Development of Electrically Conductive Thermoplastic Composites for Bipolar Plate Application in Polymer Electrolyte Membrane Fuel Cell

by

Rungsima Yeetsorn

A thesis
presented to the University of Waterloo
in fulfillment of the
thesis requirement for the degree of

Doctor of Philosophy
in
Chemical Engineering

Waterloo, Ontario, Canada, 2010

Authors Declaration

I hereby declare that I am the sole author of this thesis. This is a true copy of the thesis, including any required final revisions, as accepted by my examiners.

I understand that my thesis may be made electronically available to the public.

_____

ABSTRACT

Polymer electrolyte membrane fuel cells (PEMFCs) have the potential to play a major role as energy generators for transportation and portable applications. One of the current barriers to their commercialization is the cost of the components and manufacturing, specifically the bipolar plates. One approach to preparing PEMFCs for commercialization is to develop new bipolar plate materials, related to mass production of fuel cells. Thermoplastic/carbon filler composites with low filler loading have a major advantage in that they can be produced by a conventional low-cost injection molding technique. In addition, the materials used are inexpensive, easy to shape, and lightweight. An optimal bipolar plate must possess high surface and bulk electronic conductivity, sufficient mechanical integrity, low permeability, and corrosion resistance. However, it is difficult to achieve high electrical conductivity from a low-cost thermoplastic composite with low conductive filler loading. Concerns over electrical conductivity improvement and the injection processability of composites have brought forth the idea of producing a polypropylene/three-carbon-filler composite for bipolar plate application. The thesis addresses the development of synergistic effects of filler combinations, investigating composite conductive materials and using composite bipolar plate testing in PEMFCs.

One significant effect of conductive network formation is the synergetic effects of different carbon filler sizes, shapes, and multiple filler ratios on the electrical conductivity of bipolar plate materials. A polypropylene resin combined with low-cost conductive fillers (graphite, conductive carbon black, and carbon fibers with 55 wt% of filler loading) compose the main composite for all investigations in this research. Numerous composite formulations, based on single-, two-, and three-filler systems, have been created to investigate the characteristics and synergistic effects of multiple fillers on composite conductivity. Electrical conductivity measurements corresponding to PEMFC performance and processing characteristics were investigated. Experimental work also involved other ex-situ testing for the physical requirements of commercial bipolar plates. All combinations of fillers were found to have a significant synergistic effect that increased the composite electrical conductivity. Carbon black was found to have the highest influence on the increase of electrical conductivity compared to the other fillers. The use of conjugated conducting polymers such as polypyrrole

(PPy) to help the composite blends gain desirable conductivities was also studied. Electrical conductivity was significantly improved conductivity by enriching the conducting paths on the interfaces between fillers and the PP matrix with PPy. The conductive network was found to have a linkage of carbon fibers following the respective size distributions of fibers. The combination of Fortafil and Asbury carbon fiber mixture ameliorated the structure of conductive paths, especially in the through-plane direction. However, using small fibers such as carbon nanofibers did not significantly improve in electrical conductivity. The useful characteristics of an individual filler and filler supportive functions were combined to create a novel formula that significantly improved electrical conductivity. Other properties, such as mechanical and rheological ones, demonstrate the potential to use the composites in bipolar plate applications.

This research contributes a direction for further improvement of marketable thermoplastic bipolar plate composite materials.

ACKNOWLEDGEMENTS

This thesis arose in part out of years of research that has been done since I came to the University of Waterloo. By that time, I have had an incredible graduate experience and very joyful moments over the past four and a half years in Waterloo, Canada. I have been supported by a great number of people whose contributions in assorted ways to the research and the making of my thesis deserved special mention. It is a pleasure to convey my gratitude to them all in my acknowledgments.

In the first place, I would like to record my appreciation to Assoc. Prof. Dr. Michael Fowler and Prof. Dr. Costas Tzoganakis for their kindness to give me a great opportunity for doing my Ph.D at the University of Waterloo, and it was a major reason that I could win the scholarship for my study. They have been providing me with advice and guidance from the very early stage of this research as well as giving me an extraordinary experience throughout the work. Moreover, they have been giving me a great chance to improve efficiently through attending conferences, doing research in many places such as Polymer Technology Company and McMaster University, and being teaching assistance in chemical engineering and nano-technology programs. Their truly teacher and engineer have made them as a constant oasis of ideas and passions in teaching, which exceptionally inspire and enrich my growth as a good teacher and researcher that I want to be. I am indebted to them more than they know.

It is an honor for me to acknowledge Thai people for my Ph.D financial support through Royal Thai Government Scholarship from Ministry of Science and Technology of Thailand. My academic development has also been backed up by King Mongkut's University of Technology North Bangkok. I promise that I will do my best to serve my country in the education field and use all of my knowledge directly and effectively.

In addition, the opportunity to collaborate and to deal with other people was instrumental to this research. This thesis would not have been possible unless I did not benefit by outstanding work from researchers, technicians, my coop students and my friends in the department of chemical engineering, and mechanical machine shop.

I am thankful for the efforts of my committee members; Prof. Dr. Julia A. King, Prof. Dr. Shesha H. Jayaram, Assoc. Prof. Dr. Leonardo Simon, and Assist. Prof. Dr. Neil McManus. They contributed their valuable time to inspect me and my work, and suggested me to produce the best feasible results. I am heartily thankful to my English teacher, Mary Mcpherson whose encouragement and support from the initial to the final level enabled me to develop my English.

I am also grateful to my friends who have also been great to work with. I am happy to thank Mook, Estanislao and Gorge for their willingness to share their bright thoughts with me. Special thanks for my sister, P'Tas, your yummy foods and your kindness saved my life here, without you I would not have a happy life in waterloo. Million thanks for my lovely sisters: Ice, Pui, and Rebecca; you have been helping and making me happy. I will never, ever forget Sauder family, "My Canadian Family"; you have been very kind to me. Thank you so much.

I owe my deepest gratitude to my family: my dad, mom, aunty, and brother. Your unconditional love, overwhelming support, and encouragement have allowed me to pursue my successes. I can say "my family is my life". To the role model for a hard worker and good trainer, DAD, you have been working in your entire life, and I have not seen you give up any work. You always coach me how to live my life, and motivate me to work hard and to map my life. You always be a quizmaster that makes me have perpetual passion for knowledge. Dad and Mom, I am really proud to be your daughter, and I always want to be your pride.

Finally, I would like to thank everybody who was important to the successful realization of thesis, as well as expressing my apology that I could not mention personally one by one.

TABLE OF CONTENTS

LIST OF FIGURES

LIST OF TABLES

CHAPTER 1: Introduction

1.1 Overview

The U.S. Department of Energy (DOE) has identified Polymer Electrolyte Membrane Fuel Cells (PEMFCs) as the main candidate to replace the internal combustion engine in transportation applications [1]; however, barriers to commercialization remain. Among the fundamental technical challenges facing the commercialization of fuel cells are material and manufacturing cost and reliability.

The bipolar plate is one of the key components of PEM fuel cells, so the development of a suitable material for use as a bipolar plate is scientifically and technically important for cell commercialization. Unlike with membrane and catalyst development, little attention has been paid to bipolar plates in the published literature [1]. However, considerable recent research has covered a wide variety of bipolar plate materials, such as metal, graphite, and composite. To make PEMFCs more economical, new carbon based thermoplastic composite bipolar plate materials, which can be manufactured by low cost extrusion and injection molding, can be developed. This work explored the development of composite bipolar plates for use in the development of low-cost and light-weight bipolar plates. Although a composite plate is a promising idea, it is difficult to meet the electrical conductivity and thickness targets [2]. Therefore, increasing the electrical conductivity of the composite plate is critical if it is to be considered for fuel cell performance targets. The aim of this work was to investigate the possibility of using conductive polypropylene composites for bipolar plates in PEMFCs.

1.2 Objective

The objectives of this study include:

- The investigation of composite conductive materials for bipolar plate production;
- The development and demonstration of composite compositions and blending procedures for potential application to bipolar plates; and
- The analysis of prototype bipolar plate properties, referring to the required functionalities of bipolar plates in PEMFCs, and also the investigation of the relationship between bipolar plate properties and PEMFC performance.

1.3 Scope of Work

In this research, the focus was to work with low cost matrix materials, low cost-conductive fillers, and an intrinsic conductive polymer as an additive. Thus, conductive fillers were introduced to a polypropylene matrix to accomplish these objectives. The filled polymers used in the research were classified as random heterogeneous materials owing to their position and composition disorder. The heterogeneous materials result in a conductive network-like structure composed of conductive fillers dispersed in a polypropylene matrix. The conductivity phenomenon through a non-conductive matrix can be interpreted using percolation theory [3]. In addition, this work was concerned with the effects of additives on bipolar plate properties, conductive network investigation, and bipolar plate production modification. A number of compounding runs were completed followed by injection molding of samples were completed. The characterizations, termed in-situ and ex-situ, were relevant to bipolar plate applications in PEMFCs. These test results are discussed in relation to the feasibility of using the material in fuel cell applications. The performance of single cells and associated cell resistances during a fuel cell operation were also investigated. The approach of this research provides direction for further improvements of marketable thermoplastic bipolar plate production.

1.4 Thesis Layout

The thesis chapters follow the order of the summaries below:

Chapter 2: Background and preliminary experimental work

This chapter presents the related background information from the literature essential to understanding this research and its significance. More specifically, it presents experimental results performed to gain a fundamental understanding of PEMFC technology, bipolar plate development, and the electrical properties of bipolar plates.

Chapter 3: Experimental work

This chapter explains the main measurements and experimental techniques used for the subsequent studies. It describes the designs of composite formulation and electrical conductivity test equipment.

Chapter 4: Results and discussion

Fundamental measurements linked to material properties are used to show how knowledge of these parameters can lead to single cell performance. The discussion covers the effects of additives, filler ratios, and filler dispersion/orientation on bipolar plate properties, conductive network investigation, and the development of bipolar plate production.

Chapter 5: Conclusions and recommendations for future work

This chapter reviews the main conclusions and identifies the contributions to the scientific literature offered by this research as well as areas of future study.

CHAPTER 2: Background and Literature Review

2.1 Fuel Cell Background

Fuel cells are expected to play a major role in the economy of this century and for the foreseeable future. A number of factors provide the incentive for fuel cells to play a role in future energy supplies and for transportations, including climate change, oil dependency and energy security, urban air quality, and growth in distributed power generation [4]. The successful conversion of chemical energy into electrical energy in a primitive fuel cell was first demonstrated over 160 years ago by lawyer and scientist Sir William Grove in 1843[5]. These early devices, however, had very low current density. General Electric (GE), a more efficient design in the late 1950s for NASA's Gemini and Apollo space missions, and in addition fuel cell system provided electricity and drinking water for the crew. In developing its fuel cell technology, NASA funded more than 200 research contracts that finally brought the technology to a level that was viable for commercial application [6]. The types of fuel cells under active development include hydrogen fuelled ones such as alkaline fuel cell (AFC), polymer-electrolyte-membrane fuel cell (PEMFC) and phosphoric-acid fuel cell (PAFC) [7].

The polymer electrolyte membrane fuel cell is a good contender for portable applications and automotive propulsion applications because it provides high power density, solid state construction, high chemical-to-electrical energy conversion efficiency, near zero environmental emissions, low temperature operation (< 100 ^{o}C), and fast and easy start-up [8]. Thus, PEMFC is the fuel cell of interest in this thesis. The first development of PEMFC was

by GE for the Gemini space project, but after that, the PEMFC development became dormant. The improvement of PEMFC programs was reactivated in the 1980s, by Ballard Power Systems, subsequently recognized as the world leader in fuel cell technology [6]. The company and spin-off company Automotive Fuel Cell Corporation (AFCC) has dominated the developing automotive market and has started productions of stationary and portable power applications. For example, the largest fleet of hydrogen fuel cell buses in service was in Whistler, BC, Canada for the 2010 Olympic and Paralympic Winter Games. The twenty transit buses, powered by Ballard's FCvelocity-HD6 power module, provide a 62% reduction in greenhouse gas emissions compared to diesel buses [9].There are now more than 40 companies, for instance General Motors, Toyota, and Honda, involved in the growth of the PEMFC technology, especially in the automotive fuel cell market. Siemens and some Japanese companies have particularly focused on portable and residential fuel cell systems, where potentially high-volume markets are expected [4]. Companies such as Plug Power and Hydrogenics have made significant advances in the lift truck and back-up power market with their low pressure PEMFC technology.

2.1.1 The Operation of A PEMFC [6, 7, 10]

The fuel cell is an electrochemical energy device that converts chemical energy, from typically hydrogen, directly into electrical energy. The electrochemical reactions in fuel cells happen simultaneously on both sides of a membrane: the anode and the cathode. The basic PEM fuel cell reactions are shown as follows.

At the anode,

$$H_2 \longrightarrow 2H^+ + 2e^- \qquad (2\text{-}1)$$

At the cathode,

$$\tfrac{1}{2}\, O_2 + 2H^+ + 2e^- \longrightarrow H_2O + 286\ \text{kJ/mol} \qquad (2\text{-}2)$$

Overall,

$$H_2 + \tfrac{1}{2}\, O_2 \longrightarrow H_2O + 286\ \text{kJ/mol} \qquad (2\text{-}3)$$

The traditional PEMFC has a polymer electrolyte membrane placed between two gas diffusion electrodes, an anode and a cathode respectively, each usually containing a metal catalyst, such as Pt, supported by an electrically conductive material. The gas diffusion

electrodes are exposed to the respective reactant gases: the reduction gas (hydrogen) and the oxidant gas (oxygen/air). An electrochemical reaction occurs at each of the two junctions (three phase boundaries) where one of the electrodes, the electrolyte polymer membrane and the reactant gas interface. Figure 2-1 shows a schematic of a PEMFC.

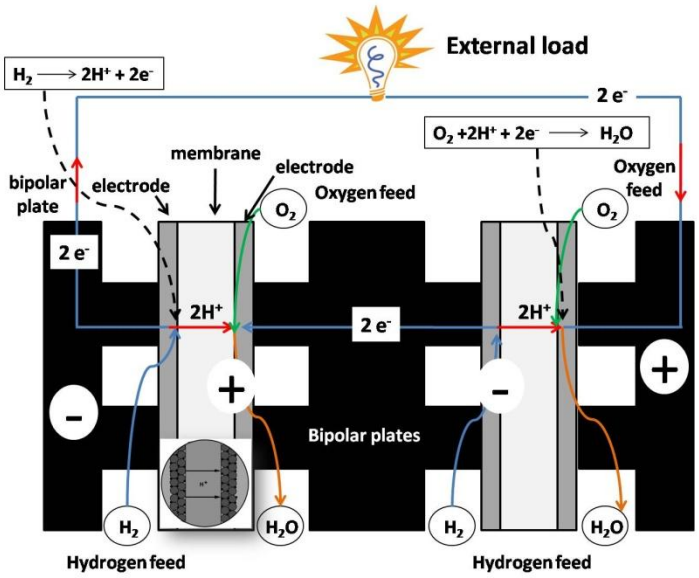

Figure 2-1: Schematic of Polymer Electrolyte Membrane Fuel Cell [6]

During PEMFC operations, hydrogen permeates through the anode and interacts with the noble metal catalyst, producing electrons and protons (2-1). The electrons are conducted via an electrically conductive material through an external circuit to the cathode, while the protons are simultaneously transferred via an ionic route through a polymer electrolyte membrane to the cathode. This polymer membrane also serves as a gas barrier so that the reactant species cannot freely combine. At the cathode, oxygen permeates to the catalyst sites where it reacts with the protons and electrons when properly hydrated, producing the reaction (2-2). Consequently, the products of the PEMFC reactions are water, electricity and heat. In the PEMFC, current is conducted simultaneously through ionic and electronic route. The efficiency of PEMFC is largely dependent on ability to minimize both ionic and electronic resistivity. The quality and functionality of fuel cells and their components can be evaluated in terms of conductivity, mechanical strength, permeability, reliability, durability, and power

output. A polarization curve is the important indicator of overall fuel cell performance (Figure 2-2).

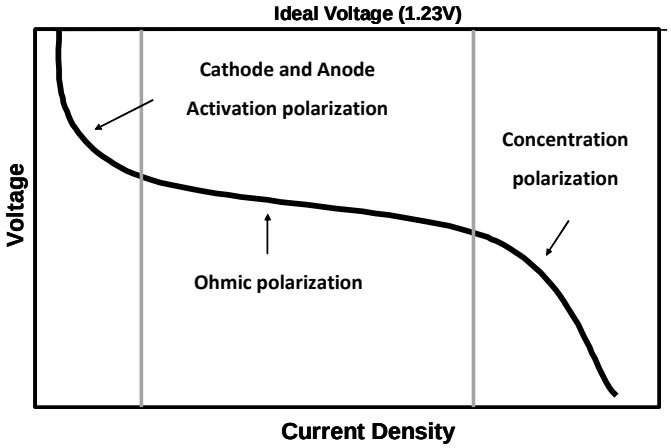

Figure 2-2: Regions of a polarization curve

The plotted curve relates the cell voltage to a changing current density. The maximum cell voltage, which occurs when the current density is zero, is referred to as the open circuit voltage (OCV). In electrochemical systems the voltage decreases as the current density increases and can be divided into three general areas: activation polarization, ohmic polarization, and concentration polarization. As shown in Figure 2-2, at the OCV, no power is produced. The power then increases with increasing current density up to a maximum, the position of which depends on the design and quality of the fuel cell components employed. Beyond the maximum, the drop in cell voltage is stronger than the increase in current density. The overall fuel cell performance is given in Equation (2-4), which signifies the cell voltage as the ideal Nernst voltage (E^o) minus different sources of voltage loss (η).

$$V_{Cell} = E^{\circ} - \eta_{activation} - \eta_{ohmic} - \eta_{concentraton} \tag{2-4}$$

When no current is flowing, the cell voltage should approach the ideal equilibrium potential (E^o). Internal currents will, however, cause losses and lower the open circuit potential below the Nernst potential.

Activation polarization ($\eta_{activation}$) is due to the energy barrier, which must be overcome in order for the electrochemical reaction to occur. The activation energy of an electrochemical reaction is a function of voltage. The oxygen reduction that occurs in the cathode of the

PEMFC has relatively slow kinetics, and consequently, the activation energy must be decreased, which results in a particularly large activation polarization. The activation loss is the dominant source of voltage loss at low current densities. The activation loss from the oxygen reduction reaction is related to effective platinum surface area ($A_{Pt,el}$), platinum loading (L_{ca}), current and exchange current density (i_o) as well as the fuel cell current (i) using Equation (2-5) [7].

$$\eta_{act} = \frac{RT}{n\alpha F} \ln\left[\frac{i}{10 \cdot \left(L_{ca} A_{Pt,el}\right) \cdot i_o}\right] \tag{2-5}$$

where T is the absolute temperature, R is the universal gas constant, n is the number of electrons transferred, α is the transfer coefficient (taken to be 0.5), and F is Faraday's constant.

The ohmic loss (η_{ohmic}) is caused by the resistance to conduction of the ionic species through the electrolyte. This loss is a linear function of current density and is proportional to the resistance of the electrolyte, and resistance through electrically conductive components such as the bi-polar plates. The ohmic losses can also be expressed as a function of current using Ohm's law as shown in Equation (2-6).

$$\eta_{ohmic} = iR_{\Omega} \tag{2-6}$$

R_{Ω} is the total cell internal resistance, which includes ionic, electronic, and contact resistance. Concentration polarization arises due to a limited supply of reactants at the electrode surface. As the fuel cell is operated at higher currents, the reaction rate at the electrode can become great enough that mass transfer to the electrode cannot replenish all of the reactants that are consumed. Accordingly, the concentration at the surface of the electrode becomes depleted and a concentration gradient is formed between the surface and the bulk, leading to a further voltage loss. At very high currents, mass transfer to the surface becomes the rate determining step, and the reactant concentration at the surface becomes zero, which is referred to as the limiting current and represents the highest current at which

the cell can operate. The value of limiting current for a cell is an important parameter for evaluating mass transfer effects. The relationship between concentrations and the concentration polarization is given by Equation 2-7.

$$\eta_{concentraton} = \frac{RT}{nF} \ln\left[\frac{C_B}{C_S}\right] \tag{2-7}$$

C_B is the bulk concentration of reactant (mol.cm^{-3}), and C_S is the concentration of reactant at the surface of the catalyst (mol.cm^{-3}).

2.1.2 PEMFC Components [11]

An expanded view of PEMFC components is shown in Figure 2-1 above. Key components include the membrane-electrode assembly (MEA), bipolar plates (flow field or separator), and seals.

The components of MEA include:

- *An electrolyte membrane* separates the reduction and oxidation half reactions, and provides an electrical and gas barrier. It allows the protons to pass through to complete the overall reaction while forcing the electrons to pass through an external circuit.
- *Anode and cathode dispersed catalyst layers* forming the electrodes are the sites for each half cell's electrochemical reaction.
- *Two Gas Diffusion Layers (GDL)* further improve the efficiency of the system by allowing direct and uniform mass transfer access of the fuel and oxidant to the catalyst layer, and mechanical support to the membrane. In addition to distributing the gases, the anode GDL also conducts the electrons away from the anode. Then the electrons go back to the anode bipolar plate and current collector. The cathode GDL conducts the electrons to the cathode catalyst layer from the cathode bipolar plate and the current collector, ensuring the complete flow of electrons. Typically, porous carbon paper or cloth is the material used for GDLs.
- *A solid polymer electrolyte* is impregnated with catalyst layers for the anode and cathode. The most common type of electrolyte used in fuel cell applications is a

perfluorosulfonic acid (PFSA) polymer, which Dupont supplies under the trade name of Nafion™.

Individual cells are combined into a fuel cell stack of the desired power. End plates and other hardware, such as current collectors, bolts, springs, intake/exhaust pipes, and fittings, are needed to complete the stack. The plates provide an integrated assembly for the entire fuel cell stack. The materials currently available for end plate production should have sufficient mechanical strength; normally steel or aluminum is used. The current collector typically functions to collect and transfer the current from the stack to an external circuit. A metal material with good electric contact and conductivity, normally copper, is suitable for the collector.

2.2 Bipolar Plates [11]

The bipolar plate performs a number of functions within the PEMFC as described below.

1. Conducting electrons to complete the circuit, including by
    - collecting and transporting electrons from the anode and cathode, as well as,
    - connecting individual fuel cells in series to form a fuel cell stack of the required voltage (i.e., fuel cells are typically arranged in a bipolar configuration);
2. Providing a flow path for gas transport to distribute the gases over the entire electrode area uniformly;
3. Separating oxidant and fuel gases and feeding H_2 to the anode and O_2 to the cathode, while removing product water and un-reacted gases;
4. Providing mechanical strength and rigidity to support the thin membrane and electrodes and clamping forces for the stack assembly;
5. Providing thermal conduction to help regulate fuel cell temperature and removing heat from the electrode to the cooling channels.

The materials of the bipolar plate must have particular properties because of its multiple responsibilities and the challenging environment in which the fuel cell operates. The ideal material should combine the following characteristics (target values below are referenced from the Department of Energy (DOE)) [12]:

1. High electrical conductivity: The electrical conductivity is the most important property for the bipolar plate, especially in the through-plane direction. A target of over 100 S/cm or 10,000 S/cm has been set by the DOE.
2. Low contact resistance with the GDL: The contact resistance, which depends on the plate material and thickness, can draw the resistance of the plate itself. Typical values for contact resistance are between 0.1 and 0.2 ohmcm^2.
3. Good thermal conductivity: Efficient removal of heat from the electrodes is imperative for maintaining an even temperature distribution and avoiding hotspots on the membrane. The heat conductivity must exceed 20Wm^{-1}K^{-1} for normal integrated cooling fluids or must exceed 100 Wm^{-1} K^{-1} if heat is to be removed only from the edge of the plate.
4. Thermal stability: The higher-temperature operation places restrictions on certain carbon polymer composites.
5. Gas impermeability: Low gas permeability avoids potentially dangerous and performance-degrading leaks. The gas permeability (specifically of hydrogen, oxygen and nitrogen) must be less than 10^{-4} cm^3/s-cm^2.
6. High mechanical strength: The bipolar plate is physically forceful and supports the thin components in the cell. The material must have suitable mechanical properties (rigidity, tensile strength, flexural strength) and must not warp. The flexural strength and tensile strength for bipolar plates must be higher than 59 MPa and 41 MPa, respectively.
7. Corrosion resistance: The bipolar plate operates in a warm and humid environment while it is simultaneously exposed to air and fuel over a range of electrical potentials. This situation is ideal for corrosion to occur. The acceptable corrosion is 1.6×10^{-3} mA/cm^2 per 5000hr.
8. Resistance to ion-leaching: If metal ions are released from the plates, they can displace protons in the membrane. The displacement diminishes the ionic conductivity.
9. Thin and lightweight proportions: A fuel cell stack requires many cells to achieve the required power levels for certain applications, so many bipolar plates are needed to

accommodate the flow channels and maintain mechanical stability. The maximum weight of a bipolar plate should be 200 g/plate.

10. Low cost and ease of manufacturing: When many bipolar plates are required, their cost should be low to reduce the total price of a fuel cell. The expected cost is $25/kW or < $10/plate.
11. Environmentally benign: Recyclability is a particular concern for fuel cell components.

Note: The values of each characteristic were set by DOE in 2007[12]

2.3 Bipolar Plate Development

Challenges facing the commercialization of PEMFCs are large scale manufacturing and materials costs, material durability, material reliability, and hydrogen storage and distribution issues [2]. Currently, efforts to improve the PEMFC cost and reliability for the industry, including the automotive industry, are comprised of reducing the cost and weight of the fuel cell stack, the goal being a 50 kW system of $35/kW and <133 kg in mass [13]. The bipolar plates in the stack require significant improvement, since bipolar plates account for approximately 55% of the PEMFC weight, and 37% of the stack manufacturing and materials cost [14, 15] as shown in Figure 2-3. Accordingly, the development of bipolar plates may present opportunities for cost and weight reductions in PEMFCs.

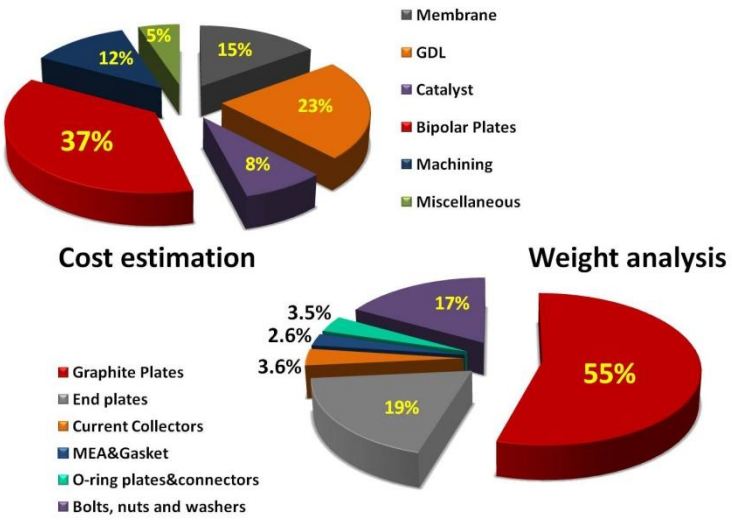

Figure 2-3: Relative cost and weight components from a PEMFC using graphite bipolar plate [14]

Moreover, bipolar plate characteristic requirements are a challenge for any class of materials, and none fits the profile characteristics exactly. Therefore, research on materials, designs and fabrications of bipolar plates for PEMFC applications is a vital issue for scientists and engineers wanting to achieve the appropriate PEMFC for global commercialization. Several types of materials are currently used in bipolar plates, including non-porous graphite plates, metallic plates with or without coating and a number of composite plates.

2.3.1 Non-Porous Graphite Bipolar Plates [2, 11, 16]

Bipolar plates in the PEMFC have traditionally been made from graphite, since graphite has excellent chemical stability to survive the fuel cell environment. Other advantages of graphite are its excellent resistance to corrosion, low bulk resistivity, low specific density, and low electrical contact resistance with electrode backing materials. This low contact resistance results in high electrochemical power output. The disadvantages of graphite plates are its high costs, the difficulty of machining it, its porosity, and its low mechanical strength (brittleness). Bipolar plates have traditionally been created from graphitic carbon impregnated with a resin or subject to pyrolytic impregnation. A thermal treatment is used in the process to seal the pores. This seal renders the bipolar plates impermeable to fuel and oxygen gases. This type of bipolar plate is available in the fuel cell market from the likes of POCO Graphite and SGL Carbon. Due to the brittle nature of graphite, graphite plates used in fuel cell stacks must typically be several millimetres thick, which add to the volume and weight of the stack.

In order to solve this problem, flexible graphite was considered the material of choice for bipolar plates in PEMFC. Flexible graphite is made from a polymer/graphite composite, in which the polymer acts as a binder. The graphite principally used for the composite is expanded graphite (EG), produced from graphite flakes intercalated with highly concentrated acid. The flakes can be expanded up to a few hundred times their initial volume [17]. The expansion leads to a separation of the graphite sheets into nano-platelets with a very high aspect ratio. This layered structure gives higher electrical and thermal conductivity. The expanded form is then compressed to the desired density and pressed to form the bipolar plate. In comparison to conventional graphite bipolar plates, the bipolar plates produced from EG are thinner.

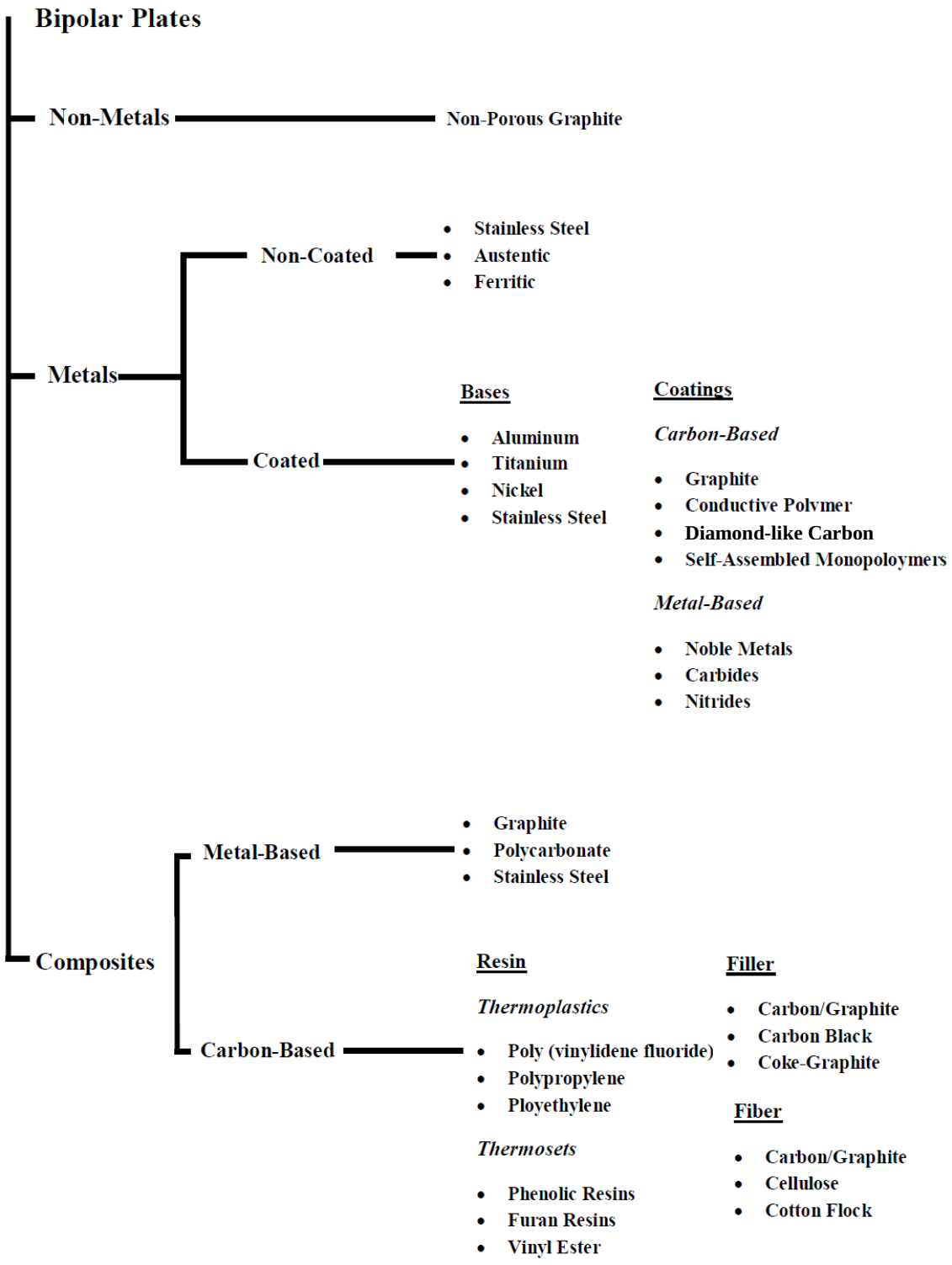

Figure 2-4: Classification of bipolar plate material [2]

Chao Du and his co-operators manufactured a compressed-expanded graphite bipolar plate with a thickness of 1mm [18]. Thinner EG plates, for example the EG/phenol, showed an

increase in flexural strength to 50 MPa [19]. However, their compression process for EG composites has not achieved mass production because the production time is too long, and the overall manufacturing cost is high. Manufacturing, for instance, may consist of two steps, pre- and main-curing [19]. In the current market, flexible graphite bipolar plates are manufactured mainly by GRAFCELL from GraphTech (Ohio, US) for the auto industry [1].

2.3.2 Metallic Bipolar Plates [1, 2, 11, 16, 20]

Metals, as sheets, are potential candidates for BP material since they have good mechanical stability, electrical and thermal conductivity and gas impermeability. They are also cheaper in the required quantities than graphite plates. Probably the most important benefit is that the resultant stack can be smaller and lighter than graphite bipolar plates. Two advantages to metallic plates that they can be stamped to accommodate flow channels and that the resultant plate can be varied thick, for example 100 μm. However, the main disadvantage of metal plates is their susceptibility to corrosion and dissolution in the fuel cell operating environment of 80^{o}C and a pH of 2–3. This degradation is harmful to fuel cell performance for the following reasons [1, 21]. First, surface oxide creation significantly enlarges the contact resistance between the plate and the GDL. Second, the corrosion process changes the morphology of the surface, potentially reducing the contact area with the GDL. Lastly, when the metal plate is dissolved, the dissolved metal ions diffuse into the PEM membrane and become trapped in the ion exchange sites [22]. This trapping results in ionic conductivity diminution, leading to increased membrane degradation. To solve these issues, researchers have considered of non-coated metal alloys, precious non-coated metals, and coated metals with a protective layer.

Precious Non-coated Metals:

Noble metals such as gold and platinum are common material choices, since they perform very similarly to graphite bipolar plates. In some cases, they have shown superior performance [23]. However, the high cost of these metals has prohibited their commercial use.

Non-coated Metals:

Aluminum, titanium, and nickel are considered to be possible alternative materials for bipolar plates in PEM fuel cells [20, 24, 25]. The advantages of these metals are their corrosion resistance, low density, low cost, and high strength. Certain higher grades of stainless steel

have also been shown to be effective. Some of these materials also have the advantage of being able to diffusion-bond with themselves, allowing complicated flow-field designs to be constructed by overlaying several layers. However, their corrosion resistance results from a passive oxide film that reduces surface conductivity or increases contact resistance. The lower contact resistance causes ohmic losses within a fuel cell. Davies et al. [26] stated that the bipolar plate performance is significantly related to the thickness of the passive layer and surface contact resistance. When the thickness and contact resistance increase, more thermal energy is generated, causing a decrease in output electric energy.

In addition to the contact resistance issues, metallic plates are also quite heavy. Therefore, plates are made as thin as can be out of these materials, allowing for smaller and lighter fuel cells. In the case of nickel, because it does not form a protective oxide layer, it will undergo corrosion in the harsh fuel cell environment. Nickel has to be subjected to surface treatment or alloyed with chromium to make it a feasible choice [20]. Stainless steel alloys are considered to be good candidates for bipolar plate materials because of their low-cost and high strength, and corrosion resistance. Despite this, the environment within fuel cells still proves a challenge for these materials, and corrosion is still a problem for some types of stainless steel such as low-chromium stainless steel [27].

Coated Metals:

To circumvent the disadvantages of metallic bipolar plates, the plates are designed with protective coating layers. The coating material should strongly adhere to the metal substrate and be resistant to cracking, blistering and pinhole formation. Furthermore, to avoid delaminating, the coating layer must have a thermal expansion coefficient similar to that of the underlying metal. Coatings must be conductive and adhere to the base materials to protect the substrate from the operating environment.

Two types of coatings, metal-based and carbon-based, have been investigated. In order to avoid the formation of an oxide layer and nickel dissolution, the SS 316L bipolar plates were coated with a gold layer, having a thickness of less than 2μm [28]. Results clearly demonstrated that there is no difference in the performance of the gold coated bipolar plates and graphite plates; however gold coated plates are relatively more expensive (even if the layer of gold is only nano layers thick). Another possible solution is to coat the metallic

bipolar plate with conducting polymer films such as polyaniline (PANI) and polypyrrole (PPy) to protect the bipolar plate while keeping contact resistance low. Shine Joseph and his team electrochemically deposited PANI and PPy on 304SS by cyclic voltammetry with 3 to 15 cycles [28]. Cost, durability and volume production were not mentioned in this study. In another development, conductive polymer coating, a team from INRS-Energie et Matériaux and McGill University in Canada has reported a method of depositing a graphitic protective coating directly onto stainless steel [29]. Current manufacturers of metallic bipolar plates include Nora (Italy) and Dana Corporation (Ohio, US) [1].

2.3.3 Composite Bipolar Plates

Composite bipolar plates are an attractive option for PEMFC use. They not only offer advantages of low cost, lower weight and greater ease of manufacturing than traditional graphite, but their properties can also be tailored through changes of reinforcements and the resin systems. The weakest point of composite bipolar plates is their low electrical conductivity compared to conventional graphite or metallic bipolar plates. To increase the electrical conductivity of the plates, electrically conductive polymers have been used as bipolar plate materials. Electrically conductive polymers are organic based materials that permit electron transfer. There are two types of conductive polymers, which can be explained as follows [30].

1. *Extrinsic Conductive Polymers:* The combination of conventional polymers (ABS, ABS/PC, and PC & PP) with conductive loads of fillers (e.g. carbon black or carbon fibers, metallic or metallic fibers, metallic powders) allows the creation of new polymeric composite materials with unique electrical properties.
2. *Intrinsic Conductive Polymers:* These materials are organic polymer semiconductors. Electrical conductivity is realized by the presence of chain unsaturation and electron delocalization effects. Much research effort and interest has therefore been devoted towards the development of polymers with intrinsic electrical conduction characteristics brought about by the presence of the conjugated group and by doping techniques.

In terms of extrinsic conductive polymers, composite materials for bipolar plates can be categorized as metal or carbon-based.

Metal-based Bipolar Plates:

Metal-based bipolar plates are made of multiple materials, such as stainless steel, plastic, or porous graphite, so that the benefits of different materials can be harvested in a single bipolar plate. For example, a composite metal-based bipolar plate was fabricated based on porous graphite, polycarbonate plastic and stainless steel [2, 6]. One of the main advantages of porous graphite bipolar plates is the production low cost. However, to produce a plate that is impermeable, the graphite plate is laminated with stainless steel and polycarbonate. The polycarbonate offers chemical resistance and can be molded to provide for gaskets and manifolding. Additionally, stainless steel also contributes rigidity to the structure, while the graphite resists corrosion. The layered plate emerges as a good alternative from reliability and cost perspectives.

Carbon-based Bipolar Plates:

Carbon-based bipolar plates can be classified as either carbon-carbon or carbon polymer composites. Carbon–carbon composites are almost entirely made of a carbon matrix reinforced with carbon fibers. The preparation of the composite plate involves an initial slurry-molding process followed by chemical-vapor infiltration (CVI) [13]. During the former process, carbon fibers and phenolic resin were formed into a plaque by means of a vacuum-molding process. After that, the surface of the plaque is sealed by the CVI technique which deposits carbon near the surface of the material, making the plate impermeable to reactant gases and greatly increasing surface electrical conductivity.

Carbon–polymer composites are created by incorporating a carbonaceous material into a polymer binder. The preference for the polymer binder is governed by the chemical compatibility with the fuel-cell environment, mechanical and thermal stability, processability when loaded with conductive filler, and cost. Two different main types of resins are used to fabricate composite plates: thermoplastic and thermosetting. Among the thermosetting resins, such as phenolics, epoxies, polyester, and vinyl ester, etc., the epoxy resin is a popular choice for carbon–polymer bipolar plate production [2]. The thermosetting resins have low viscosity, and thereby contain a higher proportion of conductive fillers. During the molding process, the thermosetting resin allows for molding of intricate details. Moreover, the resins can be

highly cross-linked through a proper curing process, and the cross-linked structure gives good chemical resistance.

Thermoplastic resins, such as polypropylene (PP), polyethylene (PE), poly (vinylidene fluoride) (PVDF), liquid crystalline polymer (LCP), poly (phenylene sulfide) (PPS), and fluoropolymer [2], are used less in bipolar plate fabrication than thermosetting resins for various reasons. These reasons are: thermoplastics are generally less chemically stable as thermosets and must operate at lower temperatures to avoid melting. On the other hand, they can be injection-molded and are therefore more beneficial in automated manufacturing. This process is suitable for mass production for future markets. However, high filler loadings limit possibilities for the injection molding process because of the higher viscosity of the composite material. As a consequence, thermoplastic composites generally have lower electrical conductivity than other technologies.

Although polymers are promising, it is difficult to meet the conductivity requirements for bipolar plate use. Therefore, the intrinsically insulating polymer resin must be filled with conductive particles. For example, Cokturk et al. [31] prepared composite materials by incorporating various nickel fillers of different shapes into polyethylene. The nickel-fillers used in this project were nickel powders, nickel filamentary powders, nickel flakes, and nickel-coated graphite fibers. It was found that the volume resistivity values of the composite materials, at maximum filler volume fraction (67 vol %), decreased more than 17 orders of magnitude with respect to neat polyethylene. Maaroufi et al. [32] investigated the effect of matrices and fillers on the location of the percolation threshold by focusing on the electrical properties of various polymers (epoxy resin, silicone, and polyurethane) filled with metal particles (cobalt and nickel). The results of this study supported the non-conducting to conducting transition that occurs as the conducting filler volume fraction increases.

A composite bipolar plate made from polyvinylidene fluoride (PVDF) as the binder and titanium silicon carbide (Ti_3SiC_2) as the conductive filler was fabricated by a compression molding technique. The metallic filler was able to improve electrical conductivity to 28.83 Scm^{-1}, but it did not meet all the criteria [33]. Instead, poor dispersion and wetting of nickel coated-graphite in the polypropylene matrix were observed [34]. The poor dispersion and

incompatibility of materials lowered the electrical conductivity when compared to the blend with synthetic graphite. This result implied that the procedure for the polymer-metal filler system needs improving to produce better dispersion composites. Moreover, the polymer-metal filler composites have the potential for ion dissolution into the fuel cell membrane, degrading performance. To solve this problem, researchers mixed a polymer with corrosion-resistant conductive particles that do not leach and thus met the conductivity target. In summary, conductive carbonaceous fillers have proven to be interesting fillers for polymer composite bipolar plates.

Graphite:

Graphite has been incorporated into polymers for bipolar plate purposes since it is able to enhance electrical properties and may offer attractive electrochemical, physical, mechanical, and economic possibilities. To reach target electrical conductivity, a high load of graphite was must be formulated for the bipolar plate material. Zhang et al. [35] produced bipolar plates through a mixture of modified phenol resin (as a binder) and natural flake-like graphite, using 84 wt% of loading. The mixture was manufactured by compression molding technology. They also observed the effects of graphite particle size and shape on the bipolar plate performance by measuring electrical conductivity, strength and other parameters. Mixing different graphite types could improve the performance of thermosetting composite bipolar plates according to Heo and his collaborators [19]. The graphite composite bipolar plates in that research were composed of expanded graphite, graphite flake and a novolak-type phenol resin, with a 75:25 wt% ratio of graphite to phenol. The production involved pre-curing and compression molding processes. The results indicated an electrical conductivity of 250 Scm^{-1}, which met the requirements for PEMFC bipolar plates, while the quantity of different types of graphite was lower than the amount used for single type graphite.

When the graphite particles are dispersed uniformly in the matrix, the bipolar plate should have improved properties: low porosity, low water adsorption, higher flexural strength and higher electrical conductivity. To demonstrate this advantage, Xiao et al. [17] first prepared a poly (arylenedisulfide)/graphite nanosheet composite via a direct ring opening

polymerization, and then graphite nanosheets were prepared by ultrasonic bathing. The plate produced was a good candidate for the bipolar plates of a PEMFC.

To achieve optimum electrical properties for these polymer graphite composites, it is essential to study not only the compositional dependence but also the effect of both processing conditions and continuous exposure to high temperatures. High temperature thermoplastic graphite composites were therefore prepared using polyphenylene sulfide (PPS) and polyether sulfone (PES) containing natural graphite powder [36]. A low resistance, in the order of 0.1 ohm, was obtained for a graphite concentration of 50 wt%. PPS/G composite with 20% PPS resin content could be produced under a molding temperature of 380 ^{o}C [37]. The plate had an electrical conductivity of 118.9 Scm^{-1}.

Carbon Black:

Carbon black (CB)-filled thermoplastic composites are widely used as antistatic and electrostatic dissipative and semi-conductive materials. To increase the electrical conductivity, polymers with high carbon powder loading have been explored. Carbon black compounds are typically loaded with 30% to 40% carbon black because CB-filled polymers have relatively low-bulk electrical conductivities, most of which were below 1 Scm^{-1} [38]. Del Rio et al. used polyvinylidene (PVDF) and carbon black to achieve a conductivity of 2.36 S/cm, corresponding to PVDF with 40wt%CB at 30°C, for example [39]. When the CB content changed from 30 to 40%, a sudden rise in conductivity was observed. The conductivity increased because the percolation threshold appeared just at this range. The best results from a performance test of a conventional fuel cell using these composite bipolar plates were obtained with the highest CB concentration (100 mW/cm^2 at 200 mA/cm^2).

Although carbon black can increase conductivity, the addition of carbon black diminishes processability of the material. Injection molding is suitable for mass manufacturing. However, processing is still difficult when a high concentration of CB is used. The high CB content increases the viscosity of the blends. Therefore, compression molding, which is a slower process than injection molding, often becomes the only method of a choice for processing when high a concentration of CB is used. An additional problem associated with high CB concentrations in polymers is the substantial reduction in the strength and ductility

of the polymer composites [40]. To address such problems, numerous studies were directed at reducing the carbon black concentration and the percolation threshold.

Carbon Fiber:

Even though fibers are frequently used to improve the strength and rigidity of polymers, several studies have considered the reinforcement of thermoplastic polymers using carbon fibers to achieve improve the thermal and electrical properties. Thus, carbon fiber composites have been used for many applications, including a limited number of trials as bipolar plates for PEMFCs. Carbon fiber composites are normally fabricated by slurry molding of chopped carbon fiber with thermosetting resin, followed by sealing with chemically vapor-infiltrated carbon (CVI) [41].

In addition to considering the influence of fiber loading on electrical and mechanical properties, some studies have been performed on fiber orientation. Fibers with finite aspect ratios can enhance the conductivity of a composite by aligning the long and more conductive axis of fiber particles in the current-flow or "through-thickness" plate direction. The fiber particles make smaller and fewer insulating gaps in the composite, resulting in a material resistivity reduction and, in turn, an increase in conductivity. This increase enables the conductive target to be achieved at lower filler concentrations, and, thus, at higher material toughness levels [42]. In response to the studies above, high loading of conductive fillers has been used to achieve satisfactory electrical and mechanical properties. However, using a high concentration of fillers leads to process difficulties. Hence, the aim of some current studies is to determine the feasibility of making conductive polymers containing lower filler concentrations with both high electrical conductivity and high mechanical strength.

Liao et al. worked with a lightweight polymer composite bipolar plate that contained vinyl ester resin, graphite powder and multi-walled carbon nanotubes (MWNTs) and was fabricated using a bulk molding compound process [43]. Results demonstrated that the bulk electrical conductivity of the composite bipolar plate with different MWNT types and contents exceeds 100 Scm^{-1}. This value was approximately 32% higher than that of the original composite bipolar plate because more continuous conducting paths resulted in better electron transfer in PEMFC (Figure 2-5). The previous investigations, mentioned above, addressed the use of a single type of carbon filler to achieve the desired conductivity, while

still allowing the material to be molded into a bipolar plate for a fuel cell. It was, however, found that a single carbon filler component could not be used for making suitable composite bipolar plates.

The addition of various carbon fillers with different physical and electrical properties, including natural flaky graphite, synthetic graphite, carbon black and carbon fibers, were found to be essential for the development of bipolar plates with the desired properties [44]. The single filler gives typical blend characteristics as follows. Carbon black has a high surface area and aggregation behavior, which are needed to achieve the desired conductivities and are also responsible for relatively low production cost. It is difficult, however, to prepare well dispersed polymer/carbon black composites containing more than 35 wt% carbon black.

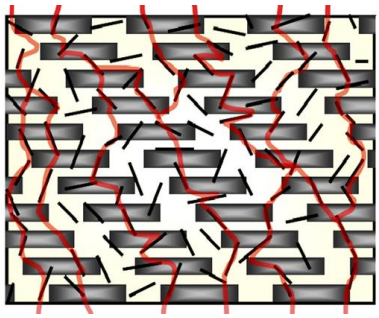

Figure 2-5: The conductive paths in MWNTs composite bipolar plates [43]

As a result, graphite is generally added to the composite to combine the electrical properties of graphite with ease of processing. High-aspect-ratio carbon fiber has also been added to polymers to increase both electrical conductivity and mechanical reinforcement. Therefore, ***the synergistic effect,*** which results from combining various types of conductive fillers, on electrical conductivity is a topic of growing interest to researchers.

The Combination of Conductive Fillers:

In previous works, the use of two filler types in polyethylene composites combined the conducting features of carbon black and carbon fiber [45]. While fibers provide charge transport over large distances, carbon black particles improve inter-fiber contacts. The results showed that for composites in which the segregated carbon black-polyethylene component was laid above the percolation threshold, the electrical inter-fiber contacts were activated

through carbon black particle bridges, leading to a rise in conductivity. The addition of sufficient amounts of carbon black must be controlled to obtain good processability. Therefore, graphite was used instead of carbon black to overcome this disadvantage. In terms of a two-filler system, composite bipolar plates composed of modified phenolic or epoxy resin, graphite particles (e.g., natural, synthesis, expended graphite), and carbon black with a thickness of less than 2mm have been successfully prepared by the bulk molding process [46-48]. Even carbon black and graphite are preferable for the production of composite bipolar plates; other fillers such as carbon fiber and organoclay are interesting materials for production [49].

Maheshwari et al. studied the comparative effect of carbon fiber mat and carbon black (10 vol%) on the various properties of the bipolar plate, while keeping the amount of natural graphite (65 vol%) and the binder resin (25 vol%) constant [41]. The results showed that the cell performance with these plates achieved 83% of the power density as compared to the commercially available Schunk plates. Ternary composites were also used as electrically conductive materials to prepare bipolar plates. Huneault formulated a new material using polypropylene (PP) and polyphenylene sulfide (PPS) as matrices and carbon black, graphite, and carbon fibers as conductive additives [50]. These formulations have properties suitable for bipolar plate manufacturing.

The University of Waterloo has investigated the synergistic effect of two and three filler systems on bipolar plate properties [34, 51]. The investigation showed that the electrical conductivity and ability of injection molding process can be improved significantly. Adding three carbon fillers (carbon black, synthetic graphite particles, and carbon fiber) to the Vectra A950RX liquid crystal polymer always resulted in an increased viscosity [52].

Intrinsic Conductive Polymers:

Intrinsic conductive polymers have been investigated for use in various applications including as bipolar plate materials. They include polymer families such as polythiophenes, polyanilines, polypyrroles, polyphenylene, polyfluorenes, polynaphthalene, and polyacetylenes. The two main groups of intrinsic conductive polymers are categorized as follows [30, 53]:

1. Polyacetylene and Polyyne

Polyacetylene (IUPAC name: polyethyne) is an organic polymer with the repeat unit $(C_2H_2)_n$. The high electrical conductivity discovered for these polymers in the 1970s accelerated interest in the use of organic compounds in microelectronics. Polyacetylenes, in which the H atoms are replaced with alkyl groups, are also known where. Polyynes are a group of organic compounds with alternating single and triple bonds, for example, buta-1, 3-diyne (diacetylene), C_4H_2.

2. Polyheterocycles as Conducting Polymers

Resonance-stabilised aromatic molecules have become one of the electronically conducting polymers because conductive organic polymers often have extended delocalized bonds. Many aromatic systems have been found to undergo electropolymerization to produce conducting polymers. These aromatic system includes pyrrole, thiophene, furan, aniline, azulene, indole, para-phenylene, as well as many substituted, multi-ring and polynuclear aromatic hydrocarbon systems.

Polymer composites prepared as a mixture of a conjugated conducting phase and classical nonconducting phase can exhibit good electrical conductivity with relatively low conducting phase content. They normally show a significant jump in the electrical conductivity at a certain critical concentration of the conducting polymer. Of specific interest to this research is polypyrrole (PPy), since it is relatively inexpensive in comparison to other conductive polymers. It is also easy to synthesize and has advantages as an industrial material. Furthermore, it has high electrical conductivity, in the range of 30 - 100 Scm^{-1}. In terms of stability, it has higher environmental stability than other conjugated conducting polymers such as polyacetylene [54].

Researchers have been interested in blends of PPy and commercial polymers to increase the electrical conductivity of materials. Conducting polymer composites of polyethylene and polypyrrole (PE/PPy), polypropylene and polypyrrole (PP/PPy), and polymethyl methacrylate and polypyrrole (PMMA/PPy) were prepared by a chemical modification method and mixing in a kneading machine to allow researchers observe the effect of the preparative route on the conductivity of polypyrrole-containing composites [55, 56]. The conductivity of PPy composites prepared by chemical modification was higher than the

conductivity of blends prepared by mechanical mixing of PPy composites in the same PPy concentration range. Omastova, M. et al. also compared the electrical conductivity of PP/PPy composites prepared by chemical modification and by mechanical melt mixing to PP/CB composites [56]. The conductivity of the PP/PPy blend was comparable to that of PP composites filled with conductive carbon black. The content level of about 2.3 wt.% PPy in PP/PPy composites or about 5 wt.% CB in PP/CB composites is the threshold concentration at which the conducting network is sufficient to remove any static charge from a sample surface. PPy has been blended with other conventional polymers such as polystyrene, polycarbonate, polyvinyl alcohol, and also other conductive polymers with the main aim of controlling the percolation threshold [57]. However most of the blends were prepared by a chemical modification process.

A recent work indicated that PPy could be included in a composite with conducting fillers by mixing PPy with synthetic graphite or carbon black using an in-situ polymerization technique [58]. PPy/carbon nanotube composites were chemically synthesized by in-situ chemical polymerization methods such as oxidation polymerization [59]. PPy blends or PPy composites in particular have attracted strong interest for fuel cell work. They have particularly been used for coating metallic bipolar plates or making membranes (i.e., PPy/Nafion membranes) [60, 61].

The possibility of using conductive polymers to produce bipolar plates is an interesting notion for fuel cell development. For example, an exploration was made of the electrical properties of polypropylene/conductive filler (i.e., graphite, carbon black, and polyaniline) composites as potential replacements for the traditional graphite bipolar plates [62]. Two methods were mainly adopted in this work for the preparation of composites: melt compounding and solution blending. The results indicated that the solution blending led to further improvement in electrical conductivity compared with the melt compounding. In reports on bipolar plate materials, less attention has been given to the use of conductive polymers than to conductive fillers in composite bipolar plates. Therefore, the aim of this research was to investigate the possibility of using the combination of polypropylene/carbon filler composites and polypyrrole to fabricate injection- molded- composite bipolar plates.

2.4 Bipolar Plate Manufacture [11, 63, 64]

Various methods for forming bipolar plates have been considered, and no single method or material is clearly the best.

Graphite Plates:

To make impermeable plates, the CVI technique is included in graphite plate production to close pores. Then, gas flow channels and other features, such as manifolds and gasket grooves, are machined into the graphite plates by means of a manual or computerized numerical control (CNC) process. These processes increase the time for producing each plate and are therefore not suitable for large-scale manufacturing. The prolonged cycle time, capital cost of CNC machines and tool wear make this sort of machining expensive. Moreover, graphite plates should be a few millimeters thick in order to maintain sufficient mechanical strength for machining flow channels and stacking assembly because of the brittleness of graphite. As mentioned, cost savings and thickness are the largest motivations to develop new materials and manufacturing techniques.

Metallic Plates:

Metals can also be manufactured by many techniques, such as forging, stamping, casting, and electroforming. Since most metallic bipolar plates also have corrosion concerns, coating processes for solid or modular metallic bipolar plates are required and physical vapor deposition techniques such as electron beam evaporation, sputtering and glow discharge decomposition, chemical vapor deposition, and liquid phase chemical techniques like electro-deposition, chemical anodization/oxidation over coating and painting. However, it is very difficult and costly to perform surface treatments on metallic bipolar plates, and little durability evaluation has been conducted.

Polymer Composite Plates:

From a processing point of view, the polymer composites offer ease of manufacturing. For instance, flow fields can be molded directly into these composites, thereby eliminating the costly and difficult machining steps required for graphite or metal hardware. The composites are used to form bipolar plates with flow channels by conventional compression or injection molding or compression-injection molding. Compression molding is favored for both thermoplastic and thermosetting matrix composites. However, if compression molding is

used, the thermoset has to be cured, and the thermoplastic material has to be cooled. Both of these processes greatly increase production time. If compression molding is used, cost-effective mass production would be more readily achievable with thermosets rather than thermoplastics because of the shorter cycle times for thermosets. With a suitable combination and operating condition, a compression molded thermoset composite can be cured comfortably in less than 10 minutes, resulting in cycle times less than those required for thermoplastics. Injection molding machines make manufacturing automation and mass-production easier, as well as ensuring short processing times, of as little as 30 seconds per plate, and with high dimensional tolerance. However, in order to accomplish practical electrical conductivities, the thermoplastic has to be highly loaded with conductive fillers, which causes the melt to flow poorly. Higher viscosity of materials has become the main concern for composite bipolar plate manufacturing.

Currently, the injection-molding industry is well ascertained and responding positively to the bipolar-plate challenge. SGL Technologies GmbH has been developing different molding technologies for graphite composite bipolar plates since 1997 [65]. Injection molding of polypropylene and phenolic-bonded graphite compounds has been identified as one of the most promising and cost-effective production processes. A range of low-cost carbon–polymer compounds with specific bulk conductivities between 5 and 150 Scm^{-1} was developed in 2005, and a production line for bipolar plates by injection molding has been set up. Quantum Composites (Ohio, US) and Ferromatik Milacron (Germany) were the first to demonstrate injection molding for a thermoset-based carbon-polymer composite based on vinyl ester [1]. Century Engineering (Michigan, US) has developed RingExtrude (12-screw) which is a technology that modernizes the method by which bipolar plates are produced [1]. Injection molding is a low cost high-productivity manufacturing method; however, other processes, such as extrusion with appropriated die, rolling and thermoforming may be alternative progressions to producing composite bipolar plates.

In recent years, some new techniques for prototyping bipolar plates for PEMFC have been reported. Huang and his collaborators used the wet-lay method to make bipolar plates. This method produced wet-lay sheets or mats consisting of graphite particles, glass or carbon fibers, and a base made of poly(phenylene sulfide) or polyester [66, 67]. The process was

comprised of a slurry-making process and then compression molding to form conductive composite plaques. The use of the wet-lay composite in the formation of bipolar plates has multiple advantages. First, it increases in-plane conductivities of the composite plate significantly, 200 - 300 S cm^{-1}, while maintaining through-plane conductivity. Second, it dramatically increases the mechanical properties of the composites. Third, one can use different components, including polymers, graphite particles, and reinforcement, for the core and outer layers of the plate, respectively, to optimize the properties and/or reduce the cost of the plate. Kuo and Chen created bipolar plates using a composite material composed of Nylon-6 and S316L stainless steel alloy fibers by the injection molding process [61]. Although this technique provided a possible alternative to graphite for bipolar plates, the performance of current PEMFC failed to match that of conventional PEMFC with graphite bipolar plates, and metal fibers are likely to impact the durability of molds and molding equipment. Inserting metal sheets into bipolar plates is another idea aimed at increasing the electrical conductivity of plates.

Hsiao and his team prepared metal mesh hybrid polymer composite bipolar plates by inserting a copper or aluminum mesh in polymer composites [68]. Poly(oxyalkylene)-diamines composites consist of 70 wt% graphite powder and 0-2 wt% modified multi-walled carbon nanotubes. Results indicated that the in-plane electrical conductivity of m-MWCNTs/polymer composite bipolar plates increased from 156 Scm^{-1} (with 0 wt% MWCNT) to 643 Scm^{-1} (with 1 wt% MWCNT). However, the aluminum mesh hybrid polymer composite bipolar plate exhibits an obvious decrease in through-plane conductivity (22.9 Scm^{-1}) due to the passive film layer on the aluminum surface. Prototype plates were successfully fabricated using a two-shot injection over-molding procedure over aluminum plates [40]. The over-molding approach is promising, but in order to reduce the contact resistance, improved polymer-metal adhesion and better matching of the aluminum and polymer blend thermal expansion coefficient is required. Direct injection without the metallic core leads to better resistivity results.

In the conventional graphite plates, the ribs and channels in the flow fields are formed while removing part of the material to create channels. Ming-San Lee and co-researchers designed new bipolar plates with specific ribs [69]. Those ribs were composed of electron conductible

carbon/graphite fiber bunches, which perpendicularly penetrated the main plastic plate body (Figure 2-6) to convey electrons from the anode of one cell to the cathode of its adjacent cell. The gas/fuel flow channels were formed between fiber bunches, and a specific pattern may be produced through arrangement of the fiber bunches location.

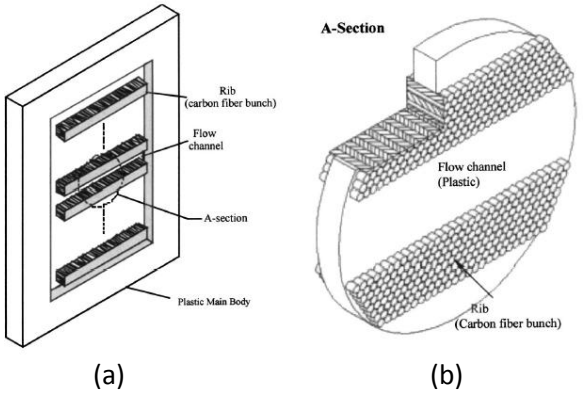

Figure 2-6: Schematic drawing of (a) the new heterogeneous composite bipolar plate and (b) the detailed structure of carbon fiber bunches inside the plate [69]

2.5 The Mechanisms of Polymer Electrical Conduction

The following section considers mechanisms for the electronic conductivity of conductive polymers. The mechanisms can be explained by different theories that depend on two types of conductive polymers: extrinsic and intrinsic conductive polymer.

2.5.1 Percolation Theory [70-74]: *for extrinsic conductive polymers*

An important theory for understanding conductivity within composite materials, especially where the polymer matrix and the filler(s) have very different characteristics, is the concept of percolation. Percolation processes were developed by Flory (1941) and Stockmayer (1943) to describe how small branching molecules react and form very large macromolecules [75]. In mathematical literature, percolation was introduced by Hammersley and Broadbent in 1957. The percolation concept originally dealt with the spread of hypothetical fluid particles through a random medium. In other words, the concept explains how the random properties of the medium influence the spread of fluid particles through it. To explain percolation theory in a simpler scenario, Stauffer applied it to forest fires (Figure 2-7): "How long does a

forest fire take to either penetrate the forest or to be extinguished?" was the question posed in this scenario.

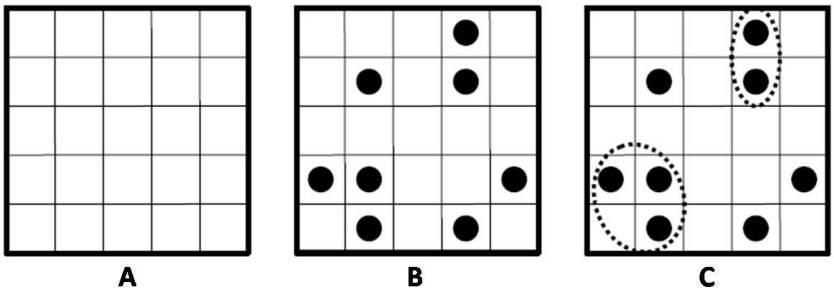

Figure 2-7: The schematic of a simple scenario for the percolation theory [70]

A represents the forest. The probability that an individual square would be occupied by a dot is p, and the probability that a site would be empty is (1-p). If p = 1, each site would be occupied by a tree. The trees in the forest are set on fire from one side, whereas the remaining trees are not on fire. In order to spread the fire, an adjacent tree must exist. If there is no tree for the fire to spread to, the forest fire is terminated. The percolation threshold is when this termination occurs in the last column, and the fire has penetrated through the entire forest. In a view of electrical conduction in a polymer matrix, electrons are free to flow through conductive filler particles. If these filler particles contact one another, a continuous path is formed through the polymer matrix, which is an insulating material, for electrons to travel through. This path is called a conductive network, and the material with the conductive network turns into a conducting material, as illustrated in Figure 2-8.

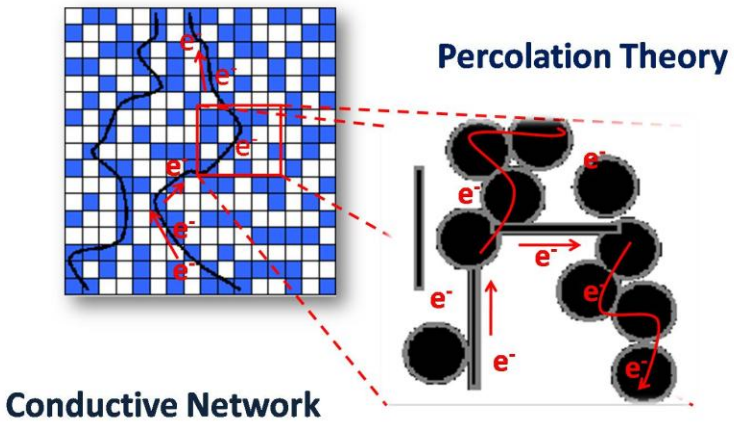

Figure 2-8: Schematics of percolation pathway

For the increase in conductive filler loading, three main regions define the relationship to the conductivity of conductive-filled-polymer composites as shown in Figure 2-9.

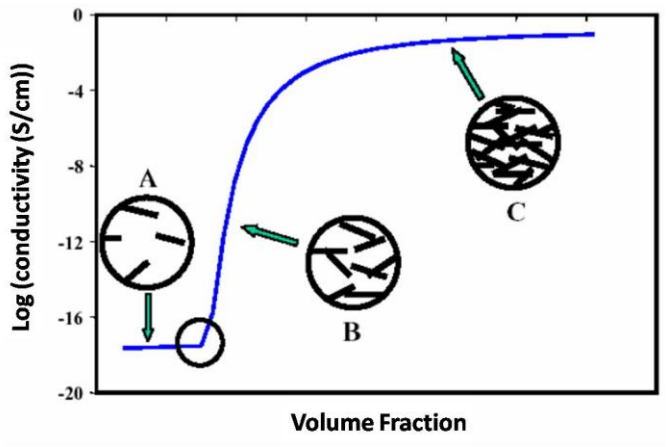

Figure 2-9: Percolation S-Curve [51]

At low filler loadings (region A), the electrical conductivity value equals zero, since no path exists for electron transport. The conductivity of the composite is still very close to that of the pure polymer matrix. At a certain critical loading, known as ***the percolation threshold***, enough filler has been introduced so that it begins to form a continuous conductive network through the composite. Following the percolation threshold is a region that produces a significant increase in conductivity with very little increase in filler amount, as displayed by region B. After this region of drastic increase, the conductivity slows its increase, and approaches that of the filler material as increase happens because the conductive network through the sample is complete. This is depicted in area C of Figure 2-9. Eventually, P_{max} is reached, at which point the addition of more filler does not increase the ease of electron movement. The addition of more filler will not enhance the conductivity to any significant degree.

2.5.2 Band Structure and Electron Delocalization [30, 54]: *for extrinsic conductive polymers*

Most commercially produced organic polymers are electrical insulators due to the material's band structure and low electronic mobility. The main property required for a polymer to be conductive is the presence of conjugated double bonds along the polymer backbone. There have been some attempts to explain the conduction mechanism of conjugated polymers with

different theories. However, the conducting mechanism of conductive polymers is quite unknown. The band theory and electron delocalization in conjugated bonds can be used to explain the electrical conduction mechanism. Conjugated polymers are polymers with alternate single and double bonds. In conjugated polymers, every single bond between the carbon atoms contains a σ bond, and every double bond contains a weak π bond. Electrons are less strongly localized in the π bonds, and thus the π electrons play a decisive role in polymer conductivity. Conductive polymers with conjugated bonds often have extended delocalized bond, composed of aromatic units (Figure 2-10).

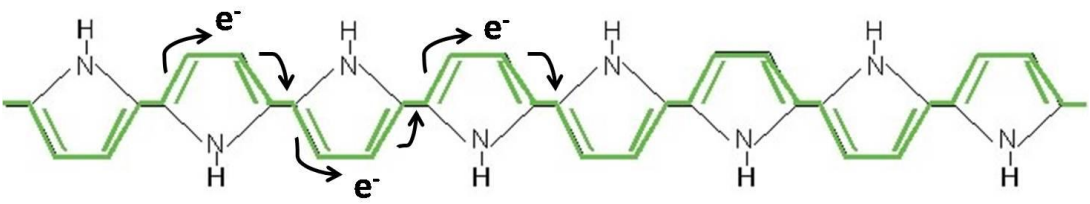

Figure 2-10: Electron delocalization on polypyrrole

When charge carriers, from the addition or removal of electrons, are introduced into the conduction or valence bands, the electrical conductivity increases dramatically. In terms of band theory, which is generally used for metals, molecular orbitals spaced together in a given range of energies form a continuous band of energy, as shown in Figure 2-11. The energy spacing between the highest occupied band and the lowest is called the band gap.

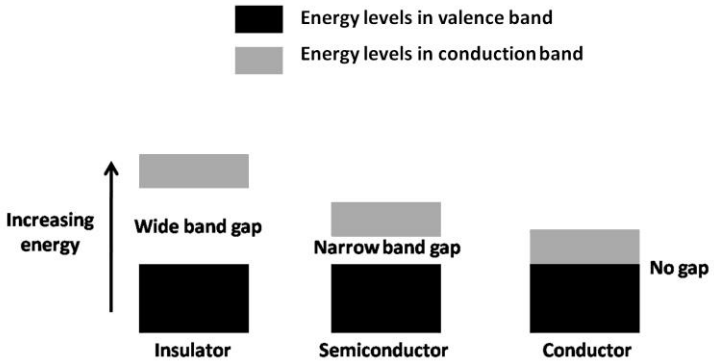

Figure 2-11: Simple band picture [30]

The highest occupied band is known as the valence band, and the lowest is called the conduction band. According to band theory, a continuous delocalization in the π system

causes the formation of a half-filled valence band. A polymer can lower its energy by bond variation, which causes it to become a large energy gap semiconductor with very low conductivity. If the polymers are covalently bonded, the material needs to be "doped" for electron flow to occur, and the polymers can be transformed into a conductor.

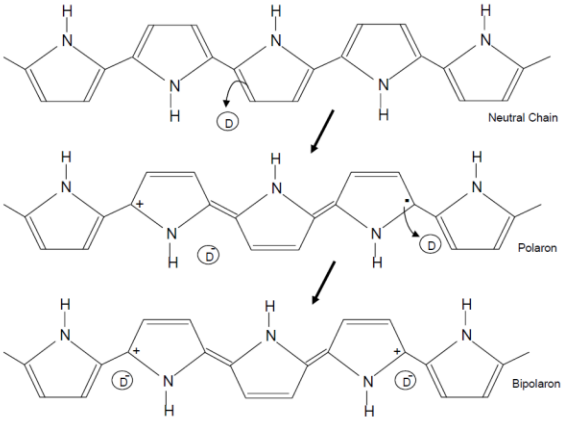

Figure 2-12: Polypyrrole doping process [54]

Doping is either the addition of electrons (reduction reaction) or the removal of electrons (oxidation reaction) from the polymer. The addition or removal of electrons localizes a charge localized over a small segment of the chain. The charge localization increases the energy of the polymer above the delocalized state, and thus, the polymer prefers to be in the delocalized state after doping. For example, the polypyrrole chain is oxidized by a dopant and transformed into a radical cation with an unpaired electron called a 'polaron' (Figure 2-12). If the polarons are on a higher doping level, the polarons will transform into a bipolaron. The continuous bipolaron bands, which are in between the conduction band and valence band are provided as shown is Figure 2-13. If heavily doped polypyrrole is generated, the polaron bands merge together between the valence and conduction bands, producing metal-like conductivity.

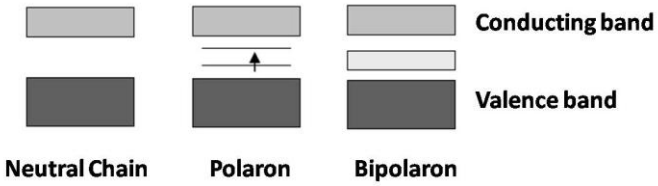

Figure 2-13: Conducting mechanism of polypyrrole with polaron and bipolaron transformations [54]

2.6 Filler Dispersion and Electrical Conductivity Improvement

The major technique for increasing the electrical conductivity of polymers is to load conductive fillers into the polymer matrix. The filler should extend continuously along the cross sectional area and through the thickness of the plate. In other words, the composite needs appropriate conductive networks to have enough electron transport paths. However, several obstacles exist, such as adhesion failure, agglomeration, and poor distribution of fillers in the matrix. Furthermore, filler distribution may increase contact resistance if the conductive filler does not fully disperse to reach the surface. The introducing of coupling agents is one technique for formulating well dispersed polymer/filler composites. A coupling agent can act as a molecular bridge at the interface between the two substrates; hence, it improves the interfacial adhesion between fillers and the matrix [76]. It also plays the role of a dispersion agent; thus, it increases the probability of conductive network formation throughout the matrix. Improvement in the electrical conductive network will diminish the percolation threshold. For example, the electrical percolation of polyethylene/carbon black composite decreases when CB is treated by a titanate coupling agent [77].

Commercially available coupling agents, such as silane and titanate, have been incorporated into carbon fiber or carbon black composites to improve electrical conductivity [78, 79]. The coupling agents have been used to improve rheological behavior, dispersion characteristics and mechanical properties of composites [80]. To the author's knowledge, of the author, there was no research publication has mentioned the use of coupling agents in the production of composite bipolar plate. This research focuses on the use of titanate coupling agents to improve conductive network formation because they can be integrated easily in the bipolar plate production process.

As in the previous attempts on employing titanate coupling agents for surface modification, the main method is as follows [78]: a solution of titanate coupling agent is prepared in an appropriate solvent, and then filler, either carbon black or carbon fiber, is immersed in the coupling solution. The fillers treated with the coupling agent were dried to remove the solvent. Finally, pre-treated fillers were incorporated into the blends in the batch mixer. Titanate coupling agent powder (CAPOW, L38/H from Kenrich Petrochemicals, Inc) can be

directly compounded with fillers and polymers in batch mixing under the optimum conditions [81]. The IUPAC name of the L38/H coupling agent is neopentyl(diallyl)oxy, tri(dioctyl)pyrophosphate titanate. The chemical structure is shown in Figure 2-14.

Titanate coupling agents consist of three main functional groups: organo-functional, hydrolysable, and Ti-O groups [81]. The organo-functional group contains pyrophosphate groups and hydrocarbon chains. The pyrophosphate group is responsible for promoting anti-corrosion properties and electron transfer control. Meanwhile the hydrocarbon chains in the region bind with the polymer matrix due to their non-polarity. These hydrocarbon chains demonstrate the concept of 'like dissolves like'. The hydrolysable group reacts with hydroxyl groups or free protons on the filler surface. This group is also responsible for the coupling, adhesion, dispersion and improvement in hydrophobicity. The Ti-O group is capable of catalyzed reactions such as repolymerization, transesterification, and transalkylation. Additionally, a condensation reaction occurs to form a Ti-O link between the functional group and the filler surface while forming methanol instead of water.

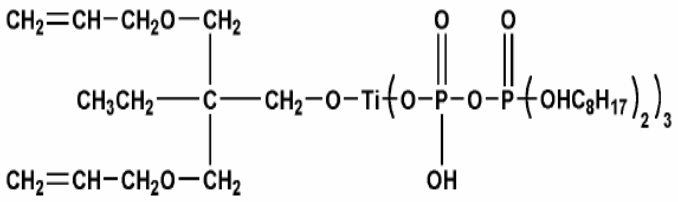

Figure 2-14: Chemical structure of L38/H titanate coupling agent [81]

A supercritical carbon dioxide process could be one approach to improve conductive network formation. The supercritical carbon dioxide process was used in extrusion for the improvement of polystyrene/polyethylene blend properties. Results showed that the viscosity of the blend was decreased with carbon dioxide dissolution, and the size of the dispersed polyethylene phase was generally reduced by increasing the concentration of CO_2 [82]. Furthermore, supercritical CO_2 was found to decrease the interfacial tension between polystyrene and polyethylene [83]. The use of carbon dioxide solution in composite mixing process was also applied to polymer/filler composite applications. For example, Matsuyama and Mishima prepared highly loaded TiO_2–polymer composite particles by rapid expansion

of carbon dioxide saturated polymer suspensions with high shear mixing [84]. The mixing process of the CO_2 saturated polymer suspension and TiO_2 accelerates the dispersion and loading of TiO_2 in the polymer matrix.

2.7 Bipolar Plate Cost

In fuel cell systems, bipolar plates are known to significantly impact the performance, durability, volume-to-weight ratio, and cost. If fuel cells are to compete in any market application, they have to be cost competitive with created with existing technology. If fuel cell vehicle engines are to become economically competitive over the internal combustion engine, the U.S. Department of Energy (DOE), based on current best technology, projects a target cost of a fuel cell vehicle $225 per kW in mass production, compared to the industry's ultimate goal of $30 to $50[85]. In terms of mass production, DOE and Directed Technologies, Inc. (DTI) have estimated costs of fuel cell stacks and fuel cell systems at a manufacturing rate of 500,000 systems per year manufacturing rate as shown in Table 2-1[86].

Table 2-1: DOE targets/DTI estimation

Source	Characteristic	Units	2005	2006	2010	2015
DOE target	Stack cost	$/kW$_{e(net)}$	$65	-	$25	$15
DTI estimate	Stack cost	$/kW$_{e(net)}$	-	$66	$30	$25
DOE target	System cost	$/kW$_{e(net)}$	$125	-	$45	$30
DTI estimate	System cost	$/kW$_{e(net)}$	-	$108	$70	$59

Recent technical cost analyses indicate that the cost for platinum electrodes is the highest influence on PEMFC cost, whereas bipolar plates rank second or third in cost, depending on the model used to estimate cost [14]. Therefore, DOE suggested suitable cost targets for bipolar plates of 10 US$/kW in 2005, 5 US$/kW in 2010, and 3 US$/kW in 2015[87]. The estimated cost of Carbon-Carbon composite bipolar plates, developed by Oak Ridge National Laboratory (ORNL), was about $26/m^2 at high volume, in which the CVI process cost was about 70% [88]. The high process cost limits the application of this approach. Cost reduction is expected through the application of high volume manufacturing processes or high

efficiency and lower cost materials. This approach can be supported by bipolar plate cost analysis, which is provided by DTI as exhibited in Figure 2-15.

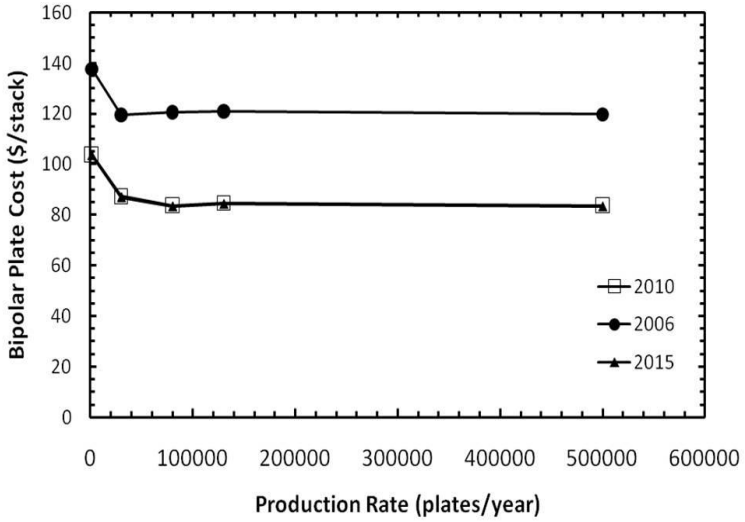

Figure 2-15: The anticipated cost of polypropylene/carbon bipolar plates [86]

The analysis provides more insight into the anticipated cost of injection molded bipolar plates at commercial volumes in the future [86]. The plates are made from the polypropylene/carbon composite with 50wt% of carbon powder loading. The plates can be flipped 180 degrees and used for both cathode and anode electrodes. The cost of this manufacturing process can be lowered by doubling plate production with a 30 second cycle time. In work done at the University of Waterloo, Mali reported the assumption of a polypropylene/carbon filler composite plate with a thickness of 3mm or 0.3 cm. and a 1:1:1 ratio with 54 wt% of fillers [51]. Comparing the result values to the previous presented target of \$0.0045/cm^2 (USD 2003), the low production level was not sufficiently competitive; mid-level production did not meet the target, but it was still reasonably competitive. At high production levels, the developed materials met the suggested bipolar plate cost, making the fuel cell a competitive technology.

2.8 Electrical Conductivity of Bipolar Plates

According to PEMFC operation, electrons must transfer through bipolar plates to complete a circuit (Figure 2-16), so one critical fuel cell performance factor is the electrical conductivity of the bipolar plate. The better the electrical transport of a bipolar plate, the fewer plates are

required to produce a given power output. This leads to a smaller fuel cell and lower cost, which are key features for market acceptance. Therefore, before single cell tests, the electrical conductivity of the composite plates must be evaluated ex-situ. Two main methods, through-plane and in-plane conductivity measurements, are employed to measure the electrical conductivity of composite plates. Prior to discussing the electrical conductivity measurements, it is essential to understand the concepts of electrical properties relevant to the measurements. The electrical conductivity is determined by the availability of "free electrons" in the material. The electrical resistance of an object is a measure of its opposition to the passage of a steady electric current. In other words, the resistance can be defined as the ratio of DC voltage to DC current, in accordance with Ohm's law (Equation 2-8):

$$R = \frac{V}{I} = \Omega \tag{2-8}$$

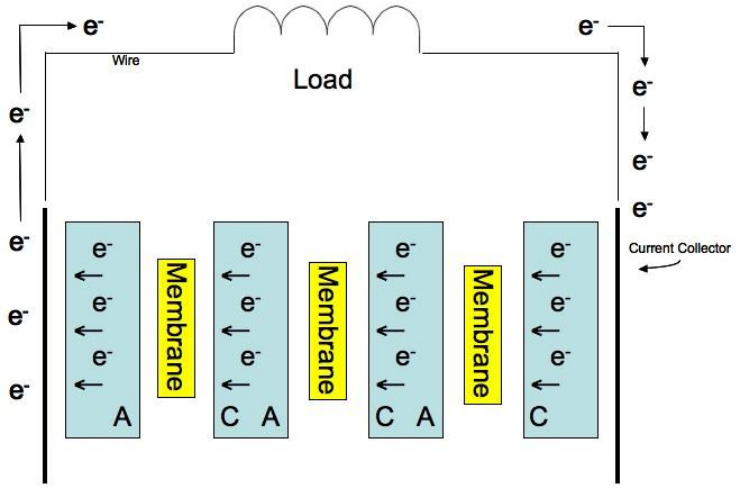

Figure 2-16: Schematic of electron transport in the cell

Bulk resistivity, on the other hand, is a measure of how strongly a material opposes the flow of electric current. The following equations were used to calculate sample resistivity and conductivity from the averaged resistance measurements [89]:

$$\text{Resistivity} = \text{Resistance} \times \frac{\text{contact area (cm}^2\text{)}}{\text{sample thickness (cm)}} = \Omega.\text{cm} \tag{2-9}$$

$$\text{Resistivity} = \frac{V}{I} \times \frac{\text{contact area } (\text{cm}^2)}{\text{sample thickness (cm)}} = \Omega.\,\text{cm} \tag{2-10}$$

$$\text{Conductivity} = \frac{1}{\text{Resistivity}} = \frac{1}{\Omega.\text{cm}} = \frac{S}{\text{cm}} \tag{2-11}$$

In terms of surface resistivity, the resistivity is determined by the ratio of DC voltage drop per unit length to the surface current per unit width as displayed in Equation 2-12. Figure 2-17 depicts a basic setup for surface resistivity measurement [90].

$$\text{Resistivity}_s = \frac{\text{voltage drop}}{\text{length}} \Big/ \frac{\text{current}_s}{\text{width}} \tag{2-12}$$

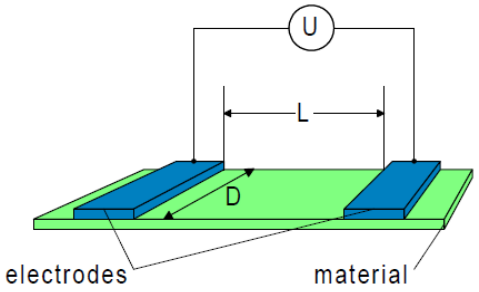

Figure 2-17: Basic setup for surface resistivity measurement [90]

2.8.1 Through-plane Electrical Conductivity Test Method

The through plane test method, developed by the US Fuel Cell Council, can measure bulk resistance and contact resistance. Both result in a voltage drop across bipolar plates. Bulk resistance is that of the bipolar plate material, and contact resistance is that of the bipolar plate and gas diffusion layer interface. To measure the through-plane conductivity, a composite specimen is placed between two conducting plates (gold-nickel-copper plates). A current source is applied through those conducting plates and the voltage drop across two conducting plates is measured with a multimeter. In a typical fuel cell, the stack of bipolar plates is held under pressure to seal the interfaces. Stress affects the electrical characteristics of the bipolar plate material; therefore, to measure the conductivity of a bipolar plate, a

sample must be placed under pressure (Figure 2-18). The conductivity can be calculated using Ohm's law (Equation 2-13) [91].

$$\text{Electrical conductivity} = \frac{\text{I}}{\text{V}} \times \frac{\text{sample thickness (cm)}}{\text{width (cm)} \times \text{length (cm)}} = \text{Scm}^{-1} \qquad (2\text{-}13)$$

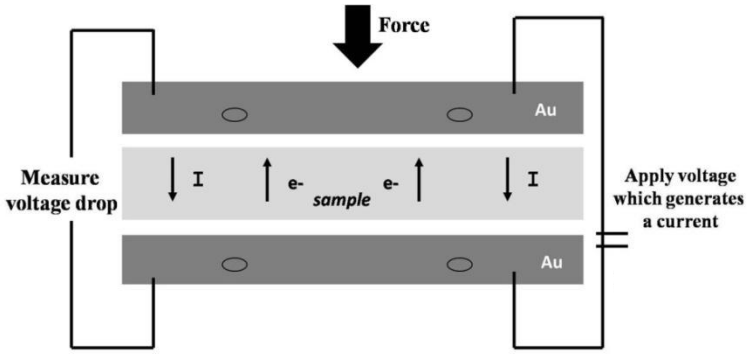

Figure 2-18: Basic setup for through-plane conductivity test method

A major source of contact resistance in a fuel cell stack comes from the interface between GDLs and the bipolar plates (Figure 2-19). A poor interface contact will decrease the actual area in contact, leading to a voltage drop across the interface [92]:

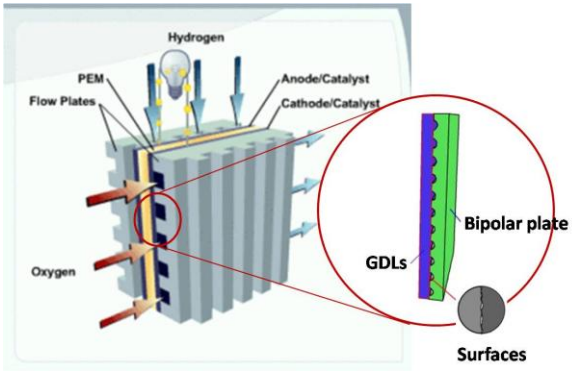

Figure 2-19: Interface contact between bipolar plates and GDL [93]

To measure contact resistance, a sample is placed between two pieces of carbon paper to create the same contact situation as in the fuel cell stack and better electrical contact of the bipolar plate with the conducting plates. In the through-plane method, some factors can affect measurement accuracy and reproducibility, such as the method used to polish the copper

electrodes, and the contact between the electrodes and the sample [94]. Equations, derived to calculate the measured resistance of a testing system, are as follows.

$$R_{Measure} = R_{Material} + R_{System} \quad (2\text{-}14)$$

$$R_{System} = R_{Instrument} + R_{Interface} \quad (2\text{-}15)$$

Combining Equations (2-14) and (2-15),

$$R_{Measure} = R_{Material} + R_{Instrument} + R_{Interface} \quad (2\text{-}16)$$

Cunningham and his coworkers pointed out that it is impossible to distinguish the resistance caused by the system from the bulk resistance of the measured material [94]. Most of research efforts use Equation (2-17) to calculate the bulk resistance of a measured material (R_{BP}) [42].

$$R_{BP} = \frac{V_{Measure} A_{Bipolar\ Plate}}{I_{Measure}} \quad (2\text{-}17)$$

Figure 2-20 illustrates the resistance components associated with the conductivity measurement for bipolar plates.

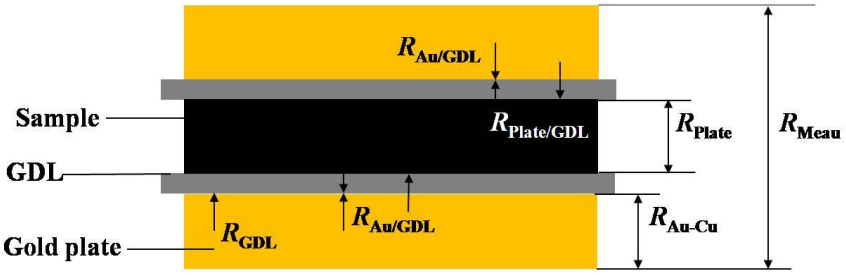

Figure 2-20: Schematic diagram of resistance measurement analysis of bipolar plate [34]

Equations to calculate the measured resistance of the bipolar plate testing system are as follows [6].

$$R_{Measure} = 2R_{Au} + 2R_{GDL} + 2R_{BP/GDL} + 2R_{Au/GDL} + R_{BP} \quad (2\text{-}18)$$

In Table 2-2, the values of R_{GDL} and R_{Au} are very small (<<1 ohm), because the gas diffusion layer and gold plate are very conductive. Therefore, one can neglect the effect of R_{GDL} and R_{Au} on the total measured resistance, $R_{Measure}$, and Equation 2-18 can be simplified so:

$$R_{Measure} = 2R_{BP/GDL} + 2R_{Au/GDL} + R_{BP} \quad (2\text{-}19)$$

Table 2-2: Nomenclature and classification of all resistances of the testing system [34]

Resistance	Nomenclature	Classification	Value
$R_{Measure}$	Measured resistance	Total resistance	Depends on measured voltage and current
R_{BP}	Resistance of sample plate	Sample	Depends on sample
R_{GDL}	Resistance of gas diffusion layer	GDL	Very Small
R_{Au}	Resistance of gold plate	Apparatus	Very Small
$R_{Au/GDL}$	Resistance caused by an interface of gas diffusion layer and gold plate	Contact resistance	Varied
$R_{BP/GDL}$	Resistance caused by an interface of gas diffusion layer and bipolar plate	Contact resistance	Varied

In Equation 2-19, the measured resistance, $R_{Measure}$, is determined by the contact resistance between the gas diffusion layer and the gold plate, $R_{Au/GDL}$, the contact resistance between the bipolar plate and the gas diffusion layer, $R_{BP/GDL}$, as well as the bulk resistance of the bipolar plate sample, R_{BP}. If the values of the two contact resistances are as small as possible, the measured resistance is approximately equal to the bulk resistance of the bipolar plate. In other words, the bulk resistance of the bipolar plate can be accurately measured by minimizing the contact resistances in the testing system caused by the interface between the bipolar plate and gas diffusion layers and the interface between the gas diffusion layer and gold plates. The bulk resistances of the gold plates and gas diffusion layers must be evaluated

and subtracted from the total measured resistance of the assembly, in order to measure the bulk resistance of bipolar plates (R_{BP}) accurately.

The bulk resistance of the gold plate, R_{Au}, can be determined by independent measurement involving only the two gold plates put together as shown in Figure 2-21. The bulk resistance of the gas diffusion layers, R_{GDL}, can also be determined by independent measurement involving only the gas diffusion layer sandwiched between the two gold plates as shown in Figure 2-22. Based on this new setup in Figures 2-21 and 2-22, the total measured resistance, $R'_{Measure}$, is expressed in Equation 2-20.

Figure 2-21: Schematic diagram of resistance measurement analysis of gold plate

$$R'_{Measure} = R_{Au/GDL} + R_{GDL} + 2R_{Au} \quad (2\text{-}20)$$

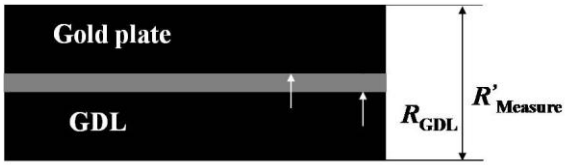

Figure 2-22: Schematic diagram of resistance measurement analysis of GDL

If one subtracts $R'_{Measure}$ from the total measured resistance, $R_{Measure}$, Equation 2-21 is further expressed as:

$$R_{Measure} - R'_{Measure} = 2R_{BP/GDL} + R_{GDL} + R_{BP} \quad (2\text{-}21)$$

The clamping of a stack of individual cells causes pressure to be applied at the interface, leading to an increase in the contact areas between fuel cell components, which, in turn, decrease the contact resistance [92]. Therefore, the electrical conductivity measurement must be done under compressive force. Another test requirement was the ability to test samples at different pressure levels. The correlation between sample test results and actual in-stack performance has not yet been standardized. The complexity of a fully functional fuel cell

makes this correlation difficult at the current stage of composite bipolar plate development. Therefore the test apparatus needed the flexibility to accommodate various pressures and sample sizes [89].

2.8.2 In-plane Electrical Conductivity Test Method

Typically, a four-point probe is used to measure the in-plane electrical conductivity of bipolar plates. This tool supplies excellent measurement results for near-surface and surface-related electrical properties of bipolar plates. However, it does not provide the same insight into electrical characteristics deep inside the bipolar plate (Figure 2-23). The four probes are arranged in a linear fashion, where the two outer probes are connected to a voltage supply, and the inner probes to a volt meter [91]. As current flows between the outer probes, the voltage drop across the inner probes is measured. The relationship of the current and voltage values is dependent on the resistivity of the material under test, and the geometrical characteristics of the probes. The theory behind the four point probe method for sheet resistivity considered two cases: the sample is infinitely thick (i.e., T>>s) and the sample is infinitely thin (i.e., T<<s) [95].

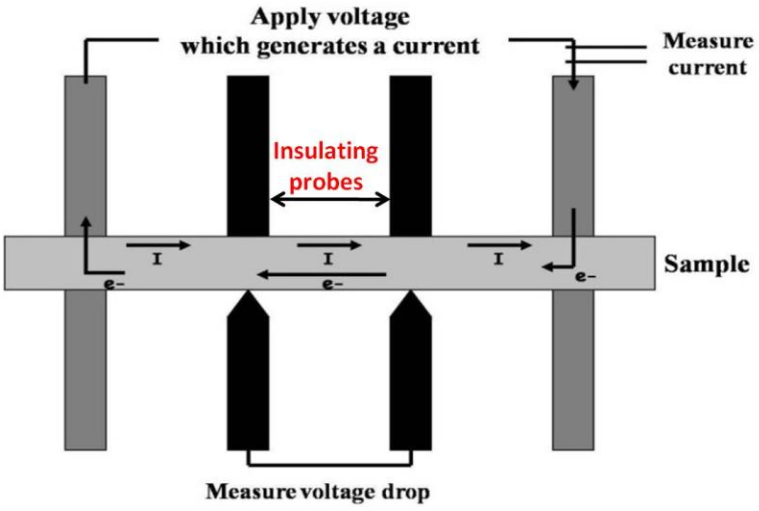

Figure 2-23: Four point probe tester

For bulk samples where the sample thickness is much higher than the probe spacing, one can assume a spherical protrusion of current emanating from the outer probe tips. The differential resistance (ΔR) is:

$$\Delta R = \rho[\frac{dx}{A}] \quad (2\text{-}22)$$

where, ρ = resistivity and A = area.

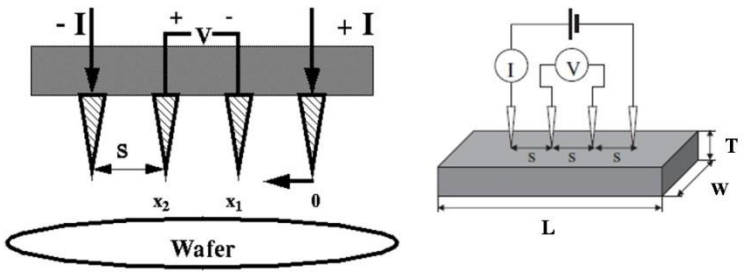

Figure 2-24: Schematic of the measurement for bar specimen resistivity [96]

If the integration between the inner probe tips takes place, the resistance is measured as shown in Equation 2-23.

$$R = \int_{x_1}^{x_2} \rho \frac{dx}{2\pi x^2} = \frac{\rho}{2\pi}\left[-\frac{1}{x}\right]\Big|_{x_1}^{x_2} = \frac{1}{2s}\frac{\rho}{2\pi} \tag{2-23}$$

If probe spacing is uniform and the superposition of current at the outer two tips takes place, R = V/2I. The resistivity is going to be:

$$\rho = 2\pi s\left(\frac{V}{I}\right) \tag{2-24}$$

In case of the thickness being much lower than the probe spacing, current rings occur instead of the current spheres. Therefore, the expression for the area is A = 2πxT. The derivation is as follows:

$$R = \int_{x_1}^{x_2} \rho \frac{dx}{2\pi xT} = \int_{s}^{2s} \frac{\rho}{2\pi T}\frac{dx}{x} = \frac{\rho}{2\pi T}\ln(x)\Big|_{s}^{2s} = \frac{\rho}{2\pi T}\ln 2 \tag{2-25}$$

The resistivity will be [96]

$$\rho = \frac{\pi T}{\ln 2}\left(\frac{V}{I}\right) \tag{2-26}$$

From the information mentioned above, this method allows measurement of bulk resistivity by applying a geometry-dependent corrector to the measured values of a voltage drop and applied current. Then the resistivity can be calculated as in Equation (2-27).

$$\rho = kT(\frac{V}{I}) \quad (2\text{-}27)$$

In the case of a thin round sample, the correction factor is a function of a sample diameter/a probe space and a sample thickness/a probe spacing [6]. Using a rectangular sample, Mironov calculated the resistivity relating to two geometric correction factors: a rectangular specimen of thickness (F_1) and a rectangular specimen of length (F_2) [96].

$$\rho = \frac{\pi T}{\ln 2}(\frac{V}{I})F_1F_2 \quad (2\text{-}28)$$

In the view of normal sheet resistivity determination, as in Equation 2-28, only F_1 is concerned. Equation 2-26 is valid for when the sample thickness is less than half the probe spacing. For thicker samples, Equation 2-29 should be used [96]. One can also assume that F_1 = 1, when the ratio of a sample thickness/a probe spacing is lower than 0.4[95].

$$\rho = \frac{\pi T}{\ln(\frac{\sinh(\frac{T}{s})}{\sinh(\frac{T}{2s})})}(\frac{V}{I}) \quad (2\text{-}29)$$

In terms of values of the finite width correction factor, F_2 is a function of the L/W ratio and W/s ratio (Figure 2-24) [96]. Researchers designed the four point probe and computed the resistivity corresponding to ASTM D-991[51]. The calculation can be expressed as Equation 2-30.

$$\rho = \frac{(VWT)}{IL} \quad (2\text{-}30)$$

2.9 Fuel Cell Resistance [6, 10, 97, 98]

In-situ characterization techniques use the electrochemical variables of voltage, current, and time to characterize the performance of fuel cell devices under operating conditions. Electrochemical Impedance Spectroscopy (EIS), one of the major methods, is a powerful diagnostic technique that can be used to characterize limitations and improve the performance of fuel cells. This technique can distinguish between ohmic, activation and concentration losses. In this method, an AC signal for which the response has known

amplitude is recorded. The process may be repeated at different frequencies, through an entire frequency spectrum.

2.9.1 AC Impedance Theory

The terms resistance and impedance both imply a hindrance to current or electron flow. When dealing with a direct current (DC), only resistors provide this effect. For the case of an alternating current (AC), circuit elements such as capacitors and inductors can also influence electron flow. These elements can affect not only the magnitude of an alternating current waveform, but also its time-dependent characteristics or phase. A resistance, with a frequency equal to 0 Hz is defined by Ohm's Law in DC theory. For AC, where the frequency is non-zero, the analogous equation is

$$V_t = I_t Z \tag{2-31}$$

In Equation 2-31, V and I are waveform amplitudes for potential and current, respectively, and Z is defined as impedance, which is the AC equivalent of resistance. Impedance measurements are usually made by applying a small sinusoidal voltage perturbation, and monitoring the system's resultant current response. The excitation signal, expressed as a function of time, has the following forms:

$$V_t = V_0 \cos(\omega t) \tag{2-32}$$

$$I_t = i_0 \cos(\omega t - \emptyset) \tag{2-33}$$

In these expressions, the ω is radial frequency, and the relationship between radial frequency ω and frequency is

$$\omega = 2\pi f \tag{2-34}$$

In general, the current response of a system may be shifted in phase compared to the voltage perturbation. This phase, shift effect is described byϕ. Following Equation 2-31, the sinusoidal impedance response of a system can be written as

$$Z = \frac{V_0 \cos(\omega t)}{i_0 \cos(\omega t - \emptyset)} = Z_0 = \frac{\cos(\omega t)}{\cos(\omega t - \emptyset)} \tag{2-35}$$

Alternatively, one can use complex notation to write the impedance response of a system in terms of a real and an imaginary component:

$$Z = \frac{V_0 e^{j\omega t}}{i_0 e^{(j\omega t - j\emptyset)}} = Z_0 e^{j\emptyset} = Z_0(\cos\emptyset + j\sin\emptyset) \qquad (2\text{-}36)$$

Typically, impedance data is plotted in terms of the real and imaginary components of impedance. The impedance of a system can therefore be expressed in terms of a real component ($Z_{real} = Z_0\cos\phi$) and an imaginary component ($Z_{imag} = Z_0\sin\phi j$). In these expressions, j represents the imaginary number. A variety of formats, such as Nyquist and Bode Plots, can be used to plot the AC impedance data. Each format offers specific advantages for revealing certain characteristics of a given test system.

2.9.2 The Nyquist Plot

The imaginary component of impedance ($Z^{//}$) is plotted versus the real component of impedance ($Z^{/}$) for each excitation frequency. From Figure 2-25, the size of these two semicircles can be attributed to the magnitude of the two (anode and cathode) activation losses. Three x-axis intercepts, identified by the semicircles mark off three impedance regions, are denoted by $Z_{\Omega,}$ Z_{fA}, and Z_{fC}.

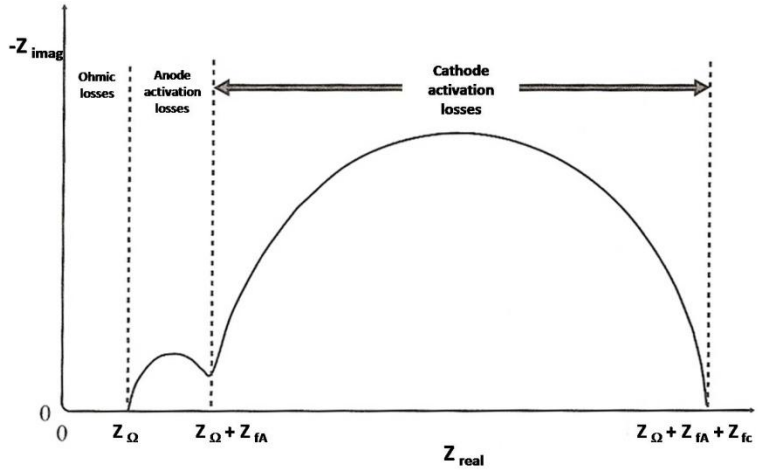

Figure 2-25: Nyquist plot from a hypothetical fuel cell [10]

The high-frequency intercept of the single impedance arc on the real axis, Z_Ω, represents the total ohmic resistance of the cell; this can be expressed as the sum of the contributions from contact resistances between components and ohmic resistances of the cell components such

as the membrane, catalyst layer, gas diffusion layer, and bipolar plates. At very low frequencies, the resulting impedances are the sum of ohmic and activation losses. The sizes of the three impedances correspond to the relative size of ohmic loss and activation losses of the anode and cathode in a fuel cell. In other words, the diameter of the kinetic semicircles is a measure of the charge transfer resistance of the electrodes.

2.9.3 EIS and Equivalent Circuit Modeling

EIS data analysis of the process that occurs inside a fuel cell is commonly carried out by fitting it to an equivalent electric circuit model. An equivalent circuit model is a combination of resistances, capacitances, and inductances, as well as a few specialized electrochemical elements (such as Warburg diffusion elements and constant phase elements) to describe the behavior of electrochemical reaction kinetics, ohmic conduction processes, and mass transport. If one measures a fuel cell's impedance spectrum and compares it to an appropriate equivalent circuit model, it is possible to extract information about the losses. The system basically consists of a potentiostat or galvanostat, frequency response analyzer and personal computer (Figure 2-26(A)). Randles equivalent impedance, which is the famous equivalent circuit of a PEMFC, has been employed for a single cell with a symmetrical gas supply arrangement [97] (Figure 2-26(B)).

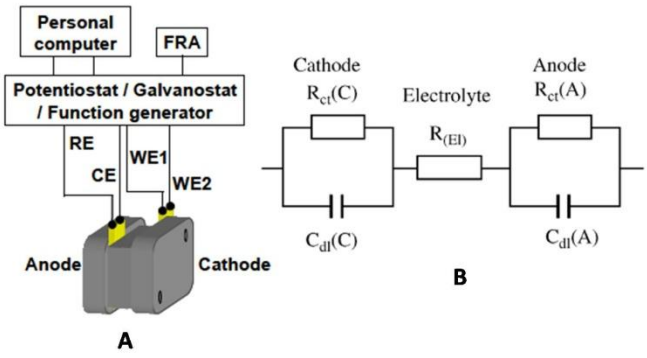

Figure 2-26: Schematic of EIS measurement system and its equivalent circuit [99]

Resistors in the equivalent circuit analog represent conductive pathways for ion and electron transfer. Those signify the materials' bulk resistance to charge transport such as the resistance of the electrolyte to ion transport or the resistance of a conductor to electron transport. Resistors are also used to represent resistance to the charge-transfer process on the

electrode surface. In terms of capacitors and inductors, they are associated with space-charge polarization regions, such as the electrochemical double layer and the adsorption or desorption processes of electrodes, respectively [100].

The main advantages of EIS as a diagnostic tool can be categorized as follows. First, EIS can provide microscopic information about the fuel cell system, which can facilitate fuel cell structure optimization and the selection of the most suitable operating conditions [101]. Second, the individual contributions of each component to fuel cell performance, such as the membrane, gas diffusion layers, and bipolar plates, can be distinguished. Therefore, AC impedance results can assist in interpretation of problems within the fuel cell components [102], and can also provide information for the design of such components. EIS also allows modeling of the system with an appropriate equivalent circuit to obtain the system's electrochemical parameters [103]. Last, EIS analysis can identify individual contributions to the total impedance of a PEMFC from different electrode processes such as the interfacial charge transfer and mass transport in both the catalyst layers [102].

A literature review finds few publications mentioning the use of bipolar plates to evaluate bipolar plate performance. For example, EIS was carried out to appraise the performance of PEMFC using alternative composite bipolar plate materials [104]. EIS was also applied to investigate the feasibility of evaluating the contact resistance of bipolar plates [99].

2.10 Summary

Bipolar plate material development is an important topic of current fuel cell research. A clear connection exists between the choice of bipolar plate materials and PEMFC cost reduction. Consequently, thermoplastic composite materials, which have many advantages in bipolar plate properties and manufacturing, have become alternative materials for bipolar plates. However, the weak point of these materials is their low electrical conductivity in comparison to the commercial target. Although considerable research has been done on using many types of conductive fillers to improve the electrical conductivity of thermoplastic composites, current literature pays to the use of conductive polymers for bipolar plate materials.

It is currently believed that conductive network formation is a key to increasing the electrical conductivity of composites and so the improvement of conductive network formation has been studied. One approach to the cost reduction of PEMFC is to produce bipolar plates by low cost manufacturing through mass production. Injection molding is also a promising technology for upcoming bipolar plate production. There is also a link between the use of high filler concentrations, which enhance the electrical conductivity of materials, and processability.

This work studies the possibility of using conductive fillers and polymers to manufacture injection molded composite bipolar plates.

CHAPTER 3: Experimental

3.1 Preparation of Polypropylene Composites

3.1.1 Material Selection

Based on the background literature and the objectives of this research, the target have for material development of bipolar plates for PEM fuel cells is to maximize the electrical conductivity while maintaining adequate properties.

Thermoplastic Matrix:

Two types of a commercially available polypropylene, produced by Equistar Chemicals, were used as the polymeric matrix: "PETROTHENE PP35FU01" and "PETROTHENE PP36KK01", with melt flow indices of 20 g/10 min and 7 g/10 min, respectively. The research objectives narrowed the preliminary resin selection to commodity polymers, which are inert and have excellent resistance to the fuel cell environment.

These polypropylenes are formulated for injection molding applications that require a balance of processability and mechanical rigidity, two important considerations in achieving high filler loading, maintaining a flow path mold pattern under compression and in a cell's operating effectively in the fuel cell environment. Moreover, to clarify the effect of process ability on composite properties, especially electrical conductivity, polypropylenes with different melt flow rates were chosen for comparison and determination of the final properties of composites. The properties of these polymers are illustrated in Tables A1 and A2 in Appendix A.

Conductive Fillers:

The choice of conductive carbon fillers to use in this research was based on their ability to impart high conductivity to the composites, while still maintaining a relatively low cost and high availability. Three carbon fillers were used in conjunction with the polypropylene to form electrically conductive composites. The fillers are a carbon black, carbon fibers, and synthetic graphite. The carbon black grade was VULCAN® XC72 (CB), produced by Cabot Corporation, was used because its highly branched, high surface area structure allows it to contact a large amount of polymer, which results in improved electrical conductivity at low concentrations. The average diameter of the carbon black particles was approximately 30 nm.

As discussed in the literature review section, it was anticipated that fibers would provide an ideal path for electron transport through the material. In order to inspect the influence of fibers on bipolar plate properties, three types of conductive carbon fibers were used in this research. The first type, Polyacrylonitrile (PAN)-based chopped carbon fiber, available from Fortafil® Fiber, was used to improve the electrical and thermal conductivity and the tensile strength of the resin. This fiber is 3 mm in length and 7 μm in diameter. Next, PAN-based milled carbon fiber (AGM-99), from Asbury Graphite Mills Inc., was combined with the chopped carbon fiber to study the effect of fiber size on electrical conductivity. The milled carbon fiber is 7-9 μm in diameter and 150 μm in length. The last type is produced by Gina New Materials Public limited company. It is a conductive carbon nanofiber with a 50 - 200 nanometer outside diameter and a 0.5 - 3 nanometer inside diameter. The fiber lengths were 10 - 70 μm. To sum it up, three carbon fibers used in this research are Fortafil® Fiber, AGM-99, and carbon nanofiber.

Additionally, introduction of graphite to the composite generally provides good electrical properties, molding characteristics, and resin compatibility. Therefore, this research used Asbury synthetic graphite 4012 (SG), produced from Asbury Graphite Mills Inc., with a particle size of 44 × 250 μm. The main properties of those fillers are presented in Tables A-3 to A-5 (Appendix A).

Conductive Polymer:

According to the results of previous research conducted at the University of Waterloo [34] the electrical conductivity of composites for bipolar plates has not yet achieved the desired target value. In order to increase the conductivity, an intrinsic conductive polymer Polypyrrole (from Sigma Aldrich) was added to the composites. The main specification can be seen in Table A-6 (Appendix A).

Additives:

Filler dispersion influences electrical and mechanical properties, so adding additives to the composites to improve filler dispersion and interfacial tension between the polymer matrix and fillers was considered. Kenrich's titanate coupling agent, neopentyl(diallyl)oxy tri(dioctyl)pyrophosphate titanate, was applied to improve filler dispersion. The preliminary selection was based on industry recommendations and availability. The effect of zinc stearate on mixing processability was also observed. It is noted that titanate coupling agent and zinc stearate in a solid powder form were introduced into polypropylene composites. The properties of additives are shown in Table A-7 (Appendix A), and the procedure of incorporating the additives into the composites are explained in the section 3.1.4.

3.1.2 Experimental Design

Preliminary investigations and earlier work demonstrated the effect of different filler types and concentrations. The results showed that a combination of three fillers (carbon black, carbon fiber and synthetic graphite) improved composite electrical conductivity. Furthermore, the blend conductivity increased with increasing filler concentration. It is important to determine a blend formulation that offers the best combination in terms of conductivity and processability. From the results, filler concentrations were higher than 55 percent by weight (%wt) diminished the efficiency of extrusion and injection molding processes. This research, therefore, was designed to use a three-filler-system at 55 %wt of filler loading as a preliminary formula for conductive composite development. The experimental approach in this research consisted of seven stages.

Stage one was the additives screening stage, where various additives were compared to determine the best candidate for further experimentation. Stage one was comprised of six

conductive composites as shown in Table 3-1. The aim of this stage was to explore the ability of additives, such as a titanate coupling agent, polypyrrole, and a processing agent (zinc stearate), to enhance the electrical conductivity of composites and to improve the mixing-processability. *Note:* The idea of applying additives with certain concentrations refers to research work in the literature review section and recommendations from additive producers.

Table 3-1: Composite formulations in stage one

Samples	Compositions
P55F	PP (45%wt)+ [CB + CF(Fortafil® Fiber) + SG](55%wt) filler ratio is 1:1:1
P55FTi	P55F + Titanate coupling agent (1 % of total composite weight)
P55FTi(s)	It has the same composition as P55FTi, but coupling agent was mixed with PP in twin- screw extruder with side stuffer.
P55FZn	P55F + zinc stearate (1 % of total composite weight)
P55FTiZn	P55FTi + zinc stearate (1 % of total composite weight)
P55FPPy	P55F + polypyrrole (1.8 % of total composite weight)

Table 3-2: Composite formulations in stage two

Sample	Composition	Filler ratio
		[CB:CF:SG]
FR2	PP (45%wt)+ [CB + CF(Fortafil® Fiber) + SG](55%wt)	1:0:0
FR3	PP (45%wt)+ [CB + CF(Fortafil® Fiber) + SG](55%wt)	0:1:0
FR4	PP (45%wt)+ [CB + CF(Fortafil® Fiber) + SG](55%wt)	0:0:1
FR5	PP (45%wt)+ [CB + CF(Fortafil® Fiber) + SG](55%wt)	0:1:1
FR6	PP (45%wt)+ [CB + CF(Fortafil® Fiber) + SG](55%wt)	1:0:1
FR7	PP (45%wt)+ [CB + CF(Fortafil® Fiber) + SG](55%wt)	1:1:0
FR8	PP (45%wt)+ [CB + CF(Fortafil® Fiber) + SG](55%wt)	4:1:1
FR9	PP (45%wt)+ [CB + CF(Fortafil® Fiber) + SG](55%wt)	1:4:1
FR10	PP (45%wt)+ [CB + CF(Fortafil® Fiber) + SG](55%wt)	1:1:4
FR11	PP (45%wt)+ [CB + CF(Fortafil® Fiber) + SG](55%wt)	2:1:1
FR12	PP (45%wt)+ [CB + CF(Fortafil® Fiber) + SG](55%wt)	1:2:1
FR13	PP (45%wt)+ [CB + CF(Fortafil® Fiber) + SG](55%wt)	1:1:2
FR14	PP (45%wt)+ [CB + CF(Fortafil® Fiber) + SG](55%wt)	1:1:1

Stage two was the filler ratio effect observation stage, during which assorted three-filler ratios were assessed to determine the impact of the amount of single filler on the electrical conductivity of the three-filler system composites. Stage two used a thirteen-run mixture response design that was developed using Stat-Ease's Design Expert 6.0 which allows for two or three factors evaluating synergetic effects of multiple fillers with a maximum of 55 wt% filler content. The formulations of the composites involved are illustrated in Table 3-2.

Stage three consisted of eight conductive composites that differ in their Titanate coupling agent concentrations, as illustrated in Table 3-3. The purpose of the compounding was to determine the optimal load of Titanate coupling agent for highly conductive composites. *Note:* The filler ratio used for this set of experiments was 1:1:1 of CB: CF: SG.

Table 3-3: Composite formulations in stage three

Sample	Main composition	Titanate coupling agent
		[%wt of composite weight]
CA0.5	PP (45%wt)+ [CB + CF(Fortafil® Fiber) + SG](55%wt)	0.5
CA1.0	PP (45%wt)+ [CB + CF(Fortafil® Fiber) + SG](55%wt)	1.0
CA1.5	PP (45%wt)+ [CB + CF(Fortafil® Fiber) + SG](55%wt)	1.5
CA2.0	PP (45%wt)+ [CB + CF(Fortafil® Fiber) + SG](55%wt)	2.0
CA2.5	PP (45%wt)+ [CB + CF(Fortafil® Fiber) + SG](55%wt)	2.5
CA3.0	PP (45%wt)+ [CB + CF(Fortafil® Fiber) + SG](55%wt)	3.0
CA3.5	PP (45%wt)+ [CB + CF(Fortafil® Fiber) + SG](55%wt)	3.5
CA4.0	PP (45%wt)+ [CB + CF(Fortafil® Fiber) + SG](55%wt)	4.0

Table 3-4: Composite formulations in stage four

Sample	Composition	Filler ratio
		[CB:CF:SG]
VE1	PP(20g/10min) (45%wt)+ [CB + CF(Fortafil) + SG](55%wt)	1:1:4
VE2	PP(20g/10min) (45%wt)+ [CB + CF(Fortafil) + SG](55%wt)	1:1:1
VE3	PP(7g/10min) (45%wt)+ [CB + CF(Fortafil) + SG](55%wt)	1:1:4
VE4	PP(7g/10min) (45%wt)+ [CB + CF(Fortafil) + SG](55%wt)	1:1:1

Stage four varied the polypropylene viscosity so that the effect on filler dispersion in the polypropylene matrix could be observed. The viscosity affects filler dispersion, which plays a critical role in the composite's conductive network. Consequently, two types of polypropylene, with dissimilar viscosities (7g/10 min or 20 g/10 min), were used as the matrix in the composites and allowed observation of the effect of polymer viscosity on electrical properties.

Stage five varied the concentration of polypyrrole so that the concentration giving the highest electrical conductivity could be determined. This stage contained eleven blends, as shown in Table 3-5. *Note:* The filler ratio used in this stage was 1:1:1 of CB: CF: SG.

Table 3-5: Composite formulations in stage five

Sample	Main composition	Polypyrrole
		[%wt of composite weight]
P55FPPy(0.5)	PP (45%wt)+ [CB + CF(Fortafil) + SG](55%wt)	0.5
P55FPPy(1.0)	PP (45%wt)+ [CB + CF(Fortafil) + SG](55%wt)	1.0
P55FPPy(1.5)	PP (45%wt)+ [CB + CF(Fortafil) + SG](55%wt)	1.5
P55FPPy(2.0)	PP (45%wt)+ [CB + CF(Fortafil) + SG](55%wt)	2.0
P55FPPy(2.5)	PP (45%wt)+ [CB + CF(Fortafil) + SG](55%wt)	2.5
P55FPPy(3.0)	PP (45%wt)+ [CB + CF(Fortafil) + SG](55%wt)	3.0
P55FPPy(4.0)	PP (45%wt)+ [CB + CF(Fortafil) + SG](55%wt)	4.0
PPy(1.8)	PP	1.8
PPy(4.0)	PP	4.0
PCBPPy	PP (45%wt)+ CB (55%wt)	1.8
PCFPPy	PP (45%wt)+ CF(Fortafil) (55%wt)	1.8
PSGPPy	PP (45%wt)+ SG (55%wt)	1.8

Stage six varied the size of carbon fiber to determine the significance of aspect ratio on a conductive network and electrical conductivity. Seven composites were formulated as displayed in Table 3-6. *Note*: The filler ratio used in this stage was 1:1:1 of CB: CF: SG.

Stage seven tested the set of composites that had the highest electrical conductivity from each previous stage. To achieve the desired target of electrical conductivity for commercial

bipolar plates, the best composites were combined together as indicated in Table 3-7. *Note*: The filler ratio used in this stage was 4:1:1 of CB: CF: SG.

Table 3-6: Composite formulations in stage six

Sample	Main composition	Polypyrrole
		[%wt of composite weight]
P55F(2F_1)	PP (45%wt) + [CB + CF(Fortafil + AGM-99) + SG](55%wt)	0.0
P55F(2F_2)	PP (45%wt) + [CB + CF(Fortafil + CNF) + SG](55%wt)	0.0
P55F(2F_3)	PP (45%wt)+ [CB + CF(Fortafil + CNF) + SG](55%wt)	1.8
		Carbon nanofiber and Polypyrrole
		[%wt of composite weight]
PCF(CNF)_1	PP	1.8 and 0.0
PCF(CNF)_2	PP	4.0 and 0.0
PPyCF(CNF)	PP	4.0 and 1.8

Table 3-7: Composite formulations in stage seven

Sample	Main composition	Polypyrrole
		[%wt of composite weight]
FR8PPy_1	PP (45%wt)+ [CB + CF(Fortafil) + SG](55%wt)	1.8
FR8PPy_2	PP (45%wt)+ [CB + CF(Fortafil) + SG](55%wt)	4.0
FR8(2F)_1	PP (45%wt)+ [CB + CF(Fortafil + AGM-99) + SG](55%wt)	1.8
FR8(2F)_2	PP (45%wt)+ [CB + CF(Fortafil + AGM-99) + SG](55%wt)	4.0
FR8(2F)_3	PP (45%wt)+ [CB + CF(Fortafil + AGM-99) + SG](55%wt)	0.0

3.1.3 Master Batch Fabrication

All composite fabrication processes are displayed as a diagram in Figure 3-1. As stressed in the discussion presented in the literature review section, it is difficult to prepare well dispersed polymer/filler composites containing high wt% filler. Prior to the compounding processes, master batches were mixed in a twin-screw extruder with side stuffer, and the

master batch runs in the extruder were chosen with the primary goal of producing a uniformly mixed composite while minimizing the degradation of the filler. A Leistritz co-rotating intermeshing twin-screw extruder, as shown in Figure A-1, with a side stuffer, Model ZSE27 HP 27mm, was used to create master batches of carbon black-filled PP and synthetic graphite-filled PP composites for this work. Master batch of carbon black-filled PP contains 40wt% of carbon black loading, and synthetic graphite-filled PP master batch contains 60 wt%. Fifteen kilograms of each master batch were produced in this work.

This extruder contained ten independent heating zones, a water-cooled feed port, and was 27 mm in diameter, with a length to diameter ratio of 40:1. The polypropylene was fed by a gravimetric feeder into the first zone, which is one of ten temperature control zones in this extruder. The first zone contains a water cooled system so that the polymer does not melt and plug the feed port. Carbon black or synthetic graphite powder used in this research was added through a side stuffer located in zone five. The side stuffer was fed by loss-in-weight feeders. The temperature profiles were respectively 150 to 220^{o}C from feed to nozzle for all formulations, and extrusion conditions and information on a screw configuration are illustrated in Tables A-8 and A-9 (Appendix A). The nozzle used for this work had three 2.5 mm-holes through which the master batch material was forced.

The three molten composite strands were forced into the water bath upon leaving the extruder. The hot strands were moved up from the water, and then they were directly blown by an air blower that allowed most of the water to evaporate off. After the master batch strands passed through the water bath, they were mechanically pelletized and, finally, kept in a sealed container.

3.1.4 Composite Mixing

3.1.4.1 The Composites in Stage 1 to Stage 4

The mixing of carbon black-filled PP and synthetic graphite-filled PP composite master batches with conductive fillers and additives was carried out in a 270-mL mixing chamber of a Haake Rheomix batch mixer (Haake Fisons Rheocord 90 - Folio Industries Inc.) with two internal screws - roller rotors. The composites mixed by this batch mixer were all composites

in stage 1 to stage 4. Each formulation was produced approximately two and a half kilograms.

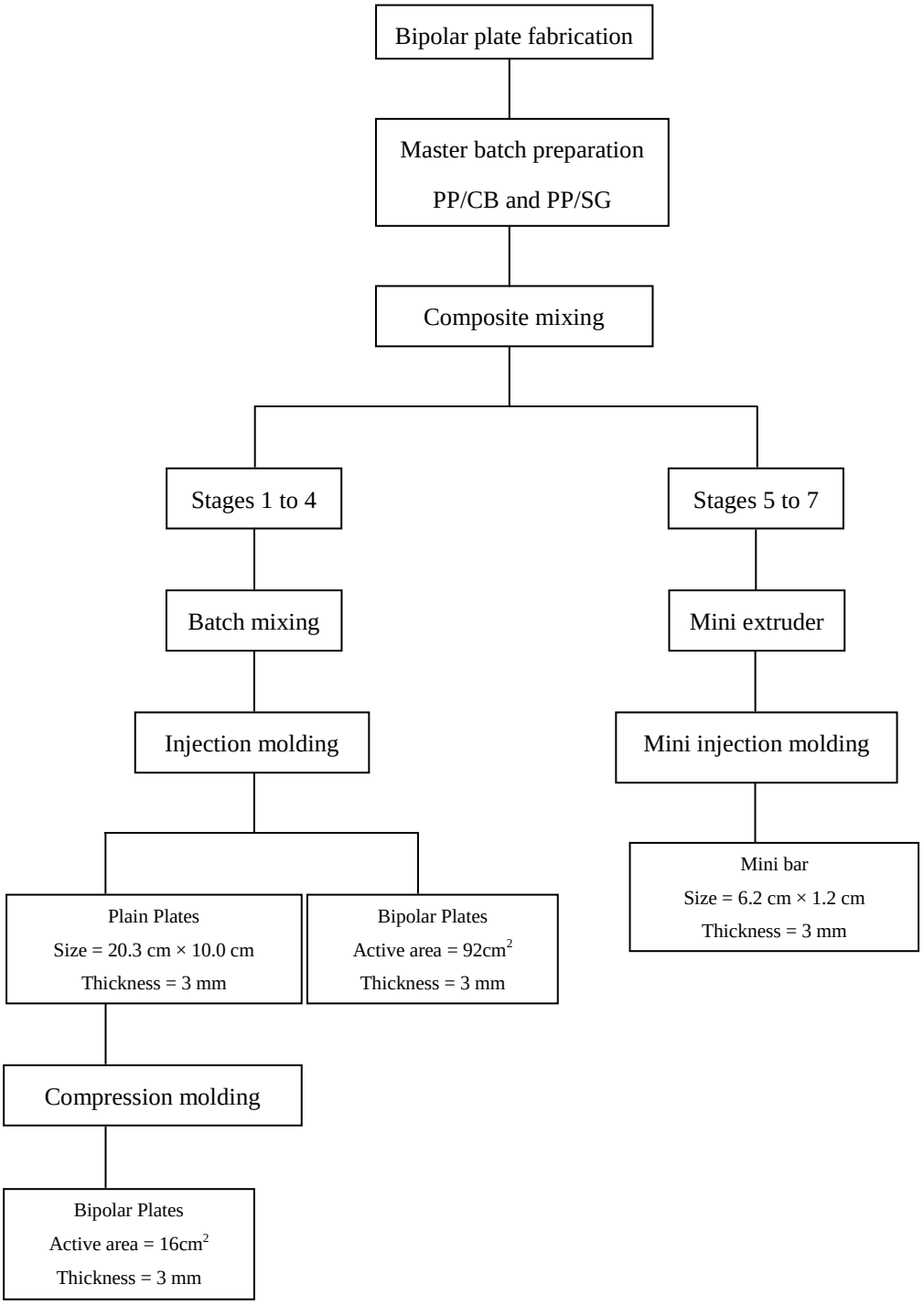

Figure 3-1: Diagram of composite bipolar plate fabrication

The specific conditions of composite mixing were 210^{o}C for melt temperature, at constant a screw speed of 80 rpm, and 25 min of mixing time. The polypropylene mixing process was as follows. First, the polypropylene was fed into the mixer and melted. Second, the additives were added, and last, the carbon black, synthetic graphite and carbon fiber were introduced into the mixer. All batches of mixtures were manipulated by the same procedure. Torque for the internal mixer and the temperature profiles in the mixing chamber were recorded as a function of time for each experiment. Due to the 'chunky' nature of composites received from the batch mixer, a size reduction step was required prior to the injection molding process. After the mixing, the composite was ground into powder by a stainless steel rotary grinder (Thomas Wiley Laboratory Mill Model 2) with a feed aperture localized on the top of the rotary cutter. In order to minimize contamination, the machine was thoroughly cleaned when grinding of one composite was completed, and before grinding of a different composite began.

3.1.4.2 The Composites in Stage 5 to Stage 7

The larger machines were not an option for the composites formulated in stages 5 to stage 7 because of the high cost of the polypyrrole and carbon nanofiber used in the blends. The composites were hand blended to obtain a uniform mixture prior to feeding into the Haake Minilab Micro-compounder (Figure A-3). Each formulation was produced approximately twenty grams. The Haake Minilab is a co-rotating 5/14 mm conical twin screw extruder with 109.5 mm of screw diameter and a cycle/flush option. For all operating conditions, the extruder's temperature profile was adjusted to maintain the compound's melt temperature beneath 220^{o}C to prevent degradation of the composite. The operating conditions of different composite formulations were set at 170 to 180^{o}C and 160 to 180 rpm. The material was conveyed by the Minilab screws, and then melting and mixing took place. A homogenized molten mixture exits at the flush orifice, in the form of strands, at the end of the die. The composite product was then pelletized with scissors into smaller pieces (approximately 5 mm long) for the injection molding process. It is important to note that each composite was mixed twice; as such thus, assume that the relative filler distribution stayed consistent throughout the process.

3.1.5 Injection Molding Process of Bipolar Plates, Composite Plaques and Composite Bars

3.1.5.1 Injection Bipolar Plates and Composite Plaques

Following the batch mixing process, the composites of stage 1 to 4 were structured into plain plaque and bipolar plates by an injection molding machine. The plain plaques were manufactured for ex-situ and in-situ tests for bipolar-plate-material characterizations, and injection bipolar plates were fabricated to investigate the feasibility of manufacturing our composites by an injection molding process for commercialization. For these composites, an Engel 85 ton rotary injection molding machine was used. An image of the injection molding machine can be seen in Figure A-4 in Appendix A. This machine has a 30 mm diameter single screw with a length-over-diameter ratio of 23.6:1, and a screw barrel holds 3.7 oz.

The injection images of the manufactured plates can be seen in Figure 3-2. First, a mold for plain plate (without gas flow channels) was assembled in the injection-molding machine. The machine was initially set at certain operating conditions, and then it was brought up to a specific operating temperature (there are four temperature control zones) for the material to be run. Then, pure PP was fed into a feed hopper dryer run to purge all of the material that might have been in the injection-molding machine previously. Conditions were kept as constant as possible and changed for different composite formulations or if operational problems were encountered. The injection-molding machine was operated until it could not fill another shot, and then the next formulation was added to the hopper. To prevent sample contamination, the next five shots were discarded. At the end of process polypropylene was used to purge the hopper until the fillers (black particles) were removed from the injection-molding machine.

The mold was changed to a new mold with gas flow channels (Hydrogenics design) for bipolar plate production. The bipolar plate production was operated similarly to the conditions of the plain plaque production. The injecting conditions can be seen in Table A-10 (Appendix A).

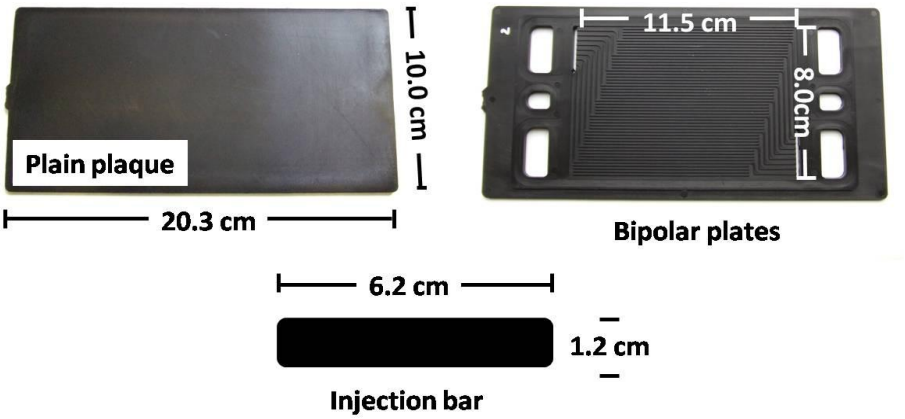

Figure 3-2: Injection composite products

3.1.5.2 Injection Composite Bar

The composite pellets produced from the mini-extruder were then injection molded using a Ray-Ran Laboratory injection molding machine, as shown in Figure A-5, to get test bars with 6.2 cm × 1.2 cm dimensions and 3 mm thickness (Figure 3-2). The composite bars were mainly used for electrical conductivity tests. The injection molding was performed keeping the barrel temperature at 190^{o}C and mold tool temperature at 55^{o}C, with injection periods of 15 sec at 100 psi. The injection molding machine transferred measured amounts of composite pellets into a barrel, where they compressed a few times by a pneumatic piston connected to high pressure air to force the molten composite into a mold. The composite was fully plasticized, and then the mold, at a lower temperature, was immediately opened. After the mold was cooled to close to room temperature, the sample bars were removed from the mold and inspected for voids and other possible defects. To avoid contamination, the machine was thoroughly cleaned before injection of a different composite.

3.1.6 Compression Molding Processes of Bipolar Plates

Small bipolar plates with a 16 cm^2 of active area were formed by a compression molding machine to minimize the quantity of composite materials. A picture of small bipolar plates is shown in Figure 3-3. The injection-composite plate (from 3.1.5.1) was cut and transferred to a mold for creating gas flow channels. The mold, shown in Figure 3-3 was designed and manufactured at the University of Waterloo. The design incorporates numerous chokes to ensure the ability to purge entrapped air from the mold as well as ejector pins which are

operated by a sling hammer from the underside of the mold. A Carver hydraulic press with heated plates was used in this work. First, the mold was preheated at approximately 170 to 180^{o}C, and a mold releasing agent was sprayed its the surfaces. Next, an injection plate was put into the chamber of the mold while the temperature was kept within 170 to 180 ℃ for 15 minutes to fully melt the composite. The temperature inside the mold was measured by a portable thermocouple. Then, the plate was pressed using 20,000 psi of pressure in the mold for five minutes, during which the pressure was released and re-established at the first minute mark to allow volatiles and entrapped air bubbles to escape.

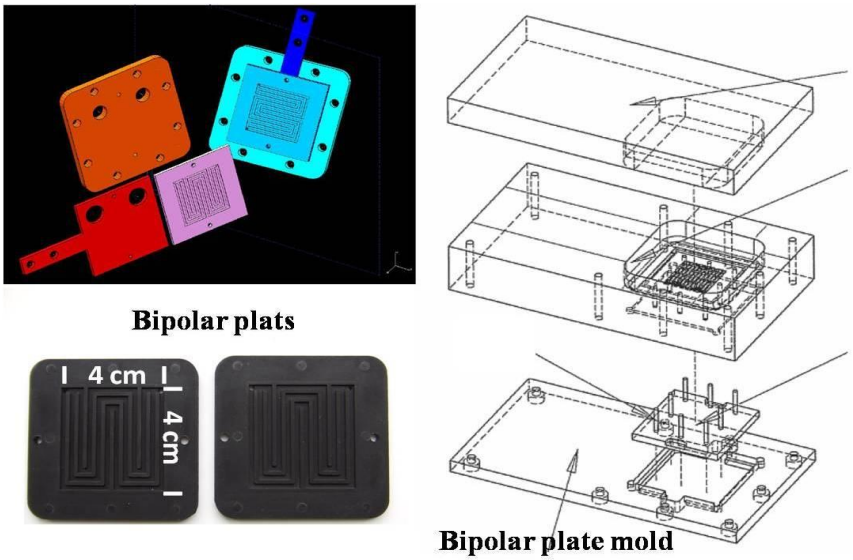

Figure 3-3: Pictures of small bipolar plates and bipolar plate mold

After five minutes, the mold containing which has the injection plate was cooled down under the pressure. Once the temperature reached 130^{o}C, a bipolar plate was removed from the mold by a sling hammer. Only plates with no major visible defects were kept for use in fuel cell performance testing. At the end of bipolar plate production, inlet and outlet holes were created in gas flow channels. Following the execution of each experiment, it was necessary to evaluate the material. The evaluation involved comparing ex-situ experiment results to in-situ fuel cell performance experiments.

3.2 In-situ Test

3.2.1 Single Cell Performance Test

3.2.1.1 Material and Test Station

The intention of this research is to relate specific bipolar plate properties, for example, electrical conductivity and thermal properties, to PEMFC performance. In single cell performance tests, single-cell fuel cells with a geometric active area of 16 cm^2 on each electrode were used. The cells were assembled using Gore™ PRIMEA® series 5510 catalyst coated membranes (CCM). The thickness of the coated layer was 18 micrometers, and the membranes contained 40 % platinum loading for both electrodes. Proprietary gas diffusion layers (GDL) from SGL carbon group were used for the cells, and the GDLs were divided into two grades for cathode and anode electrodes. The one used for the cathode side was 34 BA and has a microporous layer (MPL), and 30 BB for the anode side. The MPL is a composite of carbon particles and a hydrophobic agent that is coated on one side of the conventional gas diffusion media. The single-cell hardware is shown in Figure 3-4.

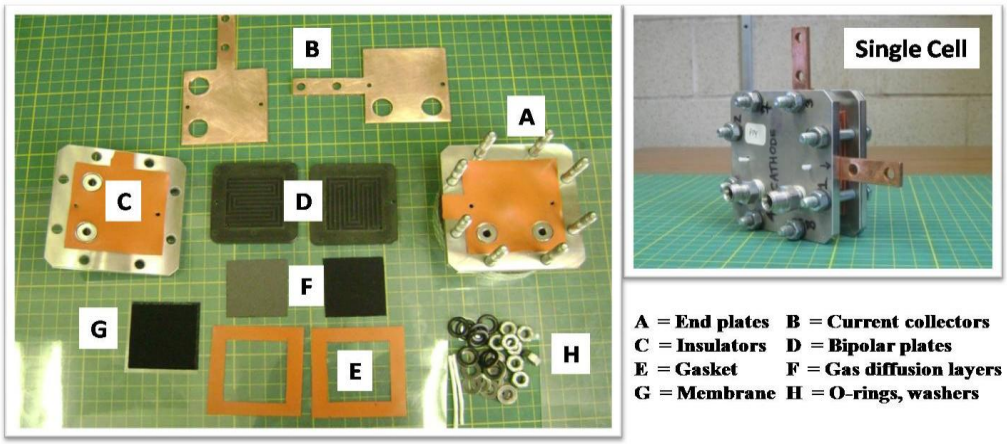

Figure 3-4: Fuel cell hardware

The two ports at the end plates of the anode side are the inlet and outlet for the hydrogen gas stream, and the other two ports, located at the cathode end plate, are the inlet and outlet for the air stream. Three sets of single-cell equipment, which had the same materials, size, and design, were used in rotation for all testing. Cells were assembled by using a torque wrench to apply a certain compression force. After the fuel cell was assembled, it was important to

ensure that the fuel cell was sealed properly and had no internal crossover. If a leak test failed, the cell was re-assembled, possibly with a new gasket, o-ring or plates, until the leak test passed. The full leak test procedures are described in Appendix A. A single fuel cell was tested on a locally designed and built test station. The representative schematic of this test station is shown in Figure 3-5.

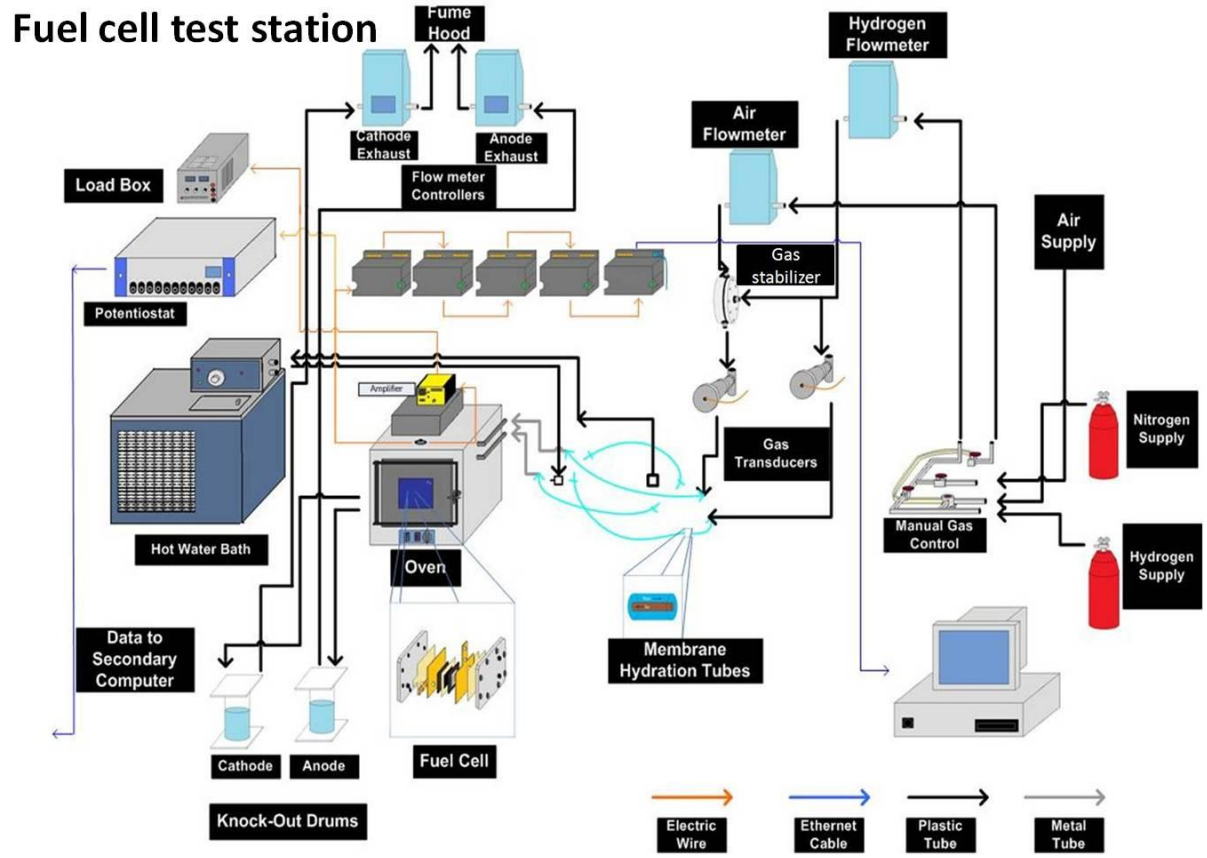

Figure 3-5: The representative schematic of the fuel cell test station.

Hydrogen gas from compressed gas cylinders and house air were supplied to the test system. The reactant gases flowed through Omega flow meters and pressure transducers before entering hydrator tubes wrapped with insulating tape to keep the temperature constant. A hydrator system in this test station consisted of a water bath and Perma Pure™ hydrators. The water bath heated deionised water up to a certain temperature, and then fed the hot water into the hydrator. Deionised water was used to eliminate the possibility of particulate and mineral deposits. The Perma Pure hydrators, used for humidifying hydrogen gas and air, consisted of small Nafion™ tubes inserted into larger polypropylene tubes. In this system

design, the gas streams flowed through the inner Nafion^{TM} tube, while deionised water was allowed to transfer through the outer tube. There were small annuli separating the outer and inner tubes. The Nafion^{TM} readily absorbed water while also maintaining a gas barrier; accordingly the gases picked up water from the Nafion^{TM} surface. The humidified gases exited the humidifiers and entered into stainless steel tubes connecting to the fuel cell inlet ports. These tubes were heated using insulating tape wrapped around the exterior of the tube to avoid gas temperature decrease. The fuel cell was kept in an oven in order to maintain the cell temperature at approximately 80°C. The temperature of deionised water from the water bath was controlled to correlate to the oven temperature to achieve a desired relative humidity (80-90%). This relative humidity required the water bath temperature to be kept between 87°C and 90°C. The anode and cathode current collectors connected to an external load via load cables, and the cell voltage was measured at the current collectors using voltage taps. The external load was a Dynaload load box (80W, 120V) which was interfaced with the data acquisition system (DAC) / PC, and allowed for control and measurement of the current. The DAC monitored and recorded operating parameters such as temperature, gas flow rates, pressure, and voltage through the computer running a locally programmed LabView virtual instrument. The fuel cell outlet gases, which were saturated with water, flowed into knockout drums. These drums captured effluent water from the fuel cell and gas streams to prevent the water entering the mass flow controllers. The mass flow controllers, positioned downstream of the knockout drums, measured the outlet flow rates of the gases as well as provided the operator with the ability to control backpressure and flow through the system. Gases exiting the knockout drums then flowed to the fume hood system.

3.2.1.2 Fuel Cell Commissioning

Prior to testing, the fuel cells were subjected to fuel cell "commissioning" for a period of six hours. The cell commissioning is accomplished at operating temperature and pressure but with a low current draw. This step permits a membrane to become fully hydrated and catalyst sites to become activated. During the fuel cell commissioning, the cell was maintained at approximately 0.6 V until performance stabilized. The cell temperature was kept at 80^{o}C, and the anode and cathode pressures were increased up to 15 psi with a differential of 0.2 psi using manual control regulator knobs. Both the anode and cathode dew point and RH were around 81^{o}C and 80%, respectively. During the "breaking-in" step, the anode and cathode

stoichiometries were analogous to the amount of excess gas delivered to the fuel cell. The stoichiometries for the anode and cathode were 2.0 and 2.5, respectively. Initial polarization curves were measured when the break-in was completed.

3.2.1.3 Polarization Curve

The operating parameters were kept constant, and the respective parameter values are given as follows.

Fuel cell temperature (oven temperature)	80^{o}C
Hydrogen Flow Rate	0.5 L/min
Air Flow Rate	0.5 L/min
Water bath temperature	87^{o}C
Dew point temperature	81^{o}C (~80%RH)
Stoichiometric ratio	1.2/2.0(Anode/Cathode)

The performance of a single cell was evaluated by measuring voltage as a function of current. The objective of a polarization curve is fully explained in the fuel cell fundamentals section. Once the temperature set points were reached, parameter values and results were first recorded at open circuit voltage (OCV). The current was increased by increments of 0.1A until the cell could no longer sustain a voltage of 0.2 volts. A single polarization curve could not provide sufficient information about cell flooding and gas flow channel blockage by condensed liquid water, so a reverse polarization curve was performed. During this polarization curve, the current was decreased (from the highest current obtained in the previous polarization curve) by 0.1A until the OCV reached. Finally, the performance of a single cell with the newly developed bipolar plates was compared to one using a commercial graphite bipolar plate to survey future possibilities for composite materials within PEM fuel cells.

3.2.1.4 Durability Testing at Multiple Current Densities

To better establish the correlation between fuel cell performance and property enhancement of the innovative bipolar plates, some cells were run at 100 and 200 mA cm^{-2}. Those experiments clarified the change in cell performance over time. The test was conducted at

gas flow rates of 0.3 L/min, stoichiometric ratios of 1.2/2 (anode/cathode), and a cell temperature of 80°C.

3.2.2 Electrochemical Impedance Spectroscopy (EIS)

The terms resistance and impedance both imply an obstruction to current or electron flow. When a process is dealing with a direct current (DC), only resistors provide this effect. Since it is non-destructive and provides useful information about fuel cell performance and its components without disturbing the system from equilibrium, EIS is a suitable and powerful diagnostic testing method for fuel cells. A diversity of formats can be used to plot the data from EIS diagnostics, and each format offers specific advantages for revealing certain characteristics of a given test system. The Nyquist plot is the most common way of analyzing impedance data. The Nyquist plot includes one, two, or three arcs: low, medium, and high frequency loops. These loops are related to mass transport resistance and charge transfer resistance combined with multi layer capacitance within fuel cell components. The principle of EIS diagnostic is described in section 2-9. Single cells with composite and commercial graphite bipolar plates were employed in order to measure the EIS, and AutoLab PGSTAT 30, controlled by Frequency Response Analyzers (FRA), was utilized for the measurement. The EIS measurements were mainly carried out at 80 ºC.

Polarization resistance of the single cells was investigated by measuring the AC impedance of the single cells with the oxygen electrode as the working electrode and the hydrogen electrode as the reference and counter electrode. The EIS was measured under potentiostatic condition, employing the amplitude of 0.01V and frequency range of 0.1 Hz to 50 kHz. After the EIS measurement, a simple equivalent circuit of a fuel cell was used to fit the EIS spectra using Boukamp software to approximate the capacitance and the change-transfer resistance of the component layers in fuel cell.

3.3 Ex-situ Test

3.3.1 In-Plane Electrical Conductivity Measurement

A four point probe is a simple apparatus for measuring the resistivity or conductivity of semiconductor samples. By passing a current through two outer probes and measuring the voltage through the inner probes allows the measurement of the substrate conductivity or

resistivity. The in-plane conductivity test procedure follows the outline in ASTM D-991 and the concept of a four-point probe method. The first four probe apparatus which abides by the ASTM standards is required for the samples injected from Engel 85. The four probe apparatus consists of two insulating plates standing parallel to each other. Four electrodes protrude from the bottom plate while two electrodes are fastened to the top plate, and an insulator is also attached to the top plate. Figure 3-6 is a general design for the apparatus.

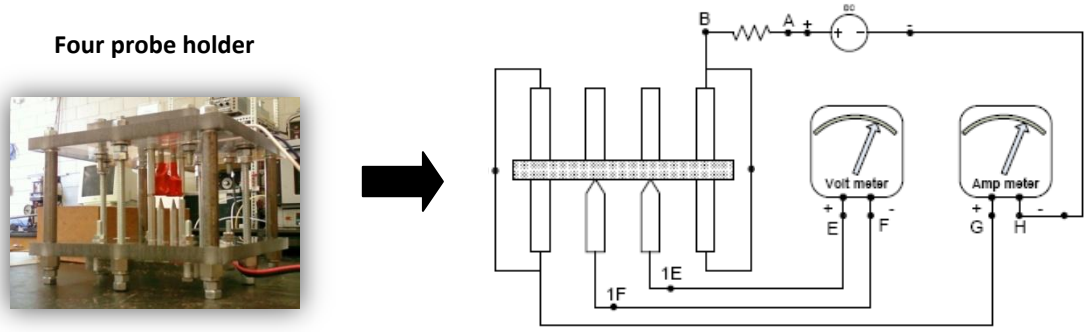

Figure 3-6: The schematic of in-plane electrical conductivity measurement

The two outer electrodes on the top and bottom are current electrodes, which carry electric current to the samples. The inner electrodes on the bottom plate are potential electrodes, and they determine the potential difference across the surface of the samples. The insulator applies downward force and allows the samples to stay leveled against the electrodes. According to material saving, the composites formulated in stage 5 to stage 7 were shaped in mini bar (Figure 3-2), therefore; a new conductivity tester was designed to accommodate these small bars. The tester was also designed to fit inside a hydraulic press for reducing contact resistance. This new design was based on an existing four-probe tester design (Appendix A), and details of the apparatus design are described in Appendix A-4.3. To achieve for reliable testing, the apparatuses were used to perform a vast amount of calibrations. Calibration tests can determine the reliability of the new tester. One can judge the viability of the new tester by testing materials with known conductivity, and compare the experimental value with literature values.

3.3.2 Through-Plane Electrical Conductivity

The four-point probe or in-plane electrical conductivity tests supplied excellent electrical conductivity measurements at the surface and near-surface of a bipolar plate, but they could

not provide the same insight into electrical characteristics deep inside the bipolar plate. The through-plane procedure (volumetric electrical conductivity) in this research followed the US Fuel Cell Council, and an experimental apparatus was devised as depicted in Figure 3-7.

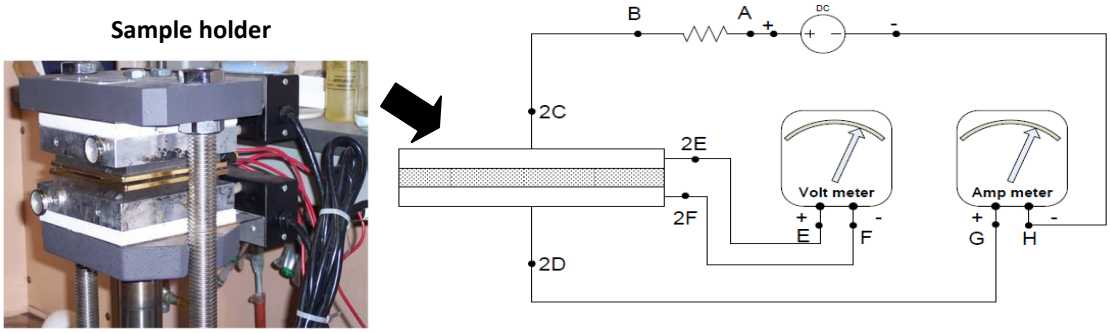

Figure 3-7: The schematic of through-plane electrical conductivity measurement

The electrical conductivity was determined by compressing a composite plate, of 3mm thickness, between two gold plated copper plates and then a constant current was passed through the two plates (Figure 3-7). The potential difference between the plates was measured. To insulate the electric circuit from the press, two polymeric insulation plates were placed between the plates of the press and the gold plates. In this test, compaction pressure (1500 psi) was applied through the apparatus to simulate conditions similar to those in a fuel cell. A composite plate was preconditioned by cycling it three times at 2000psi. After preconditioning, a sample's conductivity was measured ten times at 1500psi and the average value was calculated. For each sample, specimens were cut from different locations of an injection composite plate, and typically eight specimens were measured to obtain precise values. The concept of this method and the calculation of a conductivity value are represented in 2.8.1.

3.3.3 Thermal Analysis

3.3.3.1 Thermal Gravimetric Analysis [105]

During the extrusion and batch mixing operations, inconsistencies with the material rate would occur. Therefore, actual filler contents in each composite were validated by Thermal Gravimetric Analysis (TGA). TGA measures changes in weight in relation to change in temperature, and TGA was also used to determine thermal stability of composite bipolar plates, a property that could affect fuel cell performance. In addition, the precision of filler

loading values implies the effectiveness of filler dispersion in polymer matrix. Thermal gravimetric analysis was determined in a TA Instrument (SDT 2960 Simultaneous DTA-TGA machine) controlled by a TA processor connected to a computer for data analysis. Small amounts (approximately 15 - 20 mg) of each composite were placed in platinum crucibles, which were then loaded into the TGA chamber. Prior to the experiment, baseline and weight calibrations for the temperature were done, and then each composite was heated from ambient to 40^{o}C. An isothermal condition was held for 10 minutes for equilibrium to establish. Upon completion of the isothermal step, the sample was heated at 10^{o}C/min to 900^{o}C in an oxidative environment filled with air (at a flow rate of 130 ml/min). The equipment was then air cooled to ambient before beginning the next set of experiments. In sequential composite runs each component can be isolated to their characterized temperature range to determine decomposition temperature range and the associated weight fraction of the sample.

3.3.3.2 Differential Scanning Calorimetry [105]

Differential scanning calorimetry was carried out in a Q2000 DSC controlled by a TA processor connected to a computer for data analysis. Baseline and weight calibrations were performed in preceding steps. The calibration was firstly functioned without any samples or pans in order to obtain a baseline followed by the weight calibration involving a 96.21 mg sapphire disk (without pans) on the sample and reference positions; the temperature range was 0 °C to 300 °C under nitrogen gas. After the calibration experiments, the sample (approximately 10 mg) was then placed in an aluminum pan, crimp-sealed and loaded into the DSC chamber purged with nitrogen.

The experimental conditions comprised of 3 steps. First, a heating step from 25^{o}C to 200^{o}C, at 10^{o}C/min and under nitrogen atmosphere with a flow rate of 15 ml/min, was operated to remove any thermal history of the composites. After the heating step, samples were kept at 200°C for 5 minutes in order to promote thermal equilibrium and erase any trace of crystallinity or thermal history. Then, using a scan rate of 10°C/min, samples were cooled to 30°C and maintained at this temperature for 5 minutes. After the second step the sample was again held isothermally at 30^{o}C for 5 min. The final heating step from 30^{o}C to 200^{o}C, at 10^{o}C/min, would again melt the material. The investigation of thermal transitions of

conductive composites from DSC thermograms was correlated with other properties which are relevant to bipolar plate application. The crystallinity of a polymer can be calculated using the enthalpy of fusion (ΔH) and Equation 3-1 and 3-2.

$$\%\text{crystallinity} = \frac{(\Delta Ha - \Delta H)}{(\Delta Ha - \Delta Hc)} \times 100 \quad (3\text{-}1)$$

Where: ΔH is the enthalpy of fusion for the sample, ΔH_a is the enthalpy of fusion for a 100% amorphous standard; ΔH_c is the enthalpy of fusion for a 100% crystalline standard

$$\%\text{crystallinity} = \frac{\Delta H}{\Delta Hc} \times 100 \quad (3\text{-}2)$$

3.3.3.3 Thermal Conductivity Measurement [106-108]

The bipolar plate must be thermally conductive to conduct the generated heat (reaction byproduct) from an active part of the fuel cell to a cooling channel, therefore; thermal conductivity is a critical bipolar plate characteristic. In this research transverse thermal diffusivity of disc-shaped test specimen (1.25 mm thick and 12.5 mm in diameter) was measured at 25°C, 80°C, and 120°C by Laser Flash technique following ASTM E1461-01. The instrument used to determine the thermal conductivity was a Netzsch LFA427 (Figure A-13 in Appendix A) located in the department of mechanical engineering, University of Waterloo. A system layout and a typical temperature profile are represented in Figure 3-8. A disc specimen (i.e. sample) was placed on the Al_2O_3 holder and a laser impulse was signaled to the front face of the sample. The temperature (T) on the rear face of the sample was then measured by an IR detector. The rear-face temperature deviation signal generated from the IR detector (i.e., thermogram) can be expressed in volts or temperature units vs. time.

For the detector signal to be accepted, it must meet the following conditions: (a) irradiation time of laser pulse can be neglected, (b) the front surface of the sample is uniformly heated by the laser pulse, (c) no heat transfers, from and to outside of the sample, (d) the energy of laser pulse is perfectly absorbed, at the front surface of the sample, and (e) the sample is homogeneous. The measured signal is normalized to a baseline voltage or temperature for the

given set-point in the thermal cycle prior to the shot/impulse (i.e., ΔV/V baseline, or ΔT/T baseline).

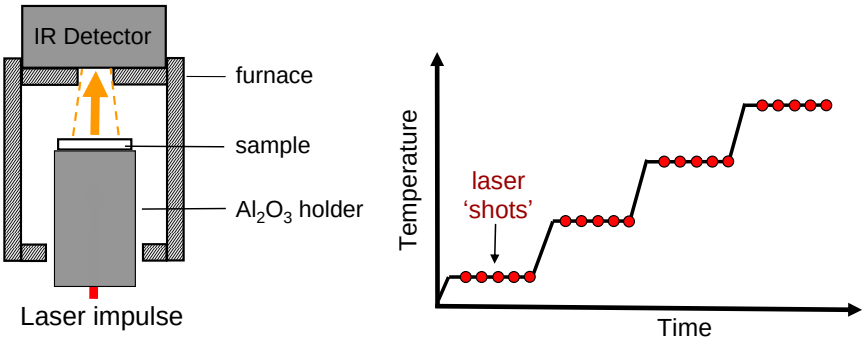

Figure 3-8: Laser flash instrument layout [108]

This convenient feature arises from the fact that the calculation of thermal diffusivity does not depend on the units of the temperature rise signal, as shown in the simplified thermal diffusivity equation below.

$$\alpha = k\frac{L^2}{t_{0.5}} \tag{3-3}$$

Where: k = half-rise constant (0.13879 under ideal conditions at half-rise), L = sample thickness, $t_{0.5}$ is the half-rise time (mm), α = thermal diffusivity (mm^2/s)

Note: Thermal diffusivity can also be calculated at the ¼ and ¾ rise times with the appropriate *k* constant in the above equation. The Netzsch software employs much more complex models that allow entire signal response fitting (i.e., the full temperature rise and stabilization/heat loss regions) and can account for pulse width effects, heat losses, etc. The example of typical thermogram and model fit is shown in Figure 3-9.

The thermal diffusivity is relevant to thermal conductivity following the equation below.

$$\alpha = \frac{k}{\rho C_p} \tag{3-4}$$

Where: k = thermal conductivity (W/ (m.K)), ρ = density (kg/m^3), C_p= heat capacity (J/(kg.K))

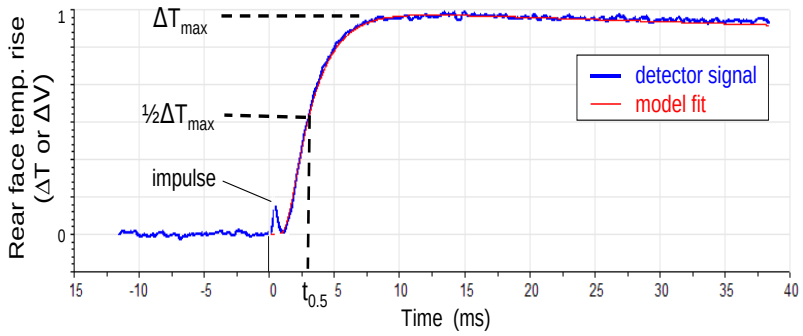

Figure 3-9: A typical thermogram and model fit of a thermal diffusivity result [108]

Heat capacity can be obtained in a single experiment with the modulated DSC (DSC Q2000). Modulated DSC differs from standard DSC in that it applies two simultaneous heating rates to the sample. The linear or average heating rate provides the same information (total heat flow rate) as standard DSC, while the sinusoidal (modulated) heating rate is used to determine the fraction of the total heat flow rate that responds to a changing heating rate. In general, this heat flow rate is caused by the heat capacity (Cp), changes in heat capacity, and by most melting. This fraction of the total heat flow is called the reversing heat flow or the heat capacity component of the total heat flow. Heat flow that does not respond to the changing heating rate is determined by subtracting the reversing signal from the total signal. This difference signal is called the non-reversing heat flow or the kinetic (time-dependent) component. Before performing the heat capacity measurement, DSC and MDSC heat capacity calibrations were required to measure accurate sample heat capacity values. These heat capacity calibrations were performed after calibration of the DSC for cell resistance and capacitance, cell constant and temperature.

The calibrations used a standard material (sapphire) with a known heat capacity at a specific temperature of interest (-50 to 200^{o}C for this research). There were three cycles to determine heat capacity as follows:

- Cycle 1: Initial temperature -50^{o}C; Final temperature 180^{o}C; heating rate of 10^{o}C min^{-1}; sample size close to 10 mg; under nitrogen at a flow rate of 50 ml/min,
- Cycle 2: Initial temperature 180^{o}C; Final temperature -50^{o}C; cooling rate of 10^{o}C min^{-1}; under nitrogen,

- Cycle 3: Initial temperature -50^{o}C; Final temperature 200^{o}C; heating rate of 10^{o}C min^{-1}.

Note: Cycle 1 was used to remove the thermal history of the composite.

3.3.4 Mechanical Property Measurement [106, 109]

The mechanical tests in this research consist of compression, tensile, flexural, creep and hardness tests. In this research, tensile, flexural (three-point bending), and compressive tests were performed on Rheometric Scientific Mini-Mat tester, equipped with a load cell of 200 N. The tests were carried out in accordance with ASTM D-3039/D3030M-00, ASTM D-790-03, and ASTM D-3410/D-3410M-03, respectively. 'Dog-bone' samples for the tensile tests were cut from injection molded plates (Figure 3-10). The specimens were dried in the oven at 80 ^{o}C for 4 hours, and then conditioned at a relative humidity of 23 ± 2°C and 50 ± 5% for at least 48 hours before testing, as suggested in the standard specification. These tests were measured in both the axial (parallel to injection flow) and transversal (perpendicular to the injection flow), and at least 5 samples were tested for each sample. Prior to the tests, exact dimensions were measured using a digital caliper and these dimensions were used in calculations of the results.

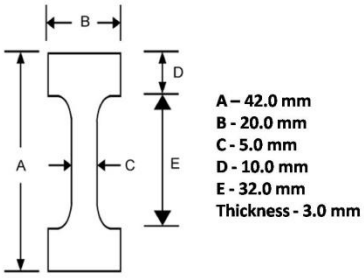

Figure 3-10: Dog-bone dimensions for mechanical tests.

All tests were carried out at room temperature, using deformation rates of 1 mm/min. The dog-bone sample was pulled at a constant deformation rate until the ultimate break point in order to study the tensile behavior of polypropylene composite. Load versus displacement was measured, and maximum strength, strength at yield, and modulus were calculated. In terms of yield stress, it is the stress needed to induce plastic deformation in the specimen. Since it is often difficult to pinpoint the exact stress at which plastic deformation begins, the

yield stress is often taken to be the stress needed to induce a specified amount of permanent strain, typically 0.2%.

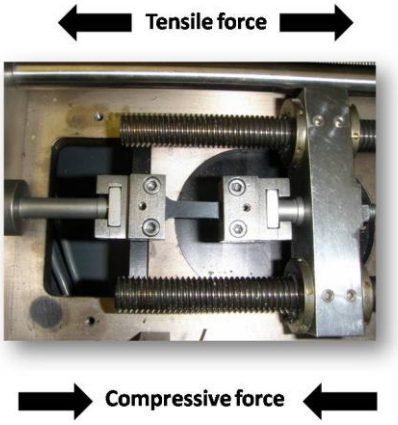

Figure 3-11: Tensile, compression, and flexural tests using Mini-Mat tester

Surface hardness (shore hardness) of the bipolar plate samples was measured by Super EX durometers (shore D from e-Asker). Hardness is defined as a material's resistance to permanent indentation. A durometer measures the depth of an indentation in the material created by a given force on a standardized presser foot. This depth is dependent on the hardness of the material, its viscoelastic properties, the shape of the presser foot, and the duration of the test. ASTM D2240 durometers allow for a measurement of the initial hardness, or the indentation hardness after a given period of time.

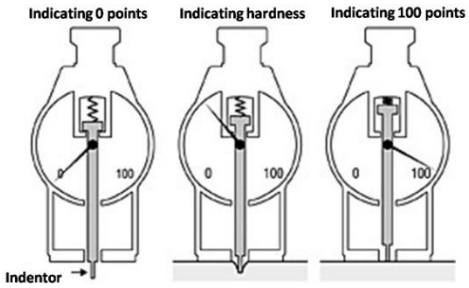

Figure 3-12: Hardness test using shore D durometer[110]

The basic test requires applying the force in a consistent manner (without shock) and measuring the hardness (depth of the indentation). If a timed hardness is desired, the force is applied for the required time and then read. The operation started with the durometer pressed against the sample and then the material resistance force and indenter spring load balanced (Figure 3-12). The depth of the indenter was measured, which provided a measure of the

material's hardness. However, as time elapsed the indicator would naturally move back. Therefore, a measurement was taken 15 seconds after the indent was made in order to ensure a stable reading. Values were based upon a 100 point scale (accuracy ±1 point).

3.3.5 Creep Behavior Test [105, 109]

To achieve good electrical contact between cell components in a fuel cell stack, the cells are compressed together. Under this compression, bipolar plate materials may experience some creep deformation. Creep is the tendency of a solid material to slowly deform permanently under the influence of stresses. It occurs as a result of long term exposure to levels of stress that are below the yield strength of the material. The creep is more severe in materials that are subjected to heat for long periods, and near the melting point, and it always increases with temperature. As indicated in the accompanying diagram, the creep of a material can be divided into three stages.

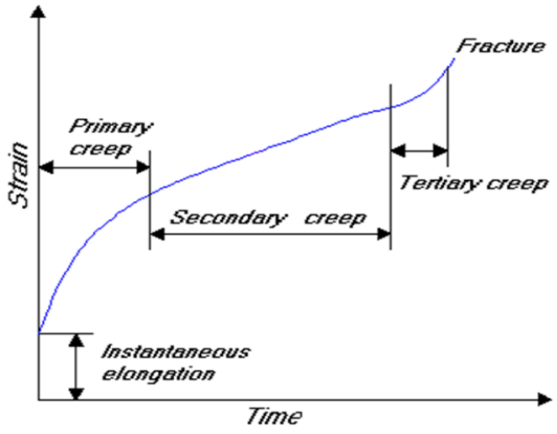

Figure 3-13: Creep behavior curve [111]

In primary creep, the strain rate is relatively high, but slows with increasing strain. This is due to work hardening. The strain rate eventually reaches a minimum and becomes near constant. This is due to the balance between work hardening and thermal softening. This stage is known as secondary or steady-state creep. This stage is the most understood. The characterized creep strain rate typically refers to the rate in this secondary stage. Stress dependence of this rate depends on the creep mechanism. In tertiary creep, the strain rate exponentially increases with strain because of necking phenomena. The experiment was operated using the laboratory parallel plate rheometer (TA Instruments AR 2000 model, see

Figure 3-14. The instrument can provide torque from 0.1 to 200 μNm, frequency from 0.12 to 100 μHz and angular velocity from 8 to 300 rad/s under controlled stress, and from 2 to 300 rad/s under controlled strain.

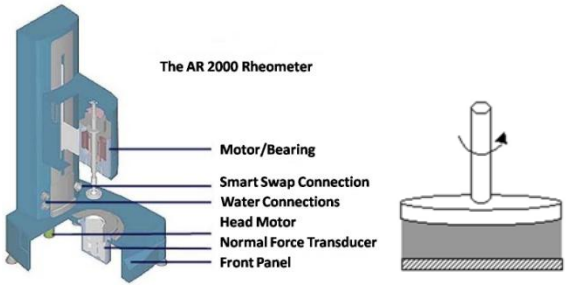

Figure 3-14: TA Instruments AR 2000[112]

It can also detect normal force from 1 to 5,000 g and a minimum strain of 6×10^{-5}. Before staring the experiment, the Rheometer was calibrated for the inertia and gap between the parallel plates. The inertia must approach the smallest possible value while the gap must be zeroed. The normal force could be calibrated to a small value, when the gap was zeroed and the plates touched each other. Disk-shaped specimens with a thickness of 2 mm and a diameter of 20 mm obtained from injection molding plates were prepared in the hot press as described previously. These disks were placed between the two parallel plates which are a pair of 20mm parallel. As soon as the sample was inside the plates, the gap was fixed at exactly 1000 μm (or gap settings according to the disk thickness). If the upper plate was lowered and touched the sample, the values of the normal force were increased dramatically. This meant that the sample was secured into that gap.

After a while, when the temperature approached the melting point of the sample, the values of the normal force started decreasing. This was an indication that the sample changed from the solid to the melt phase. To determine creep properties, a material is subjected to prolonged constant tension or compression loading at constant elevated temperature. Deformation is recorded at specified time intervals and a creep vs. time diagram is plotted. The creep rate is given by the slope of the curve at any point. If failure occurs, it terminates the test and the time for rupture is recorded. If the specimen does not fracture within the test period, creep recovery may be measured. Creep recovery, which is defined as the rate of

decrease in deformation, occurs when the load is removed after a prolonged creep test. Constant temperature is maintained to eliminate effects of thermal expansion, and measurements are taken from the time the load is zero to eliminate elastic effects. In this research, to determine the creep deformation behavior the shear stress was kept constant at 1000 Pa, and temperature, shear stress, and test duration were varied according to bipolar plate application.

3.3.6 Rheology Observation [109, 112, 113]

The addition of conductive fillers typically increases the viscosity of the polymer matrix. The viscosity of the composite must be low enough to be processed (extruded, injection-molded, compression molded, etc.) into a bipolar plate. It implies that the ability to process the material is largely dependent on the rheology of the material. The relationship between processability and composite recipes was investigated using capillary rheolometry. Additionally, rheological properties could illustrate the effects of coupling agent addition and filler dispersion on the processability of composite production. In rheological inquiry, the dependence of apparent viscosity upon shear rate can be determined over a wide temperature range by a variety of techniques that utilize some of the simple pressure or shear geometries. In this work two methods, including capillary and rotational rheometry methods, were used to study rheological behavior. The plate viscometer was used for small shear rates while the capillary rheometer was used for higher shear rates.

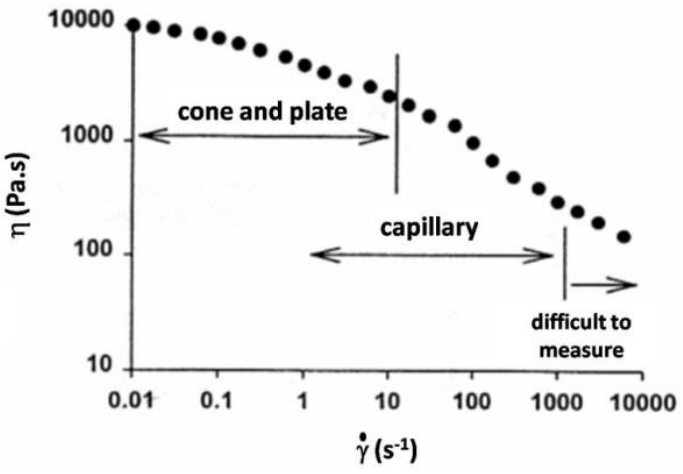

Figure 3-15: Typical flow chart of a material and application areas of rheometers[109]

3.3.6.1 Capillary Rheology

The capillary rheometry can be used over the shear rate range from 1 to 10^5 s^{-1} including most processing operations (Table 3-8). The most widely used relationship is the power-law model given as Equation 3-5.

$$\tau = k\dot{\gamma}^n \tag{3-5}$$

Where: $\dot{\gamma}$ = shear rate (1/s), τ = shear stress (Pa), k = consistency, n = power-law index

Note: k is a decreasing function while n is an increasing function of increasing temperature.

Table 3-8: Typical shear rate range for polymer processing operation [121]

Operation	Shear rate (1/s)
Compression molding	1-10
Calendering	10 - 10^2
Extrusion	10^2 - 10^3
Injection molding	10^3 - 10^4

From the Generalized Newtonian Fluid (GNF) model (Equation 3-6) the dependence of apparent viscosity on shear rate for a power-law fluid is shown in Equation 3-7.

$$\tau = \eta\dot{\gamma} = k\dot{\gamma}^n \tag{3-6}$$

$$\eta = k\dot{\gamma}^{n-1} \tag{3-7}$$

Note: n = 1, apparent viscosity is independent of shear rate, n < 1, shear-thinning behavior

In this research, rheology characterization was performed on a capillary rheometer (model 8052, KAYENESS INC) with a die L/D = 20, diameter = 0.05 inch at temperature 230 ^oC. 10^1 - 10^3 s^{-1} of the shear rate range was used.

3.3.6.2 Rotational Rheology

A TA Instruments AR2000 rheometer was used for the rheological characterization of composites. Sample preparation and instrument calibration were the same as that of the creep behavior test. In this experiment, time sweep, temperature sweep, and frequency sweep

experiments were performed in oscillatory measurement mode. In temperature sweep experiments, by varying the temperature at a specific rate, the modulus over a range of temperatures can be determined from the same experiment. On the other hand, by holding the temperature constant and varying the time, the modulus of a material over a time range can be obtained. The time sweep experiments took place at 170 ^{o}C, while a strain frequency was fixed at 1 and 0.5 Hz. A percentage of strain was set at 0.5 relating to the requirement of bipolar plate application, and the test durations were 2 and 4 hours. During the temperature sweep, a range from 80 to 170 ^{o}C was covered with 5 ^{o}C/min temperature increments. These analyses were regarding 0.5 % of strains and a strain frequency was provided at 0.5 Hz. In case of frequency experiments, the frequency was varied from 0.01 to 100 Hz. In terms of oscillatory measurements, oscillation is a non-destructive technique which is ideal for investigating structure or structural changes in materials.

The oscillation technique involves applying a sinusoidal oscillating stress (τ) wave to a material and measuring the resulting strain (γ) wave. A purely elastic (Hookean solid) material will retain all of the deformation energy applied to it and will therefore have a phase difference (phase angle) of 0 degrees, (Figure 16a). Conversely, a purely viscous (Newtonian) fluid dissipates all of the applied energy and will have a phase angle of 90 degrees, (Figure 16b). Polymeric materials are Viscoelastic and as such their responses fall somewhere between these two extremes (Figure 16c).

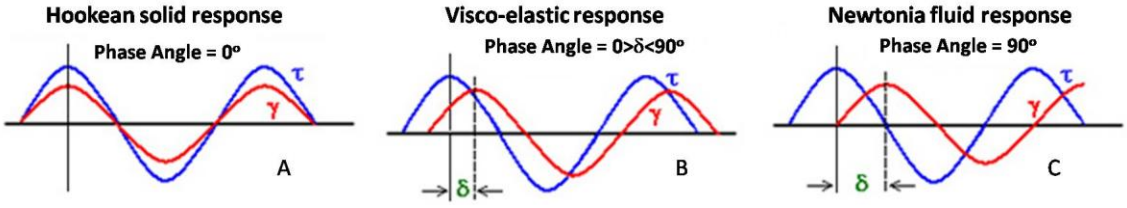

Figure 3-16: Different phase angles in oscillatory measurements

When oscillatory shear measurements are performed in the linear viscoelastic regime, the storage modulus G' (elastic response) and loss modulus G" (viscous behavior) are independent of the strain amplitude. A variety of viscoelastic properties can be calculated, as follows: [112]

- Storage (Elastic) Modulus (G'), which can be derived as:

$$G' = \frac{\text{stress}}{\text{strain}} \cos(\text{phase angle}, \delta) \quad (3\text{-}8)$$

- Loss (Viscous) Modulus (G"), which can be derived as:

$$G'' = \frac{\text{stress}}{\text{strain}} \sin(\text{phase angle}, \delta) \quad (3\text{-}9)$$

- Complex Modulus (G*), which can be derived as:

$$G^* = \frac{\text{stress}}{\text{strain}} \quad (3\text{-}10)$$

- Complex Viscosity (η*), which can be derived as:

$$\eta^* = \frac{G^*}{\text{frequency}} \quad (3\text{-}11)$$

3.3.7 Contact Angle Measurement [114]

The bipolar plate plays a crucial role in fuel cell water management and as such hydrophobicity is one of the most important features affecting the fuel cell performance, particularly at high current densities. If bipolar plates have a hydrophilic surface, the channels may flood with product water and hinder the supply of gaseous reactants to the electrodes. With an increased surface hydrophobicity, a water droplet in the gas flow channel of a bipolar plate can be swept away more easily. Since the hydrophobicity is related to the contact angle or the surface energy of the plates, the contact angle of bipolar plates was determined by using dropped water on the specimens. The contact angle is a result of the interface/surface tensions (surface free energies) between liquid and solid surrounded by vapor, and it is measured according to Young's Equation (Equation 3-12). The equation is used to explain the balance of forces that are present in phase system with solid and liquid phases.

$$\gamma_S = (\gamma_L \times \cos\theta) + \gamma_{SL} \quad (3\text{-}12)$$

Where: γ_S = Solid surface free energy, γ_L = Liquid surface free energy

θ = Contact angle, γ_{SL} = Solid/liquid interfacial free energy

When a droplet of high surface tension liquid is placed on a solid of low surface energy, the liquid surface tension will cause the droplet to form a spherical shape (lowest energy shape). The way that a liquid behaves on a solid surface is a result of the interaction between the surface energy of the solid and the surface tension of the liquid. If the solid substrate has a

surface energy large enough to overcome the surface tension, the liquid will spread or wet over the solid surface. If the surface energy is too small, the liquid will not wet the solid surface. Contact angle measurements are typically done to determine how a liquid wet a particular solid surface. Table 3-9 illustrates the correlation between contact angle and degree of wetting. According to Young's Equation the contact angle of a drop of water will be larger if the surface is hydrophobic. Hydrophilicity is indicated by smaller contact angles and higher surface energy. If the surface hydrophobicity increases, it indicates that a water droplet in the gas flow channels of bipolar plate can be swept away more easily (Figure 3-17).

Table 3-9: The correlation of contact angle, degree of wetting, and surface interaction

Contact angle	Degree of wetting	S/L interaction	L/L interaction
$\Theta = 0^{o}$	Perfect wetting	Strong	Weak
$0^{o} < \Theta < 90^{o}$	High wettability	Strong-Weak	Strong-Weak
$90^{o} \leq \Theta < 180^{o}$	Low wettability	Weak	Strong
$\Theta = 180^{o}$	Perfectly non-wetting	Weak	Strong

In this work, contact angle measurements of water drops on a bipolar plate surface was done using a VCA 2500 XE Video Contact Angle System by AST Products. A millipore deionized-water drop was placed on the bipolar plate surface using a syringe at room temperature, and images of the water drop were analyzed by VCA software. The contact angle, width, height, and volume of the sessile drops were analyzed using the VCA software accompanying the equipment.

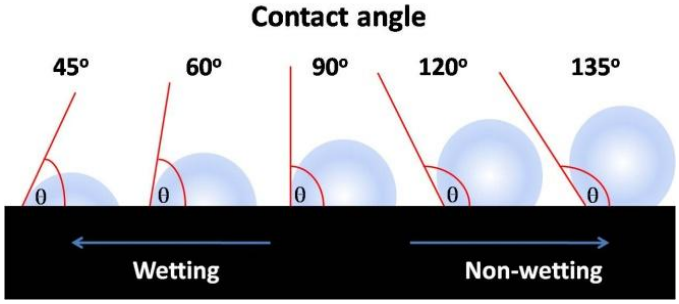

Figure 3-17: Example of liquid drops on bipolar plate surfaces.

3.3.8 Hydrogen Permeability Measurement [115]

Bipolar plates have a critical role to separate the gases in adjacent cells; therefore, they must be impermeable to hydrogen and oxygen. Since, it is much more difficult to meet thickness targets and simultaneously obtain low permeation rates when using polymer composite plates which are a porous material, the permeability of these composite materials needs to be investigated. In this research PMI Diffusion Permeameter (PMIDP) was used to discover the permeability of the composite plates. The composite plate was cut and shaped into circle samples of 1 inch diameter. The sample was placed on a sample holder (Figure 3-18) which was properly sealed. PMIDP applied hydrogen under a gas pressure of 1,000 torr to one side of a sample. Gas was maintained at a constant pressure in the inlet side and the increase in pressure in the outlet side was measured. The quantity of gas that passed through the sample into a 54 cc chamber was calculated from the pressure rise in the known volume. The rate at which the gas passed through the sample was calculated from the pressure rise in the known volume, and the flow rates were computed as in a microflow permeameter. The evacuation system allows for flow rates as low as 10^{-4} cm^3/s so that very accurate results can be obtained.

Data from the experiment was recorded with 5 minute time increments for test duration of 3 hours. Permeability was calculated using the flow rate, the cross-sectional area and thickness of the sample, and the pressure applied to the composite sample. The schematic of the PMIDP is depicted in Figure 3-19 and A-14.

Figure 3-18: Sample holder for hydrogen gas permeability measurement

PMI Diffusion Permeameter (PMIDP) software performs the following calculations in the following order:

$$\text{Flow Rate} = \frac{\text{Slope} \times \text{Chamber Volume} \times \text{Standard Temperature}}{\text{Temperature} \times \text{Standard Pressure}} \quad (3\text{-}13)$$

Note: Slope is the slope of the pressure versus time graph using least squares line fit.

$$\text{Gas Transmission Rate} = \frac{\text{Flow Rate}}{\text{Cross Sectional Area}} \quad (3\text{-}14)$$

$$\text{Permeance} = \frac{\text{Gas Transmission Rate}}{\text{Average External Pressure}} \quad (3\text{-}15)$$

$$\text{Permeability} = \text{Permeance} \times \text{Sample Thickness} \quad (3\text{-}16)$$

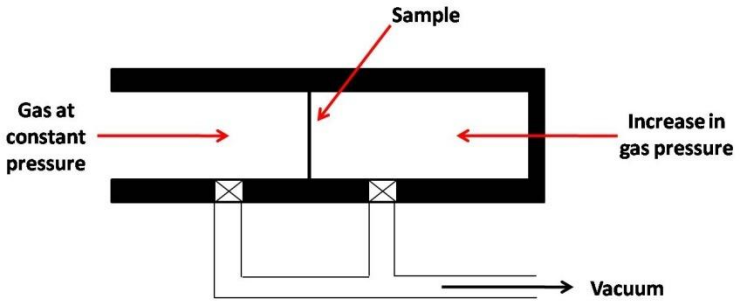

Figure 3-19: The layout of PMIDP [115]

3.3.9 Morphology

The scanning Electron Microscope (SEM) is a powerful instrument for the morphology characterization of bipolar plate material. Therefore, the morphology of conductive composites was studied by SEM, using a LEO 1530 SEM scanning electron microscope equipped with a Gemini field emission column. The surfaces of freeze broken samples obtained after compounding and after injection molding, were used for SEM analysis. Small pieces of each sample were freeze fractured using liquid nitrogen in the cross-sectional direction, and affixed to an aluminum stub using double-sided conductive tape. Then, the samples were sputter coated with gold at a thickness of approximately 10 nm prior to loading into the SEM machine. EHT was set to 10 kV, and WD was at 10 mm at the beginning of scans, and the parameters were adjusted accordingly to obtain optimal image resolution. SEM imaging of the microstructure of the bipolar plate material allows observation of the following characteristics. First, the dispersion of fillers and conductive network formation in polypropylene matrix affect to bipolar plate properties, especially electrical conductivity.

Therefore, dispersion of fillers and fiber orientation in the polypropylene were observed the interior material morphology by fracturing the samples in specific orientations (e.g., in line with the injection direction or perpendicular to it). In addition, SEM was used to indentify changes in the morphology of composites with additives such as a titanate coupling agent and conductive polymer, etc. The differences in electrical conductivity of the composite could be explored in different areas of inject composite plaques. For that reason, SEM images were analyzed with UTHSCSA Image Tool software to acquire estimates of areas, number, and sizes of contact points and agglomerations of fillers to investigate the conductive network pattern that gives high electrical conductivity.

3.3.10 Density

Density of a composite plate corresponds to other properties of bipolar plates, mechanical property and gas permeability, for instance. The density of composites was measured using the technique of water displacement, following ASTM D792. The dry weight of a sample was measured using an analytical balance in the first step. Subsequently, the sample was suspended using a non-water-absorbing string, and submersed in a beaker of deionized water. The displaced weight of the sample was measured, and the relative density of the sample was then calculated, as in Equation 3-17.

$$\text{Relative density} = \frac{\text{Dry weight}}{\text{Dry weight} - \text{Displaced weight}} \tag{3-17}$$

CHAPTER 4: Results and Discussion

This work has studied the impact of different variables in composite composition on PEMFC's conductivity and potential application as bipolar plate materials. The research has investigated in the following sections:

- The synergistic effect was different types of fillers: carbon black, carbon fiber, synthetic graphite;
- The synergistic effect of the addition of a small amount of a conductive polymer, **polypyrrole** (PPy), to improve composite conductivity;
- The effect of processing additives on the conductivity and processing characteristics;
- The effect of injection flow direction on the conductive network;
- Modifications of the surface that was improve contact resistance; and
- Innovative plate manufacturing options such as metal plate inserts.

The results of these investigations are detailed next.

4.1 Synergistic Effect of Fill Composition

One of the important functions of bipolar plates is to connect cells electrically in series and to the circuit; thus they must be electrically conductive. The greater the electrical conductivity of the bipolar plates, the better the resulting fuel cell's performance. The goal of this section is to demonstrate synergetic effects of different carbon filler sizes, shapes, and ratios on the electrical conductivity of bipolar plate materials. In order to compare the effects of fillers on composite conductivity, Stat Ease's DESIGN EXPERT 6.0 software package was applied to study the effect of two or three factors among different filler types, and to clarify the relation

of multiple fillers in composite conductivity. Table 3-2 shows the composite formulations used based on previous work [34].

Wang observed the electrical conductivity of polypropylene/fillers (CB, SG, and CF) composites with total filler loading of 45, 50, 55, 60 and 65wt%. Please note that the three-filler ratio used in Wang's work was 1:1:1. The results illustrated that electrical conductivity increases with increases of the filler loading; however, the research expectation requires both good conductivity and easy processing for bipolar plate production. Therefore, the composites with 55 and 60wt% of carbon filler loading were produced in the preliminary experiment of this research to determine the appropriate filler loading for bipolar plate production. The preliminary results indicated that the composite with 60 wt% of filler loading was hard to produce, because large amounts of solid particles gave total mixing torque that were too high during the melt-mixing process. For the remainder of this study 55 wt% of total filler loading was utilized for all composites in the entire research in order to standardize the investigations.

4.1.1 Different Types of Fillers

4.1.1.1 Electrical Conductivity of Composites

A composite series was made and studied in this section of work to clarify the role of individual fillers. These experiments would help in producing a composite plate having the desired characteristics of three different carbon filler components in different proportions. Details of experiments are given in Table 3-2 and Table 4-1.

Thermal gravimetric analysis (TGA) was applied to determine the actual filler loading (after processing) within the polypropylene matrix. This confirmation was needed due to the variations of feed rates and hopper mixing inherent in the process. Of note is that for all blends, each sample was replicated (3 times) to check the reliability of testing results. The results displayed as in Figures 4-1 to 4-2, indicate that the range of filler concentration (56-58 wt %) is close to the expected concentration (55 wt %). The trends also showed the polypropylene resin decomposition had a chemical transition (having evaporation), but those for the individual fillers overlap; therefore, the temperature range for individual carbon fillers is difficult to distinguish.

In terms of composites' thermal stability, no mass loss occurs until approximately 270°C. For all composites, the degradation temperature (at which the weight loss of material is 5%) is between 300 and 340 °C. The degradation temperatures were higher than that of PP, which is around 300°C.

Table 4-1: Filler loading of polypropylene/carbon filler composites

Composites	Loading (wt %)				Filler ratio			Electrical conductivity (S/m)	
	CB (XC72)	CF (Fortafil)	SG (4012)	PP	CB	CF	SG	In-plane	Through-plane
FR2	55	0	0	45	1	0	0	-	-
FR3	0	55	0	45	0	1	0	543	32
FR4	0	0	55	45	0	0	1	2	0.1
FR5	0	27.5	27.5	45	0	1	1	38	2.1
FR6	27.5	0	27.5	45	1	0	1	820	62
FR7	27.5	27.5	0	45	1	1	0	1,502	119
FR8	36.66	9.17	9.17	45	4	1	1	1,851	120
FR9	9.17	36.66	9.17	45	1	4	1	651	22
FR10	9.17	9.17	3.66	45	1	1	4	90	6
FR11	27.5	13.75	13.75	45	2	1	1	1,356	69
FR12	13.75	27.5	13.75	45	1	2	1	646	18
FR13	13.75	13.75	27.5	45	1	1	2	282	15
FR14	18.33	18.33	18.33	45	1	1	1	782	47

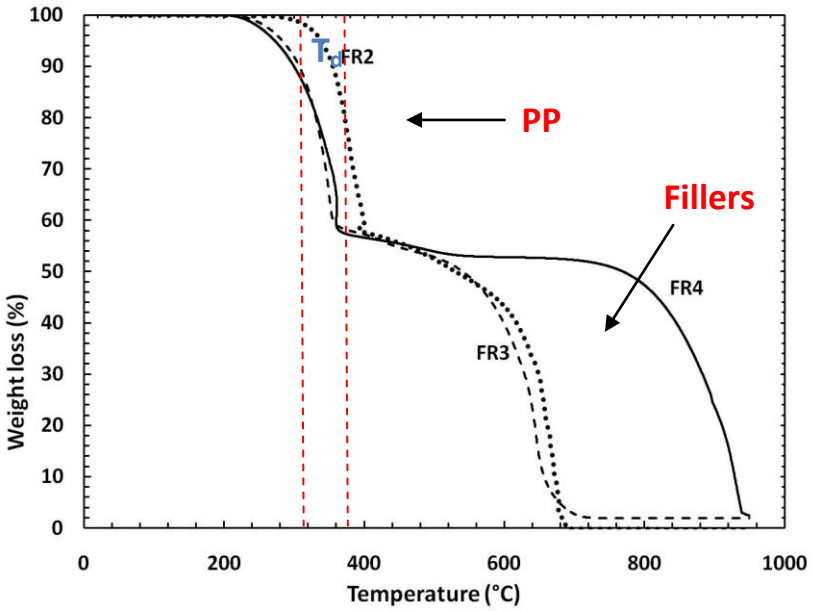

Figure 4-1: TGA thermogram of single-filler system composites

These results also confirm the good thermal stability of the bipolar plate for fuel cell application, because it is clear that all the composites showed a good thermal stability at 80 to 120^{o}C, which is the temperature range for PEMFC's operating environment. Moreover, the TGA thermograms also illustrate that the composites consisting of large quantities of carbon black particles that have a higher degradation temperature than ones with other fillers. The results indicate that carbon black increases thermal stability of the composites.

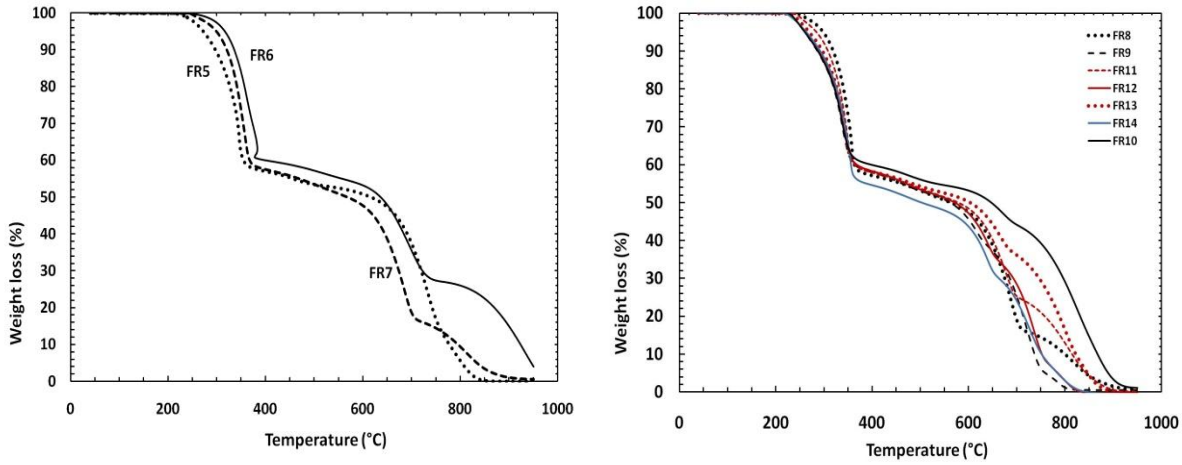

Figure 4-2: TGA thermogram of two- and three-filler system composites

The injection molded specimens of each formulation were measured in-plane and through-plane electrical conductivity. The procedure of injection molded sample preparation is described in section 3.1.5 (Chapter 3), and the electrical conductivity test methods are explained in 3.3.1, 3.3.2 (Chapter 3) and A-4.2 (Appendix A).

Single-filler System

The graphs of in-plane electrical conductivity values (average values) are presented in Figure 4-3. For single filler blends, the electrical conductivity of the PP/carbon fiber composite (CF composite) was significantly higher than that of the composite with synthetic graphite. The electrical conductivity values of PP/CF and PP/SG composites were 543.00 S/m and 2.018S/m, respectively. Researchers have typically used SG with loading higher than 70 wt% to achieve high electrical conductivity of polymer/SG composites, but doing so affects the processing capability of the composite. The increasing conductivity can be attributed to CF acting as a long-distance charge transporter. CF has a high aspect ratio with a very small diameter; therefore, the high aspect ratio enables CF to make conducting channels through

the PP matrix, which is an insulating material. However mixing and shaping processes can reduce the aspect ratio and carbon fiber length, especially with high concentrations of filler [116].

Figure 4-3 does not show the electrical conductivity of PP/carbon black because this composite could not be molded into a suitable sample. As mentioned in Chapter 2, high CB loading limits the ability of the mixing process because of the higher viscosity of the composite material. The high viscosity is due to the highly branched particles, large surface area structure of carbon black, a structure that accounts for the results in this study that show high melting torque during the mixing process (Figure 4-4). When the total mixing torque was close to the maximum (20,000 m.g) possible, the mixer closed down for safety's sake. When internal mixing is employed, the mixing torque is an imperative indicator for evaluating the processing characteristics of compounds.

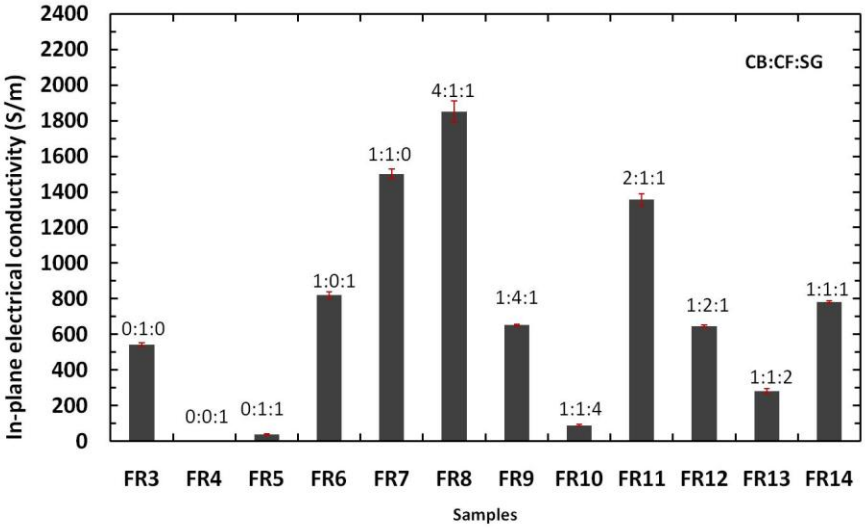

Figure 4-3: Average in-plane electrical conductivity of composites

The total mixing torque of each composite was recorded against the time of mixing. From Figure 4-4, the recorded torque can be divided into two portions: peak and stabilization. Peak torque corresponds to the peaks from starting to 5 minutes which appears on the torque versus time curves, while the stabilization torque is the torque that appears after 7 minutes of mixing. The peak torque typically corresponds to the addition of solid materials, such as PP

pellets and filler particles, during sequence described in the experimental section. The immediate increase in torque was attributed to the high shear force needed to rotate the rotor in the presence of solid particles before they were melted. The torque consequently decreased after the PP pellets melted, since the viscosity of PP decreased to under approximately 200^{o}C and high shear.

The results from Figure 4-4 also show that the peak torque of the PP/SG composite was lower than the torques of the others. In the regime of torque stabilization, the torque of the PP/CF composite was slightly lower than PP/SG's. Although the electrical conductivity of PP/SG was low, synthetic graphite can provide interconnections between the fibers by forming local conductive paths. Furthermore, the addition of SG to the PP/CB composite combines the electrical properties of graphite easily. Through-plane electrical conductivity of the single-filler composites has the same trend as in-plane electrical conductivity's values, as displayed in Figure 4-5.

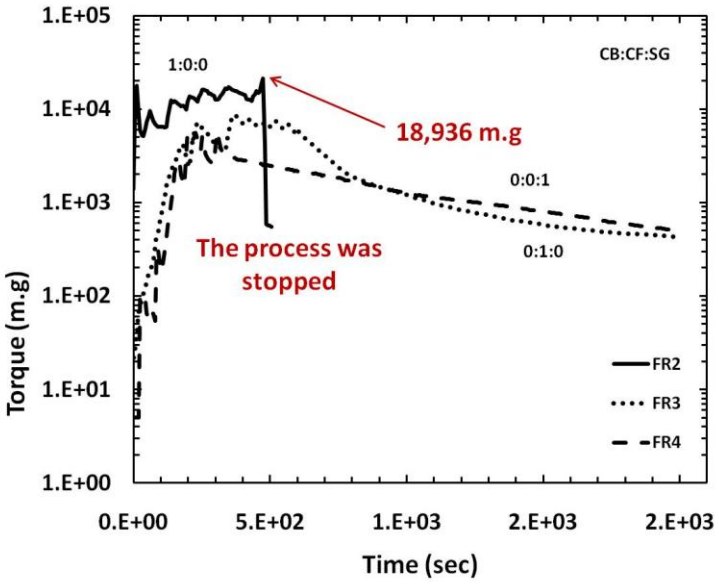

Figure 4-4: Total mixing torque of single-filler composites

In comparisons between two conductivity measurements, the through-plane conductivity shows much lower values than the in-plane. This difference is similar to the results from many research publications, for instance the work from Du's group, which found that the in-plane electrical conductivity of an epoxy/SG composite was 50 Scm^{-1} higher than the value

from through-plane [18]. This conductivity difference occurs because of the different directions for the measurements. A through-plane conductivity test measures the conductivity perpendicular to the surface of the specimens as depicted in Figure 2-18. There may be many insulating areas (PP matrix) in the direction of the measurement; therefore, there may be less electron transfer to the matrix.

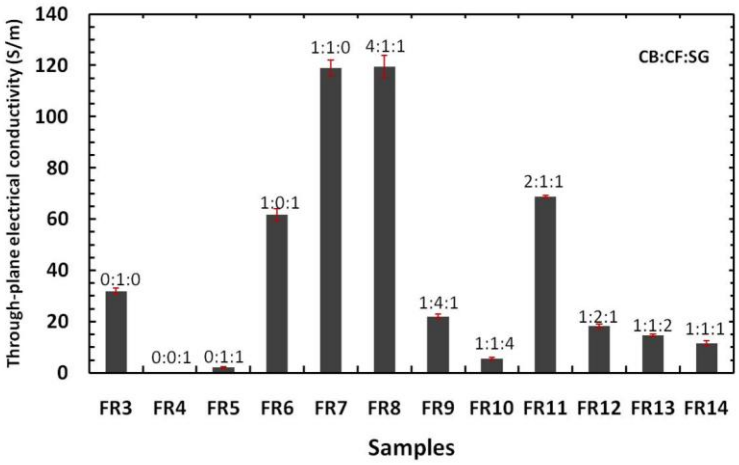

Figure 4-5: Average through-plane electrical conductivity of composites

Two-filler System

Conductive percolation networks with a synergistic effect between conductive fill types resulted in the composites having enhanced conductivity as well as improved processing characteristics. In this part of the experiments, the composites of PP and carbon black were fabricated by adding synthetic graphite or carbon fiber. Comparing results in between Figures 4-4 and 4-6 shows the total melting torque of the composite with CB dramatically decreased, SG or CF were introduced into the composites. These results imply that the melting torque reduced as the quantity of carbon black decreased. With the fixed filler loading, the conductivity of two-filler composites with carbon black exhibits very high potential (Table 4-1). In agreement with the results in Mathur's research, an introduction of CB into a phenolic resin hybrid composite (graphite, CB, and phenolic resin) could decrease electrical resistivity in approximately 10 times of the composites containing only graphite[44]. Dweiri and Sahari also stated that combining 25wt% of CB with PP/graphite composite (45wt% of graphite) increased the electrical conductivity of the composite from 1.33×10^{-3}

S/cm to 7.50 S/cm compared to that of the PP/graphite composite with 40wt% of graphite loading [62].

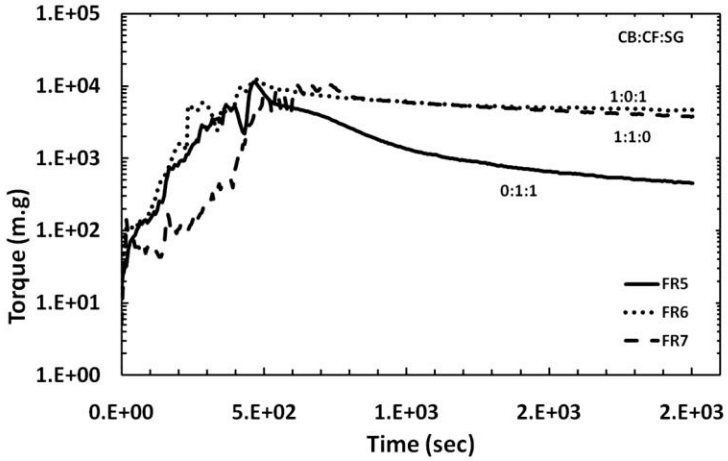

Figure 4-6: Total mixing torque of two-filler composites

CB is comprised of spherical particles aggregated together by Van der Waals forces. The unit of CB particles is basically built from graphene rings, which tend to stack in three to four layers, forming crystallographic structures. Although, the graphene layers include numerous discontinuities because of carbon atoms with sp^3 hybridization and non-carbon atoms, the electrical conductivity inside the particle is relatively high [117]. Some of the graphene layers are extended beyond adjacent particles. These overlapping layers ensure between particles of the same aggregate. The aggregates of carbon black in a PP matrix establish the conductive path that allows electrons to transport through [118]. The comparatively small CB particles also make conducting tunnels between the other particles.

Electrical conductivity results from but both methods, the electrical conductivity values of two-filler composites were found to be significantly higher than the values of single-filler composites. SEM micrographs support these results, as illustrated in Figures 4-7 and 4-8. Figure 4-7 (A) depicts the long distance charge transporter, CF, through which electrons can travel. However, there are insulating gaps (from the PP matrix) between CFs that form be obstacles to electron transport, Results in lower electrical conductivity comparing to two-filler system composites. In Figure 4-7 (B) it can be seen, at high loading of synthetic graphite, graphite particles fuse together in chunks. The chunks tend to occupy more space

than particle and percolate electrons at lower loadings [119], but such is not the case for composites with high SG loading. When the composites contain many SG chucks, longer distances between SG particles exist, and thus less conductive network and low electrical conductivity.

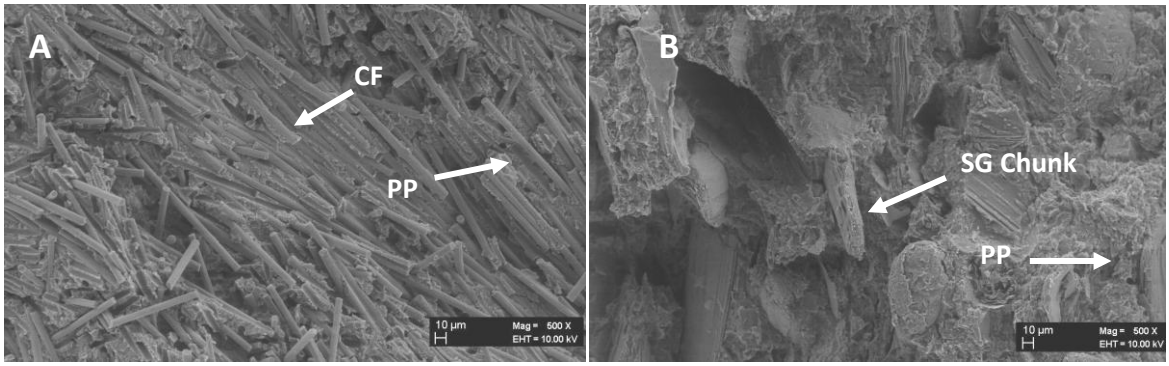

Figure 4-7: SEM micrographs of (A) PP/CF composites (FR3) (B) PP/SG composites (FR4) 500 X magnified

In the two-filler system, the concentration of SG in the PP/SG composite is half the SG loading in the PP/SG composite, so SG chucks can be expanded (during polymer processing) to become thinner layers. As a result, they can occupy more space and act as continuous conductive fillers in the composites (Figure 4-8). In this picture, SG particles are surrounded by CB aggregates that refer to a reduction in an insulating space.

The connection between CB and CF can be observed in Figure 4-9. Carbon black aggregates dispersed inside the cavity, remain after CF was pulled out (Figure 4-9 (A)). It can be implied that carbon black particles contacting the carbon fibers (as seen by those particles contained within the cavity) can produce a conductive network. In Figure 4-9 which shows SEM micrographs of PP/SG-CB composites (FR6) of 20,000X magnified The SEM micrograph (B) Figure 4-9 also shows the dispersion of carbon black in a PP matrix (27.5 %wt of CB), on the boundary of PP and CF, and on the surface of CF. These micrographs confirm that CB particles have a key influence on conductive network formation and increases electrical conductivity of multi-fill composites. The morphology of composites containing SG and CF is shown in Figure 4-10.

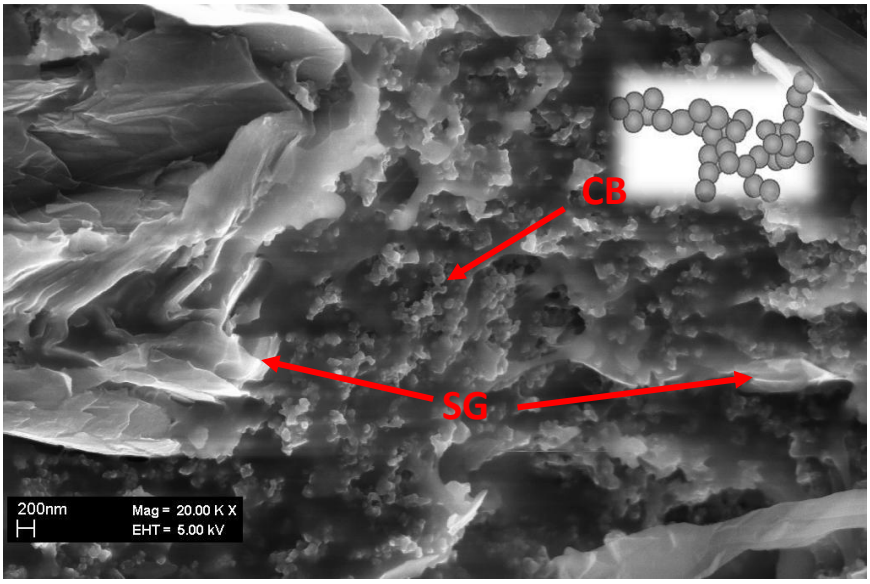

Figure 4-8: SEM micrographs of PP/SG-CB composites (FR6) magnified of 20,000X and a schematic of CB agglomerates.

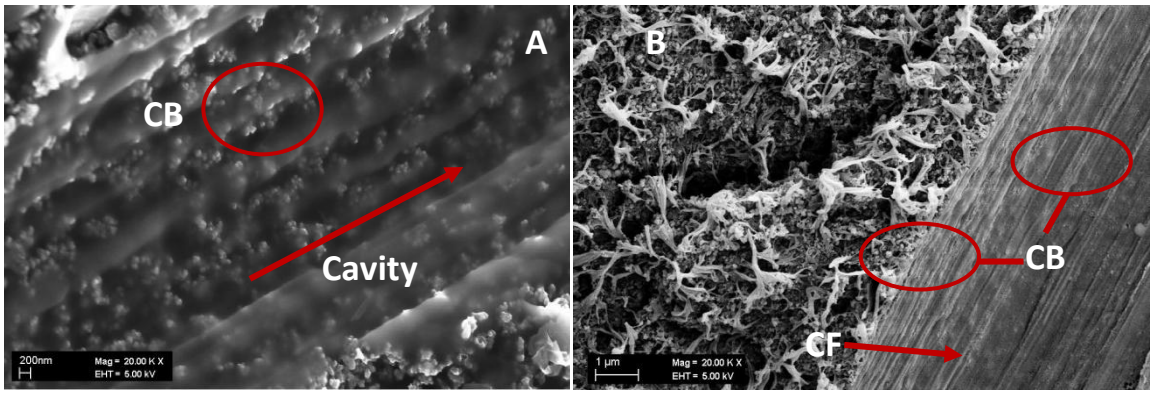

Figure 4-9: SEM micrographs of PP/SG-CB (FR7) composites magnified of 20,000X

The through-plane electrical conductivity of the PP/CF-CB composite (FR7) seems quite attractive, with the conductivity increased to 119 S/m in comparison with the value of the PP/CF composite or FR3 (32 S/m). The improved conductivity can be attributed to CB aggregates distributed on the PP matrix that served as interconnections between the fibers by forming local conductive paths. The paths in this measurement direction (perpendicular to a specimen surface) were increased. Accordingly, the conductivity of this composite was very much higher than the conductivity of composites in the single-filler systems.

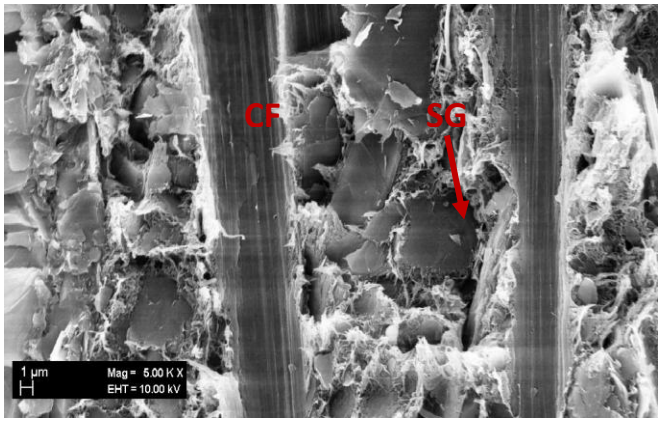

Figure 4-10: SEM micrographs of FR5 composites with magnified 5,000X

Three-filler System

Since single filler has its own specific advantage, a combination of fillers can improve the electrical property and processing characteristics of the composites, as found in the results of the two-filler system. This section explores part the effects of a three filler combination on composites' physical properties. Figures 4-3 and 4-5 indicate the influence of CB on electrical conductivity. In comparison with a 1:1:1 ratio blend (FR14), an increase in the ratio of carbon black used yields a drastic increase in electrical conductivity. Increasing the other two fillers yields marginal effects. It is noticeable that conductivity values of the composites with filler ratios of 4:1:1 and 2:1:1(CB: CF: SG) were higher than the values of other composites. The values of the composite with the filler ratio of 4:1:1were 120 S/m (through-plane) and 1851 S/m (in-plane), and values of the composite with the filler ratio of 2:1:1 were 69 S/m (through-plane) and 1356 S/m (in-plane).

In the case of FR13 and FR10, an increase in the ratio of graphite seemed to have a detrimental effect on electrical conductivity occasioned by an agglomeration of SG flakes, which reduced the conductive network in a composite. If the filler–filler interaction is stronger, the fillers tend to fuse together and are difficult to disperse. Once the fillers are separately dispersed without connection, the formation of a conductive path is retarded. These results indicate that increases in ratios of carbon fiber and solid graphite fillers do not enhance the percolation within the polymer composite.

The in-plane electrical conductivity of the composite with the filler ratio of 1:1:1 was higher than its through-plane conductivity (Figures 4-3 and 4-5) because a CF is anisotropic material, whose properties are directionally dependent. The CF affects the conducting path in the direction of in-plane measurement are greater than a path in the direction of through-plane technique, as the fibers tend to orient in the injection flow direction. If CF concentration is higher, in-plane conductivity was found to be greater. Processing characteristics of the composites in the three-filler system had the same inclination as the one in the two-filler system. The composite containing CB had a high total melting torque, whereas the composite consisting of SG or CF had a lower melting torque (Figure 4-11). Figure 4-13 exemplifies the view of the micro-structural interactions between three fillers in a cross-sectional specimen. A conductive network developed by connections of the three fillers can be observed.

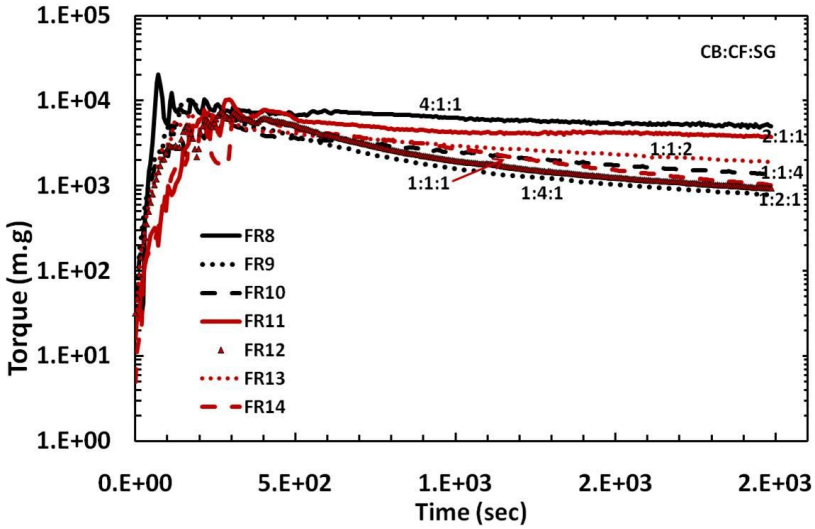

Figure 4-11: Total mixing torque of three-filler composites

The SEM micrograph (Figure 4-12) is comparable in the appearance of a conductive network to a model of the conductivity paths in a composite made of Vectra and carbon-black-coated carbon fiber-reinforced granules (Figure 4-13), as shown by Wolf and Willert-Porada[120]. In the model schematic, insulating polymer granules (white) are filled with electrically conductive carbon fibers (black). At the boundaries of the granules, there are zones of conductive carbon black (grey).

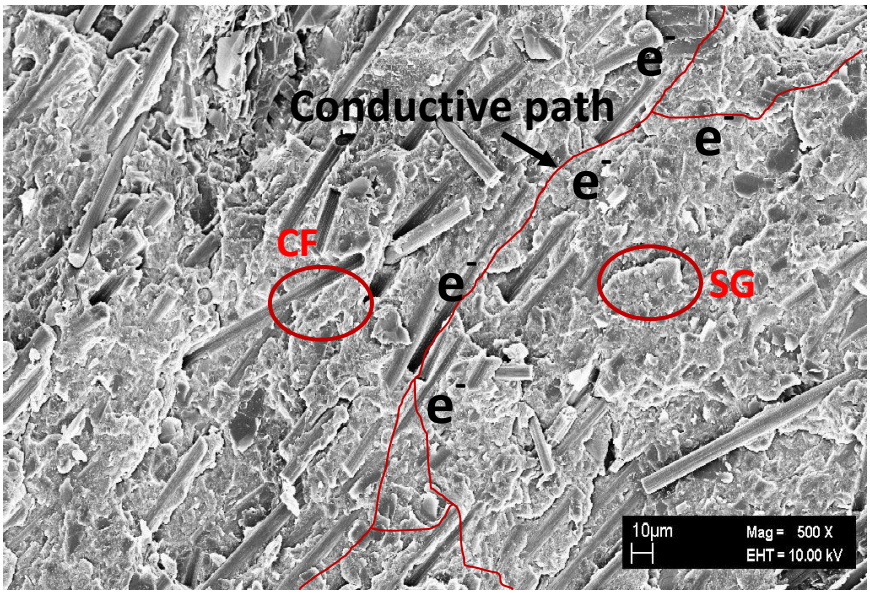

Figure 4-12: SEM micrograph of composite with filler ratio of 1:1:1 (FR14) using magnification of 500X

Figure 4-13: Schematic of a conductive path model [120]

4.1.1.2 Processing Characteristics

As mentioned above, introducing conductive fillers into a thermoplastic matrix typically increases the viscosity of the polymer matrix. The viscosity of composites has to be low enough to allow processing into bipolar plates. In this work, a capillary rheometer was used to determine the effects and interactions of fillers on composite viscosity. Composite rheological data are illustrated in a plot of viscosity as a function of shear rate. Figures 4-14 and 4-15 show the effects of fillers in single-, two-, and three-filler systems with respect to

viscosity. The range of the apparent shear rate used in this work was 10^0-10^3 s^{-1}. This shear range was not suitable for processing these composites into bipolar plates. The typical shear rate of polymer melts in the processing as follows: $10^2 – 10^3$ s^{-1} for extrusion, $10^3 – 10^4$ s^{-1} for injection molding, and 10^0-10^1 for compression molding [121].

For non-Newtonian material the relation between the shear stress and the strain rate is nonlinear, and can even be time-dependent [122, 123]. The plots from Figures 4-14 and 4-15 indicate that viscosity decreases with shear rate increases. PP/carbon filler composites exhibit shear thinning behavior; thus, they can be termed pseudoplastic. Results exhibit a decrease in apparent viscosity with increasing apparent shear rate for all composites.

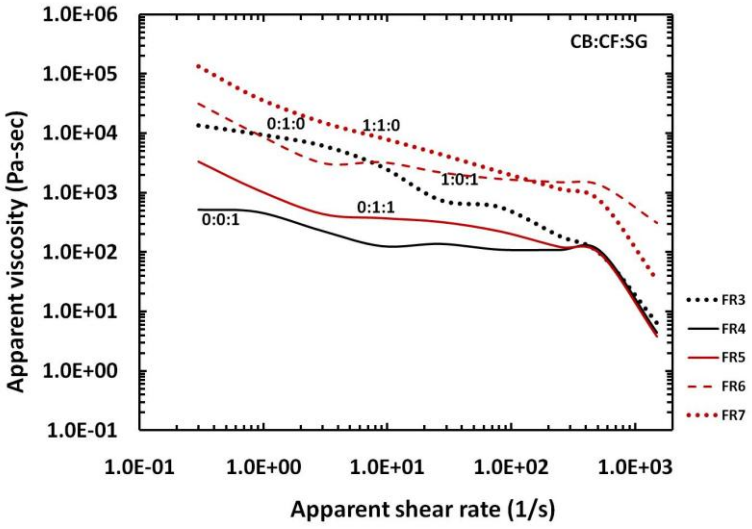

Figure 4-14: Shear viscosity plots for composites containing single and two types of fillers

Figure 4-14 indicates that carbon black particles were in increasing the apparent viscosity of the composites. The results indicated that the viscosity of the composites with added carbon black appears higher than the ones without carbon black particles. Adding solid fillers to molten polymer typically increases the viscosity of the polymer. Literature reports of carbon-filler systems indicate that more filler content leads to more viscosity enhancement [44], because these solid particles hinder polymer flow. Small filler particles, as carbon black particles, have considerable ability to increase the shear viscosity of composites, since they have higher surface area. The high surface area results in the interaction between filler particles and the interaction between fillers with molten polymer. This effect is also due to the unique connective structures that CB forms (CB aggregates) [124]. The carbon black

structure has stronger attractive forces between aggregates, and thus the dispersion process has to provide more energy to separate them, resulting in the high melting torque. If a composite has poor filler dispersion and filler agglomeration, immobilization of the polymer (some molten polymer may be entrapped in spaces between filler particles) will occur [122]. This situation causes high viscosity of the composites. The solid fillers play a significant role in viscosity increases at a low shear rate. It can be noticed that at a relatively low shear rate, the variation of the apparent viscosity was more significant than that at a higher shear rate.

A trend for convergence at high shear rates is due to the increase of yield stress in filled systems. When the yield stress is overcome, steady viscosity is largely unaffected by the filler particles [125]. At a fixed shear rate, the composite containing SG (FR4) had lower viscosity than the PP/CF composite (FR3). Mali reported similar investigations of CF effect on the flow properties of PP [51]. The viscosity of blends with CF depends on fiber orientation, and the lower shear viscosity is owing to fiber orientation in the flow direction. For a two-filler system, the combination of CB and CF provided lower viscosity than the mixture of CB and SG at the same ratio, whereas the two-filler composites containing SG and CF gave the lowest viscosity.

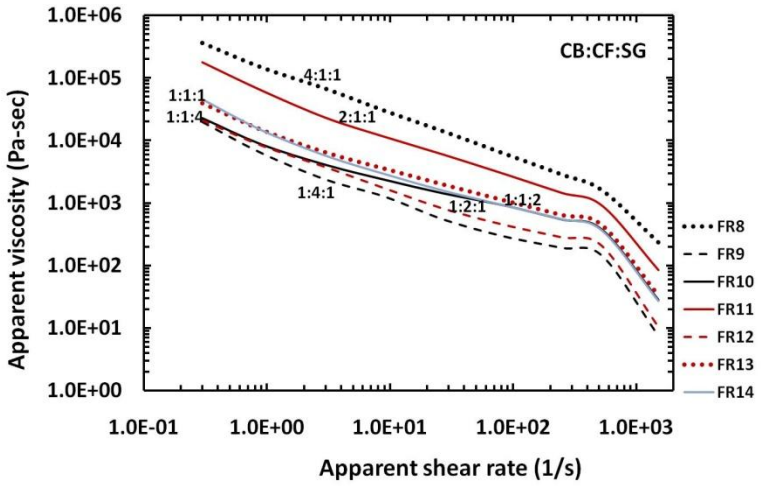

Figure 4-15: Shear viscosity plots for composites containing three types of fillers

Figure 4-15 depicts the flow property of composites in the three-filler system. Apparent shear viscosity was mainly affected by carbon black, and higher carbon black content decreased the flowability of the composites. The experiment produced some unexpected results for a three-

filler system. Higher CF or SG content was the dominating effect, resulting in the decrease of apparent viscosity. The deviation of shear viscosity is also due to how fillers disperse or distribute in the polymer matrix. At proper SG loading, the SG distribution might help carbon fibers orientate in the flow direction more easily than at low concentration. During the experiment, no significant die swell was noted for any of the composites since adding fillers to polymer results in reduced stress accumulation on polymer chains.

The non-Newtonian pseudoplastic characteristics were further corroborated by the power-law equation (Equation 3-7). By extracting the intercept and the slope of log-apparent viscosity versus log apparent shear rate, the consistency index (k) and the power-law index n were determined. The calculations were done in the range of the apparent shear rate from $1\text{-}10^2$ s^{-1} (Figures 4-14 and 4-15).

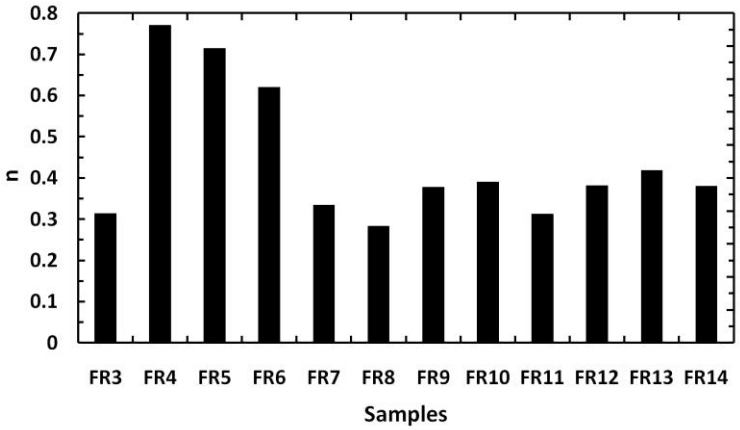

Figure 4-16: Power law index of composites

The power law index (n) is an exponent which explains the deviation of a composite's flow behavior from Newtonian fluid behavior. If n is close to one, the composite fluid has flow behavior similar to a Newtonian fluid. As implied by the results illustrated in Figure 4-16, the power law index n was less than one in all cases, which corroborated the pseudoplastic character of the melt.

For the composite containing only synthetic graphite, its power-law index was approximately 0.61, which was the highest value and occurred because graphite particles were distributed well in the polymer matrix. The power-law index values of composites in the three-filler

system ranged from 0.21 to 0.30. The degree of n decreased with the incorporation of the fillers indicating an increase in pseudoplasticity.

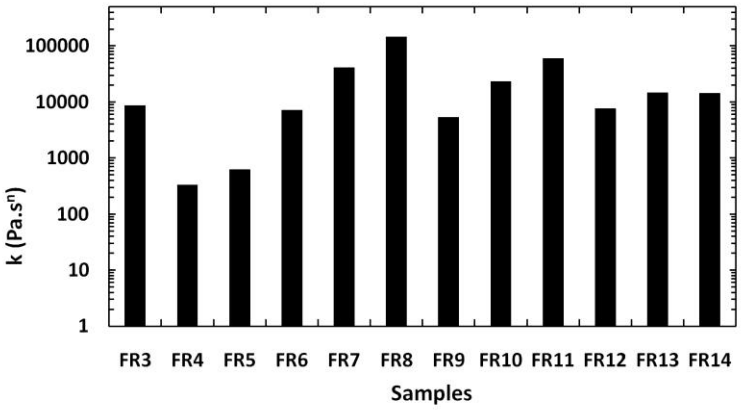

Figure 4-17: Consistency index of composites

The consistency index (k) or zero shear viscosity is shear viscosity at shear rate equals 1 s^{-1}. From Figure 4-17, the consistency index reflects the magnitude of the viscosity in the range from of 500 up to 70,000 $Pa.s^n$. The k index of FR8 and FR11, which have a high carbon black ratio were higher than those of others, since k was correlated to the fill level of CB.

All composites produced from the batch mixer were formed into bipolar plates by the injection molding process described in Chapter 3. During the injection process, operating parameters were recorded to explore the possibility of bipolar plate production by injection molding. The operating parameters fixed for whole composites were barrel temperature (200-200-210-210^oC), screw speed (420 rpm), and hold pressure (19 bars). The significant parameters adjusted during the process, to achieve a perfect bipolar plate shape, are shown in Figure 14-18. The adjustment was related to types of composites and their processing characteristics. Typically, a composite was subjected to large amounts of shear forces during the cavity filling stage in the injection molding process.

If composites are a non-Newtonian fluid, as all composites in this work were, then small variations in the shear rate can cause a large change in the viscosity. The viscosity change will make the mould filling inconsistent, resulting in shot to shot inconsistency [109]. Accordingly, the shear rate is proportional to the injection speed, and the increase in injection

speed will increase the injection pressure. Therefore, the injection pressure was regulated by adjusting the injection speed. In this work, constant injection speeds were maintained to investigate injection pressure variations.

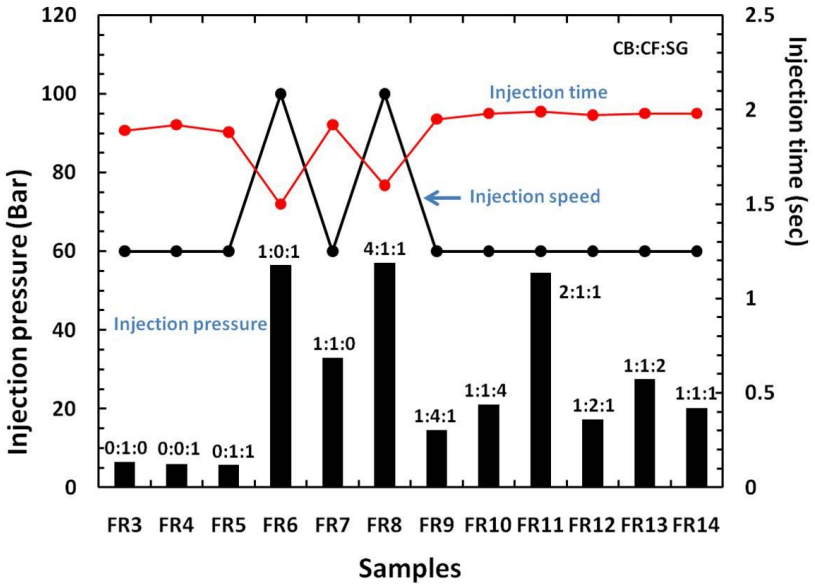

Figure 4-18: The injection operating parameters for composite bipolar plates

The results in Figure 14-18 exhibit that the high injection pressure found for the composites containing a high carbon black ratio. Since the composites containing carbon black had high viscosity, they slowly flowed into the mold. The molten composites cooled before the mold was fully filled, and then a short shot problem arose. To fabricate bipolar plates of a perfect size, increasing the injection speed and shot size was important. Composites with the high ratio of carbon fiber can be processed more easily more easily than others (as seen from the low injection pressure), since carbon fiber orientation was induced by injection pressure in the flow direction. The overall processing time for bipolar plate prototypes was approximately 25 seconds/ plate.

4.1.1.3 Mechanical Characteristics

Bipolar plates provide structural support for the fuel cell stack; therefore, they must be sufficiently strong. If each cell is to achieve good electrical contact with the GDL, cell assembly must be done under certain compression conditions, which require a bipolar plate material of a certain mechanical strength. Mentioned high electrical conductivity requires a high concentration of high loading of conductive fillers. Nonetheless, it is difficult to acquire

simultaneously high electrical conductivity and sufficient mechanical strength from the same materials. Therefore the five properties characterized in this section are compressive, tensile, flexural, and creep properties were chosen for their potential to meet these requirements.

Compressive Testing

Since for the reasons mentioned above a bipolar plate must be under compressive force in the fuel cell, compressive strength, compressive modulus, and compressive yield must be determined. Compressive testing involves compressing the specimen between two metal holders (Figure 3-11). The testing machine for this research was a Mini-mat tester. The maximum load and displacement rate were 200 N and 1 mm/min, respectively. Six specimens for each combination of fillers were tested. The compressive strength was obtained from the maximum stress or the top peak of the stress-strain curve. A 0.2% offset was used in order to determine the compressive modulus and yield strength. The compressive modulus was calculated from the average initial slope of the stress-strain curve up to the engineering yield point. This stress range is in the low-stress portion of the elastic regime.

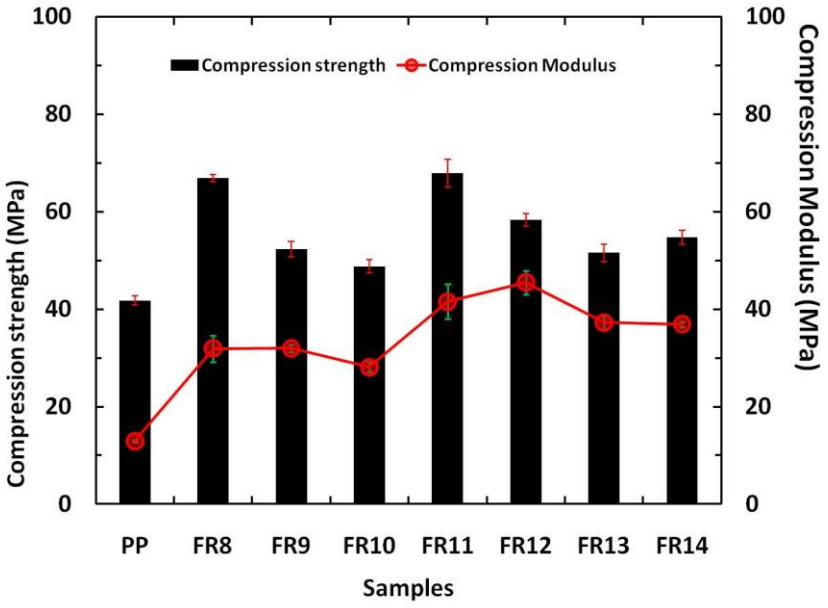

Figure 4-19: Compressive properties of composite bipolar plate with different fillers

Figure 4-19 shows the compressive test results. Filling carbon fillers into polypropylene increases the compressive strength of materials. The compressive strength of a high CB ratio (FR8 and FR 10) was more than 50% higher than that of the neat PP. These results had the

same trend that seen from the publication of Dhakate [46]. The compressive strength of a material is that value of uni-axial compressive stress reached when the material fails completely. The solid fillers distributed to a polypropylene phase, especially an amorphous phase where fillers spread to voids between polymer chains [126]. Furthermore, the application of pressure during the compression process created the compaction of polymer chain-filler composites and decreased the voids between polymer chains. Because of these actions, the composites could support higher forces than the neat PP. The compressive strength dropped with higher graphite ratios, as can be seen in the graphs of FR10 and FR13.

The reduction in strength happened because SG agglomeration occurred at high SG content. Therefore, graphite did not disperse uniformly; causing stress to concentrate at the interconnections between SG agglomerates and the PP matrix. The composite materials can therefore break easily at these points. The modulus values had the same variations as the changes in compressive strength the fillers were added to the PP. The compressive modulus corresponds to the stiffness of material in an elastic regime. It is defined as the ratio of the uni-axial stress over the uni-axial strain in the range of stress following Hooke's Law. The elastic deformation dominates in an amorphous phase, which contains polymer-chain entanglements. If fillers migrate in this region, the material will be stiffer. Since the fillers hinder the movement of polymer chains, the chains cannot rearrange as much as they do in neat PP. The higher stiffness affected the yield strength similar to the way the compressive strength was affected. It is important to note that the compressive strength (maximum stress) of these materials was the same as the compressive strength at breaking point. Figure 4-19 illustrates that the compressive strengths of all composites (the maximum ~ 68 MPa) are greater than the DOE target (50MPa) and bipolar plates in the market [12, 127].

Creep Behavior Testing

Once a fuel cell is operating the bipolar plate will be under the compression and so bipolar plate materials and creep deformation must be kept at a minimum. Creep in PP/carbon filler composites is a complex phenomenon responding material properties (morphology of material) and external factors (applied stress and temperature). Therefore, short-term creep tests in this section were performed by keeping the shear stress constant at 1000 Pa for 2 hr. The tests were operated at 80^{o}C, which is the fuel cell operating temperature. Creep

deformation of a bipolar plate occurs because of a combination of the viscous flow components of viscoelastic deformation [128]. The resulting creep strain increases non-linearly as a function of time, as shown in Figures 4-20 and 4-21. It is noticeable that the creep deformation decreased with the addition of carbon fillers, as was expected with the addition of a rigid reinforcement of a viscoelastic matrix [129]. Therefore, the deformation rates of composites were lower than that of neat PP.

At the beginning of the test (for primary creep), the strain rate was relatively high, and it slowed with increasing strain. Under the applied force and heat, some PP chains started to move, disentangle, and flow over adjacent chains. When the polymer chains move, the fillers could move as well. The force may damage aggregates of CB and SG. The next stage was known as steady-state creep. The strain rate eventually reached a maximum and became near constant due to the buildup of microstructure barriers with complete PP-chain entanglement and rigid filler reinforcement into a viscoelastic matrix. Therefore, the system needs to balance work hardening and thermal softening. The characterized creep strain rate typically refers to the rate in this secondary stage. In tertiary creep, the strain rate exponentially increases with strain because of the necking phenomena represented in the creep curve of FR10 in Figure 4-21. In single-filler systems (FR3 and FR4), in which the composites contained fillers of one type and one shape, fillers may stick together at high filler loading. The filler dispersion was not uniform; therefore, irregular curve were observed. Creep deformation of the composite with 55wt% CF (FR3) was 80% higher than the one for a composite comprised of 55wt% of SG (FR4).

SG layers would slightly spread out under constant force, so thinner SG layers could help a PP matrix to hold the force. Graphite has weak binding between the graphene sheets fused together by weak Van der Waals forces allowing for the interlamellar sliding [130]. The combination of CF and SG diminished creep deformation approximately nine times compared to pure PP.

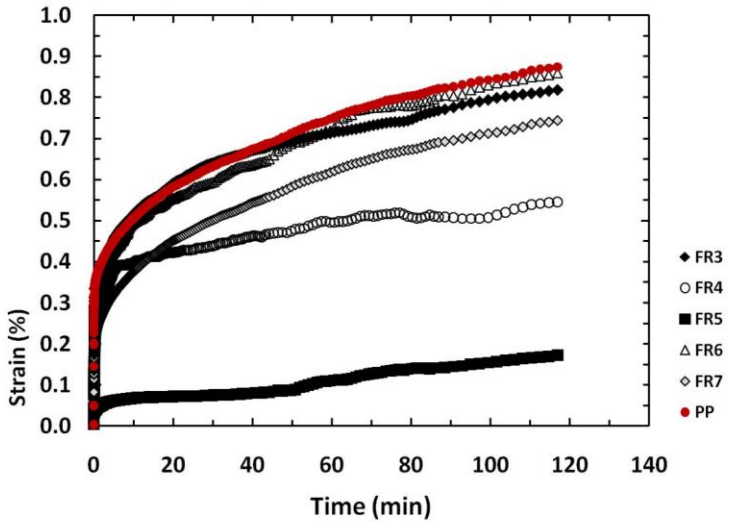

Figure 4-20: Creep deformation of composite bipolar plate in single- and two-filler systems

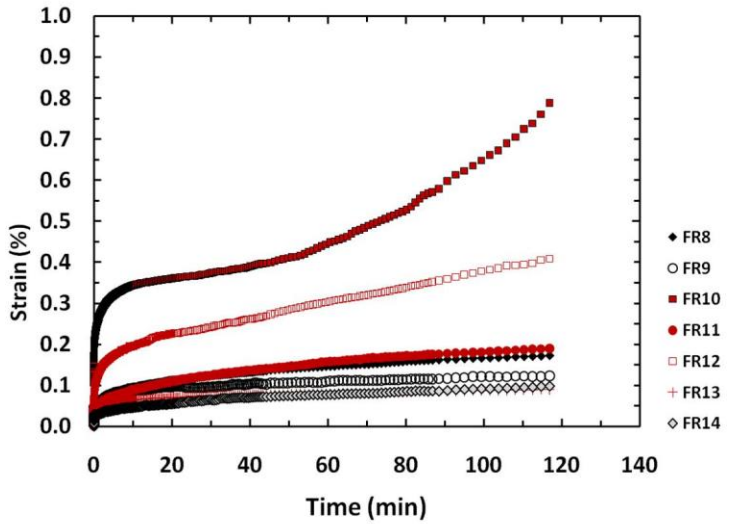

Figure 4-21: Creep deformation of composite bipolar plate in three-filler systems

Most of the samples in the three-filler system had creep deformation lower than 0.3% of strain, which was good for bipolar plate application. They also had longer steady-state creep compared to the composites in single- and two-filler systems, except FR10 and FR12. Necking phenomena was noted on FR10 curve, results correspond to the results from the compressive test. Creep behavior also relates to the variations in electrical conductivity. If bipolar plates have a high deformation rate, electrical conductivity decreases. Compression also has an effect on electrical conductivity discussed further (section 4.5.2).

Tensile Testing

Figure 4-22 shows the variations of the ultimate tensile strength for different composites containing various filler ratios in the three-filler systems. The mean plus or minus the standard deviation for composites is displayed on the graphs. No necking was observed in the samples tested, and the ultimate tensile strength was almost identical to the strength at breaking point. The addition of carbon fillers effectively decreased the ultimate strength of the PP matrix, in agreement with King [131]. Adding high levels of carbon black with a high ratio (4:1:1) caused the tensile strength to decrease from 48.6 MPa to 29.3 MPa. When the tensile force was applied, PP entanglements in the amorphous phase were allowed to release, and then PP chains were induced to align by tensile force. When the chains move close together, the intermolecular force (Van der Waals force) is stronger. The carbon black particles retarded the alignment of PP chains, and the intermolecular forces of between polymer-chains were lower than that of neat PP. Standard deviation values of the composites comprised of high carbon black ratios were wider than those of others, probably because carbon black aggregates would not disperse uniformly in the PP matrix.

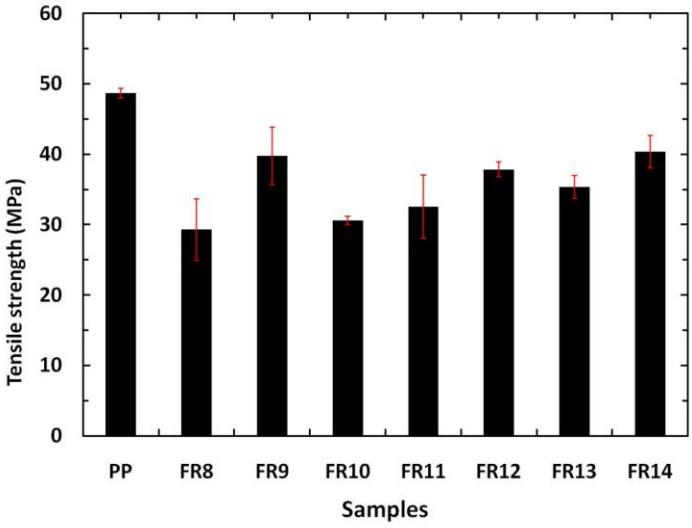

Figure 4-22: Tensile strength of composite bipolar plates in three-filler systems

Introducing carbon fibers is expected to cause the composite tensile strength to increase, since the fiber orientation in the tensile force direction could help material to carry higher forces [132]. However, in this work the tensile strength was not increased with the carbon fiber loading because of the influence of the other fillers. Nevertheless, the tensile strength values

of the composites containing a high a CF ratio (1:4:1) and (1:2:1) were 39.73 and 37.83 MPa, respectively, which were some of the higher values in this set. The results imply that CF is still effective in the composites, but the spherical and flaky particles (CB and SG) cause tensile strength to decrease. At a 1:1:1 filler ratio the tensile strength (40.32 MPa) was slightly higher than the others, and its standard deviation was around 2 MPa. In comparison to the target tensile strength for bipolar plate application, the values of FR9 and FR 14 are promising for application in for fuel cells. Entegris Inc. has produced commercial bipolar plates with a tensile strength of 30 MPa, and PlugPower has set a desired target tensile strength of greater than 41 MPa [131, 133].

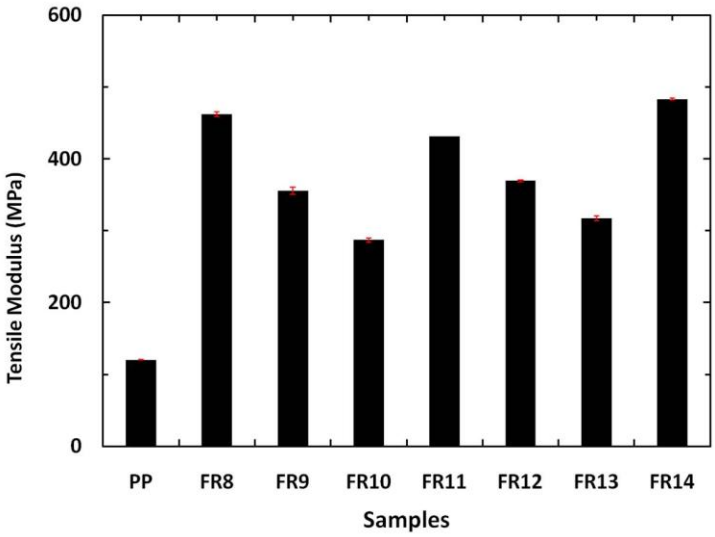

Figure 4-23: Tensile modulus of composite bipolar plate in three-filler systems

The variations of the elastic modulus of PP/carbon filler composites are illustrated in Figure 4-23. Obviously, the results indicate that the modulus for all types of composites increased dramatically from that of neat PP [131]. It is surprising that SG resulted in the lowest tensile modulus (287MPa). At this time the modulus values of composites have not achieved the target value of commercial bipolar plates [133].

4.1.1.4 Single Cell Performance

The aim of this part of the research was to investigate the effect of filler ratios in composite materials on the performance of PEMFC. Using polarization studies to evaluate performance are typical for any electrochemical system. Figures 4-24 to 4-27 show polarization curves for the one-cell PEM fuel cells with various bipolar plates containing fillers in various ratios

(CB:CF:SG). The thickness of the bipolar plates used in this research was 3 mm, and the cells had an active area of 16 cm^2. All components and operating conditions are described in section 3.2.

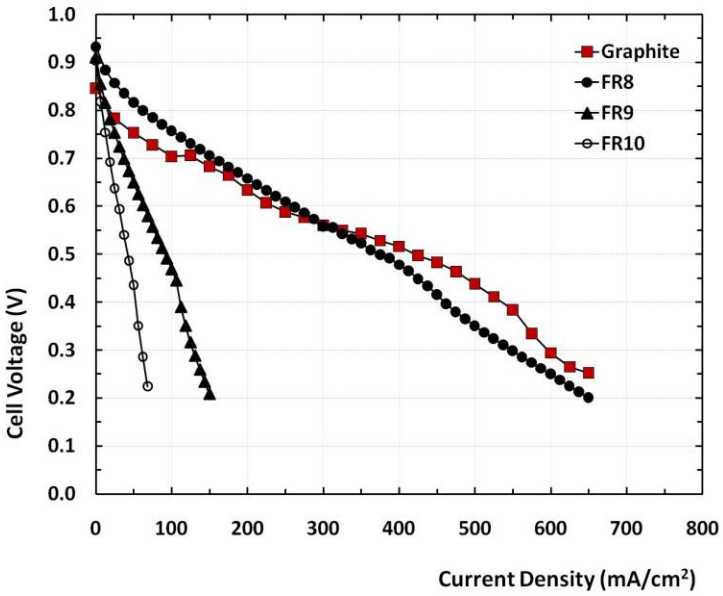

Figure 4-24: Initial performance of the single cells assembled with different bipolar plates

Figure 4-24 presents the comparative initial performance of the single cells assembled with graphite, FR8 (4:1:1), FR 9 (1:4:1), and FR10 (1:1:4) bipolar plates. It is important to note that three cells of each type of a bipolar plate were operated, and each cell showed similar results, so only the results from one cell of each type are shown. These curves were obtained by increasing the load level with scan rate: 0.1A/min from the cell and monitoring the cell voltage. The open circuit voltage (OCV) of the single cells was almost the same at 0.95 V. The OCV values dropped to a range of 0.85 to 0.93V after approximately 6 h and remained stable afterwards. Figure 4-24 indicates that the OCV of the cell assembled with graphite bipolar plates, 0.85 V, was slightly lower than those of composite bipolar plates.

At low current densities, the single cells exhibited almost the same performance. The FR8 bipolar plate showed a slightly higher performance than the graphite plate; however, its rate of voltage drop (IR loss) with increasing current density was higher than the change in the graphite plate because of its lower conductivity.

At a cell voltage of 0.6V, the current density of the single cells using graphite, FR8, FR9, and FR10 bipolar plates was 224.81, 262.313, 37.50, and 15.5 $mAcm^{-2}$, respectively. The results can probably to be attributed to the lower conductivity for single cells assembled with PP/carbon filler composites. The performance curve confirms the positive correlation between electrical conductivity and fuel cell performance: an increase in electrical conductivity yields a proportional increase in performance. For instance, FR8's in-plane and through electrical conductivity values were roughly three and four times higher than that of FR9. Subsequently, the fuel cell containing FR8 performed three times "better" than FR9. Those current densities were 184.268 and 45.97 $mAcm^{-2}$, respectively.

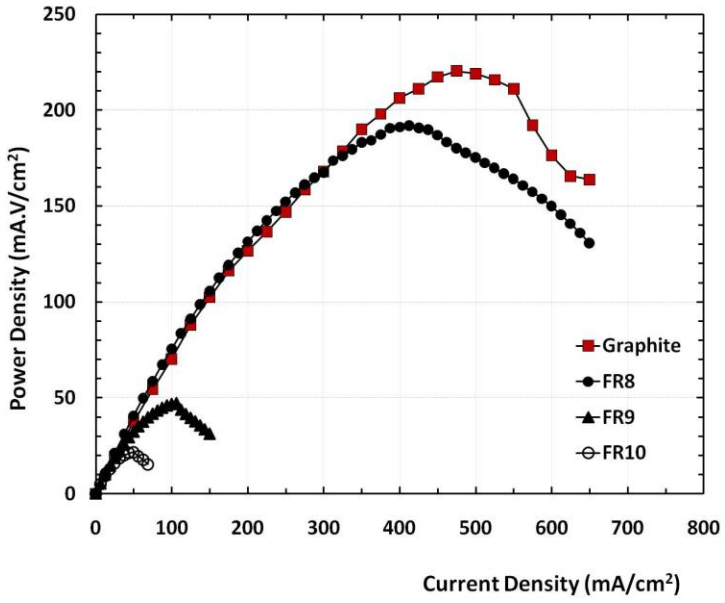

Figure 4-25: Power curves of the single cells assembled with different bipolar plates

From Figure 4-25, the best behavior of single cells using composite bipolar plates was observed for the FR8 composite, with a power density of 192.00 mW/cm^2 at 412.38 mA/cm^2. The fuel cell assembled with FR8 bipolar plates presented only slightly lower overall performance than the cell using graphite plates, although the electrical conductivity of the graphite plate was higher than that of the FR8 plate (i.e., 1,170 S/cm and 19 S/cm for in-plane conductivity). For the in-plane electrical conductivity testing, four probes were inserted below the surface of a specimen. The graphite plate had a high density of graphite particles close to the specimen's surface, whereas the FR8 plate may have lower filler dispersion close

to the surface. Under compressive force during the operation, carbon fibers in GDLs compacted with bipolar plates may penetrate the surface layer of FR8 composite bipolar plates, since the composite material is more flexible than the graphite. Subsequently, contact resistance between the GDLs and the bipolar plate would be lower, resulting in increased the cell performance.

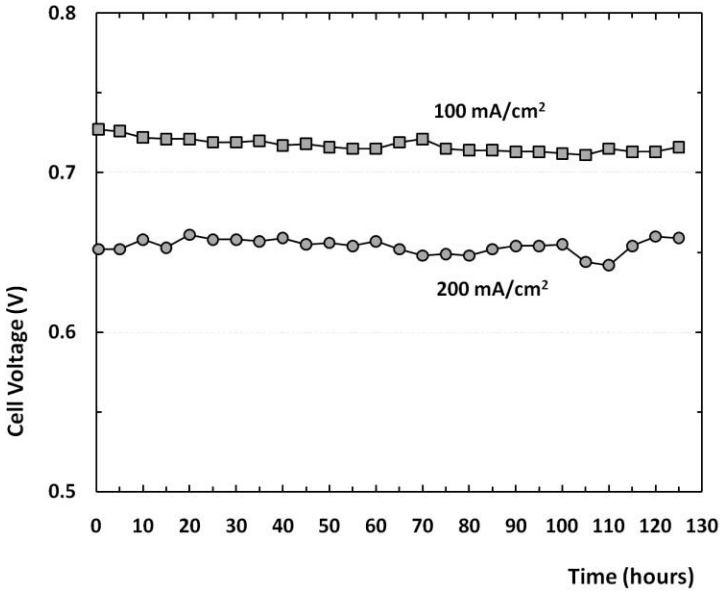

Figure 4-26: Steady-state tests of the single cell assembled with FR8 bipolar plates

Figure 4-26 shows the short-term performance of the fuel cells; the fuel cells were operated over 125 hours at a constant current density of 100 and 200 $mAcm^{-2}$. The performance did not obviously degrade; however, this operation time is not long enough for a comprehensive durability assessment, and more assessment is required.

All the results demonstrate that a high ratio of carbon black dominates the electrical conductivity of bipolar plates and the performance of the cell. This finding is confirmed by Figure 4-27, which shows polarization and power curves of the fuel cells assembled with FR11 (2:1:1), FR12 (1:2:1), FR13 (1:2:2), and FR14 (1:1:1). Results show that the single cells perform almost the same, except the one using an FR11 bipolar plate (containing a high CB ratio).

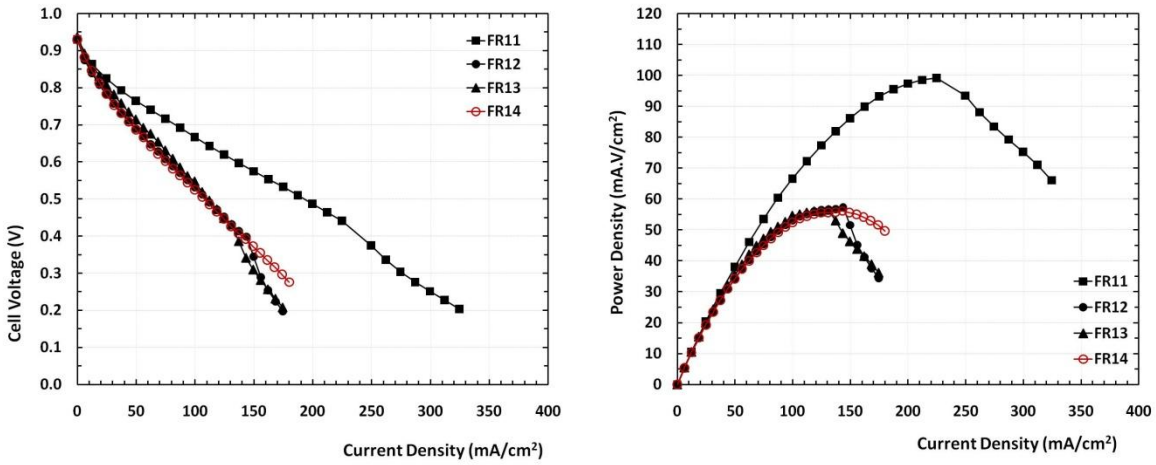

Figure 4-27: Initial performance of the single cells assembled with FR11-FR14 bipolar plates

Compared with the polarization curves in Figure 4-27, the bipolar plates containing a higher ratio of SG or CF resulted in poorer performance. Once again, this finding can probably be explained by the poor filler dispersion in the PP matrix causing less connection between conductive fill particles. The performance of PEMFCs (single cell) using carbon composites has been reported in the literature as follows. Kuo and Chen produced composite bipolar plates made of Nylon-6 and S316L stainless steel alloy fibers, with a 25 cm^2 active area [61]. Their maximum power was 0.3 W/cm^2 (W/cm^2 = $A.V/cm^2$). Carbon black (CB) and polyvinylidene fluoride (PVDF) composite bipolar plates with 50 cm^2 of active area gave 0.075 W/cm^2 [39]. Cho et al. reported the performance of a single cell (active area 25 cm^2) assembled with an unsaturated polymer/graphite (90 wt%) composite as 0.69 W/cm^2 [104]. All authors reported that composite bipolar plates were produced by a compression molding process. Heinzel el al. reported the performance of 20-cell PEMFCs that provided electrical power of 100 to 200 W [134]. These 25cm^2 fuel cells assembled with polymer/graphite composite bipolar were plates were successfully fabricated using an injection molding processes. Information from the literature and comparing the cell performance of graphite and FR bipolar plates indicates that the FR8 blend does show promise for future opportunities as a composite materials within PEMFC.

AC Impedance Characterization

AC impedance spectroscopy for single cells with different bipolar plates was conducted to clarify the internal resistance of single cells involved in the operation. The approach for this

characterization is described in Chapter 3. The intersections with the real axis in the impedance spectrum at high frequency reflect the ohmic resistance of a fuel cell. This resistance can be expressed as the sum of the contributions from contact resistances between components and ohmic resistances of the cell components such as the membrane, catalyst layer, gas diffusion layer, and bipolar plate [135]. All operation conditions and all fuel cell components, except the bipolar plates, were kept constant; the domain effect on ohmic resistance came from the type of bipolar plates [104]. The ohmic resistances support the fuel cell performance results and interpretation discussed previously (Figure 4-27). These resistance values ranged from 8.80×10^{-2} to 0.48 ohm, and the decrease in ohmic resistance had the identical trend to the fuel cells' change in polarization. The resistances the fuel cell using graphite and FR8 bipolar plates were 8.82×10^{-2} and 8.80×10^{-2} ohm, respectively (Table 4-2).

Table 4-2: Fuel cell resistance at high frequency of single cell using different bipolar plates

Samples	In-situ ohmic resistance (Ω)
Commercial graphite	0.0800
FR8	0.0830
FR9	0.2286
FR10	0.4799
FR11	0.1134
FR12	0.2217
FR13	0.2168
FR14	0.2104

4.1.2 Conductive Polymer and Different Types of CF_S

4.1.2.1 Electrical Conductivity of Composites

Polypyrrole Effects

As mentioned in Chapter 2, intrinsic conductive polymers such as polyaniline and polypyrrole can increase the electrical conductivity of polymer blends significantly. For of fuel cell applications, researchers typically use intrinsic conductive polymers for MEA electrical conductivity improvement in the electrode. Less attention has been given in the literature to the use of conjugated conducting polymers in composite bipolar plates' perhaps

because conductive polymers are quite expensive. Melt compounding was adopted in this research, and polypyrrole (PPy) was used as an additive for the preparation of composites to explore the ability of PPy to increase the electrical conductivity of the material. The composite formulations in this section are described in Tables 3-5 and 3-7, Chapter 3. To study the effect of PPy on the electrical conductivity of composites, 1.8wt% of PPy was introduced into PP/carbon filler composites (with 55wt% of carbon filler loading) in a preliminary experiment. The formulation of PP/carbon filler composites with PPy prepared in the batch mixer is reported in Table 3-1, and mixing parameters are described in section 3.1.4.1. The torque in the mixer was measured during the melt-mixing process. A comparison between PP/carbon filler composition and the composite prepared with 1.8wt% of PPy is shown in Figure 4-28.

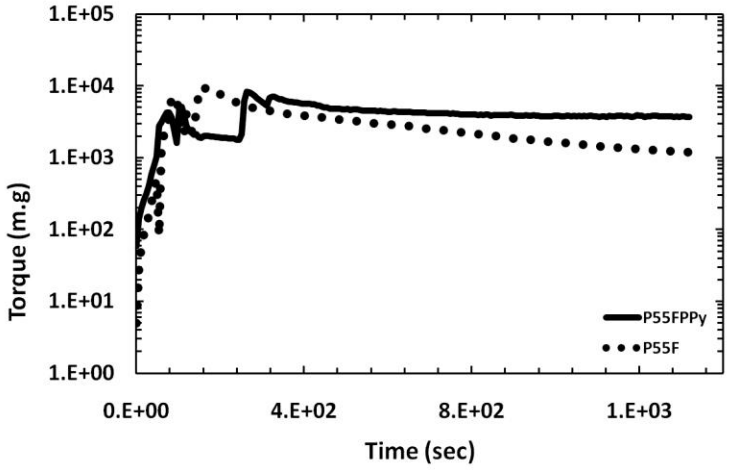

Figure 4-28: Total mixing torque of PP/filler composites with and without PPy

The torque curves were recorded from the point when the fillers were added to the polymer already melted until the value was constant (uniform flow conditions). The sequence for adding filler into the polypropylene composite is described in section 3.1.4.1. Approximately four minutes were spent to complete the addition of fillers to the melted polypropylene in each experiment. As shown in Figure 4-28, adding PPy into the composite required a higher torque to promote mixing between filler and matrix. PPy is a chemical compound formed from a number of connected pyrrole ring structures, giving it a rigid backbone (Figure 2-10); moreover, the intermolecular forces of PPy chains are of the hydrogen bonding type. Since

PPy has high stiffness chains, which are harder to flow and to disperse in the PP matrix, higher torque was required compared to torque of the composites without PPy content.

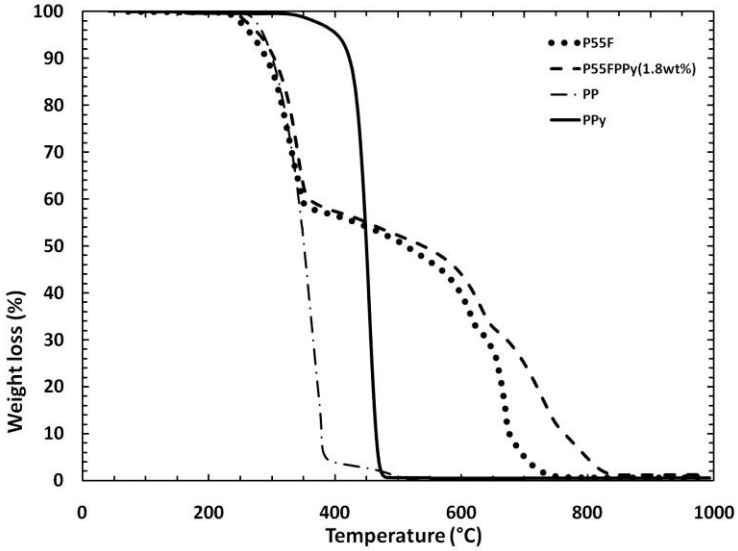

Figure 4-29: Thermogravimetric curves of the composites with and without PPy content

The composites produced by the batch mixer were shaped into bipolar plates by an injection molding process as described in Chapter 3. Although the difference in their torque was discovered, bipolar plates of both composites could be injected with identical operating parameters, which can be seen from the injection parameters of FR14 in Figure 4-18. TGA was used to determine the actual filler loading and thermal stability for each sample (Figure 4-29) after the compounding.

The composite shows weight losses at these two regions, the first of which corresponds to the burning of polypropylene, while the second corresponds to the burning of fillers. The change in weight directly translates to the amount of fillers in the composite. Because of a very small amount of PPy and the overlapping of filler decomposition and PPy, the change in weight because of PPy content could not be identified. In Figure 4-29, the decomposition temperature was obtained. PP decomposition occurs at around 350^{o}C, while polypyrrole burns off at approximately 450^{o}C. The PPy decomposition temperature in this research is close to the value reported by Veeraraghavan et al.[58], and agrees with the PPy value of PPy specified by Sigma Aldrich 9 (Appendix A).The composites decompose close to the PP matrix, and the composite containing PPy has a somewhat higher decomposition temperature

than the composite with no PPy. The influence of the PPy at 1.8wt% on the electrical conductivity of composites was first investigated in a preliminary experiment, as shown in Figure 4-30.

The blend was produced with an intrinsically conductive polymer, polypyrrole, at a level of 1.8%wt. The in-plane conductivity (in the injection flow direction) of the 55%wt composite with PPy is 22% higher than that of the blend without PPy (P55F). Perpendicular to the injection flow direction the value of P55FPPy is around 7% higher than P55F's. PPy can also play a role in the composite conductivity for through-plane electrical conductivity, and the values increased by 6%. This suggested that applying PPy as a conducting additive was successful in further improving electrical properties of the composites, since the PPy enhances the connectivity of the conductive filler electrical percolation matrix, in agreement with the research done by Omastova and Pavlinec[55].

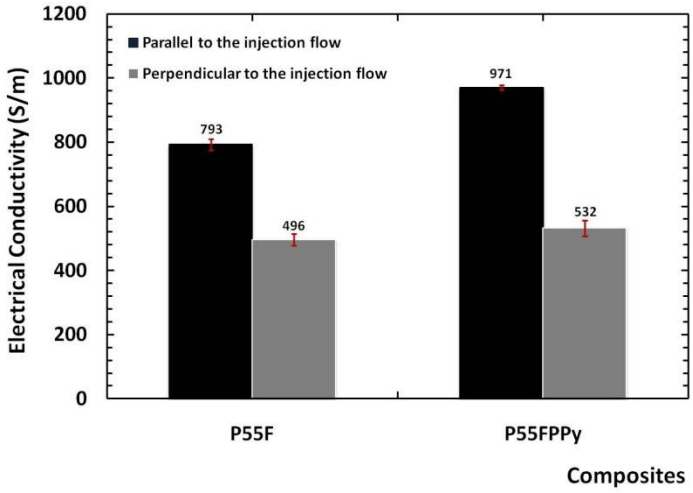

Figure 4-30: In-plane conductivity of P55F and P55FPPy composite with 1.8% PPy.

Typically, PPy mixes with PP as an immiscible blend [55] and may also coat the surface of fillers [136]. FourBier et al. [137] noted that conductive polymer (PPy) increases the electrical conductivity of epoxy/CB composites, and Radwan et al. concurred with this assumption [62]. Radwan and Jaafar added polyaniline (PANI) to PP/graphite and PP/CB composites for the bipolar plate application. On the other hand, research published by Omastova in 2003 showed that the electrical conductivity of a with composite filled CB particles which had surface modification by PPy and PANI, was about one order of magnitude lower than an

unmodified CB composite [138]. From Figure 4-30, the samples cut in the direction of the injection flow gave a greater increase of in-plane electrical conductivity.

This finding can be explained by the contribution of surface conductivity. Four probes for measuring in-plane conductivity were inserted into the surface of a specimen and touched the filler surfaces. There was more opportunity to touch CF surfaces because carbon fibers were induced by injection pressure to orientate in this direction. If part of a filler is coated with PPy, more electrons run along the through conductive paths. In contrast, there are less conductive connections in perpendicular to injection flow direct that is because of more numbers of insulating gaps (Figure 4-31). Unlike the previous results, the electrical conductivity data of specimens cut in both directions was slightly changed in the through-plane technique.

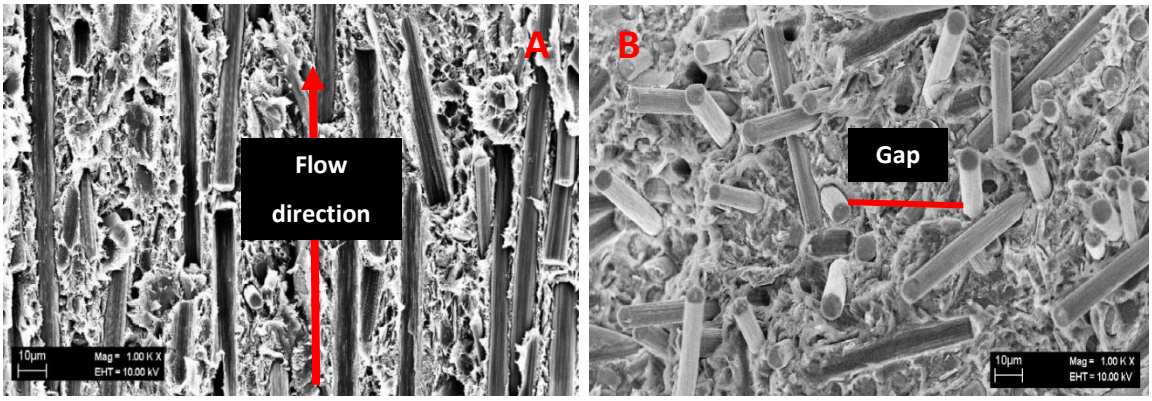

Figure 4-31: SEM micrographs of P55FPPy injection specimens cut in parallel (A) and perpendicular (B) to injection flow direction (magnification: 1kX)

To further explore the effect of PPy on electrical conductivity, composites comprising of various PPy loadings were characterized in order to observe the effect of PPy concentration on their conductivity. Composites in this section were compounded in a micro-compounder as explained in section 3.1.4.2. The total mixing torque during the processes was recorded; it appears that the torque increased with increased PPy concentrations from 127 to 170 N.cm (Table B-1, Appendix B). Composites produced with the micro-compounder were injected into small bars at injection pressures ranging between 80 to 90 psi (section 3.1.5.2).

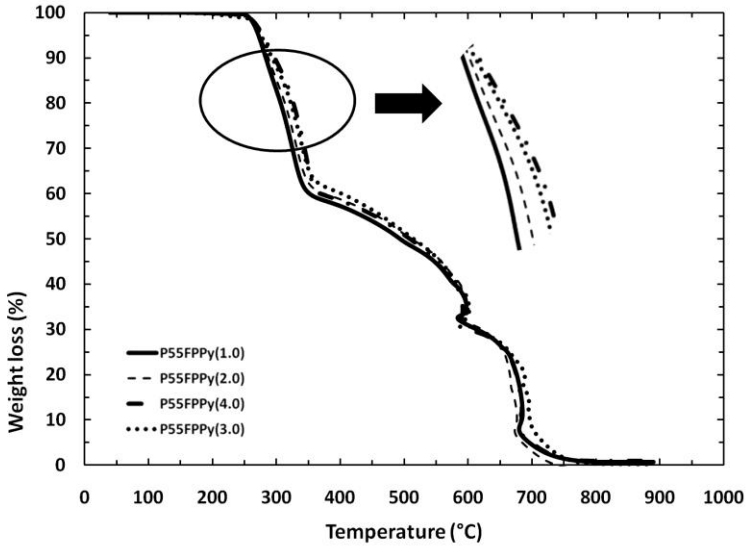

Figure 4-32: Thermal behavior of PP/filler composites with different PPy concentration

TGA was also performed to observe the thermal stability of composites as a function of time. The stability improves as PPy loading increases (Figure 4-32) due the synergistic influence of PPy, which has a higher decomposition temperature than the PP matrix.

The data in Figure 4-33 indicate an increase in the composites' conductivity as PPy concentration increases. This observation appears to agree with that of Ketpang and Park, who explored a positive effect of PPy on the electrical conductivity of PVDF/PPy/MWNTs composites [139]. The in-plane conductivity of the PP/carbon filler composite was increased by incorporating PPy up to 3 wt% (271S/m), and then the conductivity slightly decreased from this value when the PPy level was brought to 4 wt%. The percolation threshold is observed in the vicinity of 2wt%, since the conductivity significantly increased after this point. In terms of through-plane electrical conductivity, the percolation threshold is in the locality of 1.5 wt%, and the highest conductivity is 89 S/m at 3wt% of PPy. These synergistic effects can be explained by the enrichment of the PPy at the interface between fillers and PP matrix [62]. *Note*: the in-plane conductivity represented in Figure 4-33 was measured using small four point probes.

The influence of polypyrrole levels in the PP/PPy, PP/SG/PPy and PP/CF/PPy composites on their through plane electrical conductivity was also investigated (Table 4-2). All formulations of the composites are indicated in Table 3-6. The reported values in Table 4-2 represent the

average of twelve readings for each sample. The results exhibit the expected trend of an increase in conductivity as PPy is incorporated into the composites and as PPy loading is increased.

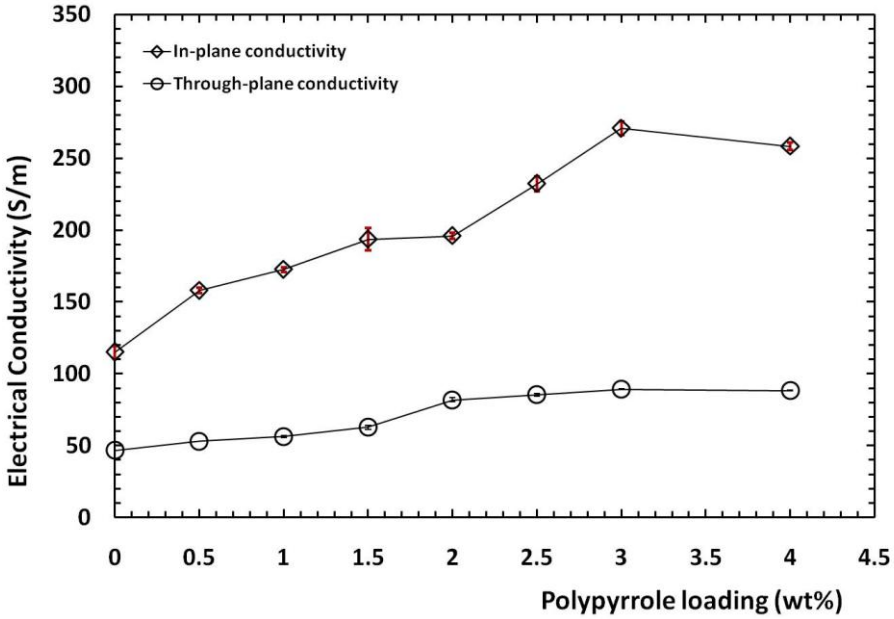

Figure 4-33: Electrical conductivity of PP/filler composites as a function of PPy loading

Applying PPy into PP/SG (55wt %) and PP/CF (55 wt %) composites can increase the electrical conductivity from 0.099 and 31.867 S/m up to 1.201 and 35.786 S/m, respectively. The blends of PP/PPy with 1.8 and 4wt% of PPy loading can increase the electrical conductivity of material; the change in values are, however, quite low. It is important to note that both conductivity values of PP/PPy blends in Table 4-3 are in the range of those measured by Omastova[55] .

Table 4-3: Absolute values of through-plane electrical conductivities of composites

Sample	Through-plane electrical conductivity (S/m)	SD
PPy(1.8)	1.266E-10[a]	1.531E-11 (n = 12)
PPy(4.0)	3.611E-10[a]	4.386E-11 (n = 12)
PCFPPy	35.786	4.507 (n = 12)
PSGPPy	1.201	0.043 (n = 12)

Note: [a] Through-plane electrical conductivity was measured using Agilent E4980
A Precision LCR Meter (Frequency 1 kHz, Voltage 20V, and Current 900 nA)

Figure 4-34 shows that PPy in the PP/PPy blend (i.e., no carbon fill) tends to distribute as small spherical granules within the PP matrix. The phase separation remains due to the interfacial tension between PPy and PP matrix, and then causes electrical conductivity of the blend to be low. The interfacial tension occurs because PP contains non-polar polymer chains, while PPy chains are polar molecules. In other words, the PPy spherical granules do not make contact with their nearest neighbors due to partial wetting by the PP matrix.

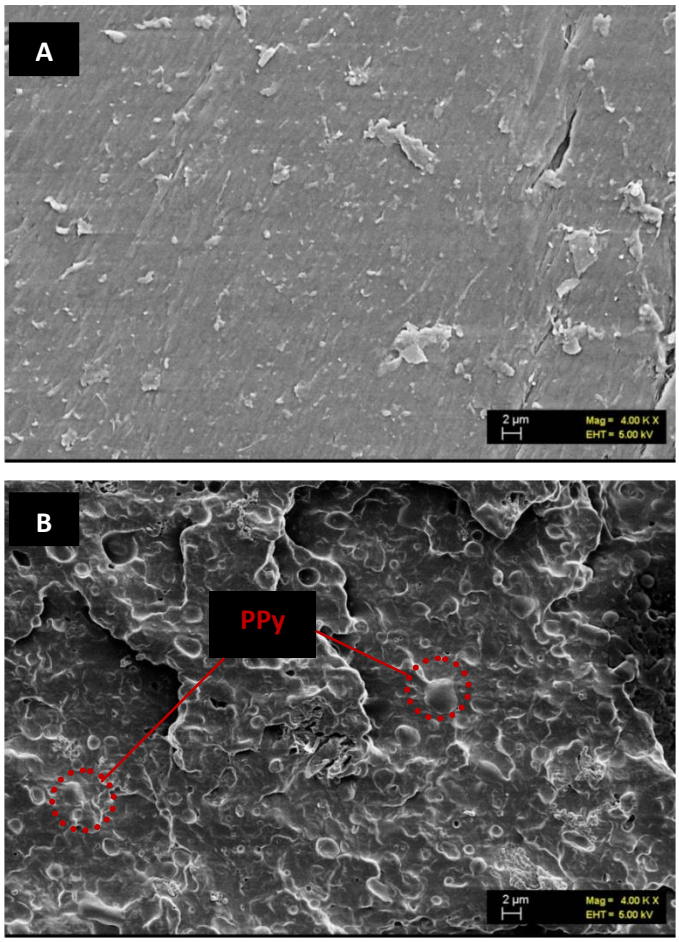

Figure 4-34: SEM micrographs of (A) PP and (B) PP/PPy(4wt%) composite (magnification 4kX)

The picture of PP/PPy composite (B) is similar to the SEM micrograph published by Lee et al. [140]. All results imply that filler connections play a main role on electrical conductivity of the material. PPy acts as a conducting additive dispersing on the interface between fillers and the polymer matrix, and it can also coat some parts of filler surfaces. These functions of PPy improve the number of conductive paths. Regards to cost of PPy itself and its

significance to improve conductive paths, PPy is recommended to use as an additive instead of the PP/PPy blend for a bipolar plate application.

Effects of Different Sizes of Carbon Fibers

As mentioned, the aspect ratio of fillers affects on conductive network formation; thus, investigating a combination of fillers with different sizes and the changes in electrical conductivity is worthwhile. Three carbon fibers, their diameters and lengths are shown in Table 4-4. These were used in this section of work. All composite formulations used to investigate the influence of CFs are explained in Table 3-6, and the results from TGA are presented in Appendix B.

Table 4-4: Sizes and diameter of three carbon fibers

Carbon Fibers	Diameter	Length
CF(A) (A = Fortafil® Fiber)	6-7 μm	6 mm
CF(B) (B = AGM-99)	7-9 μm	150 μm
CF(C) (C = Carbon nanofiber)	50-200 nm (outer)	10-70μm

The two-fiber combination's influence on electrical conductivity is shown and is shown in Figures 4-35 and 4-36.

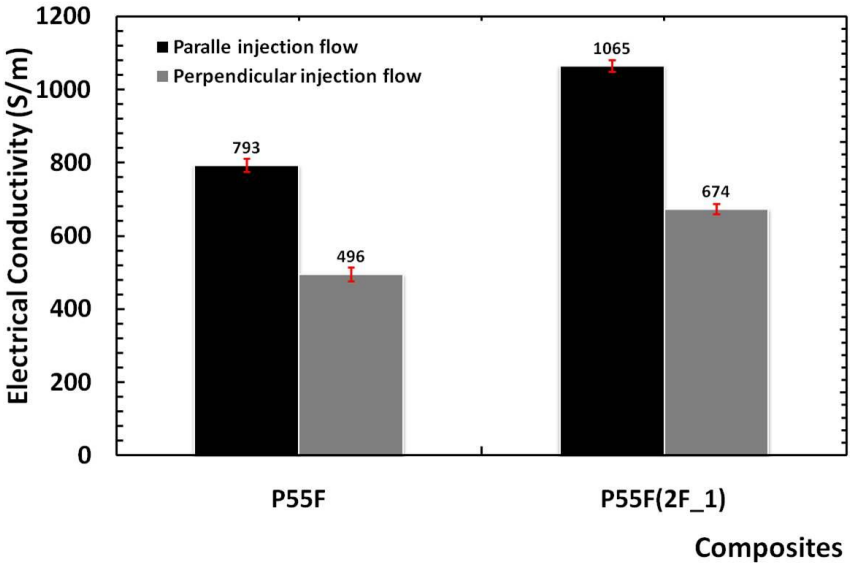

Figure 4-35: The in-plane electrical conductivity of composite with CF (A) and CF (B)

The combination of CF (A) with CF (B) has a synergistic effect on that conductivity. The maximum achievable in-plane conductivity was 1065 S/m, while the through- plane conductivity was 57 S/m. These values are roughly 1.34 times higher than those of composites that used only one type of a carbon fiber (for the in-plane). Note: the in-plane conductivity represented in this section was measured using a small four-point probe tester. The reason for these results can be explained with the aid of the images in Figure 4-37.

Figure 4-37 reveals that smaller fibers are located in a space (which might be an insulating space) between other fibers; thus, the fiber insert is able to increase a network's conductively, especially in the through-plane direction. If the composite contains fibers of a variety of fiber lengths, fibers can fill into different sizes, as seen in Figure 4-37.

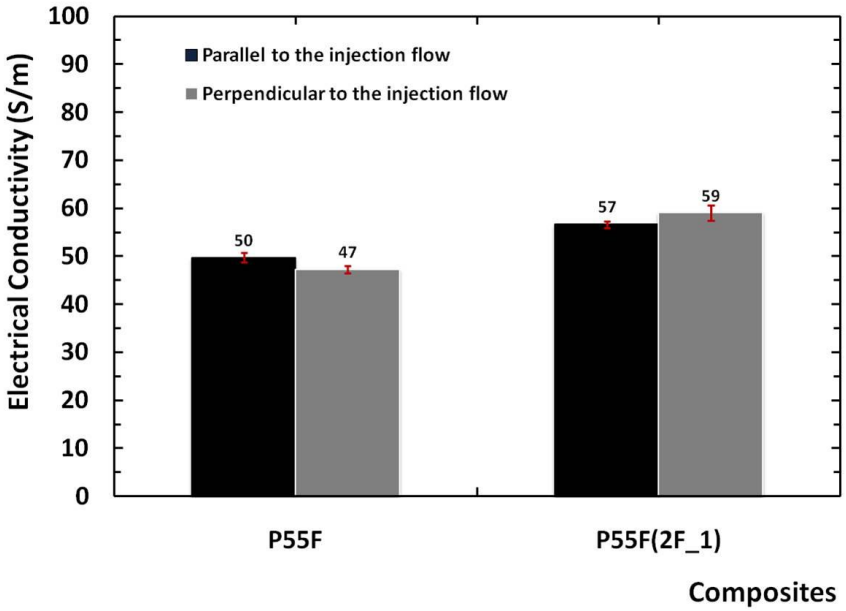

Figure 4-36: The through-plane electrical conductivity of composite with CF (A) and CF (B)

In addition to these two types of fibers, carbon nanofibers were combined with PP/carbon fillers, since carbon nanofibers (CNF) have a high aspect ratio. Formulations of composites containing CNF are described in Table 3-6. First, PP/CNF blends and PP/CNF/PPy blends (Table 4-5) were tested. CNF leads to an increase in the electrical conductivity of the blend, and the reported conductivity values of the blend containing 1.8 wt% and 4wt% of CNF are within the range of the reported conductivity of PP/carbon nanotube composites (10^{-9} - 10^{-5}

S/cm) [141]. These values are; however, lower than those of the PP/three-carbon filler composites.

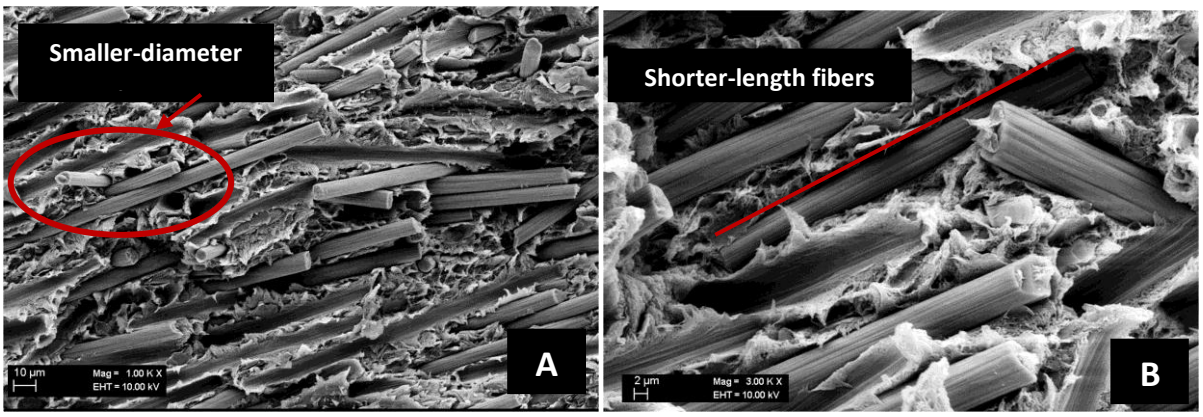

Figure 4-37: Morphological pictures of P55F (2F_1) composite
(magnification: 1kX (A) and 3kX (B))

Although, CNFs have a very high aspect ratio, enabling them to create conductive systems at a low-volume fraction, conductive network formation depends on many factors, the factors include for example: CNF aspect ratio, nanofiber dispersion, nanofiber distribution, nanofiber conductivity, polymer matrix crystallinity, and polymer matrix surface tension [142].

Table 4-5: Absolute values of composites' through-plane electrical conductivities [a]

Sample	Through-plane electrical conductivity (S/m)	SD
PCF(C)_1	4.835E-09	6.921E-10 (n = 12)
PCF(C)_2	4.493E-05	1.420E-05 (n = 12)
PPyCF(C)	7.167E-05	2.381E-05 (n = 12)

Note: [a] Through-plane electrical conductivity was measured using Agilent E4980 A Precision LCR Meter (Frequency 1 kHz, Voltage 20V, and Current 670 μA)

SEM micrographs reveal that CNFs distribution to the in the PP matrix and CNT aggregates can be found in some areas (Figure 4-38). CNF distribution on the PP matrix is quite homogeneous, but less conductive connections were formed [143]. Since the size of CNFs is very small, a higher amount of 3.5wt% of CNF is required to achieve a conductive percolation threshold [141]. This supposition, the effect of incorporation of CNF with CF (A) on composite conductivity, was also investigated.

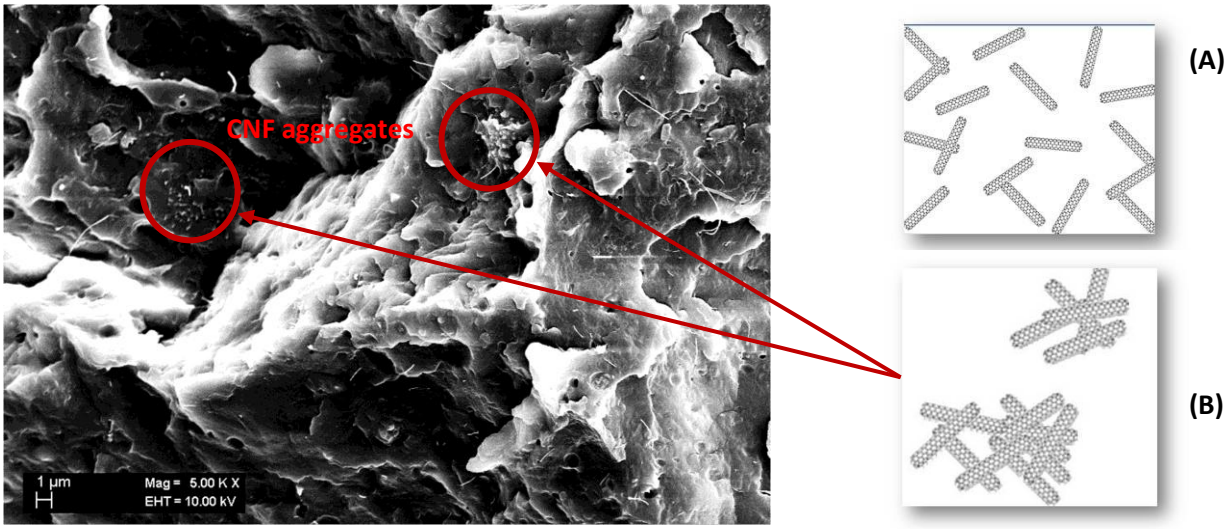

Figure 4-38: SEM pictures of PP/CNF blended with 1.8wt% of CNF loading (magnification 500 kX):(A) CNF connections and (B) CNF aggregates

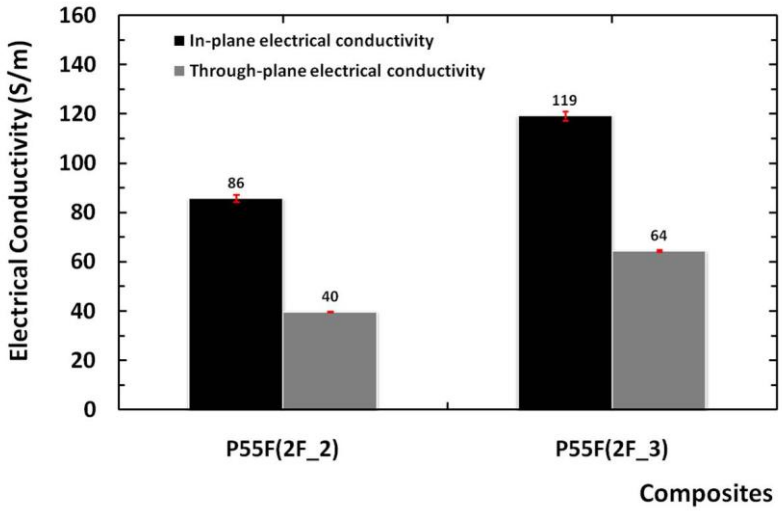

Figure 4-39: Electrical conductivity of composites consisting of two fiber types, (CF (A) and CF(C))

The results in table 4-4 also illustrate that PPy slightly increases the electrical conductivity of the PP/CNF blend. In previous experiments, the PP/carbon fillers composite with 55wt% of filler concentration was fabricated using a filler ratio of 1:1:1(CB: CF: SG). In this section the ratio of filler was changed to 1:0.5:0.5:1 (CB: CF (A) and CF(C): SG). Note that CF(C) is CNF. In comparison to the conductivity values in Figure 4-39, CNF decreased the electrical conductivity of composites from 115 to 86 S/m and from 53 to 40 S/m for in-plane and

through-plane conductivity, respectively. Adding PPy (1.8 wt%) into the composites with CNF can increase in-plane and through electrical conductivity as displayed in Figure 4-39.

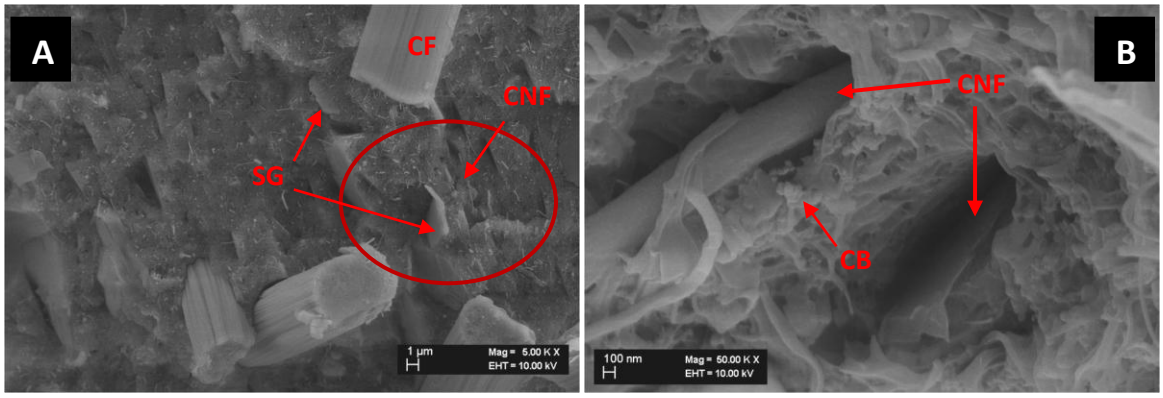

Figure 4-40: SEM photos of P55F (2F_2) composite with magnification 5kX (A) and 50kX (B)

Even the small size of CNFs is useful for creating a conducting network formation in small and narrow areas; however, the electrical conductivity of this composite did not increase. Because of the huge difference between CNFs and filler sizes, the connections cannot be associated successfully, as seen in Figure 4-40. The area inside the red circle shows CNFs dispersed (white small particles) in the PP matrix, but they cannot connect directly with SG and CF particles. In other words, reducing the quantity of CF causes a reduction in long-distance conducting transporters.

4.1.2.2 Processing Characteristics

Polymer rheological data is typically illustrated in a log plot of viscosity as a function of log shear rate. Figure 4-41 shows the effect of carbon filler and polypyrrole content and the combination of two sizes of carbon fibers. Comparison of the melt viscosities of the materials shows the significant effect of the filler content. When the range of shear rate was at 10^1 - 10^3 s^{-1}, the molten composites show higher viscosity compared with that of neat PP. When shear rate is increased, PP/carbon filler composites exhibit shear thinning effect, while the neat PP exhibits only smaller shear rate dependence [144]. From Figure 4-41, it can be seen that Newtonian plateau does not exist within the shear rate range investigated. The viscosity curves of composites indicate a steep slope at low shear rate. The increase in viscosity is due to the confinement of polymer chains with the filler and fiber entangled together, and thus

forming an interconnected structure (Figure 4-41). Therefore, the viscosity of the molten confined polymer is greater than that of bulk chains. This assumption was also reported by Teng et al. [145].

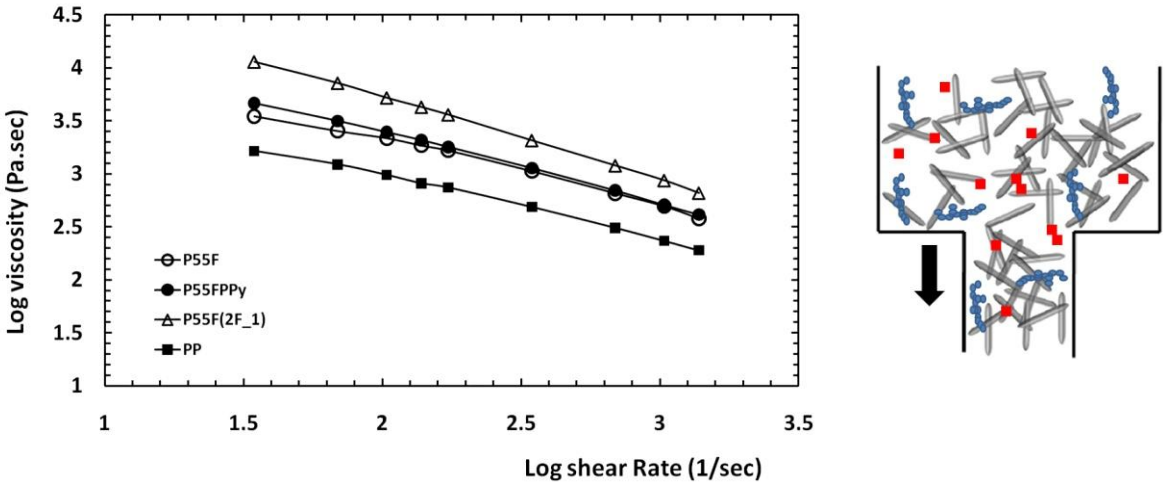

Figure 4-41: A log plot of the viscosity as a function of the shear rate and the flow schematic of the composites in a capillary rheometer

Table 4-6: The power law index and consistency index of the PP/filler composites

Samples	Power law index (n)	Consistency index (k) Pa.s^n
PP	0.3545	21,081.43
P55F	0.3898	34,914.03
P55FPPy	0.3278	56,584.84
P55F(2F_1)	0.2292	171,711.7

The composite containing two types of carbon fibers shows the highest viscosity in the group, while P55FPPy indicates only slightly higher viscosity than normal P55F. The difference in CF sizes enhances the fiber network and fiber entanglement; therefore, has hindering effect on the flow of molten PP.

In the case of P55FPPy, the rigid polymer-chains of PPy and hydrogen bonding also retard the composite flow. The values of the power law index of materials exhibits those different sizes of carbon fibers leads to the behavior composites having a more non-Newtonian pseudoplastic characteristic (Table 4-6). The power law indexes (n) of P55FPPy and of P55F

(2F_1) were further from ones comparing PP and P55F. The consistency index of the composite was increased from 34,914.03 $Pa.s^n$ to 56,584.84 $Pa.s^n$ (P55FPPy) and 171,711.7 $Pa.s^n$ (P55F (2F_1)).

This consistency index reveals the magnitude of the viscosity at a very low shear rate. Conversely, at the higher shear rate at which injection molding operated, the melt viscosity of composites is close to that of the neat PP, as can be assumed from the smaller slope of the viscosity curves. The effect of the viscosity combining two types of CFs or PPy with the PP matrix at a high shear rate is insignificant.

4.1.2.3 Single Cell Performance

The increase in fuel cell performance (Figure 4-42) of the single cells assembled with P55FPPy and P55F (2F_1) bipolar plates is similar to the trend of their electrical conductivity, as expected. To evaluate the performance of composite bipolar plates, single fuel cells were made using both graphite and PP composite bipolar plates. The individual cell sample had comparable open circuit voltage (OCV) measurements (0.85-0.93V). The OCVs of the cells ranged from 0.903 and 0.93, which are higher values than for the fuel cell using graphite bipolar plates. At low current densities, the single cells exhibited almost the same performance; and P55FPPy and P55F (2F_1) bipolar plates gave cell performance really close to that of single cells assembled with graphite bipolar plates.

At an intermediate current density, PPy and the combination of two CFs showed an expected higher performance than the normal PP/carbon filler composite; at a cell voltage of 0.6V, the current densities of the single cells using P55FPPy, P55F(2F_1), and P55F bipolar plates were 74.79, 83.11, and 45 $mAcm^{-2}$, respectively. At this voltage, the performances of graphite bipolar plates are approximately 1.6 and 1.8 times higher than those of P55F (2F_1) and P55FPPy, respectively. However, the performances of the PP blends with PPy and two types of fibres are still lower than that of the cell made from commercial graphite and FR8 composite plates. The fuel cell assembled with P55F (2F_1) and P55F generated a maximum power lower than that of the one with graphite bipolar plates, about 103 and 90 $mA.V/cm^2$ (mW/cm^2) for P55F (2F_1) and P55FPPy, respectively (Figure 4-43). Once again, all results indicate that PPy and different sizes of CFs improve PEMFC performance by improving the electrical conducting network within the composites.

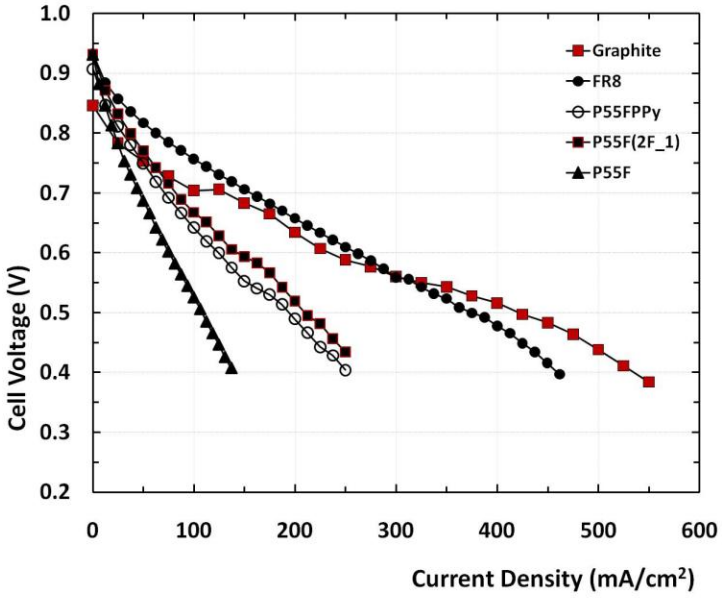

Figure 4-42: Polarization curves of single cells using different bipolar plates

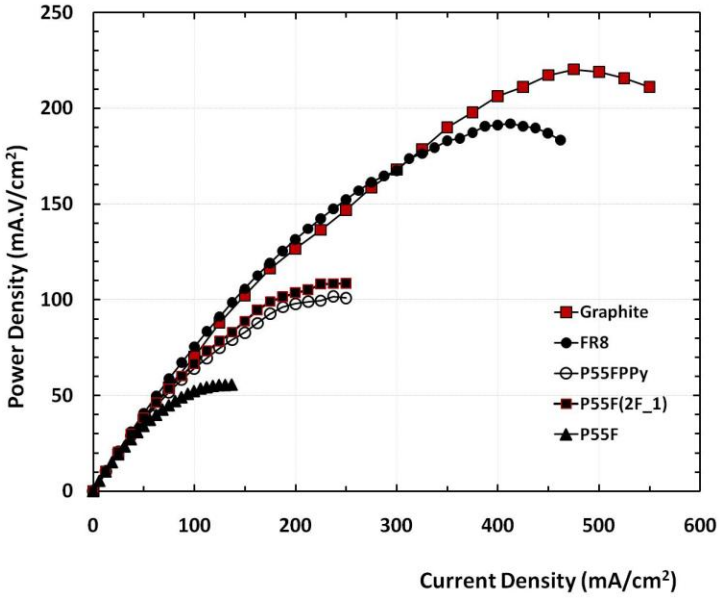

Figure 4-43: PEMFC performance of single cells using different bipolar plates

Figure 4-44 shows the short-term performance of the fuel cells; the fuel cells were operated over 121 hours at a constant current density of 100 and 200mAcm^{-2}, and then the voltage was measured at 100 and 200 mAcm^{-2}. There was some voltage degradation perhaps these changes might because of water flooding in the gas flow channels. P55FPPy's performance

did not obviously degrade, and it is assumed that cell resistance is quite stable for this period of fuel cell operation.

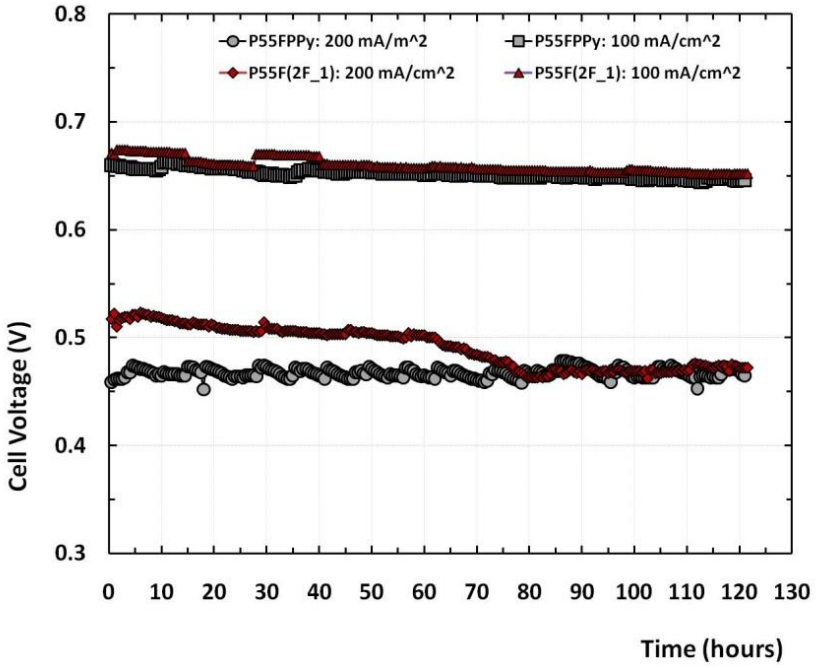

Figure 4-44: Steady-state tests of single cells

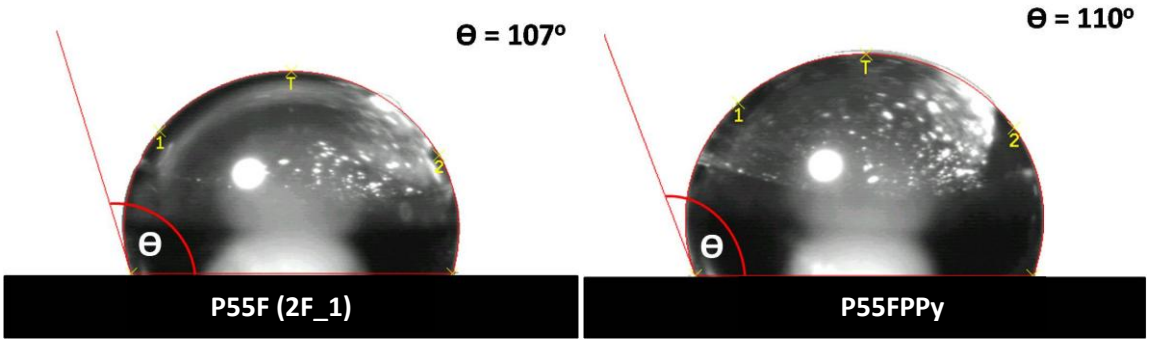

Figure 4-45: Contact angle of injection molded specimens

Figure 4-45 depicts the contact angle of composites containing PPy is higher than that of P55F (2F_1) due to PPy's structure, which provides a stronger hydrophobic surface than 2F_1 values since the PPy molecule is polar. The contact angle result can help explain more constant performance of the cell using P55FPPy bipolar plates than the performance of the cell using P55F (2F_2) bipolar plates. This result indicates that water droplets in the gas flow channels of P55FPPy bipolar plates can be swept away more easily by the gas stream under

relatively low flow rate conditions than that water droplets can in the channels of P55F (2F_1) bipolar plates[146]. In other words, the cell using P55FPPy exhibits content performance as a function of time (for a relatively short-term test).

AC Impedance Characterization

Table 4-7: Effect of Polypyrrole on fuel cell resistance at high frequency

Samples	In-situ ohmic resistance (Ω)
Commercial graphite	0.0800
FR8	0.0830
P55F	0.2104
P55FPPy	0.1411
P55F(2F_1)	0.1074

The performance curve confirms the positive correlation among electrical conductivity, fuel cell performance, and cell resistance: an increase in electrical conductivity yields a proportional increase in performance and reduction in cell resistance. The observation of AC impedance was performed at OCV, since at OCV fuel cell electrochemical reaction does not generate much water. Therefore, the resistance of fuel cell components is a domain effect on ohmic resistance. Table 4-7 shows that the ohmic resistances of single cells reduce when PPy is added two types of CFs are combined in the composite. The influence of a CF combination on the ohmic resistance is higher than that of PPy. The ohmic resistances of the two cells is 0.1078 and 0.1419 Ω for P55F (2F_1) and P55FPPy, respectively.

4.1.2.4 Mechanical Characterization

Mechanical properties are one of most important properties of a bipolar plate in a PEMFC. The plate must retain mechanical stability in order to prevent the stack from leaking and to ensure that the plate does not damage the membrane.

Compressive Test

Figure 4-46 shows the change in compressive strength when three carbon fillers were added to PP to form composites, with error bars showing one standard deviation. Based on average values of the property as displayed in the figure, it appears that all four types of PP/carbon filler composites possess values for higher all compressive properties compressive strength,

compressive modulus, and yield strength, than pure PP did. The compressive strengths of every composite (the maximum ~ 60 MPa) are greater than that of compressive strength of current commercial bipolar plates (~ 50 MPa) [127]. Please note that six specimens for each combination of fillers were tested. The compressive strength was obtained from the maximum stress or the top peak of a stress-strain curve. A 0.2% offset was used in order to determine the compressive modulus and yield strength.

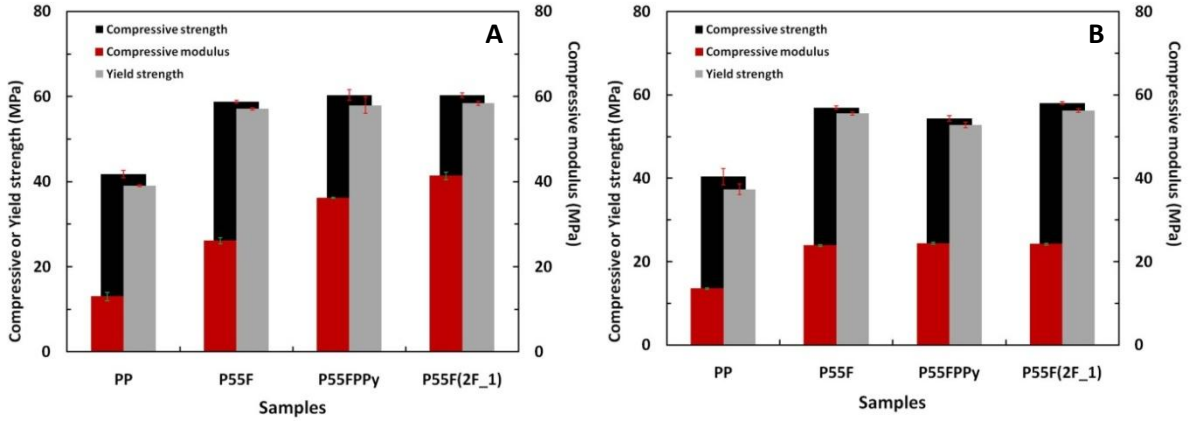

Figure 4-46: Compressive properties of composite bipolar plates:
(A) injection specimens were cut parallel to and (B) injection specimens were cut perpendicular to the flow injection direction

Note that PPy and a two-CF mixture have no significant effect on the compressive properties of composites. The injection specimens cut perpendicular to the flow direction gave 5-10% lower compressive strength than that of the specimens cut in the flow injection. According to the orientation of fillers, especially CFs, in the flow direction, higher compressive force is required to crack a specimen, since almost all of the force is used to rupture the fillers, which are rigid and stiff materials.

Tensile Test

The data for Young's modulus, tensile strength, and the yield strength of the injected composites obtained from the tensile testing are shown in Figure 4-47. The composite modulus increases as fillers are introduced into the PP matrix as discussed in the previous section. It seemed apparent from the trend shown in the figure that the material comprised of PPy shows the more improvement in tensile modulus, while the composites using two CFs were less effective in modifying this property of the composite. Short carbon fibers in P55F

(2F_1) have less ability to handle tensile force than do long fibers since the former entangle with other fibers or with PP chains less than the longer ones can do. In other words, long carbon fibers have a much higher strength than short fibers [132]. These results conflict with the tensile strength results reported by Thomason [147].

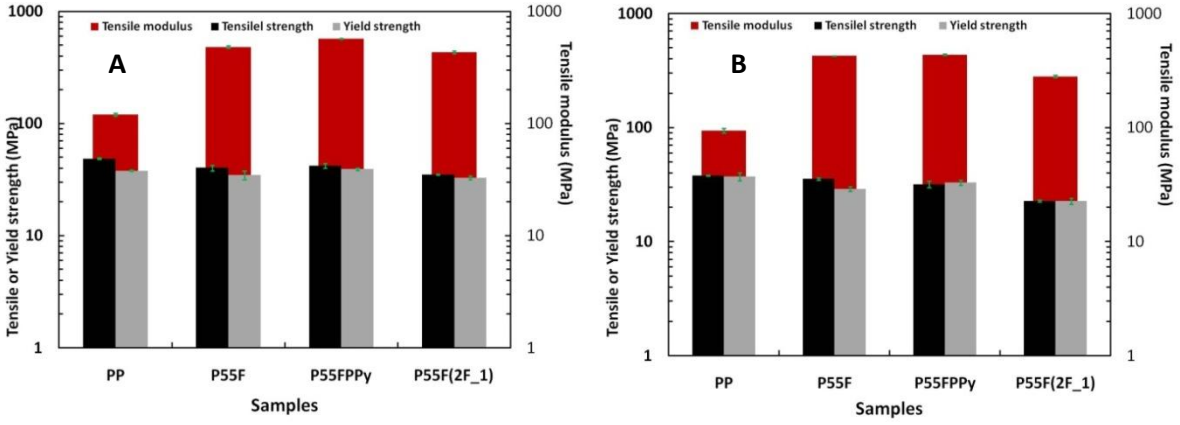

Figure 4-47: Tensile properties of composite bipolar plates: (A) injection specimens were cut parallel to flow injection, (B) injection specimens were cut perpendicular to flow injection

It can be seen that the tensile and yield strengths of all composites decreased with the addition of fillers into the PP matrix. The tensile properties of composite specimens cut perpendicularly to injection flow are lower than specimens cut in the injection flow direction. All tensile properties of perpendicular-cut specimens appear to fall on a similar trend line, indicating another direction. In comparison to tensile strength for commercial bipolar plates (30-41 MPa) [131], the values of all composites in this set are in the target range.

Flexural Test

The flexural strengths of the composite bipolar plates can be obtained from Figure 4-48. As the combination of CF (A) and CF (B) in PP/filler composites increases, the flexural strength, yield strength and flexural modulus decrease. As PP content decreases, the surface interaction between filler particles and the PP matrix is poor [48]. Consequently, the flexural strength of composite bipolar plates declines. The flexural strength of the P55F composite decreased roughly 0.62 MPa when PPy was introduced into the composite. Its flexural strength also diminished, from 33.38 MPa to 31.86 MPa, as combining to in response to the combined types of CFs in the composite. The results indicate that PPy plays less of a role in

the decrease of flexural strength than the two-CF combination used in the composite. These results agree with the assumption stated by Fu et al. [132] who reported the decrease in composite strength caused by the reduction in mean fiber length. Changes in the flexural modulus and yield strength of composites have the same general trend as the flexural strength. It can be also seen that the trends for flexural properties of composite specimens in both directions are almost identical (B-4, Appendix B).

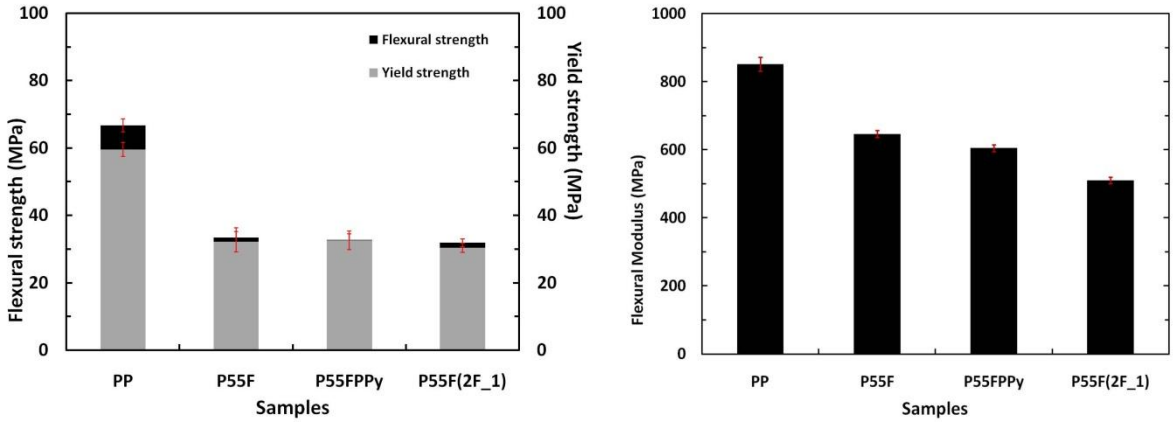

Figure 4-48: Flexural properties of PP/carbon fiber composites
(specimens were cut in the injection flow direction)

The maximum in this set of composite flexural strength values was 33.38 MPa, whereas the flexural strength of the Poco^{TM} graphite bipolar plate is 45MPa [48]. The ElectroPhen bipolar plates fabricated by Bac2 Limited have flexural strengths of 30 MPa [148]; therefore, all composites described in this section can be applied for PEMFCs.

Hardness Test

Figure 4-49 shows the changes in shore hardness that result from adding CB, CF and SG to the PP matrix. The hardness value increased by about 9% (from 70 (PP) to 79 (P55F)), probably because rigid filler particles were inserted among PP chains, and because voids developed in the fillers and resin interface during polymer processes [149]. The experiments thus reveal that the addition of PPy (1.8%) to the composite did not improve the hardness of bipolar plates, but did it sacrifice the hardness of composite bipolar plates. DOE's hardness for bipolar plate hardness requirement is >50 and the hardness values of existing commercial bipolar plates is detailed in the publication of Dhakate et al. [46]. The values are 60 for Schunk

bipolar plates and 52 for the bipolar plate of fuel cell store. The results reveal that PP/carbon filler composites are sufficiently hard for bipolar plate application.

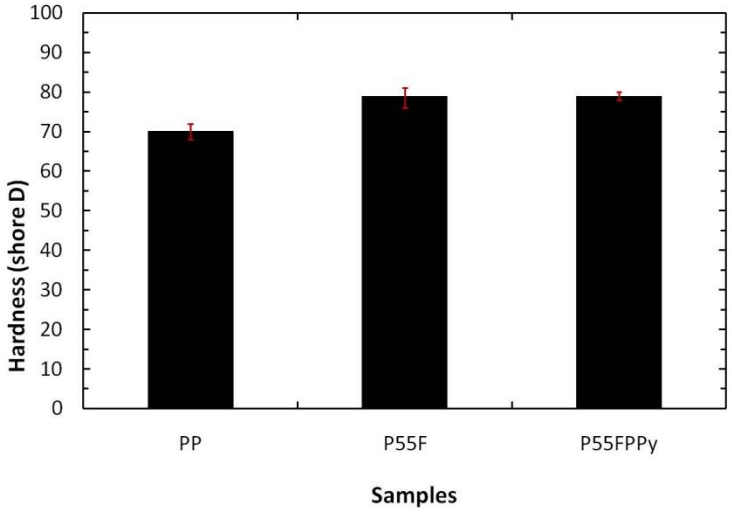

Figure 4-49: Shore hardness of PP/filler composites

4.1.3 Synergistic Effect of CB, PPy and The Combination of Two Fibers

All results from the beginning of this chapter show the strong points of each component to develop the electrical conductivity of the PP/carbon filler composite. The electrical conductivity was strongly influenced by high ratios of CB, PPy and the combination of two types of CFs. The formulations of composites studied in this part of the study are described in Tables 3-6 and 3-7. It is important to note that the in-plane electrical conductivity measurements were obtained with a small four-point-probe tester obeying the theory as explained in Equations 2-22 to 2-29. The in-plane and through-plane electrical conductivity values of hybrid composites are given in Figure 4-50. The high ratio of carbon black is main factor that affects electrical conductivity increase.

The electrical conductivity from both measurements was abruptly increased after a high ratio of carbon black and two types of CFs were mixed together. The conductivity of the FR8 (2F_2) composite increased by about nine times for in-plane and eight times for through-plane, compared with the conductivity of P55F. The highest electrical conductivity values of the two methods are provided by the FR8 (2F_2) composite: 2139.18 S/m (in-plane) and 773.30 S/m (through-plane). The synergistic potential of fillers and additives to enhance

electrical conductivity is easily seen in this set of composites because the conductive network in the composites was enlarged, and then the percolation threshold was decreased. As is known, the electrical conductivity of a composite is strongly dependent on percolation threshold.

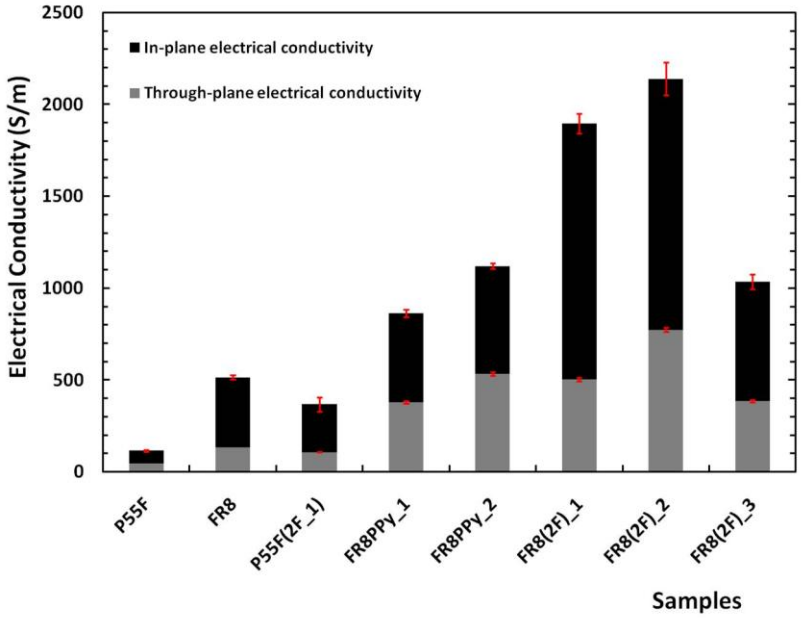

Figure 4-50: The electrical conductivity of composites containing a high ratio of CB, PPy and the combination of two types of CFs

It is necessary to consider that incorporating PPy and a high ratio of carbon black results a significant increase in composite viscosity. This viscosity increase was found for the composite bars produced by mini-injection molding. A temperature in the range of 200 - 210^{o}C was used to inject molten composites into the mold, while 190^{o}C was typically used for all other composites. Finally conductive injection moldable thermoplastic composites in this research can be achieved, although equivalency to the DOE target (100 S/cm or 10,000 S/m for through-plane) and to that of conductive composite bipolar plates existing in the current market (114 S/cm for in-plane and 32 S/cm for through-plane) [148] has not yet been achieved. The blends do show promise for future opportunities as composite materials within PEMFC, and they may be used in portable or stationary applications which do not require such a high power density.

4.2 Effect of Additives

The electrical conductivity of insulating polymer matrices can be increased with relatively high filler compositions of a conductive fill such as carbon. However, the non-uniformity of material properties is a major problem in a highly filled polymer system due to poor dispersion of fillers in the polymer matrix. Besides filler concentration, the electrical conductivity also depends upon filler dispersion, interaction between composite constituents, and process conditions. Therefore, the application of some additives, such as a coupling agent or processing agent, in particulate filled polymer has usually been controlled to overcome the dispersion problem. This section investigates the effect of coupling and processing agents on bipolar plate properties.

4.2.1 Titanate Coupling Agent

This research focused on the use of a titanate coupling agent to improve the quality of filler dispersion and overall material processability. The titanate coupling agent was selected because the new generation of titanate coupling agents is more user-friendly and more cost effective than previous ones. The titanate coupling agent can easily be incorporated with higher aspect ratio fillers and could eliminate the need for filler pretreatment steps during processing. Details of composite formulations for the study in this section are given in Table 3-1.

4.2.1.1 Electrical Conductivity

A titanate coupling agent affects on in-plane electrical conductivity was measured in two directions: parallel and perpendicular to the injection flow direction. The two directions were tested because filler orientation, carbon fibers especially, will affect the polymer blend's conductivity. Theoretically, fillers with a high aspect ratio will be oriented parallel to the injection flow, and thus, the measurement in this direction will give higher electrical conductivity. Figure 4-51 shows results for the in-plane electrical conductivity versus a titanate coupling agent weight percent. The in-plane conductivity in both directions slightly increased as the titanate coupling agent loading was varied from 0 to 1wt%. The electrical conductivity abruptly increased when the titanate coupling agent loading was changed from 1 to 2 wt%. However, the conductivity was found to decrease with increased concentration of

the coupling agent higher than 2wt%, so there is an optimal loading point for the titanate coupling agent.

The results indicate that the titanate coupling agent enhances the wettability of filler surfaces by the polypropylene matrix (non-polar polymers) and promotes interfacial adhesion [150]. The coupling agent provides molecular bridges at the interface between two substrates. Figure 2-14 shows the chemical structure of the agent used in this research.

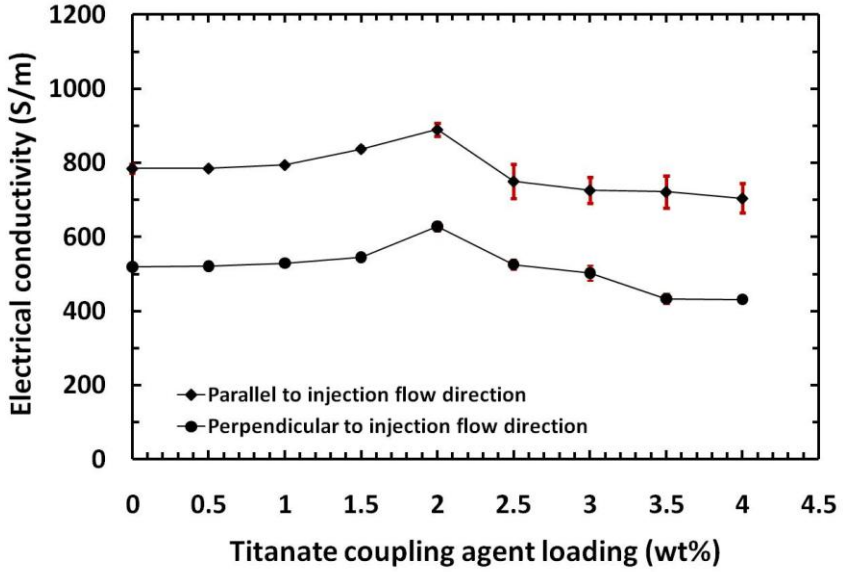

Figure 4-51: Effect of titanate coupling agent on in-plane electrical conductivity of carbon filler filled PP

Improved interfacial adhesion can develop filler dispersion in the matrix; thus, more conductive connections can form a situation that agrees with results from Yu et al. [151]. The mechanism of titanate reaction on a filler surface was explored by Wah et al. [152], who explained that hydroxyl groups at the inorganic filler surface react with titanate coupling agents. The reaction results in the formation of a monomolecular layer on the inorganic filler surface, which increases the compatibility of the filler/polypropylene interface. A schematic of the reaction is depicted in Figure 4-52. Titanium-derived coupling agents have been used, typically on inorganic fillers, and similar coupling surface treatments have been applied to carbon fibers or carbon black reinforced plastics [77, 79].

Chiang et al. have reviewed the fundamentals of carbon fiber surface chemistry [153]. Chemical and spectroscopic analyses identified the presence of the carbonyl and alcohol groups on polyacrylonitrile fibers, which are similar to the carbon fibers used in this research. It is also known that carbon blacks have chemisorbed oxygen complexes (i.e., carboxylic, hydroxyl groups and others) on their surfaces. Since carbon fibers and carbon black in PP/carbon filler composites contain the hydroxyl group, they can be coupled with titanate coupling agents.

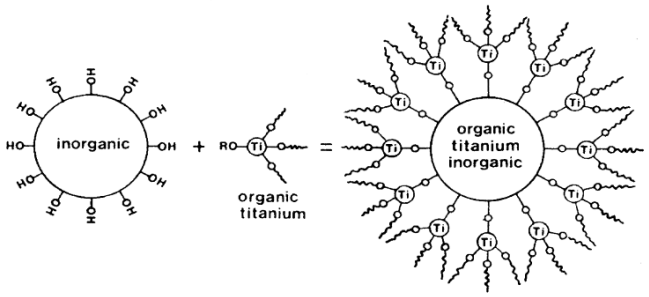

Figure 4-52: Mechanism of titanate reaction on inorganic filler surfaces [152]

Micrographs of PP composites with and without coupling show that the coupling agent has the potential to significantly improve the interface between fillers and a polymeric matrix, as illustrated in Figure 4-53. The SEM image of PP composites without a titanate coupling agent shows the poor interfacial adhesion between the fillers (especially CF) and the PP matrix, and graphite agglomerates can be found (red marking circles). The pictures of PP composites with the coupling agent indicate better filler dispersion in the PP matrix. The filler dispersion and interfacial interaction between fillers (CFs especially) and PP improve as the coupling agent loading increases.

At higher magnification (2kX), the insulating gaps that electrons cannot transfer through, can be observed clearly (Figure 4-54 (A)), while the composites with 2wt% indicates that polar fibers have good compatibility with a non-polar polymer matrix (B) in the present of the additives. The micrographs support the electrical conductivity results in Figure 4-51.

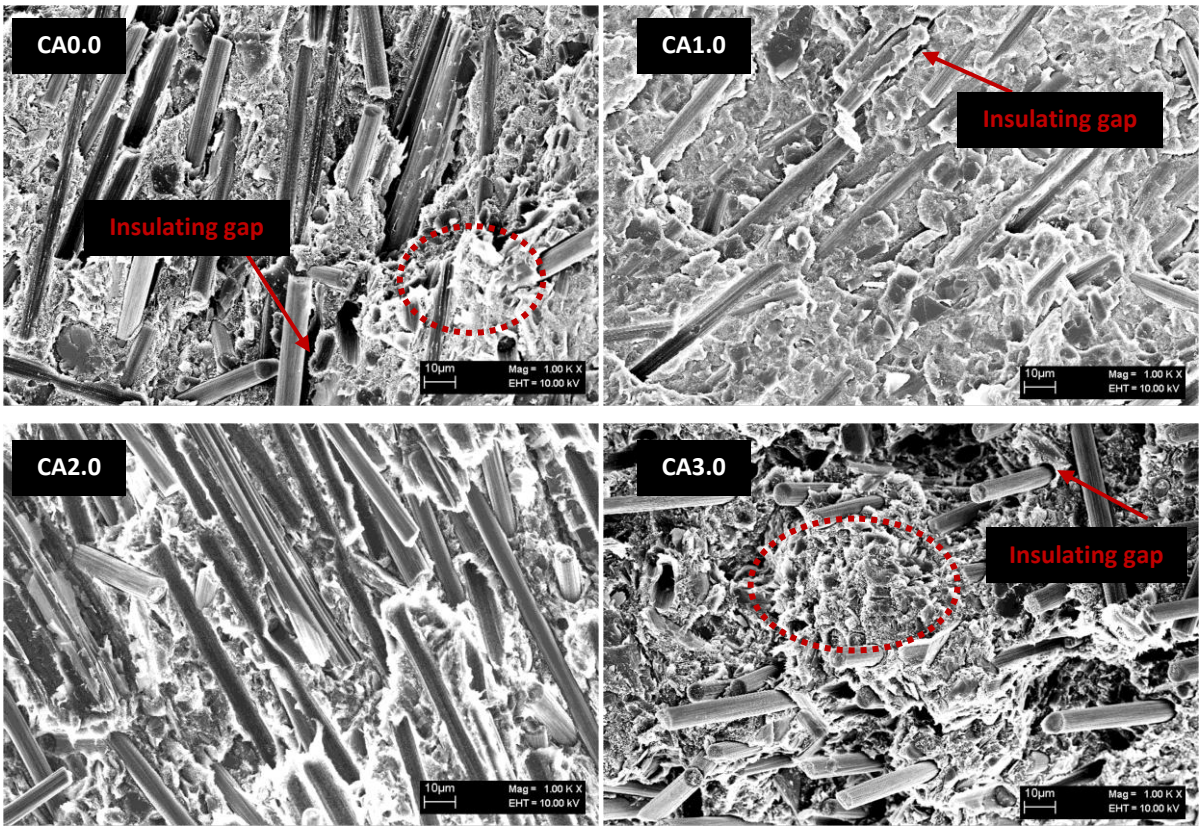

Figure 4-53: SEM micrographs compare PP composites with and without titanate coupling agent (magnification 1,000X)

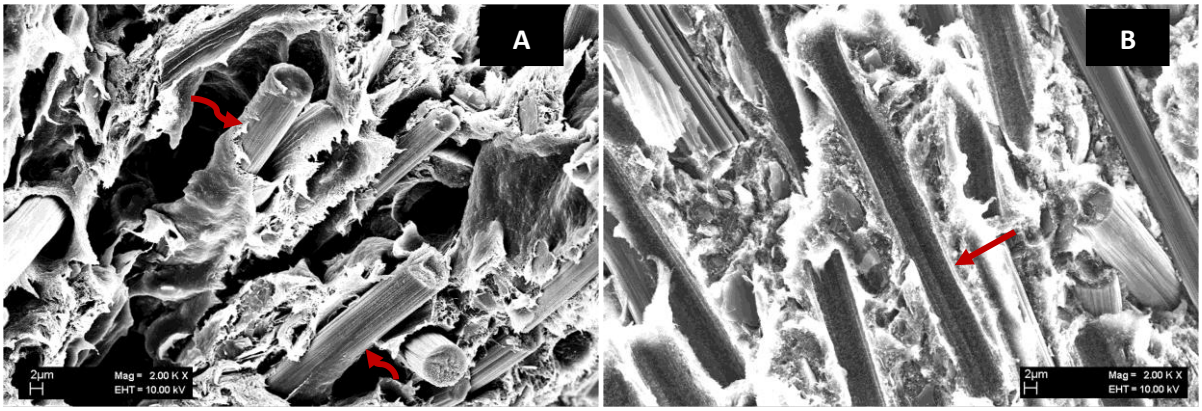

Figure 4-54: SEM micrographs of CA0.0 composites (A) and CA2.0 composites (B) magnified 2000X

In terms of carbon black dispersion, SEM pictures of PP composites without a coupling agent show carbon black clusters (Figure 4-55(A)), whereas 2wt% of coupling agent loading

improves the distribution of carbon black particles (B). Organofunctional titanate causes filler/polymer interface to be more compatibility, and air voids in the system are eliminated.

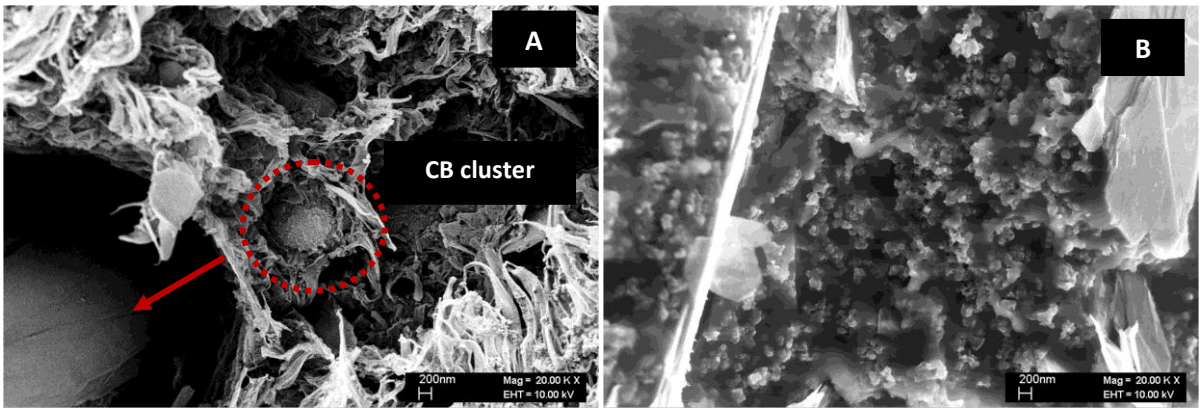

Figure 4-55: SEM micrographs of CA0.0 composites (A) and CA2.0 composites (B) with 20kX of magnification

Subsequently, de-agglomeration and more uniform dispersion in melt composite results [152]. Coupling agent concentration above 2wt% causes poor filler dispersion and poor surface adhesion Figure 4-54. SEM micrographs support the trends seen in electrical conductivity results. It is considered that filler-filler interfacial forces may be stronger than the polymer-filler interfacial forces, since the coupling agent may also couple filler-filler interfaces. Therefore, the fillers tend to agglomerate into clusters and be unevenly distributed throughout the non-polar polymer matrix during compounding processing [154].

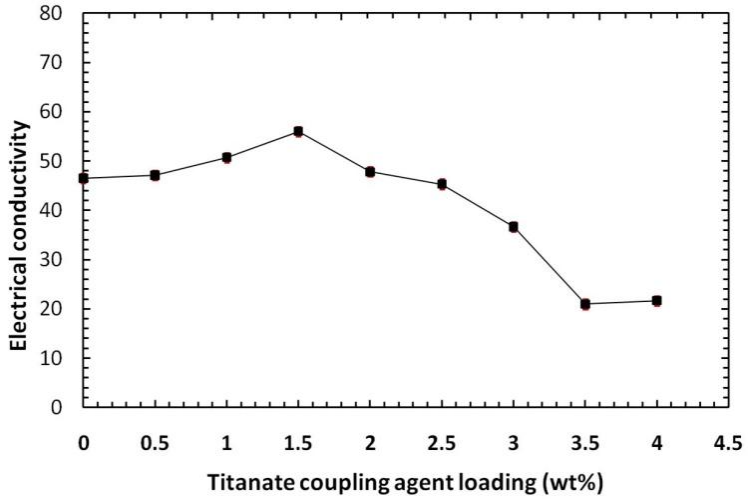

Figure 4-56: Effect of titanate coupling agent on through-plane electrical conductivity of carbon fillers filled PP

On the other hand, the formation of a conductive network structure could be obstructed by the coupling agent because fillers could be thickly coated with an insulation layer of the coupling agent [141].

Through-plane conductivity shows the same general in which change the coupling agent loading increases with in-plane conductivity (Figure 4-56). The limitation of the use of the titanate coupling agent was observed at 1.5wt%, which is lower than that of in-plane conductivity. Moreover, the conductivity diametrically decreased with the coupling agent loading, varying from 1.5 wt% to 3.5wt%.

4.2.1.2 Single Cell Performance

Figure 4-57 shows the I-V characteristics of single fuel cells prepared with an individual PP/three carbon filler composite bipolar plate. The bipolar plate consists of coupling agents with various loadings: 0, 1, 2, 3.5 wt%. The polarization curves demonstrate increased performance when bipolar plates contain the titanate coupling agent at a concentration increasing from 0 to 2 wt%. On the other hand, the performance deteriorated at 3.5 wt% of coupling agent loading, as expected. The polarization curve of the fuel cell assembled with composite bipolar plates containing 2 wt% of titanate coupling agent performs best. Observation of the fuel cell performance it showed that the power density continuously increased up to the current density of 225 $mAcm^{-2}$ corresponding to the maximum power density of 84.5 $mWcm^{-2}$.

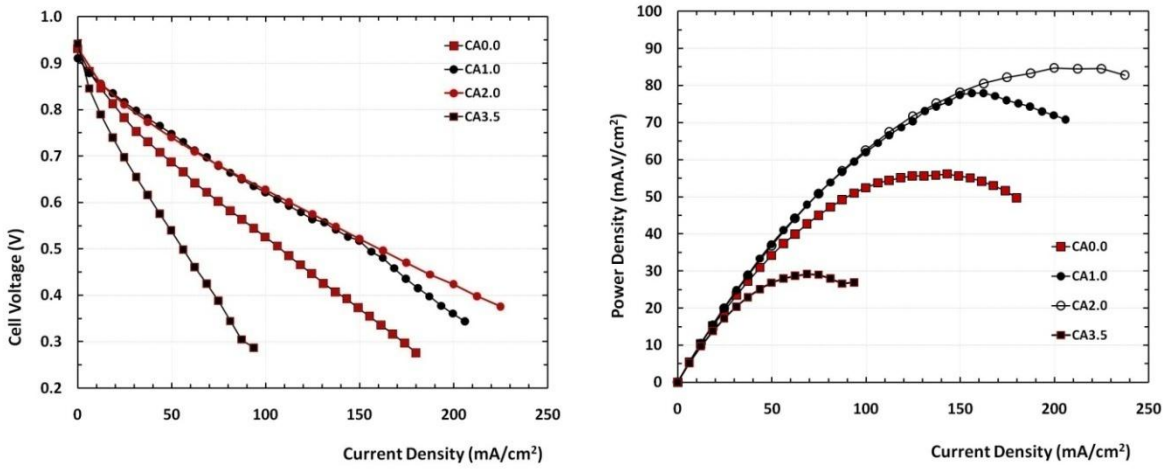

Figure 4-57: Performance of single fuel cell assembled bipolar plates containing various concentrations of coupling agent

The composite bipolar plates using 1 wt% of the titanate coupling agent reduced the fuel cell performance slightly below that of bipolar plates using 2wt% of coupling agent. The cell voltage dropped by 19% at 100 $mAcm^{-2}$ of an average current density, when the composite bipolar plates do not have the coupling agent. The performance results confirm the results from electrical conductivity measurements.

AC Impedance Characterization

The activities of the titanate coupling agent were evaluated using in-situ EIS. Table 4-8 presents four single-arc Nyquist spectra obtained at OCV. The electrochemical impedance spectra were recorded in the 0.5 Hz $\leq$ f $\leq$1 kHz frequency range. Ohmic resistance at high frequency decreased as coupling agent loading increased due to the coupling agent encouraging conductive filler connections. The titanate coupling agent loading used for a PP composite causes overall fuel cell and electron transfer resistance to increase. All impedance results relate to the results represented previously.

Table 4-8: Effect of titanate coupling agent on fuel cell resistance at high frequency

Samples	In-situ ohmic resistance (Ω)
CA0.0	0.2111
CA1.0	0.1744
CA2.0	0.1454
CA3.5	0.3281

4.2.1.3 Contact Angle

Hydrophobicity is one of the important features affecting cell performance, principally at high current densities. In this section, the surface hydrophobicity of all the composites was obtained by measuring the water contact angles.

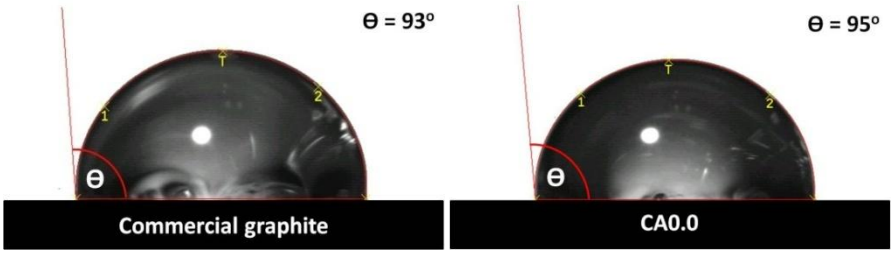

Figure 4-58: Contact angles of graphite and PP/three filler composite bipolar plates

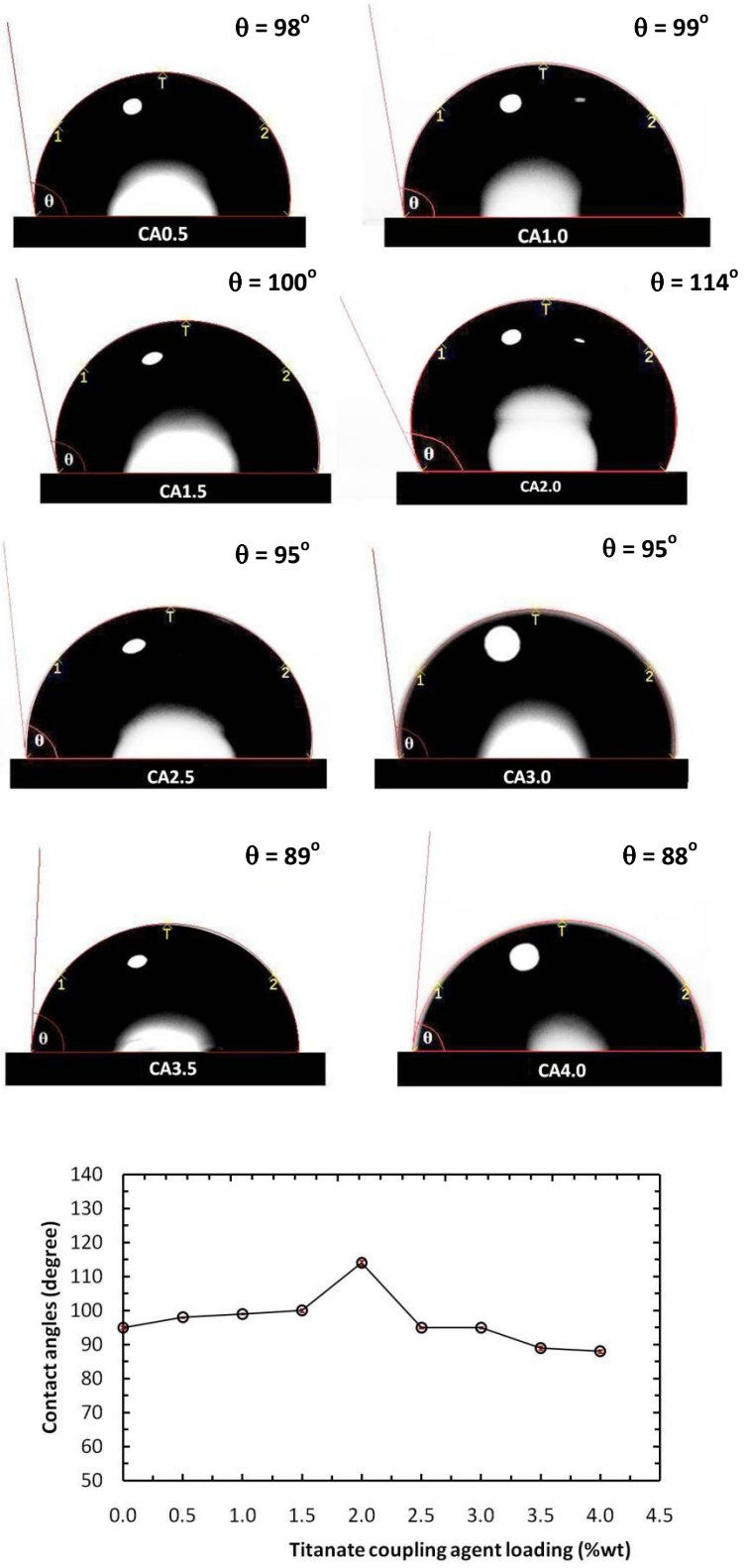

Figure 4-59: Contact angles of graphite and PP/three filler composite bipolar plates containing various coupling agent concentrations

It is noted that a neat PP plate has a contact angle of approximately 88^{o}. PP composite bipolar plates also have stronger hydrophobic surfaces than the graphite bipolar plates used in this research (Figure 4-58). Typically, graphite composite bipolar plates have contact angles of about 93-100^{o} [17, 114]. The contact angles in Figure 4-59 indicate that a water droplet in the gas flow channels of composite bipolar plates containing the titanate coupling agent (0.5 to 2.0 wt% of loading) can be swept away more easily with an increase in coupling agent loading. Hence the PEMFCs can perform better even at low flow rates, in agreement with performance results in Figure 4-57. The change in the contact angle is related to chemical change of the bipolar plate surface. Contact angles of bipolar plates decreased from 114^{o} to 88^{o} when the coupling agent loading increased from 2 to 4 wt%. The result is reflected in the performance of PEMFC assembled with bipolar plates containing 3.5 wt% of coupling agent loading (Figure 4-57). The PEMFC showed a high rate of voltage drop, especially at high current density. Rapid voltage decay suggests flooding conditions, which may result from water trapped in the flow field channels.

4.2.1.4 Rheological Characteristics

Capillary Rheological Characteristics

Processing characteristics are important in the ability to cheaply apply composites to fuel cell applications for the larger numbers of bipolar plates in a fuel cell stack. The effect of the titanate coupling agent on rheological behavior was studied using a capillary rheometer.

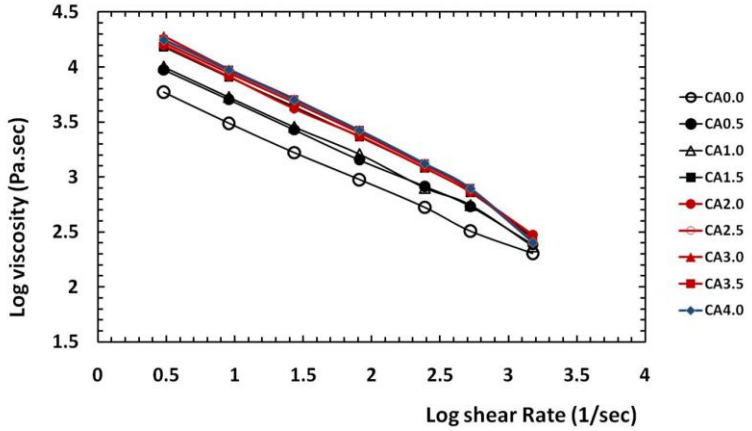

Figure 4-60: Effect of titanate coupling agent on capillary rheological behavior

The relationship displayed in Figures 4-60 shows the non-Newtonian flow of the composite on a log shear rate versus log viscosity. The addition of rigid particulate fillers to polypropylene restricts molecular motion in the PP matrix, and hence imposes resistance to flow. As a result, it gives a higher viscosity value than adding filler a PP matrix. Here, upon introducing a titanate coupling agent to the filled system, the viscosity values were observed to increase with respect to the agent's concentration. Typically, an increase in viscosity value indicates inferior molecular motion between polymer chains, perhaps because the coupling agent improves interface interaction between the PP and fillers, or because the improvement creates more uniform filler dispersion. At high coupling agent concentration, stronger filler-filler interaction may be induced by a coupling agent, so filler agglomeration occurs. The results in this experiment showed flow behavior similar to the results of mixing torque in the batch mixer (Figure 4-61).

Melting Torque Characteristics

In all cases, an initial loading peak was registered at the beginning of the experiment, reflecting the high viscosity of unmelted PP.

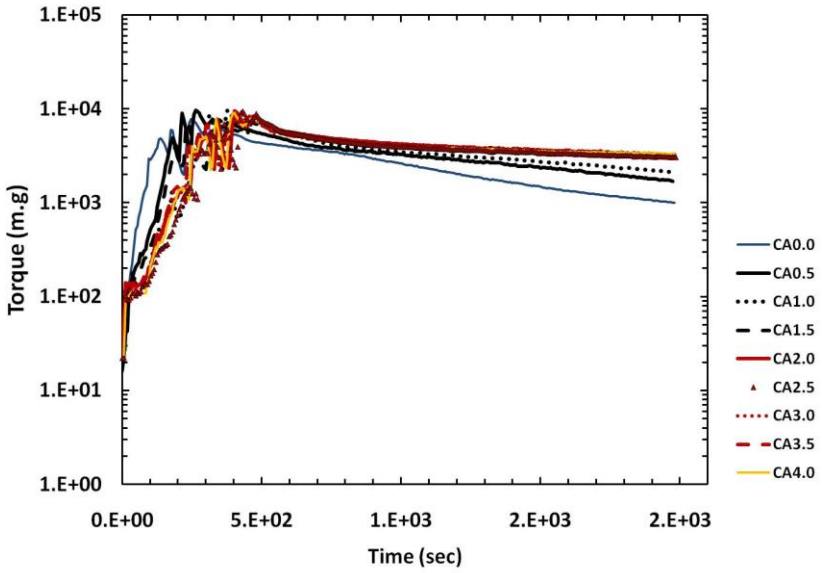

Figure 4-61: Effect of titanate coupling agent on mixing torque

The addition of the filler and coupling agent components produced again an increase of the torque, which was followed by a decrease as the titanate coupling agent melted and the filler particles were dispersed in the PP matrix. The melting torque was observed to increase when

adding the coupling agent into filled composites. The torque values significantly increased as a function of coupling agent concentration from 0.2 to 2.0wt%. The changes in coupling agent loading did not affect the torque values when the loading was higher than 2wt%.

Dynamic Oscillary Rheological Characteristics

The rheological properties of the melt composites are sensitive to the structure, shape and surface properties of the dispersed filler. Evaluating the rheological behavior clarifies the effect of the fillers on internal structures and processing properties of polymer/carbon filler composites. It is also used for investing the effect of the titanate coupling agent on the flow properties of composites.

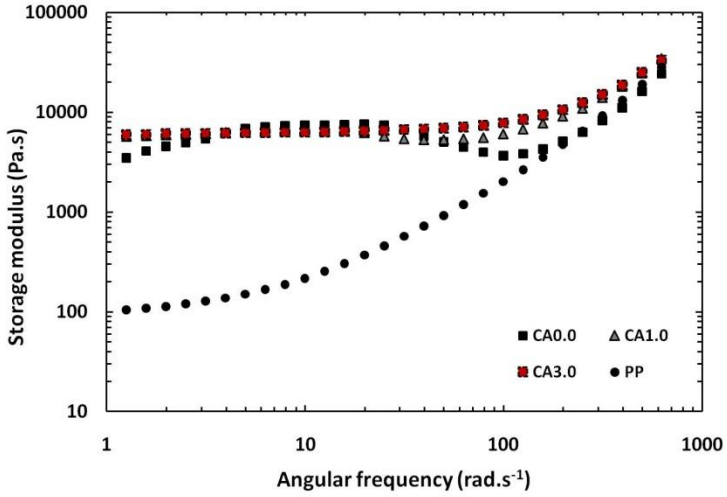

Figure 4-62: Effect of carbon fillers and titanate coupling agent on storage modulus

The frequency dependence of a storage modulus for neat PP and composites with and without a titanate coupling agent measured at 170 ^{o}C is illustrated in Figure 4-62. The result reveals that when loading carbon fillers into neat PP, the storage modulus (G′) dramatically increases and becomes less frequency dependent at low frequencies, where plateau line regimes can be observed. The G′ values of PP/carbon filler composite in the low frequency region are significantly higher than that corresponding to neat PP. When titanate coupling agent is added to the PP/carbon filler composite, the storage modulus of the composites was further increased as expected. The terminal slopes of PP/carbon filler composite curves show great decreases with adding titanate coupling agent increases. The increase in storage modulus is interpreted by the relaxation and mobility being considerably hindered by the

confined spacing constructed by carbon filler particles when the fillers form a conductive network [155]. The reduced frequency dependence at low frequencies indicates the non-terminal behavior in the storage modulus versus angular frequency curve. This behavior can be attributed to the construction of interconnected filler connections in the polymer matrix. It is also known that highly concentrated coupling agent and incompatible composites show non-terminal solid-like behavior at lower frequency ranges [156]. The non-terminal behavior was stronger when coupling agent were added to the composites, since the coupling agent causes the increase in interactions between filler particles and the polypropylene matrix as well as between filler particles. The pressure of coupling agent also results the increased polypropylene chain entanglements with fillers, because fillers have better dispersion in the polypropylene matrix.

The curves of PP composites containing 1wt% and 3wt% of titanate coupling agent loading do not exhibit any change in G′. It seems like in highly concentrated PP/carbon filler composites, higher titanate coupling agent loading does not have any further potential for homogeneous dispersion of carbon fillers and does not shows the significant improvement of interfacial interaction between PP matrices and filler particles. At high angular frequency, G′ of all composites and neat polymer show very close values. The relaxation and mobility of polypropylene chains are a domain rheological property at low frequencies, whereas the rheological property at high frequencies relates to the movement of partial polypropylene chains, segments and methyl groups joined on the backbone for instance, within a small timescale [157].

The complex viscosity of molten PP/carbon filler composites with and without the titanate coupling agent is shown in Figure 4-63. The observed results illustrate that neat PP has flow behavior closer to Newtonian fluid than the PP composites. Adding three fillers to the polypropylene matrix increases the complex viscosity of the material radically at low frequency. It was found that frequency thinning is initiated at lower frequency ranges. As the results in Figure 4-63, show the coupling agent did not play a crucial role in the interfacial interaction between a polypropylene matrix and carbon filler particles at low frequency, but improvement was observed at high frequency. The results also show that the various

concentrations of titanate coupling agent do not have any effect on complex viscosity of the composites.

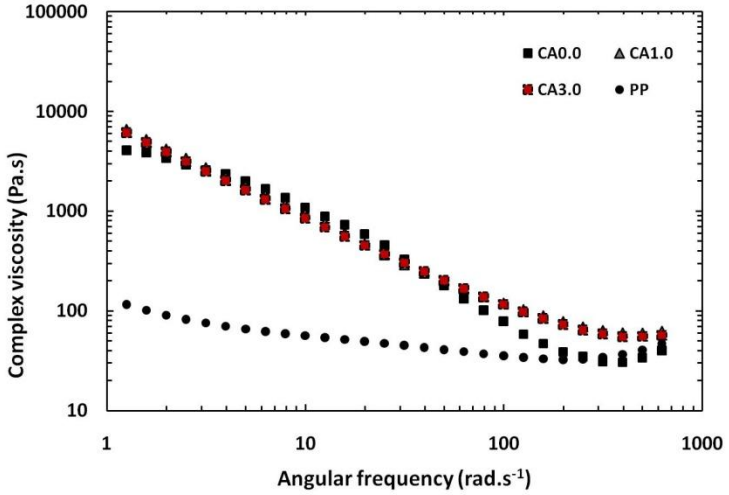

Figure4-63: Effect of carbon fillers and titanate coupling agent on complex viscosity

4.2.1.5 Differential Scanning Calorimetry

The effect of carbon fillers and titanate coupling agents on the crystallization parameters of neat PP and PP/carbon filler composites was observed by differential scanning calorimetry. The results are shown in Table 4-9. The DSC thermograms of neat PP and PP composites are shown in Appendix C. A specimen's degree of crystallinity can be calculated from the melting heat of crystallization regrinding a process represented in Equation 3-2. The melting heat of 100% crystalline polypropylene used for the calculation is 207.1 J/g, which was reported by Sui et al. [143]. The crystallization melting temperature (T_m) of the PP composites did not significantly change from that of the neat PP. Introducing fillers into polypropylene increased the peak temperature of crystallization by approximately 5.3 ^oC. The values of calculated degree of the crystallinity (X_c), melting heat (ΔH_m), and crystallization heat (ΔH_c) decreased when fillers were applied to the PP matrix.

Table 4-9 also illustrates the effect of coupling agents on crystallization parameters. It was found that the degree of crystallinity slightly increased when the titanate coupling agent was added to the filled system. When the intermolecular reaction between filler surfaces and the polypropylene phase is improved, filler dispersion occurs. Therefore, more energy is consumed for the mobility of polymer chains, which may explain the increase in melting

heat, since the degree of crystallinity was determined from the melting heat as an increase in the melting heat. The degree of crystallinity of composites is also important for bipolar plate application, because lower crystallinity results in decreased mechanical properties and increased gas permeability of bipolar plates.

Table 4-9: Crystallization parameters of neat PP and PP/carbon filler composites

Samples	**Tm (^{O}C)**	**T_c (^{O}C)**	**ΔH_m (J/g)**	**ΔH_c (J/g)**	**X_c (%) of samples**	**X_c (%) of PP in composites**
PP	165.57	126.99	78.60	84.86	38.00	38.00
CA0.0	164.07	132.28	37.98	40.20	18.30	40.67
CA1.5	165.04	131.81	41.78	43.07	20.20	44.89
CA2.5	164.42	132.72	40.10	40.5	19.40	43.11
CA3.5	164.67	132.31	38.25	38.97	18.50	41.11

4.2.1.6 Mechanical Characteristics

Compressive Test

Bipolar plates require good mechanical strength to withstand the high clamping forces of stacking and vibrations during applications. The addition of titanate coupling to three filler filled polypropylene has resulted in some small changes of the compression modulus (Figure 4-64). Fillers naturally disperse in the amorphous phase more than in the crystalline phase of a semicrystalline polymer, so elastic deformation is affected by the rigid particle more than the crystalline region. The titanate coupling agent reduced the composites' elastic deformation, since the compatibility of PP with fillers and the filler dispersion were promoted. The compressive modulus dropped when the composites consisted of the coupling agent with a higher loading than 1wt%.

Although a decrease in modulus was found, the compressive modulus values of all composites were higher than the composites without the titanate coupling agent. The compression strength of composites was almost independent of titanate coupling agent concentration. The results correspond to the degree of crystallinity of composites which was slightly increased when the titanate coupling agent was added to the filled system.

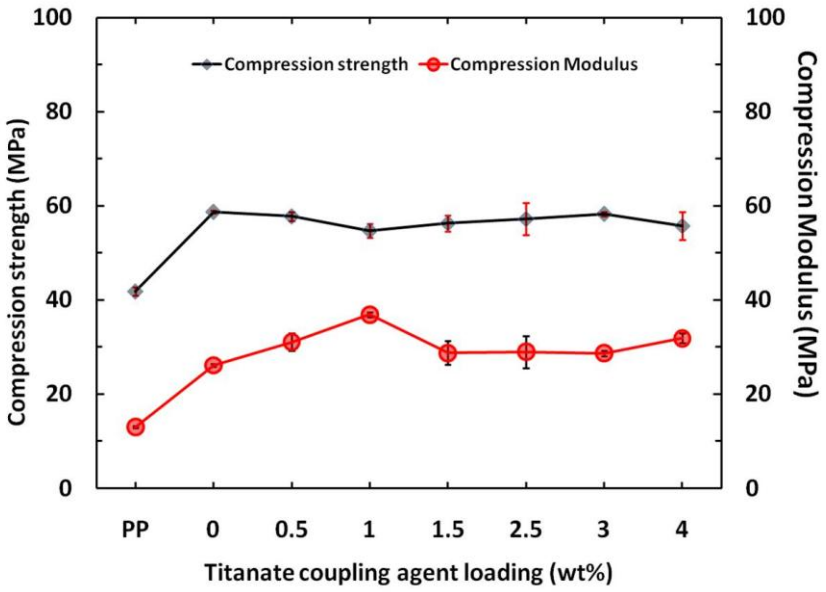

Figure 4-64: Effect of titanate coupling agent on compressive properties

Tensile Test

Figure 4-65 illustrates the tensile strengths of carbon filler reinforced PP composites with and without titanate coupling agent treatment. Composites treated with interface modifiers exhibited slight better tensile strength than the untreated ones.

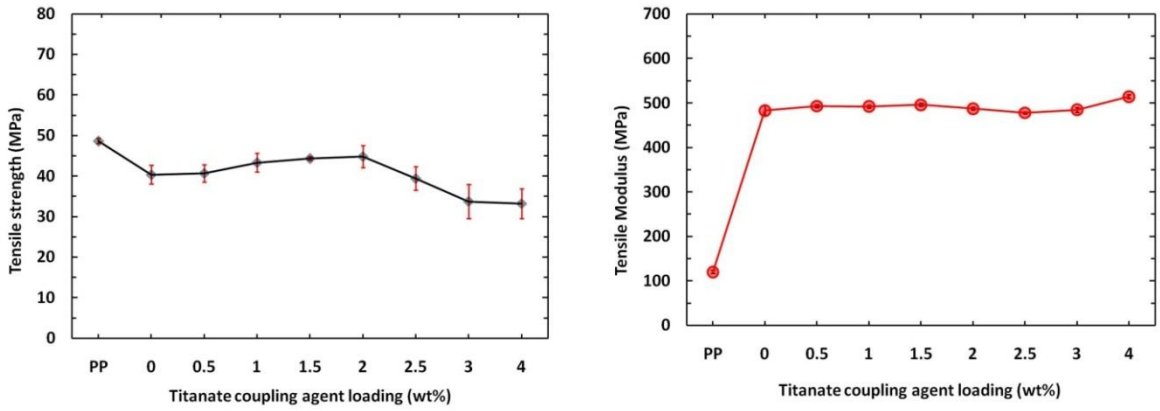

Figure 4-65: Effect of titanate coupling agent on tensile properties

The tensile strength obviously decreased as coupling agent loading varied from 2.5 to 4 wt%. On the other hand the coupling agent can improve the tensile modulus of the composites of composite. The tensile modulus of the composites with 4wt% of coupling agent increases

around 6.5 % from that of the composites without coupling agent (from 483.17 MPa up to 514.44 MPa).

Two procedures for mixing the titanate coupling agent with the composites were carried out to compare the effect of mixing procedure on electrical conductivity. First, the titanate coupling agent was added into the composites during the batch mixing process; this procedure was followed to preparing composites in the hold section. In the second case, PP was treated with the titanate coupling agent by pre-mixing in a plastic bucket, prior to compounding, and then the PP-coupling agent was mixed with carbon black to prepare a PP-carbon black master batch (40wt% of CB) in the twin screw extruder with side-stuffer. This master batch was used for further composite mixing in a batch mixer. A 1 wt% of coupling agent loading was used in this study. Table 4-10 represents the in-plane and through-plane electrical conductivity of composites mixed with titanate coupling agent in different procedures.

Table 4-10: Electrical conductivity of the composites with a titanate coupling agent

Samples	In-plane electrical conductivity (S/m)		Through-plane electrical conductivity (S/m)	
	Parallel	Perpendicular	Parallel	Perpendicular
P55FTi	812.446	503.779	52.175	53.722
P55FTi(s)	613.344	436.935	34.205	31.591

The results from Table 4-10 illustrate that the composite mixed with the coupling agent in a batch mixer (P55FTi) had higher electrical conductivity values than the composites mixed with the coupling agent in the twin screw extruder (P55FTi(s)). This unexpected result may have occurred because the polypropylene and carbon black surfaces in the P55FTi(s) composite may be coated by the titanate coupling agent more than the surfaces in the P55FTi composite. Good interfacial adhesion between CB and polypropylene results in better PP coating on CB particles. However, an insulating layer of PP on CB surfaces breaks the conductive path. Moreover, when the coupling agent is added to the master batch, the agent reacts mostly with PP and CB. Therefore, less unreacted coupling agent can react with CF and SG during the batch mixing process, leading to poor filler dispersion would occur in the composite.

The composite also has more insulating voids because of poor adhesion between the fillers and the PP matrix. The idea can be confirmed by the SEM picture (Figure 4-66) which depicts larger filler agglomerates and poor interfacial adhesion on carbon fiber surfaces. The comparison of fuel cells assembled with P55FTi and P55FTi(s) bipolar plates confirms the positive correspondence between in-plane and through-plane electrical conductivity and fuel cell performance: an increase in electrical conductivity yields a proportional increase in performance (Figure 4-67).

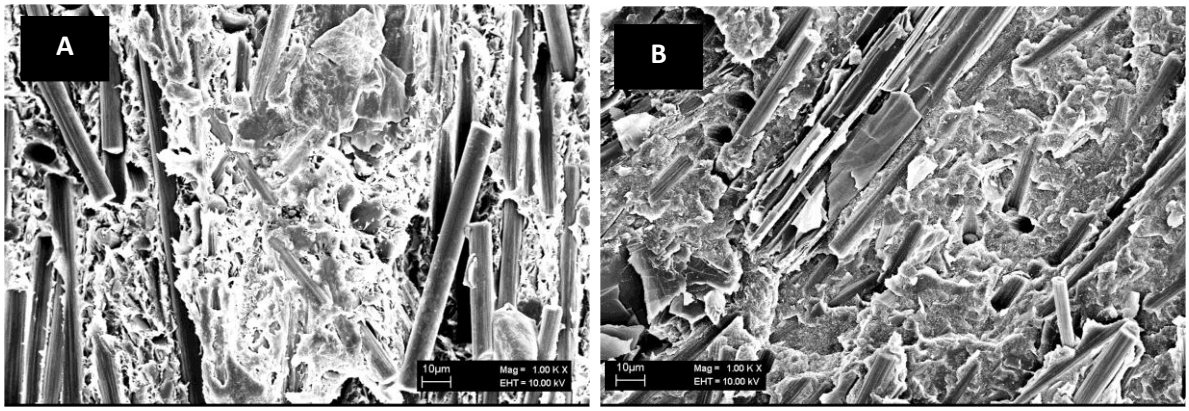

Figure 4-66: SEM micrographs of (A) P55FTi(s) and (B) P55FZn composites (magnification: 1,000X)

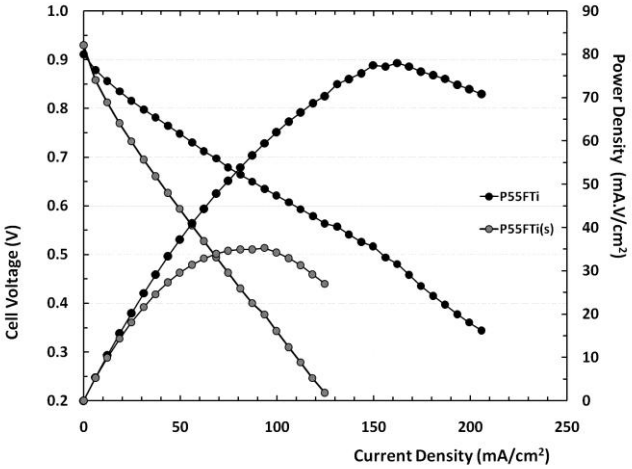

Figure 4-67: Performance of the fuel cells assembled with P55FTi and P55FTi(s) bipolar plates

The fuel cell with P55FTi bipolar plates had two times higher current density than that of the fuel cell using P55FTi(s) at a cell voltage of 0.6 V. The maximum cell power densities of those two cells are 77.96 and 35.29 mA.V/cm^2, respectively.

4.2.2 Processing Agent

As discussed previously, the viscosity of molten composites was increased by the addition of adding three carbon fillers. The processing agent, zinc stearate (Zn ($C_{18}H_35O_2)_2$), was applied to a composite to observe its effect on the electrical conductivity and flow property of the composite. In comparison with a composite with no processing agent, a composite with one has a drastic reduced electrical conductivity. The electrical conductivity of composites with and without processing agents is represented in Table 4-11. A composite containing multi-additive (a processing agent and coupling agent) was also produced and its electrical conductivity measured.

Examining the effects of processing agents in more detail, requires further characterization of the material's flow property. The capillary rheological characteristics of composites with and without processing agents are represented in Figure 4-68 and Table 4-12. The results show that a processing agent significantly decreases composite viscosity and the power law index of the composites is increased with the addition of the processing agent. The increase in power law index implies that the composite adopts more Newtonian fluid behavior. The plateau regime can be observed at a high shear rate, meaning the viscosity is less dependent on that rate. The consistency index indicates the decrease in viscosity of low shear rate when a processing agent was used.

Table 4-11: Electrical conductivity of the composites with and without processing agent

Samples	In-plane electrical conductivity (S/m)		Through-plane electrical conductivity (S/m)	
	Parallel	Perpendicular	Parallel	Perpendicular
P55F	792.836	495.612	49.713	47.191
P55FZn	627.140	453.669	40.340	42.410
P55FTiZn	636.272	468.205	46.906	45.530

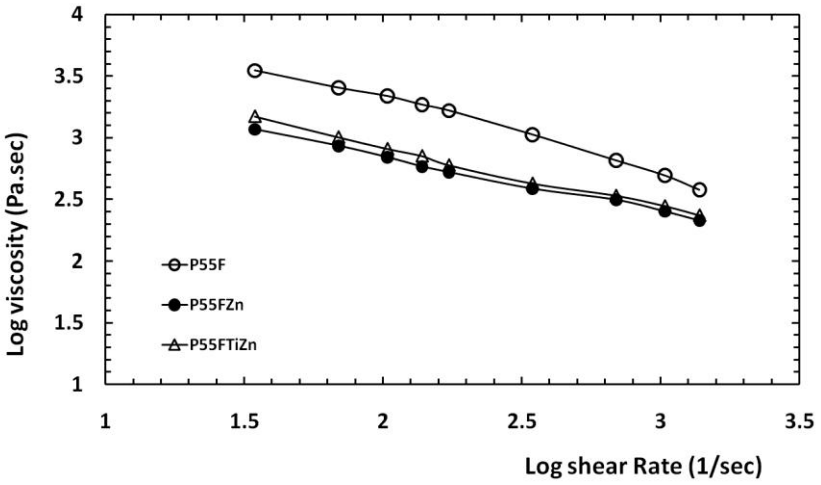

Figure 4-68: The effect of processing agent on capillary rheological behavior of the composites

Zinc stearate, which is a much shorter molecule than a polypropylene chain, can localize between the polymer chains causing a decrease in Van der Waals force between the polypropylene chains. Thereby, the viscosity of the composites is reduced. The processing agent also diminishes the friction of polymer bulk during polymer flow and reduces the friction between the barrel wall of an extruder or injection molding. This lubricant behavior of the processing agent results in poor filler dispersion, causing the electrical conductivity to decrease. The SEM micrograph of the composites with processing agent is depicted in Figure 4-66.

Table 4-12: The power law index and consistency index of the composites with and without processing agent

Samples	**Power law index (n)**	**Consistency index (k) Pa.s^n**
P55F	0.3898	34,914.03
P55FZn	0.5501	5,601.44
P55FTiZn	0.5130	7,883.45

Using additives, titanate coupling and processing agents for the PP/carbon filler composite tends to increase the electrical conductivity and shear viscosity, since the coupling agent improves the filler dispersion.

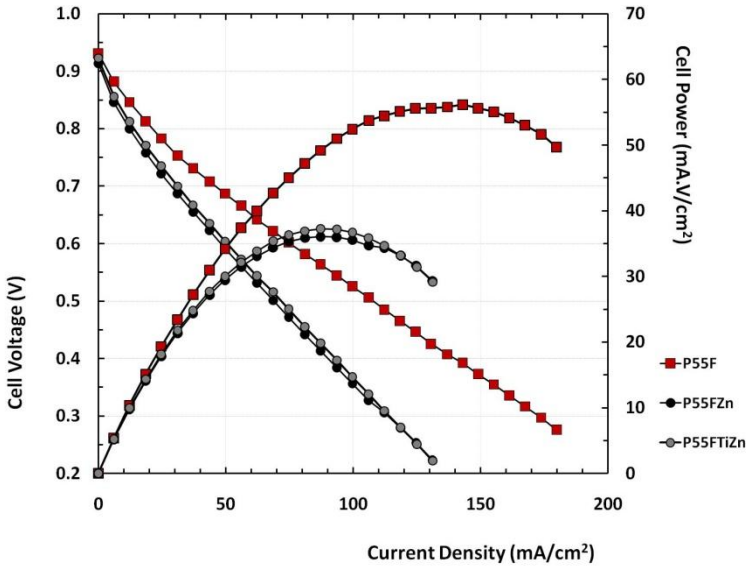

Figure 4-69: The effect of processing agent on fuel cell performance

As expected, based on the ex-situ test results, the performance of fuel cells with an added processing agent reduces by around 55% in comparison with the fuel cell using P55F bipolar plates (Figure 4-69). All results relating to composites with Zn stearate indicate that using processing agent did not give an advantage to fuel cell application; it increases the bipolar plate material cost.

4.3 Effect of Polypropylene Viscosity

Drubetski et al. stated that the higher level of fiber orientation in hybrid carbon black/carbon fiber polypropylene composites is due to the increased viscosity combined with the higher shear stresses required during polymer processing [158]. This statement suggested the idea of investigating polypropylene matrix viscosity may be related to the electrical conductivity of composites. To observe the matrix viscosity effects on fiber orientation and filler dispersion that result in composite electrical conductivity, two grades of PP were compared as matrix polymers in PP/three carbon filler composites. The melt flow rate values for the two grades

of PP used in this study are 7 g/10 min and 20 g/10 min. To ensure that it was the viscosity of a PP matrix affecting the electrical conductivity of composite bipolar plates, two systems of composites with different ratios of fillers were studied as described in Table 3-4.

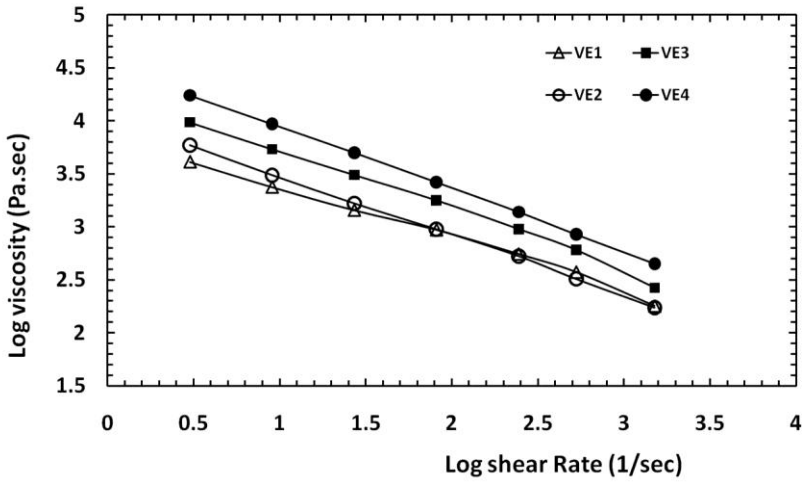

Figure 4-70: Capillary flow behavior of composites with low and high viscosity PP matrix

Figure 4-70 indicates that the viscosity of composites using low viscosity PP (VE1 and VE2) was lower in both systems as expected. For example the power law index of VE2 (0.309) performed slightly higher than that of VE3 (0.411). VE2 shows slightly more Newtonian flow behavior than VE4 does.

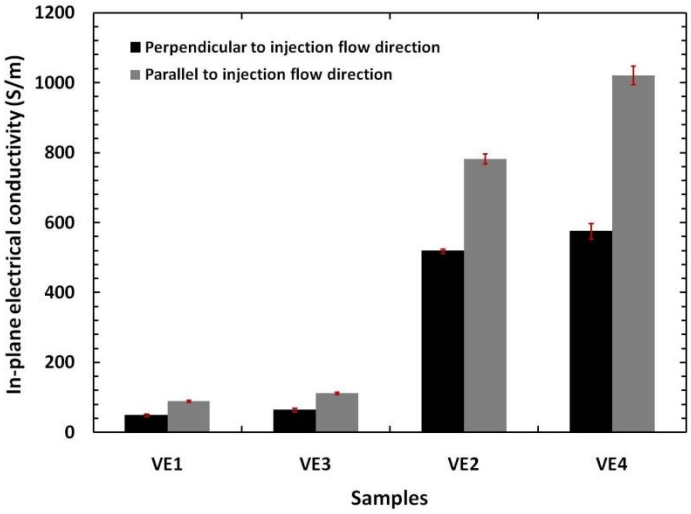

Figure 4-71: In-plane electrical conductivity of composites with different grades of PP

Figure 4-71 and 4-72 exhibit in-plane and through-plane electrical conductivity values of the composites based on the different viscosity values of PP matrix. Since these values are statistical averages, their standard deviations are given in terms of error bars to indicate the variance in the data. The higher viscosity (VE3 and VE4) based composites exhibit in-plane and through-plane electrical conductivity values higher than those of the composites based on the lower viscosity matrices (VE1 and VE2). Relative to micro morphological observation by SEM, the higher viscosity PP composites display slightly enhanced fiber orientation and graphite dispersion, reducing the quantity of filler contacts as seen in Figure 4-73.

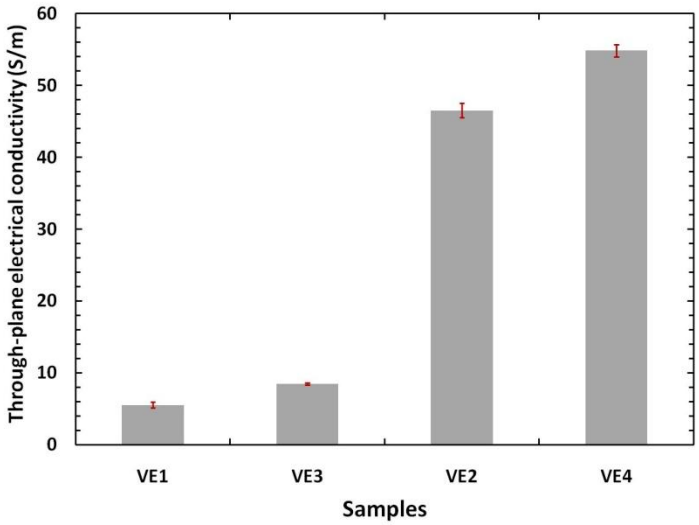

Figure 4-72: Through-plane electrical conductivity of composites with different grades of PP

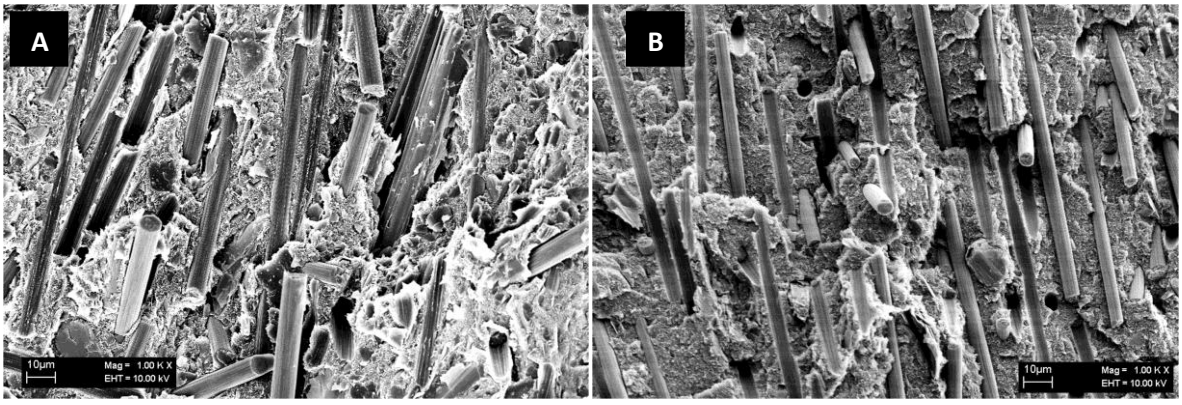

Figure 4-73: SEM micrographs of VE2 (A) and VE4 (B) at 1,000X magnification

Hypothetically, fiber orientation in the composite should be higher, contrary to the observations made in this research. Some CF, SG, and CB interactions and local conflicts of the SG particles to the flow pattern possibly caused less fiber orientation than was anticipated in the presence of SG and CB; which is in agreement with the discussion of Drubetski et al.[158].

Relating the direction of current flow to electrical conductivity, it is evident from the in-plane parallel samples that electrical conductivity is highest when current is applied in the direction of injection flow. In comparison, in-plane perpendicular conductivity is consistently approximately two-thirds of that of in-plane parallel, and through-plane conductivity is minimal across all sample plates. The higher in-plane conductivity can be related to the plate's manufacturing method; as the carbon fiber is pushed through the mould during injection molding, their alignment will mostly become oriented in the direction of the plane because of their rod-like geometry.

4.4 Effect of Injection Flow on Conductive Network

The need for injection molded bipolar plates in future commercialization as demand increases because it gives the capability for high-volume-production and high geometrical freedom of gas-flow channel design. The injection molded polypropylene composites display anisotropic characteristics, since the fillers are dispersed during the process. It was found that the electrical conductivity values of injected specimens cut from different areas of an injected plaque were different, since the electrical conductivity depends largely on the carbon fiber alignment, filler dispersion, and filler distribution.

The injection parameters, such as injection speeds and melt temperature, strongly affect filler orientation [159] and thus should affect the electrical conductivity of the blends. Although the conductive injection moldable composites can be produced in this research, electrical conductivity of bipolar plates, especially through plane conductivity, has not yet achieved the commercial target. For that reason, simulation of fiber orientation in injecting plaque using Moldex 3D/Solid program was carried out with the support of Compuplast Canada Inc to an investigate the effect of an injection flow on fiber orientation on conductive networks.

This simulation provides a guideline for further understanding the effect of graphite and carbon black dispersion on conducting paths. The simulation was performed from the basic plaque geometry used in this research, and the size of the plaque is 10.0 cm of width and 20.3 cm of length. The setting process conditions for this simulation are illustrated in Appendix B. The picture simulation outputs are illustrated in following pictures, and the definitions of the output are explained as follows. In the post-processing of fiber orientation, the biggest eigenvalue and its corresponding eigenvector are plotted together to show the complex fiber orientation phenomena. The orientation of the vector shows the most favorable orientation direction, while the magnitude of it (displayed in color) shows the degree of orientation.

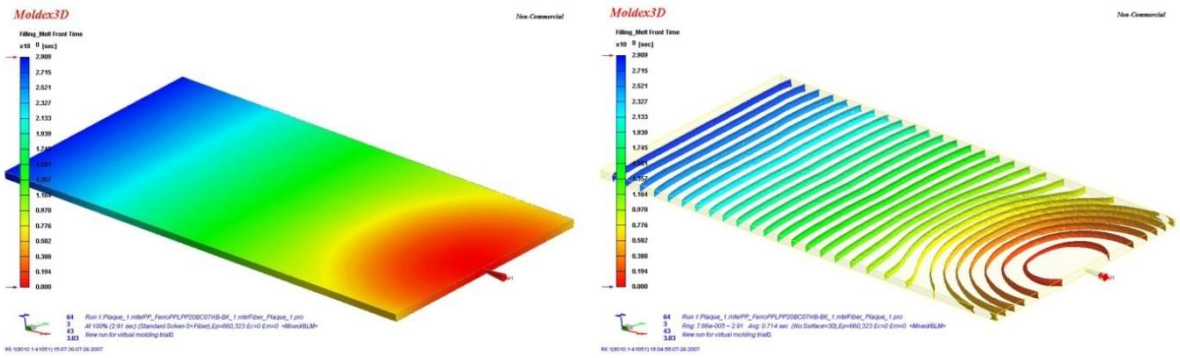

Figure 4-74: Simulation output filling pattern

From the pictures, it can be explained that the molten composite flows into a mold due to injection pressure at different times. In Figure 4.74, the blue zone represents the region to which a molten composite flows over the longest time (2.909 sec.), whereas the composite takes the shortest time for the red zone (0.000 sec.).

The Moldex3D/Solid analysis outputs are fiber Orientation (Skin) and fiber Orientation (Figure 4-75). ‘Fiber Orientation (Skin)’ is the fiber orientation on the skin layer near the surface of the plate, while fiber orientation is the three-dimensional fiber orientation distribution across the part. Therefore, users can use the slicing function to visualize its details. In summary, for a random orientation, the maximum eigenvalue would be 1/3; for a fully aligned orientation, the maximum eigenvalue would be 1.

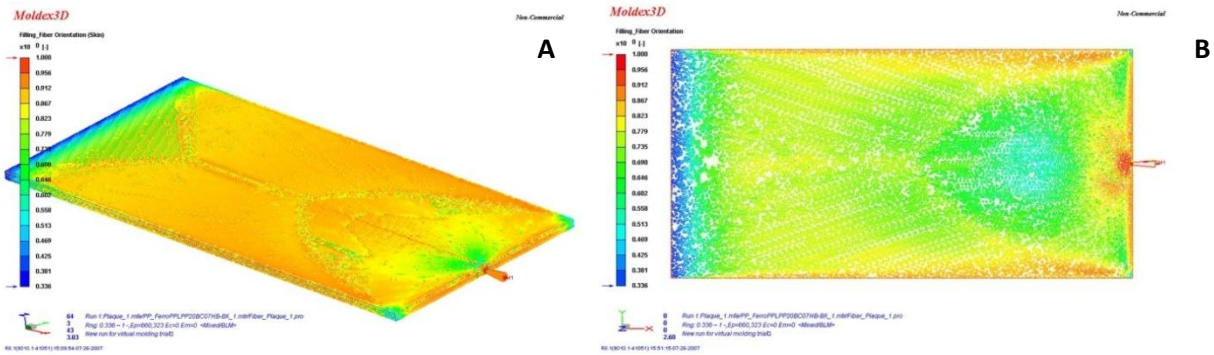

Figure 4-75: Simulation output: (A) fiber orientation (skin) and (B) fiber orientation

This injection simulation cannot explain the true fiber orientation of the composites in this research, since setting conditions are not exactly the same as the real conditions used for producing the composite plaques. This simulation was also performed for the PP/CF system, but the composites in this research contain three carbon fillers. SG and CB dispersion would affect fiber orientation. However, the simulation suggests ways to an idea to further electrical conductivity measurement. To address the influence of injection flow on bipolar plate electrical conductivity, conductivity values for a particular bipolar plate were assumed to vary by region and direction of applied current. Thus, electrical conductivity values were measured for different regions of the same plate as well as with current being applied in different directions. Specimens for measuring conductivity were prepared according to Figure 4-76. For each prototype plate, electrical conductivity values for regions A to M were measured. Note that four specimens from four composite plates for each sample were required to determine the effects of current direction on electrical conductivity values.

For in-plane samples, current was passed along the direction of the plate plane. The arrows in Figures 4-76 (a) and 4-76 (b) indicate the direction through which current was applied. Perpendicular and parallel designations refer to the direction of the applied current relative to the direction of injection flow during to the injection molding process. In-plane parallel samples were cut along the direction of injection flow, while in-plane perpendicular samples were cut perpendicularly to the injection flow. Lastly, for through-plane samples, current was passed directly through the plate plane.

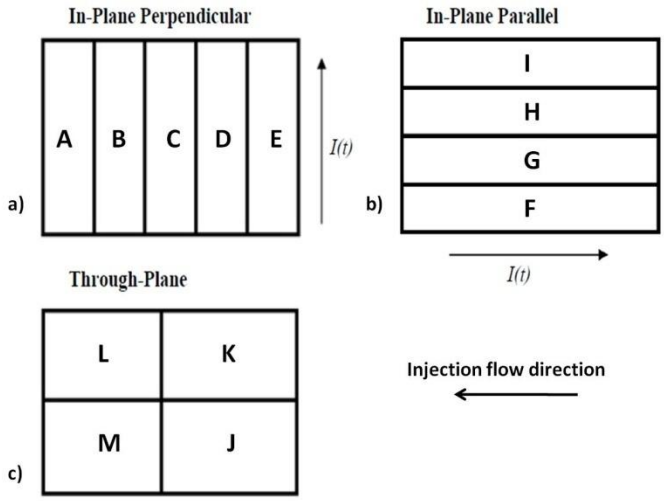

Figure 4-76: Electrical conductivity testing sample preparation

Through-Plane Electrical Conductivity

Three injection plates were cut into four areas (J, K, L, and M) as shown in Figure 4-76 (c). The through-plane electrical conductivity values of three composite systems were measured in different locations as illustrated in Figure 4-77. The electrical conductivity results of the FR3 composite, containing 55wt% of carbon fiber loading, is first discussed, since this composite system is more similar to the composite in the simulation work than the others. The electrical conductivity ranking of FR3 plates is M > L > J > K, and the result discussions are related to the simulation output pictures. In Figure 4-78, three areas from slice number 5 to 7 were focused onto simulate the fiber orientation.

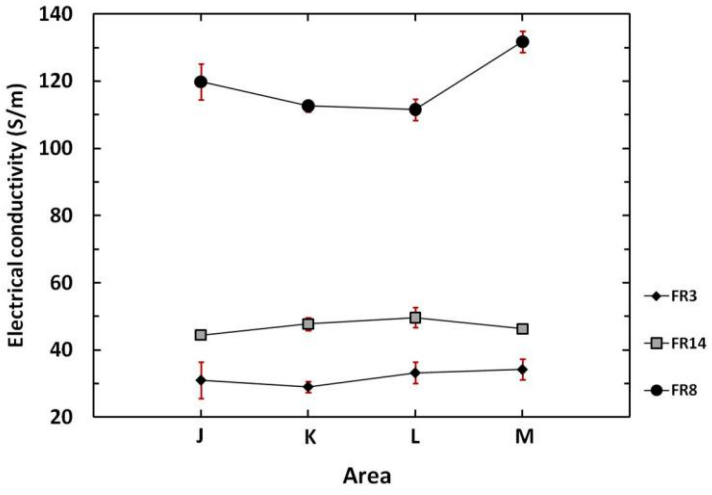

Figure 4-77: Through-plane electrical conductivity of composite plates in different locations

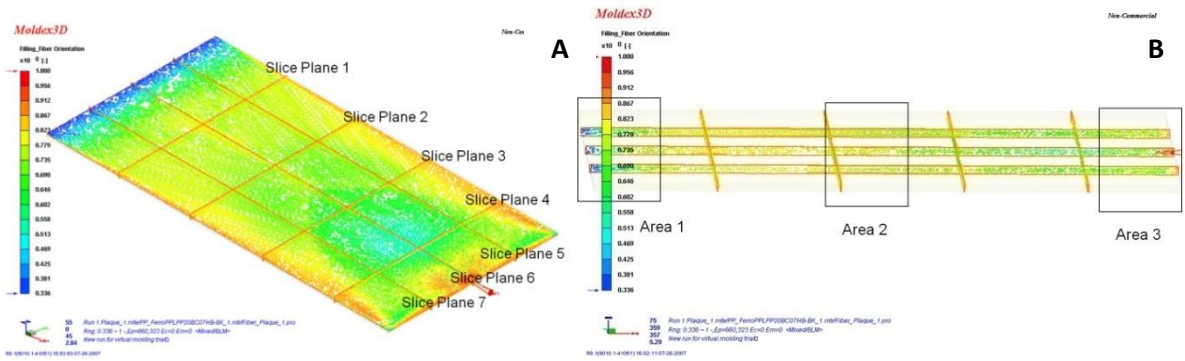

Figure 4-78: Various areas of the fiber orientation simulation output

As the results show, area M had the highest electrical conductivity, and the fiber orientation patterns can be seen in Figure 4-79. The M specimen covers area 1 of slice 7 and half of slide 6; it also covers half of area 2 in slice 7 and half of slice 6. It can be seen that the fibers were disorderly in the middle and the end of slices 7 and 6 (area 1). This fiber disorder is in the highest disorientation range, represented by dark blue color. In area 2, which is the center region of an injection plate, more orientation appears in the middle of slices 6 and 7. Most fibers align quite orderly along the flow direction on both edges of slices 6 and 7. To sum up, a conductive network can be successfully formed in which the fiber orientation ranges from green (~0.690) to dark blue (~0.381). The electrical conductivity of the L specimen was slightly lower than that of M. The result corresponds to the simulation output, since the degree of fiber disorientation in area 1of slice 5 is slightly lower than that of slice 7.

The specimens J and K mainly represent area 3, the location near an injection gate. The carbon fiber orientation in both sides of the injection gate (Figure 4-79) is quite alike. The carbon fibers orientated slightly in both sides of the injection gate, but with disorder alignment fashion in the middle region along the flow line from the injection gate (the light blue color), probably because a fountain flow effect happens during injection molding, pushing composite layers on the melt front that entered the cavity outward[160]. In comparison with an end plate area, the area near the gate exhibits better fiber orientation. The fibers in the area close to the injection gate were induced to align by injection and melt pressure more than the fibers at an end of filling area. The distribution in fiber connection in the area close to the gate may cause the composites to lose conductivity. The wide error bar of specimen J's conductivity shows the electrical conductivity distributions in the area near an injection gate.

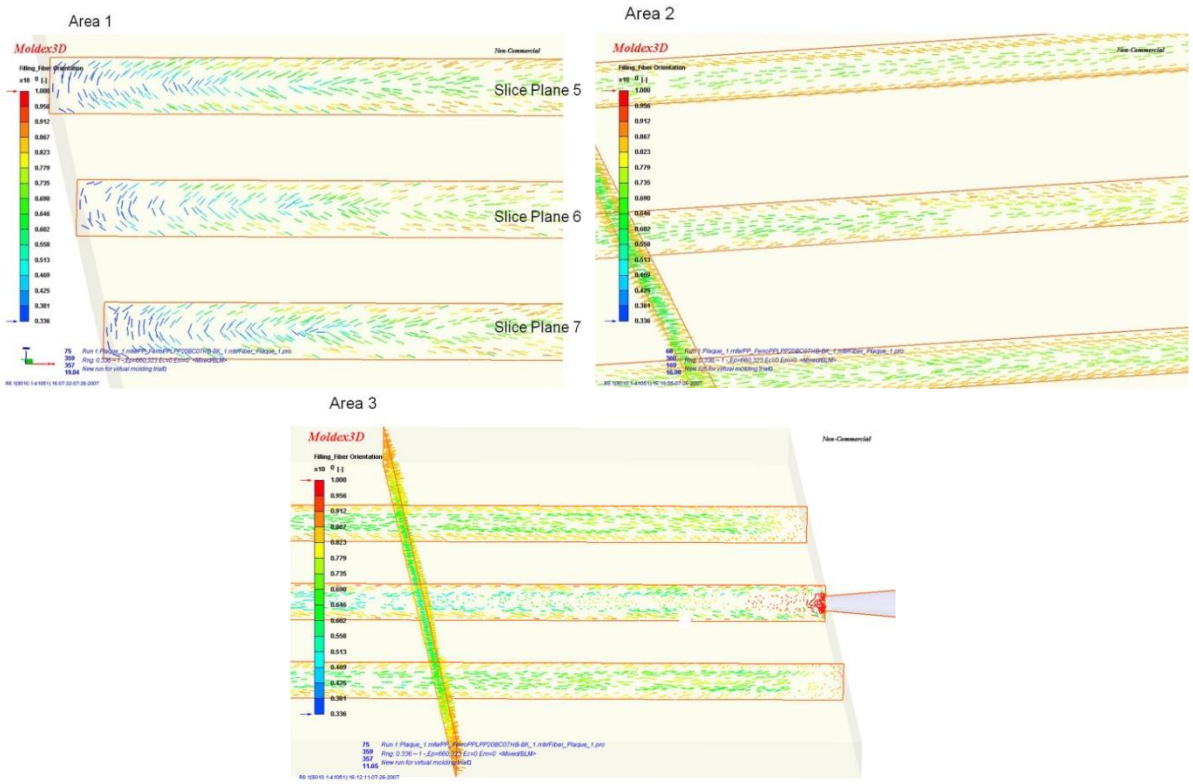

Figure 4-79: Zoom in on the three investigating areas

In terms of FR14 composites, the three filler system, the through plane electrical conductivity ranks L > K > M > J. This order of electrical conductivity does not correspond to the simulation output. During injection molding of composites, mechanical shear induces dispersion and distribution of SG and CB particles in the matrix. SG and CB distribution or SG agglomerates may disrupt fiber orientation. The electrical conductivity values of FR14 in different locations did not show a drastic change. In the case of FR8, the electrical conductivity measured from the area near the gate (J and K) shows lower values than at the end of the filling area. Note that FR8 contains a high carbon black ratio of 4:1:1 for the CB: CF: SG ratio.

The electrical conductivity of composite specimens from two areas significantly varied. This fact confirms that the distribution of carbon black aggregates strongly influence the orientation of carbon fibers as well as the conductivity. In this research, the electrical conductivity in many plate areas of composites with different filler ratios were also observed, as shown in Figures B-9, Appendix B. The results in different systems gave different

tendencies of changes in electrical conductivity. In reality, the fiber orientation and filler distribution could be due to the complex interactions among many factors during injection molding that affect the final distribution and dispersion of fillers [161]. Further detailed study of this effect is warranted, but beyond the scope of this project.

In-Plane Electrical Conductivity

The in-plane electrical conductivity values were measured parallel (Figure 4-80) and perpendicular to the injection direction (Figure 4-82). The specimens were cut as described in Figure 4-76.

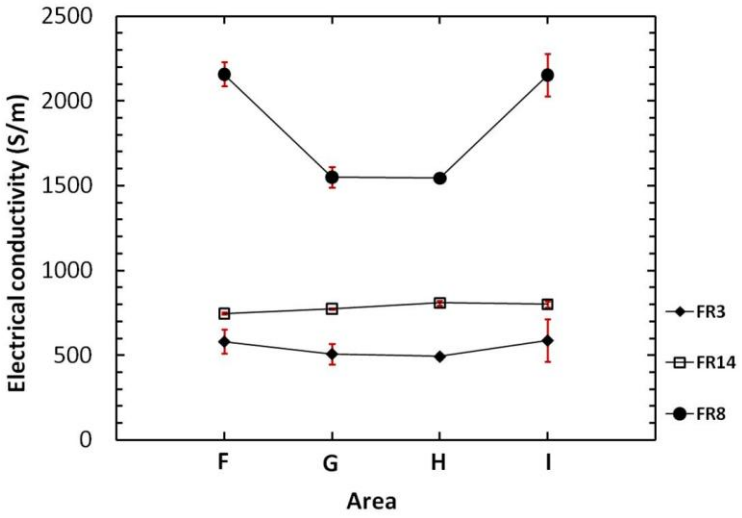

Figure 4-80: In-plane electrical conductivity of composite plates in different locations (1)

The electrical conductivity of FR3 plates, from Figure 4-80, shows two levels of conductivity values. Electrical conductivity values can correspond to the simulation output fiber orientation-skin in Figure 4-81. The simulation output indicates that the fibers are highly orientated, notably on the surface of composite plates.

The orientation on the skin is one reason that in-plane electrical conductivity is higher than through-plane electrical conductivity. This is also the reason for higher in-plane electrical conductivity in parallel to the injection flow direction compared to the value measured perpendicular to the flow direction. Higher electrical conductivity values of the F and I specimens are due to the carbon fibers orderly orientated on both sides of the plate skin layer, and they are aligned well in the core layer along the injection flow from the gate.

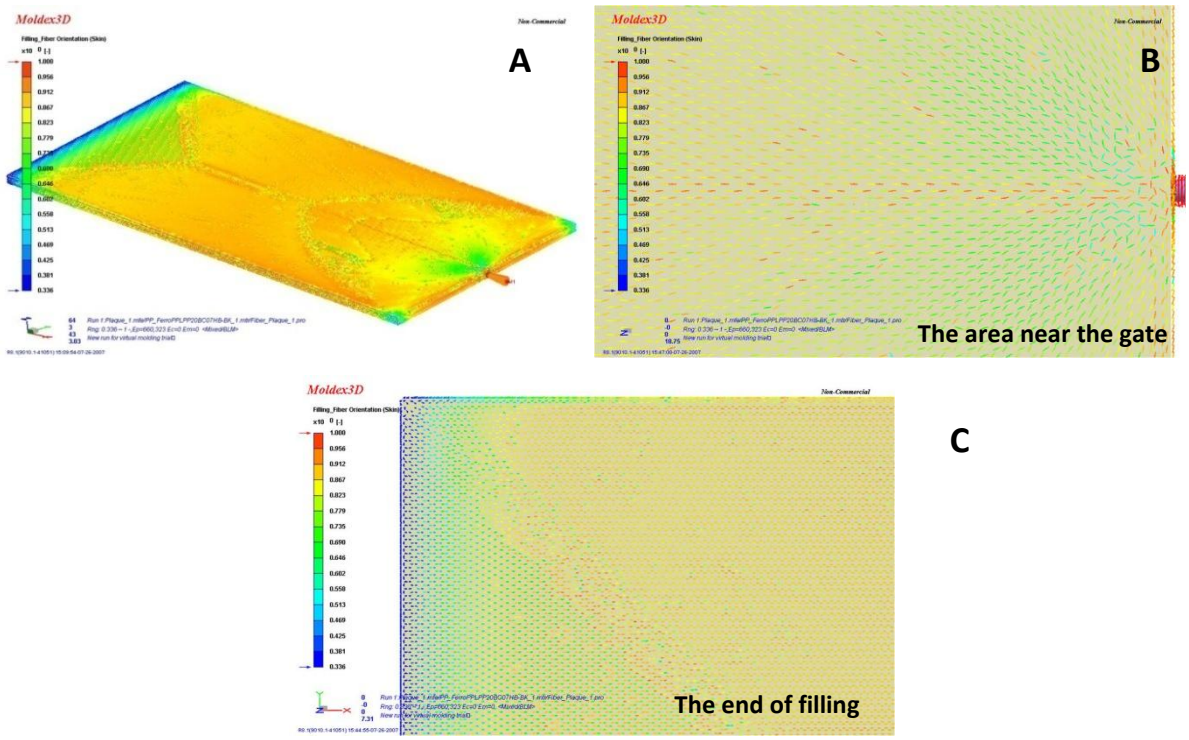

Figure 4-81: Simulation output fiber orientation-skin

The fiber orientation powerfully affected in-plane electrical conductivity, since the current was applied in the same direction as the orientation. Therefore, high conductive paths are provided for the flow of electrons. As results show, the electrical conductivity of the G and H specimens was slightly decreased, because fibers become disorderly in the layer near the filling gate. When the composites consist of hybrid fillers, the in-plane conductivity has the same general tendency as the conductivity of FR3 composites.

The difference of FR8's electrical conductivity between the side and centre regions is much higher than that of FR3 and FR14. The high ratio of carbon black in FR8 composites enhances a poor filler arrangement, especially in the area near the injecting gate. In-plane electrical conductivity in many plate areas of composites with different filler ratios was also observed (Figure B-10, Appendix B). Almost of the results indicate that the combination of carbon fillers has no significant effect on filler orientation at the surface of the composite plates. Therefore, this simulation has potential to be used for the investigation of the change in carbon fiber interconnections.

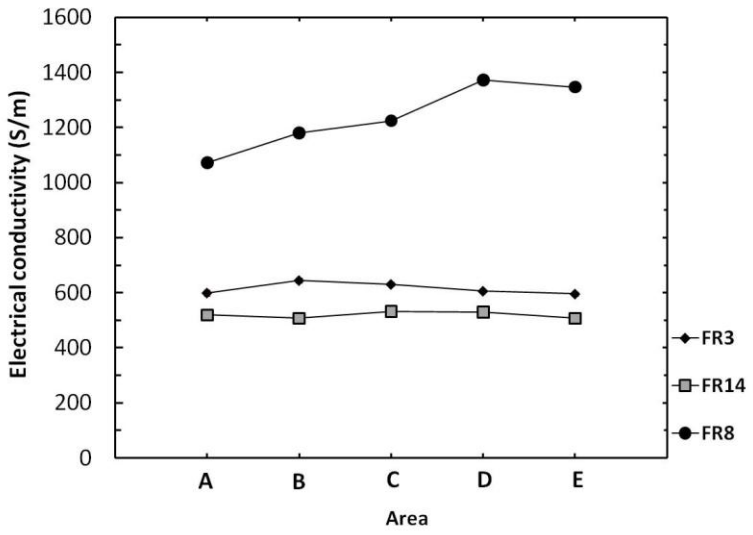

Figure 4-82: In-plane electrical conductivity of composite plates at different locations (2)

The in-plane electrical conductivity of the samples vertically cut to an injection flow direction has overall values lower than the values of samples cut in the parallel direction. That is because of lower numbers of fiber interconnections in the direction of electron flow. There was little difference in the composites' electrical conductivity measured from area A to E, and this result was unexpected. The electrical conductivity determined from areas A and E should be higher than that of the other zones, since the carbon fiber is randomly distribution. For that reason, more conducting paths would be enlarged in the direction of the measurement. In the case of the FR8 composite, the conductivity increased from the area at the end of filling to the area near the gate. A feasible reason for this phenomenon is poor fillers dispersion at the end of filling; thus connecting paths may be broken.

From Figure 4-81 (B), near the gate, a large quantity of fiber contacts can be observed. If there are good filler distributions around that area, more conductive filler networks will be associated. However, this trend did not exist in all composite systems as seen in Figure B-11, Appendix B. For further study, FR8 composite plates were cut into many pieces as depicted in Figure 4-83, and those specimens were measured for through-plane electrical conductivity. The through-plane electrical conductivity of the composite diverged in various areas (Figure 4-83) as expected, since carbon fillers are randomly distributed in a polymer matrix. It is hard to determine the actual pattern of filler network formation to give each a conductive value.

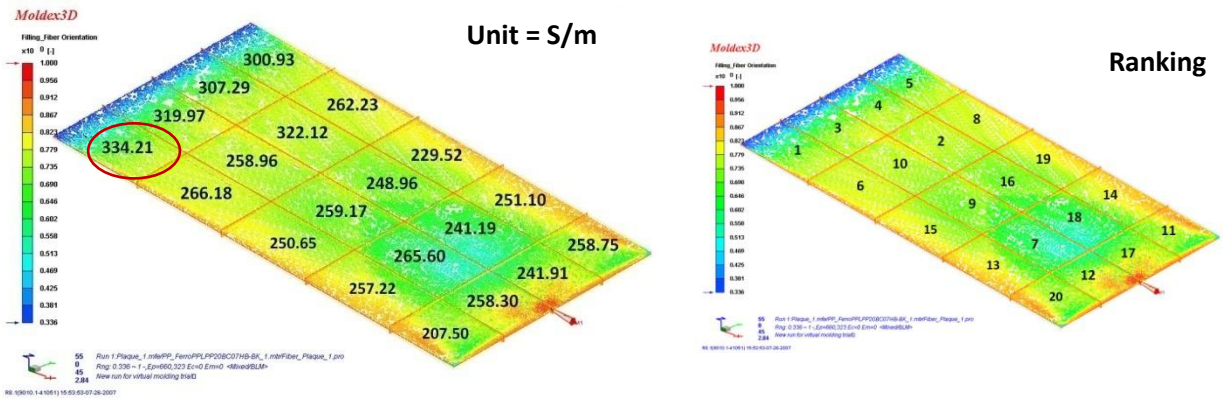

Figure 4-83: Through-plane electrical conductivity of composite plates in twenty locations

To summarize the results, the highest electrical conductivity (334.21 S/m) was found from an end filling area (marking red circle), and the last row of the end filling area gave the highest conductivity compared to other zones. The results positively correspond to the previous discussion describing a relation between through-plane electrical conductivity and the simulation output. As described previously, the degree of orientation is represented by the degree of orientation in different colors. Composite specimens from each color shade were prepared to investigate the morphological characteristic of composites in that area by SEM images (Figure 4-84). For further experiments, the SEM images were used to determine a number of fillers (SG and CF), a number of connection points, and filler contact areas using UTHSCSA ImageTool Version 3.0. Micrographs (with 3kX of magnification) having an area of approximately 4,872 μm^2 were used for the determination. Note that five areas were snapped for each SEM specimen, and five specimens were required to determine those values. The results from ImageTool are illustrated in Table 4-9.

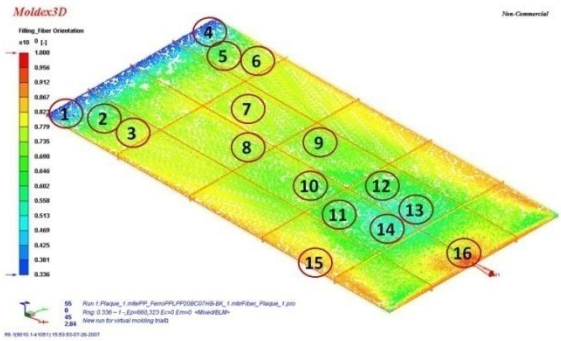

Figure 4-84: The areas in a composite plate observed by their morphology by SEM

Table 4-13: The results from ImageTool

Area	#SG	#CF	#SG-CF contacts	SG-CF contact area mm^2	#SG-SG contact	SG-SG contact area mm^2	Total # number of contact
1	10	6	6	12.856	6	6.223	11
2	22	3	3	8.610	6	11.209	9
3	10	10	3	13.901	3	8.626	6
4	17	5	3	7.405	3	8.626	6
5	17	3	2	13.664	7	11.524	9
6	10	7	2	3.115	2	7.682	4
7	5	6	4	9.401	1	1.096	5
8	4	4	4	20.672	1	6.982	5
9	8	7	2	22.120	3	12.027	4
10	19	6	2	27.462	4	6.821	6
11	11	7	3	9.291	5	6.301	8
12	11	9	5	8.563	3	5.072	8
13	9	5	3	9.604	6	7.072	9
14	21	5	4	8.743	3	2.426	7
15	13	13	1	4.963	3	9.463	4
16	8	11	3	8.798	1	0.665	4

As the results in the table show, the total number of filler contacts in a dark blue zone is highest, and the overall values from a light green zone to a dark blue zone are higher than a red zone. Results in Table 4-13 can be related to the electrical conductivity values in Figure 4-84. It could be concluded that a smaller degree of fiber orientation gives fillers a higher opportunity to form more conducting paths, resulting in increased electrical conductivity values.

According to previous results, a supercritical carbon dioxide (CO_2) technique was introduced in order to create a random orientation of filler. Lee and Tzoganakis have applied supercritical carbon dioxide into polymer extrusion for the improvement of polymer blend properties [82]. In this experimental work, composite plates were shaped into circles with diameter of 1 inch, and then a specimen was placed into a steel chamber, which is a closed system. After the chamber was heated up to a certain temperature, a metered amount of CO_2 was directly injected into the chamber under constant pressure (2,000 psi). The operating

conditions were also varied to investigate the effect of conditions on morphology change. The temperatures used in the processes were 150, 180, 200^{o}C, and the process intervals were 1 and 2 hrs. After the process was done, the through-plane electrical conductivity of final specimens was measured to observe the change in electrical conductivity.

Table 4-14: The effect of supercritical carbon dioxide (CO_2) technique on electrical conductivity

Conditions	**Through-plane electrical conductivity (S/m)**
No supercritical carbon dioxide (CO_2)	42.09 (SD = 0.876, n = 9)
150 ^{o}C, 1hr., 2200 psi	43.72 (SD = 3.189, n = 9)
180 ^{o}C, 1hr., 2200 psi	56.70 (SD = 1.900, n = 9)
200 ^{o}C, 1hr., 2200 psi	61.59 (SD = 1.666, n = 9)
200 ^{o}C, 2hr., 2200 psi	60.42 (SD = 2.307, n = 9)

Note: The composite used for this experiment was P55F composite

As shown in Table 4-14, the supercritical carbon dioxide (CO_2) improved electrical conductivity of the composites from 42 S/m to 60.42 S/m. The process operation under a temperature lower than the melting point of PP cannot increase the electrical conductivity of the composites, since polymer chains do not have enough energy to flow and allow for fiber reorientation. Therefore, CO_2 molecules did not penetrate into the polypropylene phase. The electrical conductivity slightly increased as the temperature increased, but the longer time spent for the process did not cause an increase in electrical conductivity. Supercritical CO_2 was found to decrease the interfacial tension between polymers, and it also affected on the dispersed phase size during melt blending [83]. The dissolution of CO_2 may decrease interfacial interaction between filler-fillers, thus the agglomerates and aggregates of fillers would decrease. Therefore, dissolution of CO_2 can develop filler dispersion in a polypropylene matrix, and an increase in electrical conductivity. The SEM micrographs of the composite after the supercritical CO_2 process were also observed; however, no clear change of composite morphology before and after the process could be found.

4.5 Contact Resistance

4.5.1 Effects of Tightening Torque

To reduce the fuel cell resistance, not only must the electrical conductivity of fuel cell component materials be decreased, but a reduction in the contact resistance of fuel cells. If the contact resistance is adequately decreased, the overall fuel cell resistance has a greater chance to meet the target at reduced filler loadings. External factors such as the clamping of a stack of individual fuel cells results in increased pressure applied at the interface, leading to an increase in the contact area between fuel cell components (i.e. the plate and GDL); which, in turn, decreases the contact resistance. In this section, the clamping torque on supportive screws was varied to observe the effect of assembly pressure on fuel cell resistance and fuel cell performance. Asghari et al. investigated the effect of non-uniform tightening of the supportive tie rods [162]. Results indicated that the uneven assembly pressure can reduce the fuel cell performance due to a non-uniform fuel cell assembly pressure. Therefore, all fuel cells in this research were assembled with tightening supportive screws tightened in order, as shown in Figure B-12; Appendix B.

Prior to tightening the supportive screws in order, a fuel cell was assembled by uneven tightening of the supportive screws to observe the basic effect of tightening order. Results obtained from the test gave the following information. The non-uniform tightening resulted in poor cell sealing, and also in oxygen starvation at the cathode and hydrogen leaks that created in a safety concerns. Moreover, GDL penetrated into a gas flow channel, resulting from non-uniform compression of the GDL, and blocked the flow channel (Figure 4-85(A)). The uneven pressure also damaged the bipolar plates, as seen in (Figure 4-85(B)).

Total cell resistance of a single cell can be expressed as a sum of contributions from uncompensated wire/contact resistance, the ohmic resistances of fuel cell components, and the contact resistances between the cell components. The clamping torque on supportive screws was varied from 1 to 5 Nm to investigate the effect of assembly pressure on contact resistance. The increase of single cell performance is proportional to the increase of the clamping torque, as seen in Figure 4-86. These findings indicate that clamping torque, and accordingly assembly force have an essential role on the performance of PEMFC.

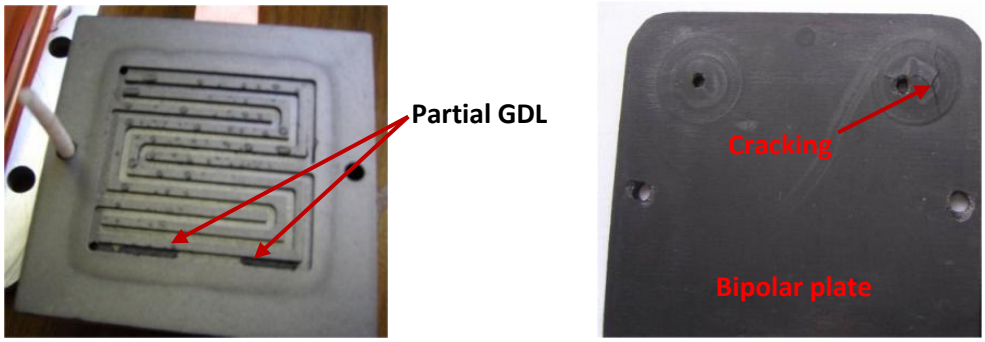

Figure 4-85: (A) partial GDL in gas flow channels of a cathode bipolar plate, (B) cracking of bipolar plates

Unsatisfactory assembly force leads to leakage of gases and high interfacial contact resistance between fuel cell components, resulting in increased ohmic polarization losses. The change in ohmic polarization losses can be observed in Figure 4-86. At intermediate current densities (0.5 V of cell voltage), the current densities of the single cell clamped by varied torque from 1 to 4 Nm were 34.79, 42.49, 53.73, and 97.86 $mAcm^{-2}$, respectively. The maximum power density values were 37.16, 46.25, 56.02, 101.69 $mA.Vcm^{-2}$ (or $mWcm^{-2}$), respectively.

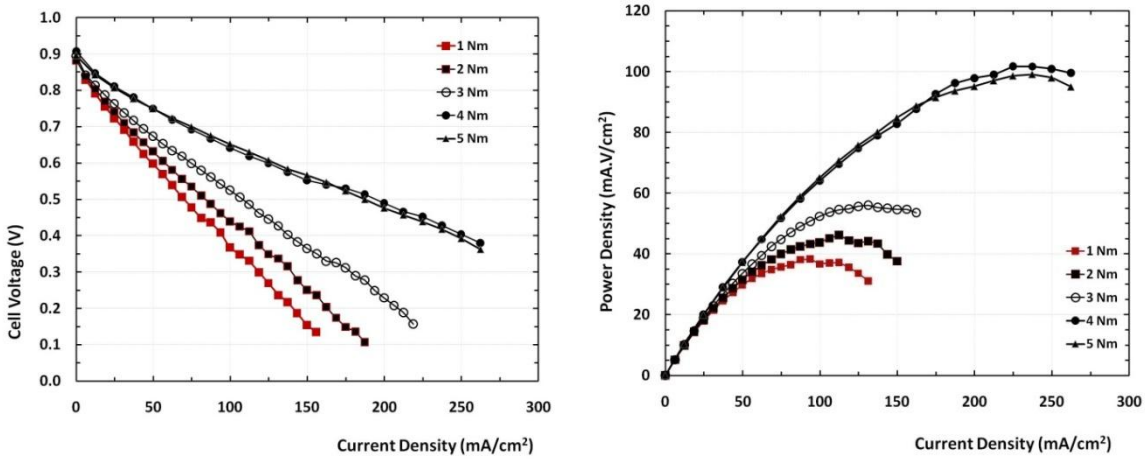

Figure 4-86: Performance of PEMFC using P55FPPy bipolar plates, assembled with different degree of torque tightening

On the other hand, increasing torque to 5 Nm did not increase the fuel cell performance by much. The cell voltage of the fuel cell assembled at 5 Nm was slightly higher than that of the fuel cell assembled at 4 Nm for medium current density. For instance, the cell voltage values,

at a current density equal to 137.250 $mAcm^{-2}$, of the fuel cell assembled at 4 Nm and 5 Nm were 0.575 and 0.584 V, respectively. In contrast, the cell voltage drop of the fuel cell assembled at 5 Nm, in a high current density regime was higher than that of the one with 4 Nm. Although the overall cell resistance of 5 Nm was almost identical to that of 4 Nm, its charge transfer resistance was obviously higher than that of 4 Nm. It can be interpreted that too high force reduces the porosity of GDLs, resulting in increased the mass-transport overpotentials at high current density [119], especially at the cathode side, because moisture generated at the cathode cannot be completely removed and so affects the transport of oxygen in the diffusion layer.

Too much torque also causes damage to the GDLs', it could fracture or deform the bipolar plates. The failure of bipolar plates could be observed in the case of graphite bipolar plates. A cracked bipolar plated is depicted in Figure B-13, Appendix B. The AC impedance method was measured in this study to analyze the effect of the clamping torque on overall fuel cell resistance illustrated in Table 4-15. The ohmic resistance of the fuel cell reduced with as clamping torque increased, probably because of the compression of the GDL as well as in the reduction in conduct resistance.

Table 4-15: Fuel cell resistance at high frequency of single cell with different clamping torques

Torque	In-situ ohmic resistance (Ω)
1Nm	0.3031
2Nm	0.2713
3Nm	0.2165
4Nm	0.1426
5Nm	0.1423

4.5.2 Effects of Compression Force

The through-plane electrical conductivity of composite bipolar plates, as an ex-situ test, was also measured at conditions with different loading compression forces. Compression forces

applied for the test include 2,500, 5,000, 7,500, 10,000, and 15,000 lbs, respectively. Note that the size of specimens used in this experiment was 36.15 mm (width) × 97.61 mm (Length) × 2.96 mm (Thickness). Four specimens were used to repeat the test, and average values were used to plot graphs. The electrical conductivity measurement of a composite plate sandwiched between GDLs used for a fuel cell in this research was also conducted in this experiment. As expected, the measured conductivity increases with increasing compression force for both bipolar plate samples with and without different GDLs (Figure 4-87).

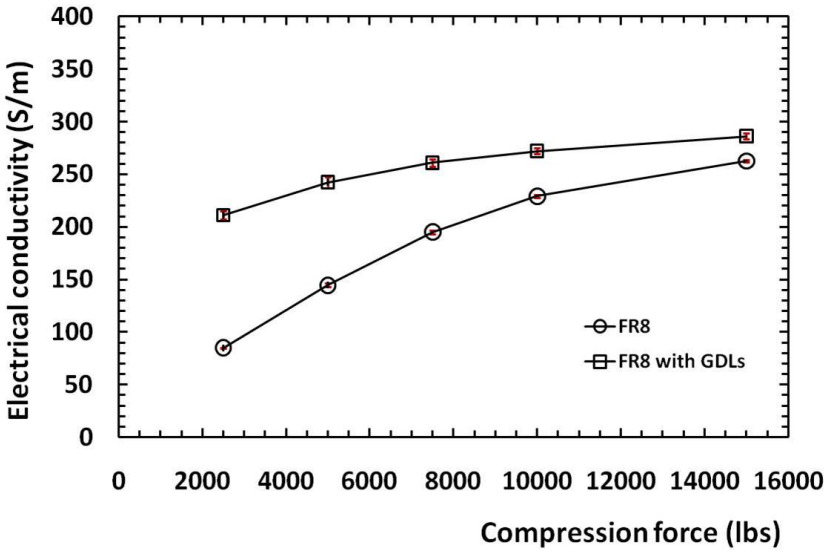

Figure 4-87: Effect of Compression force on through-plane electrical conductivity

For the specimen with GDLs, two possible reasons can be used to explain the contact resistance reduction. First, forces applied to the interface lead to an increase in the contact area between the bipolar plate and GDLs, which in turn, decreases the interfacial contact resistances. Second, carbon fibers in GDLs penetrate into the surface of composite bipolar plates and so conductive paths are propagated. The graph in Figure 4-87 also indicates that the dependence of contact resistance versus compression is non-linear, which is in agreement with results in the literature, such as those of Fu et al. [163].

4.5.3 Effects of Temperature

Many researchers have been interested in the effect of operating temperature on PEMFC performance. Yan et al. found that an increase of proton mobility or enhancement of the

membrane hydration level as temperature rises results in membrane conductivity improvement [97]. Freire et al. also stated that water transport through the membrane from the cathode to the anode, when the temperature increases, affects membrane hydration [164]. Better membrane hydration can reduce the ohmic resistance of a fuel cell; and charge transfer resistance decreases as the operating temperature increases owing to the faster oxygen reduction reaction [162]. Besides the improvement of those parameters, temperature increases also influence the electrical conductivity of composite bipolar plates. The effect of temperature on through-plane electrical conductivity was studied, and the results are shown in Figure 4-88. This experiment was conducted under 5,000 lbs (1,500 psi) of compacting force. As the results shown in Figure 4-88 indicate, the electrical conductivity increased when the temperature increased, in agreement with Fu et al. [163].

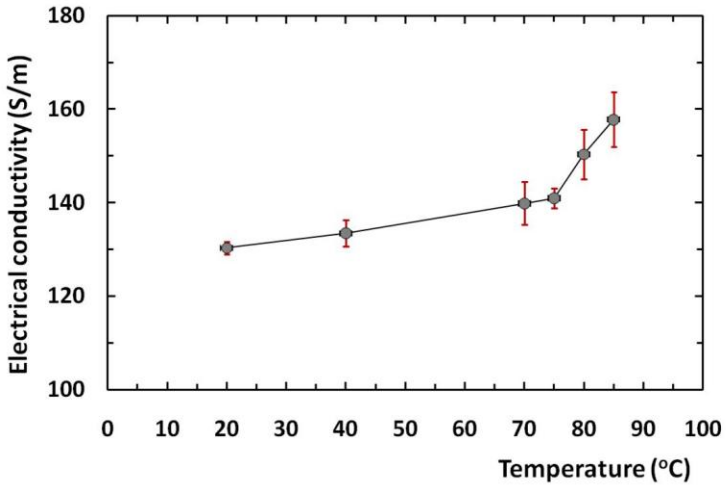

Figure 4-88: Effect of temperature on through-plane electrical conductivity

The results indicate that the internal electrical resistance of PEMFC using composite bipolar plates is going to be lower at the fuel cell operating temperature. Bipolar plate characteristics must relate to three effects: temperature, time, and compressive force, all at the same time under fuel cell operating conditions. Therefore, the creep behavior of composite plates was studied to determine the possibility of using these composite materials in bipolar plates. Figure 4-89 displays the creep behavior of P55F composite at various applied stress levels. Creep graphs display two main different zones of behavior for the creep strain rate as a function of time. First, in the initial primary creep regime, the creep strain rate drastically increased when stress was applied.

In the secondary regime, the creep strain is almost constant over time. In this experiment, the third region, where the creep strain rate increases until failure cannot be observed, the composite plate did not show any trend towards damage the fuel cell operating temperature (80^{o}C) as a function of time. Creep deformation did increase when higher applied stresses were introduced. The change in creep deformation at low stress was slow; for example, the deformation changed approximately 0.073% when the stress increased from 1,000 to 2,000 Pa. The change in strain became much higher when the stress was higher than 2,000 Pa. Different applied stresses proved the previous postulation of the compacting force effect on the electrical conductivity of composite bipolar plates.

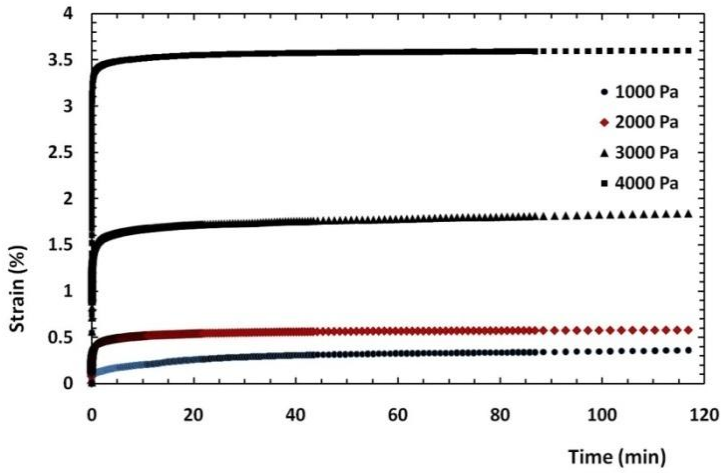

Figure 4-89: Effect of stress on creep behavior of P55F composite under 80^{o}C over two hours

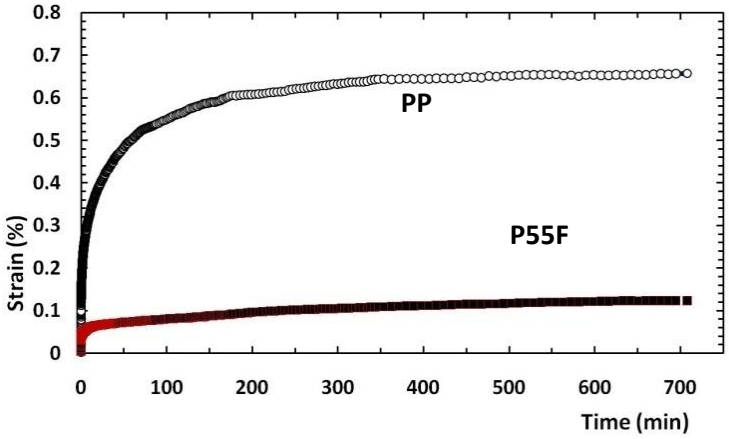

Figure 4-90: Creep behavior of P55F composite under 80^{o}C with 1,000 Pa of stress

In order to determine longer time creep deformation, the shear stress was kept constant at 1000 Pa for 12 hours, as showed in Figure 4-90. It is noticeable that the creep deformation decreases with the addition of carbon fillers, as expected from the addition of a rigid reinforcement into a viscoelastic matrix. Although the testing interval is up to 12 hours, the creep strain is approximately constant. Furthermore, there is no evidence of plate rupture, since the strain remained stable throughout the relevant time period examined. From visual observation, the diameter of the P55F specimen after the test was similar to the diameter before the test (1 inch).

As mentioned, PEMFC may be able to operate under higher temperatures and thus to improve fuel cell performance. Therefore, the creep behavior of composite plates under different temperatures was investigated in this work (Figure 4-91).

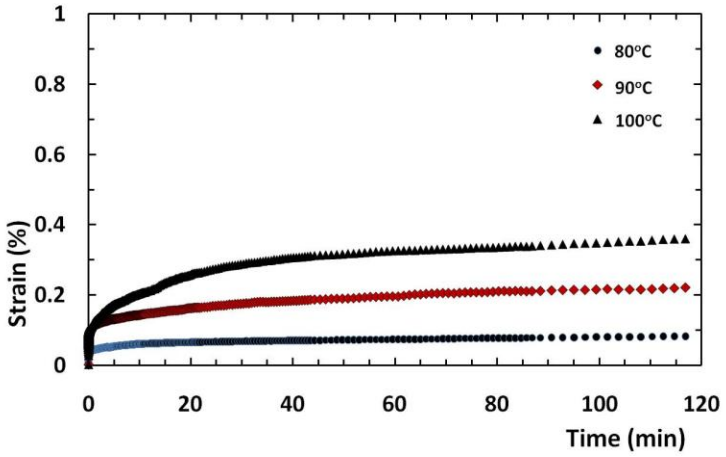

Figure 4-91: The effect of temperature creep behavior of P55F composite (1,000 Pa of stress)

The results show that creep deformation increased as the temperature increased. The results indicate that composite bipolar plates produced in this work can be used under basic fuel cell operating temperatures (65-85 ^{o}C), since the strain is very low (< 0.1%) and remains constant as a function of time. These bipolar plates can be applied to the higher temperature PEMFC system as well, because there is no significant change in strain rate (<0.3%) with the temperature raised up to 100^{o}C.

Oscillatory time sweep measurements revealed a pronounced time dependence of G' and G" of composite plate (P55F) (A) and neat PP (B), as shown in Figure 4-92. The storage modulus (G') in a polypropylene composite, which is a viscoelastic solid, represents the elastic portion, whereas the loss modulus (G") represents the viscous portion. Based on the time dependency of the elastic and loss moduli of the neat PP and the PP composite, it can be seen that the addition of carbon fillers leads to at least a ten-fold increase in the composite moduli compared to those of the neat PP. Carbon fillers cause the mobility of PP to decrease. For the neat PP, both moduli keep decreasing as a function of time, since PP chains is more flexible and can move a part of adjacent chains more easily. On the other hand, the elastic and loss moduli of the PP composite increased when the testing period increased from 0 to 4000 s, and then they slightly decreased after that.

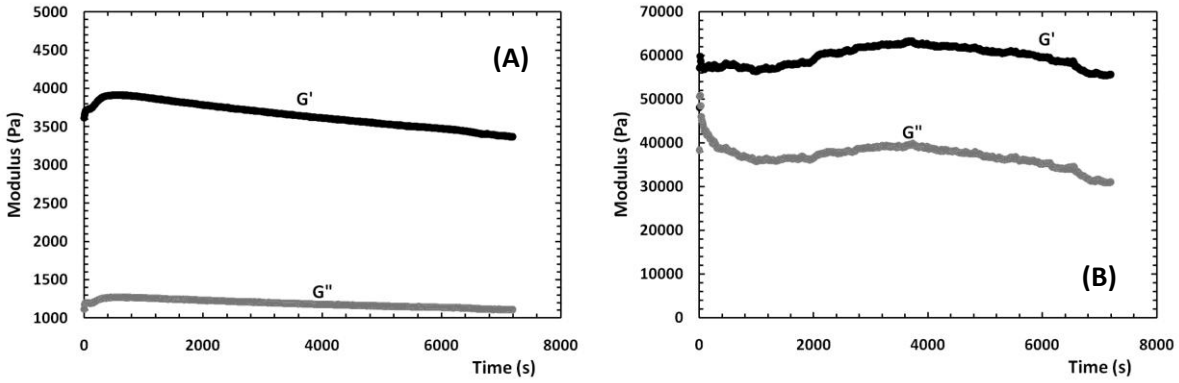

Figure 4-92: G' and G" of neat PP (A) and P55F composite
(B) as a function of time at 170 ^{o}C

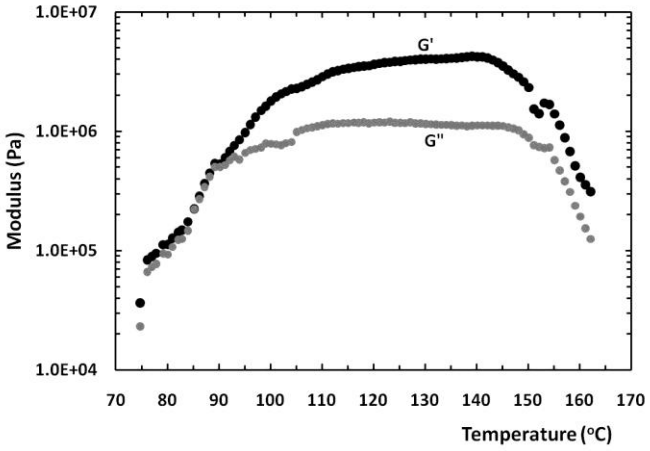

Figure 4-93: G' and G" of P55F composite as a function of temperature

The slight decrease in the moduli suggests that the polymer chains are extended, but the values of the moduli still remain high throughout the time period examined. In brief, this PP/carbon filler composite bipolar plate has ability to support mechanical strength of PEMFC. The observation of the effect of temperature was also performed and the results are displayed in Figure 4-93. As previously discussed, storage and loss moduli increased due to the mobility and thermodynamics effects. When the temperature was in a range of 110 to 140 ^{o}C, a plateau regime could be observed. The filler network declined, when the temperature above than 140 ^{o}C; the slope of the curve decreases, indicating that the elasticity is enhanced. This phenomenon stems from a competition between mobility and thermodynamics.

4.6 Bipolar Plate Modification

4.6.1 Mechanical Surface Treatment

In addition to about the interfacial contact resistance in PEMFC, which comes from the interface between the bipolar plates and GDLs, the mechanical surface treatment is another interesting approach to reducing the interfacial contact resistance of bipolar plates. In this part of the research, a mechanical treatment was used to remove the polypropylene-rich layer on the bipolar plate surface. Many methods of surface activation are currently used in industry, including sanding and abrasion. In this research, surfaces of bipolar plates and composite plane plates were polished using an Automet polisher. Each plate was gently hand polished by Carbimat sandpapers of 240 grit size until the shiny surface of the polymer layer was removed. Finally, surfaces of the polished bipolar plates were cleaned with isopropanol and dried to remove any particle remains [165].

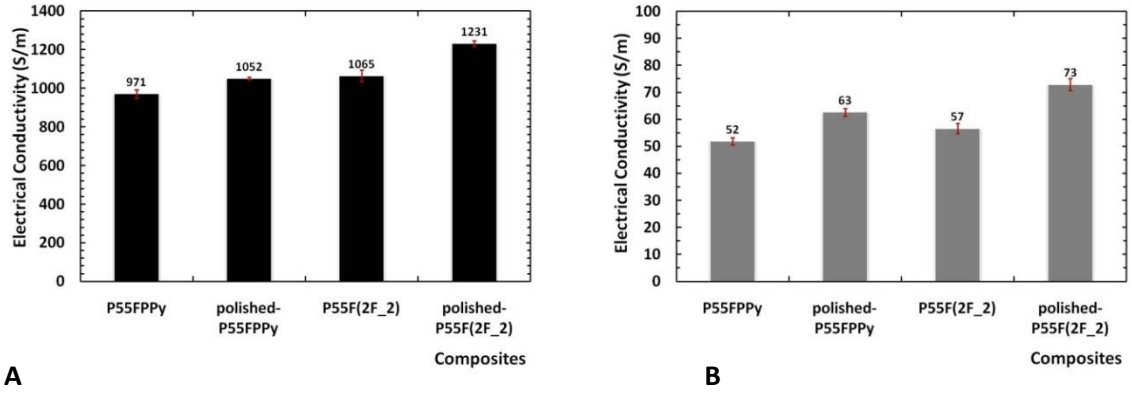

Figure 4-94: Electrical conductivity of non-polished and polished bipolar plates

As anticipated, and graphed in Figure 4-94, the electrical conductivity of composite plates increased after their surfaces were polished with sandpaper. Typically, the polypropylene composite bipolar plates can be fabricated by an injection process with quite a high concentration of polypropylene. The molding process results in the formation of a polymer-rich skin over the surface of the molded part; subsequently, a rich non-conductive layer on a bipolar plate contact region leads to an increase in the contact resistance at the bipolar plate and GDL interface. The surface treatment can also minimize the surface roughness of bipolar plates, leading to a decrease in the overall fuel cell resistance as well. The interfacial contact resistance constitutes an important source of the ohmic resistance due to the insulating layer at the interface. PEMFC performance can be improved if the contact resistance can be minimized.

The fuel cells with un-polished bipolar plates performed less well than that the bipolar plates whose surface was polished, in disagreement with Avasarala and Haldar [165]. When a non-conductive layer is removed from a bipolar plate surface, the surface is enriched with conductive fillers. For that reason, the association of conductive GDLs and conductive surface of bipolar plates can form better conducting paths for electron transport.

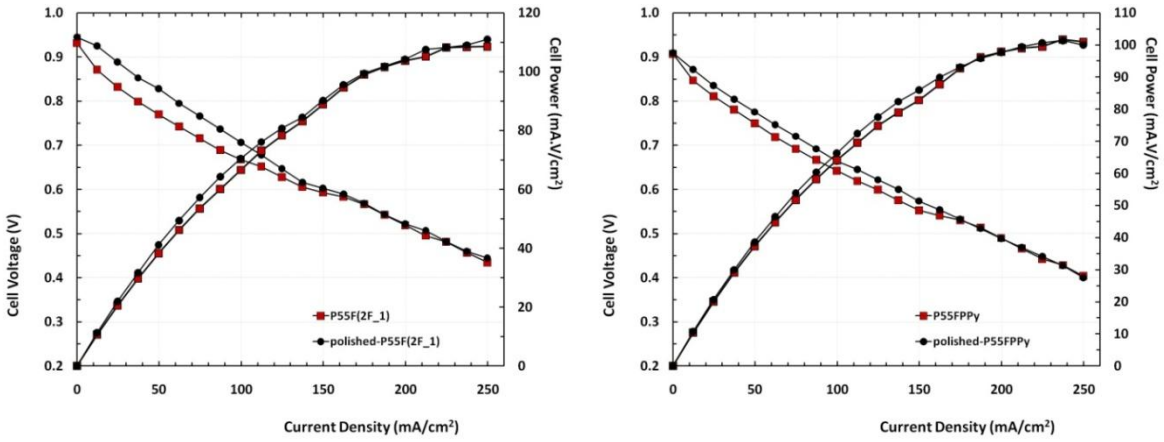

Figure 4-95: Effect of surface polishing on fuel cell performance: (A) the fuel cell using P55F (2F_1) bipolar plates, (B) the fuel cell using P55FPPy bipolar plates

The results in Figure 4-95 confirm this supposition. In the ohmic overpotential region, the cell voltage of the fuel cell assembled with polished bipolar plates was slightly higher than that of the fuel cell using un-polished bipolar plates. However, at higher current density, the

performance of fuel cells using both types of bipolar plates is nearly independent of surface polishing. That is, the domain effect of the performance in this regime is mass transport limitation through the GDL.

4.6.2 Copper Sheet Insertion

As known, electrical conductivity of a conductive composite relatively increases with an increase in conductive filler concentration. High loading of conductive fillers into the composite bipolar plates is necessary for achieving the minimum electrical conductivity required. However, high filler loading may cause a substantial reduction in other bipolar plates properties, and it also results in the decrease of injection processability. Inserting or overmolding copper sheets into bipolar plates has been explored to meet the electrical conductivity target at reduced filler loadings.

Hsiao et al. reported that the power densities of a single fuel cell using copper or aluminum mesh composite bipolar plates were more stable than those using neat polymer composite bipolar plates [68]. Wang produced metal insert bipolar plates by compression molding; and the results exhibited very high in-plane conductivity results; however, their performance in single cell testing was not as encouraging [34]. This copper insert technique is based on the concept that electrons can easily transfer through the copper sheet to form an electric circuit and thus improve the electrical conductivity of bipolar plates can be improved. Figure 4-96 depicts the manual fabrication scheme for copper sheet polypropylene/carbon composite bipolar plates used in this work. The manufacturing of copper insert composite plates is described in Appendix B.

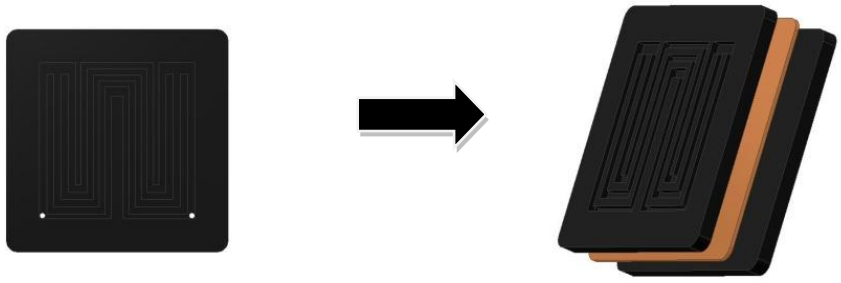

Figure 4-96: Schematic of the structure of copper hybrid composite bipolar plates

Table 4-16: Effect of copper sheet insert on electrical conductivity of composite plates

Samples	In-plane electrical conductivity (S/m)	Through-plane electrical conductivity (S/m)
P55FZn	617.922 (SD = 27.008, n = 16)	30.740 (SD = 1.018, n = 16)
Copper insert-P55FZn	2502.186 (SD = 87.898, n = 16)	55.900 (SD = 4.095, n = 16)

The copper sheet insert bipolar plates were tested for both in-plane and through-plane conductivity, and compared with the results of those without metal sheet inserts. The testing results are summarized in Table 4-16.With the metal mesh insert technique, the in-plane and through-plane conductivity values were increased approximately 4 and 1.8 times, respectively. These results are likely lower than expected as an oxidation layer formed on the copper sheet surface. The surface energies of a copper sheet surface and PP composite surface typically differ, thus, a PP composite cannot perfectly coat a copper sheet, leading to an increase in interfacial contact resistance. In other words, the conductive network is broken by the insulating gap between the copper sheet and PP composite.

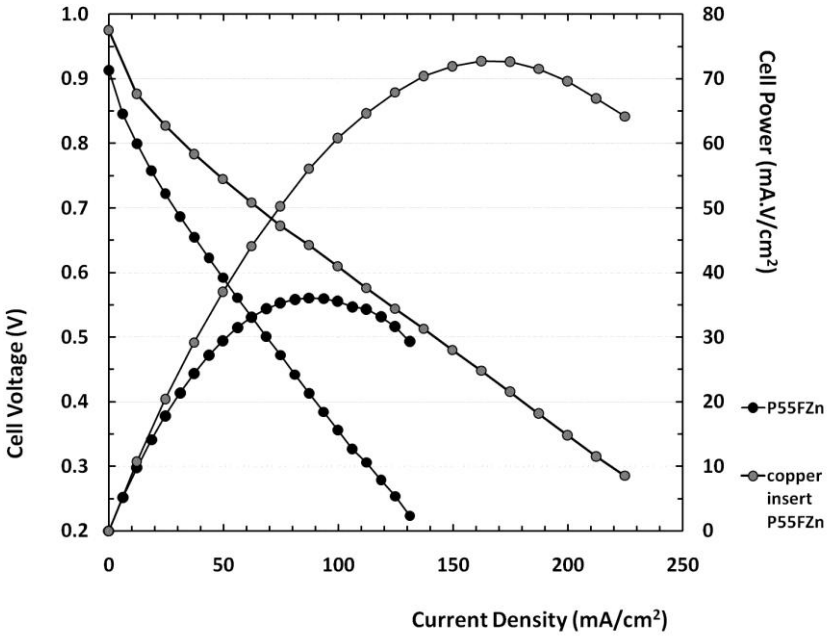

Figure 4-97: Effect of copper sheet insert on fuel cell performance

Figure 4-97 presents polarization curve results of the single cells compressively assembled with P55FZn composite and copper insert-P55FZn. The open circuit voltages (OCV) of the

single cell using copper insert-P55FZn bipolar plates was obviously higher than that of plates using P55FZn; the OCV of both cells were 0.976 V (copper insert-P55FZn) and 0.913 V (P55FZn). The current densities at 0.5V of both fuel cells are 137.250 and 68.625 $mAcm^{-2}$ for the fuel cells assembled with a copper insert-P55FZn and P55FZn respectively. The single cell with copper insert-P55FZn bipolar plates possesses two times higher maximum power density than that with P55FZn, in agreement with Hsiao et al. [68].

4.7 Other Properties of Composite Bipolar Plates

4.7.1 Hydrogen Permeability

Bipolar plates have a critical role separating the gases in adjacent cells; therefore, they must be impermeable to hydrogen and oxygen. Because, it is much more difficult to meet thickness targets and simultaneously obtain low permeation rates when using polymer composite plates, the gas permeability of composite plate materials needs to be investigated. This part of the research addresses hydrogen permeation concerns associated with the thickness and density of the composite bipolar plates.

Table 4-17: Hydrogen permeability of composite bipolar plates

	Hydrogen permeability ($cm^3cm^{-2}s^{-1}$)			
Samples	T = 0.5 mm	T = 1.0 mm	T = 2.0 mm	T = 3.0 mm
PP	-	-1.28E-08	-	-
P55F	5.96E-05	4.95E-06	1.75E-07	1.14E-08
P55FPPy	8.16E-06	1.77E-06	7.29E-09	4.39E-10
P55F(2F_1)	1.46E-08	3.26E-05	-	-
FR8	3.43E-05	9.44E-06	1.22E-07	-

Table 4-17 illustrates the hydrogen permeability values of composite bipolar plates produced in this research; almost all of the values are higher than the DOE target of 2.0×10^{-6} $cm^3cm^{-2}s^{-1}$[46]. According to Fick's law, which relates the diffusive flux to the concentration field, this last finding can be explained according to the one-dimension differential equation as expressed by Equation 4-1[166].

$$j = -DS\frac{dp}{dx} = -P\frac{dp}{dx} \quad (4\text{-}1)$$

The mass flux (j) is proportional to the permeability (P) of the medium times a negative gradient of a pressure potential driving force (dp/dx) (or the chemical potential gradient). Since for ideal gases such as H_2 that do not interact with the polymer composite, the partial pressure is almost equivalent to the chemical potential. Therefore, hydrogen gas permeability depends upon the chemical structure and the morphology of the composites, as well as other factors such as the thickness of specimens, temperature, and humidity. The addition of conductive carbon fillers to the PP matrix causes the hydrogen permeability to increase radically, since the fillers increase the porosity of materials. As discussed in the previous section, conductive fillers prefer to disperse in the amorphous region, which there are a number of voids between polymer chains. The fillers may make the voids bigger, since the intermolecular force is decreased. A schematic of the relationship between electron transfer and hydrogen diffusion, was outlined by Blunk et al., as shown in Figure 4-98.

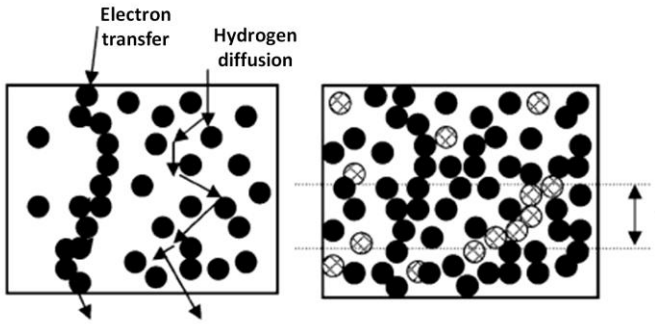

Figure 4-98: The schematic of electron transfer and hydrogen diffusion [166]

The hydrogen permeability of composites can be ordered as P55F (2F_1) > FR8 > P55F > P55FPPy. The hydrogen permeation rate decreases when the density of composite plates increases; the density values of P55FPPy, P55F, FR8, and P55F (2F_1) are 1.298, 1.284, 1.230, and 1.200 gcm^{-3}, respectively. Hydrogen permeation rates were also measured as a function of sample thickness. The hydrogen permeability of composite specimens significantly decreases as specimen thickness increases. In the case of P55FPPy, a large rate of decrease was realized between a thickness of 0.5 and 3 mm, in with which the permeability dropped approximately four orders of magnitudes of order. The hydrogen permeation values decreased from 8.16×10^{-6} to $4.39\times10^{-10}cm^3cm^{-2}s^{-1}$. This situation is explained by the schematic in Figure 4-98.

In the case of an inhomogeneous composite with high filler loadings, when the thickness of the specimen is reduced, a percolation path of voids can develop. Therefore, diffusion-driven transport converts to convection-driven transport, causing a huge increase in hydrogen permeation. However, the permeability decreases with an increase a thickness, as in the case of P55F (2F_1). The combination of two filler sizes may result in the configuration of voids in the composite.

4.7.2 Thermal Conductivity

As a PEMFC generates electricity, it also generates water and heat. The generated heat has to be dissipated from the PEMFC stack through the bipolar plate to a cooling channel in order to maintain constant operating temperature in the fuel cell system. The heat is typically removed from the fuel cell by water or air flowing through cooling channels inside the plate; and heat will partly leave the fuel cell with the produced water. Therefore, consideration of the thermal conductivity of bipolar plates also requires management of the heat in PEM fuel cell stacks. The thermal conductivity of bipolar plates should be higher than 20 $W(mK)^{-1}$ for heat dissipation when fuel cells are operated above temperature $70^{o}C$[46]. Moreover, heat accommodated in fuel cells must be removed to prevent proton exchange membrane degradation from hot spot formation. In this research, through-plane thermal conductivity was measured using the Laser Flash technique explained in Chapter 3. This through-plane thermal conductivity was determined because the heat generated in the bipolar plate during operation may be efficiently transferred from the inside to outside of a stack through in-plane thermal conductive layers.

The results exhibited in Table 4-18 show that the thermal conductivity and heat capacity of polypropylene composites are higher than those of neat PP at the same temperatures. Unfilled polypropylene has a very low thermal conductivity of 0.21 $W(mK)^{-1}$[167]. The increase in thermal conductivity occurs because of the intrinsic thermal conductivity of carbon fillers; for example the thermal conductivity of pure graphite is about 600 $W(mK)^{-1}$[18]. However, all composite thermal conductivity values were lower than the target value, in part, because carbon black has relatively low thermal conductivity due to its amorphous carbon and porous structures (0.2-0.3 $W(mK)^{-1}$)[168].

It was found in the literature that polymer composites at filler loading lower than 50 wt% vary in their the thermal conductivities varing from 1.0 to 5.0 $W(mK)^{-1}$[169, 170]. However, many reasons may cause low thermal conductivity of polymer composites, for example, the interfacial thermal resistance between the filler and matrix, the shape and size of filler particles, the contact and interaction between filler particles, the thermal conductivity of each filler particle, and filler orientation [167, 171]. The results also indicate that the thermal conductivity of composites increases with an increase in temperature. In conclusion, the thermal conductivity of PP/carbon filler composites produced in this work needs more improvement for bipolar plate application.

Table 4-18: Thermal properties of PP composites

Sample	Temperature (^oC)	Thermal diffusivity (m^2/s)	Heat capacity J/kg.K	Density kg/m^3	Thermal conductivity W/mK
P55F	25	4.530E-07	455.2	1298	2.6477E-01
	80	3.560E-07	838.5	1298	3.8328E-01
	120	3.180E-07	1123.0	1298	4.5853E-01
FR8	25	3.890E-07	483.8	1200	2.3148E-01
	80	3.120E-07	816.5	1200	3.1334E-01
	120	2.780E-07	1083.0	1200	3.7032E-01
P55FPPy	25	4.870E-07	397.2	1230	2.5108E-01
	80	3.890E-07	879.6	1230	4.4413E-01
	120	3.420E-07	1249.0	1230	5.5445E-01
P55F(2F_1)	25	4.470E-07	307.1	1284	1.6473E-01
	80	3.580E-07	941.4	1284	4.0443E-01
	120	3.160E-07	1361.0	1284	5.1609E-01

CHAPTER 5: Conclusions, Recommendations, and Contributions

A typical PEMFC in vehicle application will include 200 to 400 bipolar plates, so the development of low cost materials and manufacturing processes is critical for widespread application of PEMFC. This research reported in this thesis has focused on the production of polypropylene/carbon filler composites that could be used as a relatively low cost material. Different types of additives such as conductive polymers, carbon nanofibers, titanate coupling agents, and processing agents were used in this work to improve the electrical conductivity and processing characteristics of bipolar plate materials. The major advantages and disadvantages of composite bipolar plates over graphite bipolar plates in PEMFC were investigated. Particular emphasis was placed on improving the electrical conductivity of polypropylene/carbon filler composite bipolar plates. Moreover, manufacturing of the composite bipolar plates using an injection molding technique has been studied as a promising production process.

To provide more information for future bipolar plate development and to further clarify the effects of filler dispersion on electrical conductivity enhancement, the conductive networks in the injection molded bipolar plates was observed. Furthermore, techniques such as polishing bipolar plate surfaces, inserting a copper sheet into bipolar plates, and using super critical CO_2 to improve conductive network formation were investigated as potential options to improve the electrical conductivity of bipolar plates and overall performance of PEMFC.

5.1 Conclusions and Recommendations

5.1.1 Synergistic Effect: Different Type of Fillers

5.1.1.1 Conclusions

The objective of this part of the research was to determine the effects and interactions of each filler and filler combination on bipolar plate properties such as electrical conductivity, process characteristics, mechanical properties, and single cell fuel cell performance. Carbon black (CB), carbon fiber (CF) and synthetic graphite (SG) were used as filler types. Adding carbon fillers to the polypropylene matrix resulted in an increased electrical conductivity of material from approximately 10^{-12} S/m to 10^{2} S/m (10^{-14} S/cm to 10^{0} S/cm).

Different filler systems, single-, two-, and three-filler systems, were formulated to fabricate composite bipolar plates. At 55wt% of filler loading, the composite containing carbon fiber gave the highest electrical conductivity in this group: 615.30 S/m (6.153 S/cm) of in-plane electrical conductivity and 31.87 S/m (0.3187 S/cm) of through-plane conductivity. It is important to note that at 55wt% of carbon black, the composite could not be processed because the molten composite was varied viscosity. All combinations had a significant synergistic effect that increased the composite electrical conductivity, but carbon black caused the greatest increase.

Different ratios of fillers also affected the electrical conductivity, and the best composite for electrical conductivity can be formulated from a composite containing a high carbon black ratio relative to the other fillers. FR8 composites, created from a 4:1:1 of CB: CF: SG ratio, gave the greatest electrical conductivity: 1239 S/m (12.39S/cm) for in-plane measurement and 120 S/m (1.20 S/cm) for the through-plane technique. However, introduction of carbon fillers to the PP matrix resulted in an increased viscosity, especially adding carbon black. The blends did show promise for future opportunities to produce bipolar plates using an injection molding process. The average overall operating time of injection molding was roughly 25 seconds/plate. The fuel cell assembled with FR8 bipolar plates displayed comparable performance to the cell using graphite bipolar plates, and this result corresponded to the results from an AC impedance measurement of conductivity.

In terms of the mechanical properties of bipolar plates, the compressive properties of composites met the commercial target, whereas the tensile strength of polypropylene was reduced by the addition of solid fillers, but the fillers increased the tensile moduli of the materials. The tensile strength of composites was close to the commercial target. The creep behavior of most of the composite bipolar plates under fuel cell operating temperature ($80^{o}C$) indicated acceptable strain value, which was a strain as less than 0.2%, as a function of time.

5.1.1.2 Recommendations

For fuel cell bipolar plate applications, the results obtained from this section of work suggest that a multiple filler approach with synthetic graphite, carbon fiber, and carbon black may be a good strategy to improve the electrical conductivity of bipolar plates. However, an improving the electrical conductivity of composites is still needed for commercial bipolar plate application. There are two main potential extensions and applications of this work. First, additional study of multi-filler electrical percolation thresholds and rheological percolation thresholds of the composites in a three-filler system is recommended. Interfacial interaction energies of filler-polymer and filler-filler would also be interesting information to acquire since this would help to clarify how to improve processability of the composites.

5.1.2 Synergistic Effect: Conductive Polymer and Different Types of CFS

5.1.2.1 Conclusions

This study has demonstrated the feasibility and advantages of the using polypyrrole as an additive for improving the electrical conductivity of composites. Combining PPy with PP/three carbon fillers is an effective technique for developing higher conductivity composites; electrical conductivity increases as PPy concentration increases, but PPy concentration was kept low as is it an expensive polymer. The best conductivity results for composite bipolar plates are obtained by introducing 3wt% PPy into the composites. The best conductivity values are higher than that of the composite without PPy by approximately 2.4 times for in-plane conductivity and 1.7 times for through-plane conductivity.

The percolation threshold is observed in the vicinity of 2wt% and 1.5wt% for in-plane and through-plane conductivity, respectively. In view of the PEMFC power outputs, the composites with PPy are better than the one without PPy (performance increases 100%).

Adding carbon nanofibers into the PP/three carbon filler composites increases the electrical conductivity of materials by about 3.5% (in-plane) and 20% (through-plane) compared to the conductivity of composites using normal fibers. Mixing two carbon fibers for the composites shows the synergistic effect on electrical conductivity, since different sizes of fibers assist fillers to enlarge conducting paths. The composites formulated from the incorporation of the best characteristics of conductive fillers and conductive additives appear to significantly increase electrical conductivity. Blending PPy or CNF with polypropylene without carbon fillers is not effective at low PPy or CNF loading, since their dispersion cannot form the desired conductive network. The best formulation is PP/three filler composite with 4wt% of PPy, and the composite contains a 4:1:1 of CB: CF: SG ratio.

The fiber composition of this composite comprises two types of fibers of different sizes. This composite gives 2139.18 S/m (21.3918 S/cm) for in-plane and 773.30 S/m (7.733 S/cm) for through-plane in electrical conductivity which are 19 times (in-plane) and 15 times (through-plane) the conductivity values belonging to basic PP/three carbon filler composites. Their mechanical and rheological properties show possibility to use the composites produced in this section as bipolar plate applications.

5.1.2.2 Recommendations

PPy addition offers a good alternative to bipolar plate applications; however, some improvement in conductivity is still needed for commercial fuel cell use. This situation illustrates the necessity of determining a proper approach of blends that can give high electrical conductivity with low PPy concentration, and a cost benefit analysis should be conducted. Note that the incorporation of PPy in the synthesis of a copolymer may improve miscibility and overall polymer characteristics.

5.1.3 Effect of Additives and Effect of Viscosity of Polypropylene

5.1.3.1 Conclusions

Although carbon fillers can offer the resulting composites greater electrical conductivity, the polar surfaces of carbon fillers have inherently low compatibility with non-polar polymer matrices, especially hydrocarbon matrices such as polypropylene. The incompatibility causes problems in the composite processing and material properties. Filler agglomerates also result,

which can randomly distribute throughout the polypropylene matrix during the compounding process. To solve this problem, applying a titanate coupling agent to PP/carbon filler composites is beneficial as doing so develops the wettability of the filler surfaces by polypropylene and promotes interfacial adhesion. This results in the improvement of filler/PP interfacial interaction, which in turn results in conductive path formation. The in-plane and through-plane conductivity increased as the titanate coupling agent loading was increased. Nevertheless, there was a certain optimal amount of the titanate coupling agent. This can be seen from the increase in electrical conductivity when the titanate coupling agent was higher than 2wt% for in-plane and 1.5 wt% for through-plane. The enhancement of fuel cell performance confirms the increase in electrical conductivity. Other properties of composites such as mechanical properties, flow behavior, and contact angle of the composites bipolar plates can be improved by applying a titanate coupling agent. However, the use of a titanate coupling agent also imposed a loading limitation on the material's property improvement. As shown, the viscosity of molten composites increased with the addition of as adding three carbon fillers.

Using zinc strearate as a processing agent to reduce the viscosity of the composites resulted in a decline of the composites electrical conductivity. The decrease in electrical conductivity also happened when the composites contained low viscosity polypropylene. The results have shown that higher levels of conductive filler connections result from an increased viscosity combined with the higher shear stresses required during polymer processing.

5.1.3.2 Recommendations

Based on the results of this section, addition of a processing agent is not suggested for fuel cell application, because it does not contribute significantly to the key characteristic of conductivity and would also increase the bipolar plate material cost. Other additives, such as a blowing agent, which could affect conductive network creation, should be studied. However, applying many components to improve the electrical conductivity of composites will increase the bipolar plate's cost and may negatively affect some bipolar plate properties.

5.1.4 Effect of Injection Flow on Conductive Network

5.1.4.1 Conclusions

The orientation of carbon fibers in composites is typically influenced by the geometry of injection flow. It was determined that the electrical conductivity values of injected specimens cut from different areas of an injected plaque varied, since the electrical conductivity depends largely on the carbon fiber alignment, filler dispersion, and filler distribution. In this experimental work, the simulation of fiber orientation in an injected plaque using the Moldex 3D/Solid program was done to investigate the effect of injection flow on fiber orientation in a conductive network. Injection composite samples were cut from different areas and different directions of an injection molded plank to measure in-plane and through-plane electrical conductivity. In-plane and through-plane electrical conductivity of the composite containing only carbon fibers as filler has a positive correlation with the simulation output; however, the final distribution and dispersion of the filler were caused by complex interactions among many factors during injection molding. Therefore, the simulation output could not explain the orientation of carbon fibers in the composites containing hybrid fillers. Most of the in-plane electrical conductivity results, from the specimens cut in the flow direction, indicate that the combination of carbon fillers does not show any significant effect on filler orientation at the surface of composite plates.

In order to investigate the morphological characteristics of composites in that area by SEM, the composite specimens were also cut into small pieces following the degree of fiber orientation reported by the simulation output. The SEM micrographs were used to determine a number of fillers (SG and CF), a number of connection points and filler contact areas using the UTHSCSA Image Tool. It could be concluded that lesser degrees fiber orientation give fillers a greater opportunity to form more conducting paths, resulting in the electrical conductivity increase. A supercritical carbon dioxide (CO_2) technique was used to create random orientation and the results from this process showed the capability to improve electrical conductivity of the composites.

5.1.4.2 Recommendations

Using the simulation of flow injection to describe the conductive network pattern is useful, as the combination of fillers in a hybrid filled system and various process parameters used in the

injection molding process significantly affect the formation of conductive networks. The experiment on supercritical CO_2 performed in this research was a preliminary investigation of filler dispersion development. If supercritical carbon dioxide (CO_2) was used in extrusion or batch mixing, the combination of shear stress, melt pressure, and CO_2 dissolution would provide some impact on the filler dispersion.

5.1.5 Contact Resistance

5.1.5.1 Conclusions

Contact resistance of a fuel cell system originates from the interface between fuel cell components, especially bipolar plates and GDLs. Increasing clamping torque is one solution to decrease contact resistance. Clamping torque was varied to observe the effect of assembly pressure on fuel cell resistance and fuel cell performance. The single cell performance and ohmic resistance increased with increase of the applied clamping torque up to 4 Nm and remained unchanged with further torque increase to 5N.m. The results from this section indicate that too high a force reduces the porosity of GDLs, increasing the mass-transport losses at high current density. The through-plane electrical conductivity of composite plates under various pressures supports the effects of clamping torque; the measured conductivity increases with increasing compression force for both bipolar plate samples with and without different GDLs. Time and temperature were found to affect electrical conductivity.

5.1.5.2 Recommendations

The observation of contact resistance effect is a good idea; however, the actual contact resistance between bipolar plates and GDLs or between bipolar plates and current collectors is difficult to determine. There is a need to design an approach for determining actual contact resistance between bipolar plates, and to evaluate long term creep behavior.

5.1.6 Bipolar Plate Modification

5.1.6.1 Conclusions

Inserting a copper sheet into bipolar plates is one possible way to meet the electrical conductivity target at reduced filler loadings. The results show that the copper sheet insert technique can increase the in-plane and through-plane conductivity values and performance of the fuel cell. Feasible reasons for the lower-values than an expected values include an

interfacial contact resistance between the copper sheet and oxidation layer formed on the copper sheet surface. As well, the polishing bipolar plates' surface as a mechanical treatment to remove the polypropylene-rich layer on that surface enhanced electrical conductivity and performance of the fuel cell. However, it did improve the fuel cell performance at high current density.

5.1.6.2 Recommendations

Bipolar plate fabricated with a metal insert is useful for PEMFC applications; and an injection molding process creates a suitable metal insert bipolar plates. However, an appropriate mold design must be provided for a metal insert plate; and the surface modification for the metal sheet is needed to reduce interfacial contact resistance. An important problem found in this work is that the weight of the copper insert bipolar plate is 2.5 times greater than that of the original composite plate.

5.1.7 Other Properties

5.1.7.1 Conclusions

The hydrogen permeability values of composite bipolar plates produced in this research achieved the DOE target. The hydrogen permeability of composite specimens significantly decreases as specimen thickness increases. The thermal conductivity and heat capacity of polypropylene composites was increased by adding carbon fillers to the PP matrix, because the carbon fillers offered higher thermal conductivity behavior to neat PP. However, the thermal conductivity values of all composites are lower than that of DOE target.

5.1.7.2 Recommendations

The use of more synthetic graphite concentration is recommended to improve thermal conductivity of composites [172]

5.2 Work Summary of Targets and Suggestion for Future

Work Summary of Targets

Table 5-1comparises of the properties of commercial and PP/composite bipolar plates developed in the word. Electrical conductivity targets for the commercial application in bipolar plates have not yet been achieved for these blends, but some properties of the PP/composite bipolar plates have meet most of the requirements. The blends do show

promise for future opportunities as composite materials within PEMFCs. The costs of composites, created in this research, for bipolar plate production are exemplified in Table D-19, Appendix D. Clearly the cost of the PPy will come down as it is more widely commercialized (i.e. it is really only now available in laboratory amounts), but also the weight percent in the blend of the PPy will dramatically influence the cost of any such blend.

Table 5-1: Comparison of properties between commercial and PP/composite bipolar plates [46, 148, 171]

Bipolar plates properties	Unit	DOE Target	Dupont Thermoset composite	SGL Thermoset composite	Bac2 Thermoset composite	Dhakate * Thermoset composite (65%G+1%MWNT)	P55FPPy (1:1:1:)1.8% PPy **	FR8 (4:1:1) **
Electrical conductivity								
In-plane	Scm^{-1}	100	-	>100	114	178	9.7	13.0
Through-plane	Scm^{-1}	20	25-33	>20	32	30	0.5	1.2
Mechanical properties								
Compressive strength	MPa	50	-	-	-	-	60	68
Flexural strength	MPa	25	>50	40	30	56	35	30
Tensile strength	MPa	41	-	-		-	32	-
Hardness	Shore D	50	-	-	67	57	75	80
Thermal Properties								
Thermal conductivity	$W(mK)^{-1}$	20	-	20	-	50	0.44	0.31
Thermal stability	^{o}C	-	-	-	180	-	>300	>300
Physical Properties								
Density	gcm^{-3}	1.9	-	1.97	1.83	1.82	1.23	1.20
Contact angle	degree	90	-	-	-	-	110	108
H_2 Permeability	$cm^3cm^{-2}s^{-1}$	2×10^{-6}	-	-	-	-	7.209×10^{-9}	1.22×10^{-7}

Note: * Bipolar plate was produced by Dhakate at al.,

** Bipolar plates produced were in this research (PP/three carbon fillers (55 wt%)

Suggestion for Future Work

Research can continue in the future and expand the following topics:

- Investigation of multi filler electrical and rheological percolation thresholds of the composites in three filler system.
- The incorporation of PPy in the synthesis of a copolymer to improve miscibility and overall polymer/carbon filler composite characteristics.
- Using the simulation of flow injection to describe the conductive network pattern for the combination of fillers in hybrid filled system and various process parameters used

in the injection molding process significantly affect the performance of forming conductive network.

- Conductive network improvement by incorporating supercritical carbon dioxide (CO_2) in extrusion or batch mixing or injection molding process.
- The use of other additives, such as blowing agent, which could affect on conductive network creation.
- Design an approach for determining actual contact resistance between bipolar plates, and to evaluate long term creep behavior.
- Design an appropriate mould design must be provided for a metal insert plate; and the surface modification of metal sheet is needed to reduce interfacial contact resistance.

5.3 Contributions

This research contains a number of contributions to the scientific community and publically available knowledge. For fuel cell commercialization, this work provides alternative of conductive composite formulas that are a guideline for bipolar plate production, specifically the use of conductive polymers such as PPy as additives for bipolar plate production. This research also provides information about filler characteristics and the synergistic effect of multiple fillers on the electrical conductivity and processability of materials. This information is important for the design of conducting composite formulations in any applications. This work also permits evaluation and comparison of processing characteristics of different composites, fundamental phenomena for conductive material fabrication. This evaluation represents the feasibility of conductive composite blends produced by injection molding techniques for future mass production. Filler dispersion is one of the major keys to improving conductive network. Therefore, the effect of an injection flow on filler dispersion and fiber orientation on the electrical conductivity were investigated regarding the simulation of fiber orientation.

This research also contributes to the development of methods and instruments for characterizations of bipolar plates, especially electrical conductivity and cell resistance analysis. Ultimately, all information from this research provides a data base for conductive composites and bipolar plate development in academic and commercial fields.

References

1. Brett, D. and Brandon, N., *Bipolar Plates: The Lungs of The PEM Fuel Cell.* **The Fuel Cell Review**, 2005. **2**(1): p. 15-23.
2. Hermanna, A., Chaudhuria, T., and Spagnol, P., *Bipolar Plates for PEM Fuel Cells: A review.* **International Journal of Hydrogen Energy**, 2005. **30** p. 1297 – 1302.
3. Janssena, H.K. and Tauber, U.C., *The Field Ttheory Approach to Percolation Processes.* **Annals of Physics**, 2005. **315** p. 147-192.
4. Weaver, G., *World Fuel Cells - An Industry Profile with Market Prospects to 2010* 1st ed. 2002, New York: Elsevier 234.
5. Sopian , K. and Daud, W.R.W., *Challenges and Future Developments in Proton Exchange Membrane Fuel Cells.* **Renewable Energy**, 2006. **31**: p. 719-727.
6. Barbir, F., *PEM Fuel Cell*. 2005, UK: Elsevier Inc.
7. Larmininie, J. and Dicks, A., *Fuel Cell Systems Explained*, ed. 2nd. 2003, West Sussex, England: John Wiley and Sons Ltd.
8. Vishnyakov, V.M., *Proton Exchange Membrane Fuel Cells.* **Vacuum**, 80(2006)1053-1065., 2006. **80**: p. 1053-1065.
9. Kusie, J., Knight, J., and Morton, J., *News Release*. 2010, Ministry of Transportation and Infrastructure BC, Canada.
10. O'Hayre, R., Cha, S.W.,Colella, W.,Prinz, F.B., *Fuel Cell Fundamentals*, ed. 2nd. 2009, New York: Jonhn Wiley and Sons, Inc.
11. Mehta, V. and Cooper, J.S., *Review and Analysis of PEM Fuel Cell Design and Manufacturing.* **Journal of Power Sources**, 2003. **114** p. 32-53.
12. Cooper, J.S., *Design Analysis of PEMFC Bipolar Plates Considering Stack Manufacturing and Environment Impact.* **Journal of Power Sources**, 2004. **129**: p. 152-169.
13. Besmann, T.M., Klett, J. W., Henry, J. J., Lara, C.E., *Carbon/Carbon Composite Bipolar Plate for PEM Fuel Cells.* **Journal of The Electrochemical Society**, 2000. **147**(11): p. 4083-4086.
14. Jayakumar, K., Pandiyan, S., Rajalakshmi,N., Dhathathreyan, K.S., *Cost-benefit Analysis of Commercial Bipolar Plates for PEMFC's.* **Journal of Power Sources**, 2006. **161**: p. 454–459.
15. On, I.B., R. Kirchain, and Roth, R., *Technical Cost Analysis for PEM Fuel Cells.* **Journal of Power Sources**, 2002. **109**: p. 71-75.
16. Dihrab, S.S., K. Sopian , Alghoul, M.A., Sulaiman, M.Y., *Review of The Membrane and Bipolar Plates Materials for Conventional and Unitized Regenerative Fuel Cells.* **Renewable and Sustainable Energy Reviews**, 2009. **13**: p. 1663–1668.

17. Xiao, M., Lub,Y. Wang ,S.J., Zhaoa,Y.F., Menga,Y.Z., *Poly(arylene disulfide)/graphite Nanosheets Composites as Bipolar Plates for Polymer Electrolyte Membrane Fuel Cells.* **Journal of Power Sources**, 2006. **160**(1): p. 165-174.
18. Du, C., Ming, P., Hou, M., Fu,J., Shen,Q., Liang, D., Fu,Y., Luo,X., Shao, Z., Yi, B., *Preparation and Properties of Thin Epoxy/Compressed Expanded Graphite Composite Bipolar Plates for Proton Exchange Membrane Fuel Cells.* **Journal of Power Sources**, 2010. **195**: p. 794–800.
19. Heo, S.I., K.S. Oh, Yun,J.C., Jung, S.H., Yang,Y.C., and Han, K.S., *Development of Preform Moulding Technique using Expanded Graphite for Proton Exchange Membrane Fuel Cell Bipolar Plates.* **Journal of Power Sources**, 2007. **171**: p. 396–403.
20. Tawfika, H., Hunga, Y., and Mahajan, D., *Metal Bipolar Plates for PEM fuel cell - A review.* **Journal of Power Sources**, 2007. **163**: p. 755-767.
21. Antunes, R.A., Oliveira, M.C.L., Ett,G., and Ett,V., *Corrosion of Metal Bipolar Plates for PEM Fuel Cells: A Review.* **International Journal of Hydrogen Energy**, 2010. **35**: p. 3632-3647.
22. Hung, Y., El-Khatib, K.M., and Tawfik, H., *Corrosion-resistant Lightweight Metallic Bipolar Plates for PEM Fuel Fells.* **Journal of Applied Electrochemistry**, 2005. **35**: p. 445-447.
23. Wind, J., et al., *Metallic Bipolar Plates for PEM Fuel Cells.* **Journal of Power Sources**, 2002. **105**: p. 256-260.
24. Davies, D.P., Spah, R., Kaiser, W., and Bohm, G., *Bipolar Plate Materials for Solid Polymer Fuel Cells.* **Journal of Applied Electrochemistry**, 2000. **30**: p. 101-105.
25. El-Enin, A., Abdel-Salam, S.A., and Omar, E., *New Electroplated Aluminum Bipolar Plate for PEM Fuel Cell.* **Journal of Power Sources**, 2008. **177**: p. 131–136.
26. Davies, D.P., Adcock, P.L., Turpin, M., and Rowen, S.J., *Stainless Steel as A Bipolar Plate Material for Solid Polymer Fuel Cells.* **Journal of Power Sources**, 2000. **86**: p. 237-242.
27. Wang, H., Sweikart, M.A., and Turner, J.A., *Stainless Steel as Bipolar Plate Material for Polymer Electrolyte Membrane Fuel Cells.* **Journal of Power Sources**, 2003. **115**: p. 249-251.
28. Joseph, S., McClure, J.C., Chianelli, R., Pich, P., and Sebastian, P.J, *Conducting Polymer-coated Stainless Steel Bipolar Plates for Proton Exchange Membrane Fuel Cells (PEMFC).* **International Journal of Hydrogen Energy**, 2005. **30**: p. 1339-1344.
29. Cunningham, N., Dodeleta, J.P., Guaya,D., and Ross, G. G., *RBS and XRD Analyses of Carbon-coated Stainless Steel Plates,* **Surface and Coatings Technology**, 2004. **183(**2-3): p. 216-223
30. Ku, C.C. and Liepins, R., *Electrical Properties of Polymers: Chemical Principles*. 1987, New York: Hanser Publishing.
31. Cokturk, H.S., Fiske, T.J., and Kalyon, D.M., *Effects of Particle Shape and Size Distributions on the Electrical and Magnetic Properties of Nickel/ Polyethylene Composites.* **Journal of Applied Polymer Science**, 1993. **50**: p. 1891-1901.
32. Maaroufi, A., Haboubi, K., Amarti, A. E., and Carmona, F., *Electrical Resistivity of Polymeric Matrix Loaded with Nickel and Cobalt Powders.* **Journal of Materials Science**, 2004. **39**: p. 265-270.

33. Bin, Z. and Bingchu, M., *Study on The Electrical and Mechanical Properties of Polyvinylidene Fluroide/titanium Silicon Carbide Composite Bipolar Plates.* **Journal of Power Sources**, 2006. **161**: p. 997–1001.
34. Wang, Y., *Conductive Thermoplastic Composite Blends for Flow Field Plates for Use in Polymer Electrolyte Membrane Fuel Cells (PEMFC)*, in *Department of Chemical Engineering*. 2006, University of Waterloo: Waterloo, Canada.
35. Zhang, J., Jiang, D.D., and Wilkie, C.A., *Thermal and Flame Properties of Polyethylene and Polypropylene Nanocomposites Based on An Oligomerically-modified Clay.* **Polymer Degradation and Stability**, 2006. **91**: p. 298-304.
36. Radhakrishnan, S., Ramanujam, B.T.S., Adhikari, A., Sivaram,S., *High-temperature, Polymer–graphite Hybrid Composites for Bipolar Plates: Effect of Processing Conditions on Electrical Properties.* **Journal of Power Sources**, 2006. **163** p. 702–707.
37. Xia, L. and Li, A., *Effects of Resin Content and Preparing Conditions on The Properties of Polyphenylene Sulfide Resin/graphite Composite for Bipolar Plate.* **Journal of Power Sources**, 2008. **178**: p. 363–367.
38. Wu, M. and Shaw, L.L., *A novel Concept of Carbon-filled Polymer Blends for Applications in PEM Fuel Cell Bipolar Plates.* **International Journal of Hydrogen Energy**, 2005. **30**: p. 373-380.
39. Rio, C.D., Rio,C. D., Ojeda, M. C., Acosta, J. L., Escudero, M. J., Hontan, E., and Daza, L., *New Polymer Bipolar Plates for Polymer Electrolyte Membrane Fuel Cells: Synthesis and Characterization.* **Journal of Applied Polymer Science**, 2002. **83**: p. 2817.
40. Mighri, F., Huneault, M.A., and Champagne, M.F., *Electrically Conductive Thermoplastic Blends for Injection and Compression Molding of Bipolar Plates in The Fuel Cell Application.* **Polymer Engineering and Science**, 2003. **44**(9): p. 1755-1765.
41. Maheshwari, P.H., Mathur, R.B., and Dhami, T.L., *Fabrication of High Strength and A Low Weight Composite Bipolar Plate for Fuel Cell Applications.* **Journal of Power Sources**, 2007: p. 1-10.
42. Blunk, R.H.J., Daniel, J. L., Yoo,Y.E., and Tucker III, C.L., *Enhanced Conductivity of Fuel Cell Plates Through Controlled Fiber Orientation.* **AIChE Journal**, 2003. **49**(1): p. 18-27.
43. Liao, S.H., C.H. Hung, Ma, M.C.C., Yen,C.Y., Lina,Y.F., and Wenga,C.C., *Preparation and Properties of Carbon Nanotube-reinforced Vinyl Ester/nanocomposite Bipolar Plates for Polymer Electrolyte Membrane Fuel Cells.* **Journal of Power Sources**, 2008. **176**: p. 175–182.
44. Mathur, R.B., Dhakate, S.R., Gupta, D.K., Dhami, T.L., and Aggarwal, R.K., *Effect of Different Carbon Fillers on The Properties of Graphite Composite Bipolar Plate.* **Journal of Materials Processing Technology**, 2008. **203**: p. 184-192.
45. Calleja, F.J.B., Bayer, R.K., and Ezquerra, T.A., *Electrical Conductivity of Polyethylene-carbon-fibre Composites Mixed with Carbon Black.* **Journal of Materials Science**, 1988. **23**: p. 1411-1415.
46. Dhakate, S.R., Mathur, R.B., Kakati,B.K., and Dhami, T.L., *Properties of Graphite-composite Bipolar Plate Prepared by Compression Molding Technique for PEM Fuel Cell.* International **Journal of Hydrogen Energy**, 2007. **32**: p. 4537 – 4543.

47. Du, L. and Jana, S.C., *Highly Conductive Epoxy/graphite Composites for Bipolar Plates in Proton Exchange Membrane Fuel Cells.* **Journal of Power Sources**, 2007. **172**: p. 734–741.
48. Hui, C., Hong-Bo, L., Jian-Xin, L., Li, Y., and Yue-De,H., *Characteristics and Preparation of Polymer/Graphite Composite Bipolar Plate for PEM Fuel Cells.* **Journal of composite materials**, 2009. **43**(7).
49. Yen, C.-Y., Liao,S.-H., Lin,Y.-F., Hung,C.-H., Lin,Y.-Y., and Ma,C.-C. M.., *Preparation and Properties of High Performance Nanocomposite Bipolar Plate for Fuel Cell.* **Journal of Power Sources**, 2006. **162**(1): p. 309-315.
50. Huneault, M.A., Mighri, F., and Champagne, M.F., *Conductive Polymer Blends for Injection Molded Bipolar Plates.* **ANTEC2003**, 2003: p. 1330-1334.
51. Mali, T.J., *Thermoplastic Composites for Polymer Electrolyte Membrane Fuel Cell Bipolar Plates,* in *Department of Chemical Engineering*. 2006, University of Waterloo: Waterloo, Canada.
52. King, J.A., Tambling, T. M., Keith, J. M., Cole, A.J., and Morrison, F. A., *Synergistic Effects of Multiple Carbon Fillers on The Rheology of Liquid Crystal Polymer Based Resins.* **Polymer Composites**, 2009. **30**: p. 111-119.
53. Shirakawa, H., MacDiarmid, A., and Heeger, A., *Twenty-five Years of Conducting Polymers.* The Royal Society of Chemistry, 2003: p. 1-4.
54. Joseph, S., *Conducting Polymer-coated Corrosion Resistant Metallic Bipolar Plates for Proton Exchange Membrane Fuel Cells* in *Materials Science and Engineering*. 2005, The University of Texas At El Paso: Texas.
55. Omastova, M. and Pavlinec, J., *Synthesis, Electrical Properties and Sability of Polypyrrole-containing Conducting Polymer Composites.* **Polymer International**, 1997. **43**: p. 109-116.
56. Omastova, M., Chodak, I., and Pionteck, J., *Electrical and Mechanical Properties of Conducting Polymer Composites.* **Synthetic Metals**, 1999. **102**: p. 1251-1252.
57. Wang , L.X., Li, X.G., and Yang, Y.L., *Preparation, Properties and Applications of Polypyrroles.* **Reactive & Functional Polymers**, 2001. **47**: p. 125-139.
58. Veeraraghavana, Paulb, J., Harana, B., and Popov, B., *Study of Polypyrrole Graphite Composite as Anode Material for Secondary Lithium-ion Batteries.* **Journal of Power Sources**, 2002. **109**: p. 377–387.
59. Wu, T.M., Chang, H.L., and Lin, Y.W., *Synthesis and Characterization of Conductive Polypyrrole/multi-walled Carbon Nanotubes Composites with Improved Solubility and Conductivity.* **Composites Science and Technology**, 2009. **69**: p. 639–644.
60. Feng, C. and Chan, P.C.H., *Catalyzed Microelectrode Mediated by PPy/Nafion Composite Film for Microfabricated Fuel Cells.* **Electrochemistry Communications**, 2007. **9**(1): p. 89-93.
61. Kuo, J.K. and Chen, C.K., *A novel Nylon-6–S316L Fiber Compound Material for Injection Molded PEM Fuel Cell Bipolar Plates.* **Journal of Power Sources**, 2006. **162** p. 207–214.
62. Dweiri, R. and Sahari, J., *Investigations on The Electrical Properties of Carbon-based Polypropylene Composites for Bipolar Plates in Polymer Electrolyte Membrane Fuel Cell (PEMFC)*, **Journal of Power Sources**. 2007. p. 1-31.

63. Li, X. and Sabir, I., *Review of Bipolar Plates in PEM Fuel Cells: Flow-field Designs.* **International Journal of Hydrogen Energy**, 2005. **30**: p. 359-371.
64. Baurens, P. and Crouvezier, J.P.P., *Innovative Concepts for Bipolar Plates.* CLEFS CEA, 2005. **winter 2004-2005**(50/51).
65. Muller, A., Kauranen, P., Ganski, A., and Hell, B., *Injection Moulding of Graphite Composite Bipolar Plates.* **Journal of Power Sources**, 2006. **154**: p. 467-471.
66. Huang, J. and Baird, D.G., *Compression Molding of Highly Conductive Fuel Cell Bipolar Plates from A Thermoplastic Composite.* **ANTEC2003**, 2003: p. 2151-2155.
67. Huang, J., Baird, D.G., and McGrath, J.E., *Development of Fuel Cell Bipolar Plates from Graphite Filled wet-lay Thermoplastic Composite Materials.* **Journal of Power Sources**, 2005. **150**: p. 110–119.
68. Hsiao, M.C., Liao, S.H., Yen, M.Y., Ma, C-C.M., Lee,S-J., Chen,Y-H., Hung, C.H., Lin, Y.-F., and Xie,X-F., *Electrical and Thermal Conductivities of Novel Metal Mesh Hybrid Polymer Composite Bipolar Plates for Proton Exchange Membrane Fuel Cells,* **Journal of Power Sources**, 2010. **195**(2): p. 509-515.
69. Lee, M.-S., Chen, L.-J., He,Z.-R., Yang,S.-H., *The Development of A Heterogeneous Composite Bipolar Plate of A Proton Exchange Membrane Fuel Cell.* **Journal of Fuel Cell Science and Technology**, 2005. **2**: p. 14-19.
70. Clingerman, M.L., *Development and Modelling of Electrically Conductive Composite Materials*, in *Chemical Engineering*. 2001, Michigan Technological University: Michigan. p. 1-299.
71. Heiser, J.A., *Conductive, Shielding, Tensile, and Impact Properties of Carbon-filled Nylon 6,6 Based Resins*, in *Chemical Engineering*. 2003, Michigan Technological University: Michigan.
72. Kovacs, J.Z., et al., *Two Percolation Thresholds in Carbon Nanotube Epoxy Composites.* Composites Science and Technology, 2007. **67**: p. 922-928.
73. Kirkpatrick, S., *Percolation and Conduction.* **Reviews of Modern Physics**, 1973. **45**(4).
74. Sahimi, M., *Applications of Percolation Theory*. 1994: Tylor & Francis Ltd.
75. Stauffer, D., *Introduction of Percolation Theory*. 1985, London: Tylor and Francis.
76. Brovko, Rosso, O.P., and Friedrich, K., *Adhesion Between Differently Treated Fibers and A Hybrid Resin System.* **Journal of Materials Science Letters**, 2002. **21**: p. 305-308.
77. Yu, G., Zhang, M.Q., and Zeng, H.M., *Carbon-black-filled Polyolefine as A Positive Temperature Coefficient Material: Effect of Composition, Processing, and Filler Treatment.* **Journal of Applied Polymer Science**, 1998. **70**: p. 559-566.
78. Koysuren, O., Yesil, S., and Bayram, G., *Effect of Surface Treatment on Electrical Conductivity of Carbon Black Filled Conductive Polymer Composites.* **Journal of Applied Polymer Science**, 2007. **104**: p. 3427-3433.
79. Chiang, W.Y. and Ao, J.Y., *Effect of Surface Treatment of Carbon Fiber on The Electrical and Mechanical Properties of High-impact Polystyrene Composite.* **Journal of Polymer Research**, 1995. **2**(2): p. 83-89.
80. Wah, C.A., Choong, L.Y., and Neon, G.S., *Effects of Titanate Coupling Agent on Rheological Behaviour, Dispersion Characteristics and Mechanical Properties of Talc Filled Polypropylene.* **European Polymer Journal**, 2007. **26**: p. 789-801.

81. Monte, S.J., *Neoalkoxy Titanate and Zirconate Agent Additive in Thermoplastic.* **Polymer and Polymer composites**, 2002. **10**(1): p. 1-51.
82. Lee, M., Tzoganakis, C., and Park, C.B., *Effects of Supercritical CO_2 on the Viscosity and Morphology of Polymer Blends.* **Advances in Polymer Technology**, 2000. **19**(4): p. 300–311.
83. Xue, A., Tzoganakis, C., and Chen, P., *Measurement of Interfacial Tension in PS/LDPE Melts Saturated With Supercritical CO_2.* **Polymer Engineering and Science**, 2004. **44**(1): p. 18-27.
84. Matsuyama, K. and Mishima, K., *Formation of TiO_2–polymer composite microparticles by rapid expansion of CO_2 saturated polymer suspensions with high shear mixing.* **Journal of Supercritical Fluids**, 2007. **40**(1): p. 117-124.
85. Rose, R., *Questions and Answers about Hydrogen and Fuel Cells*. 2009, Breakthrough Technologies Institute. p. 1-13.
86. James, B.D. and Kalinoski, J.A., *Mass Production Cost Estimation for Direct H_2 PEM Fuel Cell System for Automotive Applications*. 2008, **Directed Technologies**, Inc.: USA. p. 1-41.
87. Adrianowycz, O., *Next generation bipolar plates for automotive PEM fuel cells*. 2009, Graf Tech International Ltd.: USA. p. 1-26.
88. Carlson, E.J., Kopf, P., Sinha, J., Sriramulu, S., and Yang, Y, *Cost Analysis of PEM Fuel Cell Systems for Transportation*. 2005. p. 1-98.
89. Landis, L. and Tucker, J.L., *Making Better Fuel Cells: Through-plane Resistivity Measurement of Graphite-filled Bipolar Plates*. 2002, Keithley Instruments, Inc.
90. Maryniak, W.A., Uehara, T., and Noras, M.A., *Surface Resistivity and Surface Resistance Measurements Using a Concentric Ring Probe Technique*. 2003, Trek Inc.
91. Kim, J.W. and Kim, N.H., *Synergy Effects of Hybrid Carbon System on Properties of Composite Bipolar Plates for Fuel Cells.* **Journal of Power Sources**, 2010. **195**: p. 5474–5480.
92. Mishra, V., F. Yang, and Pitchumani, R., *Measurement and Prediction of Electrical Contact Resistance Between Gas Diffusion Layers and Bipolar Plate for Applications to PEM Fuel Cells.* **Transactions of the ASME**, 2004. **1**: p. 1-9.
93. Fuel Water, *Water Fuel Cell vs. Hydrogen Fuel Cell* 2010 [cited 2010 20 July]; http://www.waterfuel.ws/water-fuel-cell.htm.
94. Cunningham, N., et al., *Measuring The Through-plane Electrical Resistivity of Bipolar Plates (Apparatus and Methods).* Journal of Power Sources, 2005. **143**: p. 93-102.
95. Smits, F.M., *Measurement of Sheet Resistivities with The Four-Point Probe.* **Bell System Technique Journal**, 1958: p. 711-718.
96. Mironov, V.S., Kim J.K., and M. Lefevre, Lebrun,G., Dodelet, J.P., *Comparison of Electrical Conductivity Data Obtained by Four-Electrode and Four-Point Probe Methods for Graphite-Based Polymer Composites.* **Polymer Testing**, 2007. **26**: p. 547–555.
97. Yan, X., Hou, M., Sun, L., Liang, D., Shen, Q., Xu, H., Ming,P., and Yi,B., *AC Impedance Characteristics of a 2 kW PEM Fuel Cell Stack Under Different Operating Conditions and Load Changes.* **International Journal of Hydrogen Energy**, 2007. **32**(17): p. 4358-4364

98. Yuan, X.Z., Song,C., Wang,H., and Zhang, J., *Electrochemical Impedance Spectroscopy in PEM Fuel Cells*. 2010, USA: Springer-Verlag London Limited 262.
99. Ishibashi, Y., A. Nishikata, and T. Tsuru, *Electrochemical Impedance Spectroscopy of PEM Fuel Cell with Metal Bipolar Plates*. 2006, The Electrochemical Society meetings.
100. Brunetto, C., Moschetto, A., and Tina, G., *PEM Fuel Cell Testing by Electrochemical Impedance Spectroscopy.* **Electric Power Systems Research**, 2009. **79**: p. 17-26.
101. Pattamarat, K. and Hunsom, M., *Testing of PEM Fuel Cell Performance by Electrochemical Impedance Spectroscopy: Optimum Condition for Low Relative Humidification Cathode.* **Korean Journal Chemical Engineering**, 2008. **25**(2): p. 245-252.
102. Rubio, M.A., Urquia, A., and Dormido, S., *Diagnosis of Performance Degradation Phenomena in PEM Fuel Cells.* **International Journal of Hydrogen Energy**, 2009. **35**(7): p. 2586-2590.
103. Ciureanu, M. and Roberge, R., *Electrochemical Impedance Study of PEM Fuel Cells. Experimental Diagnostics and Modeling of Air Cathodes.* **Journal of Physical Chemistry B**, 2001. **105**: p. 3531-3539.
104. Cho, E.A., Jeon,U.-S., Ha,H.Y., Hong,S.-A., and Oh,I.-H., *Characteristics of Composite Bipolar Plates for Polymer Electrolyte Membrane Fuel Cells.* **Journal of Power Sources**, 2004. **125**: p. 178-182.
105. Fried, J.R., *Polymer Science and Technology*, ed. 2nd. 2005, China: Pearson Education, Inc.
106. Shackelford, J.F., *Introduction to Materials Science for Engineering*, ed. 7th. 2009, New York: Pearson Education. Inc.
107. Thomas, L.C., *Modulated DSC® Paper #9 Measurement of Accurate Heat Capacity Values*. 2009: USA.
108. Turriff, D.R.M., *NETZSCH LFA 427 Operation Instrctions*. 2009: Canada.
109. McCrum, N.G., Buckley, C.P., and Bucknall, C.B., *Principles of Polymer Engineering*, ed. 2nd. 1997: Oxford University Press.
110. instruments, H., *Durometer Super Ex Series*. 2009, Hoto instrument: Japan.
111. Mark, J., Ngai, K., and Graessley, W., Mandelkern, L., Edward, S., Koening, J., and Wignall, G., *Physical Properties of Polymers*, ed. 3rd. 2003: Cambridge University Press.
112. Psarreas, A., *Nitroxide-Mediated Controlled Degradation of Polypropylene*, in *Chemical Engineering*. 2006, University of Waterloo: Waterloo. p. 47-50.
113. Yanovsky, Y.G., *Polymer rheology : theory and practice*, ed. 1st. 1993, Landon: Chapman & Hall.
114. Lee, H.S., Kima, H.J., Kima,S.G., and Ahna,S.H., *Evaluation of Graphite Composite Bipolar Plate for PEM (proton exchange membrane) Fuel Cell: Electrical, Mechanical, and Molding properties.* **Journal of Materials Processing Technology**, 2007. **187-188**: p. 425-428.
115. Porous Materials, I., *Diffusion Permeameter*. 2008: New York.
116. Konell, J.P., King,J. A., and Miskioglu,I., *Tensile Modulus Modeling of Carbon-Filled Nylon 6,6 and Polycarbonate-Based Resins.* **Journal of Applied Polymer Science**, 2003. **90**: p. 1716–1728.

117. Pantea, D., Darmstadt, H., Kaliaguine, S., Sümmchen, L., and Roy, C., *Electrical Conductivity of Thermal Carbon Blacks Influence of Surface Chemistry.* **Carbon**, 2001. **39** p. 1147–1158.
118. Huang, J.-C., *Carbon Black Filled Conducting Polymers and Polymer Blends.* **Advances in Polymer Technology**, 2002. **21**(4): p. 299-313.
119. Blunk, R., Hassan,M., Elhamid,A., Lisi,D., and Mikhail,Y., *Polymeric Composite Bipolar Plates for Vehicle Applications.* **Journal of Power Sources**, 2006. **156**: p. 151-157.
120. Wolf, H. and Willert-Porada, M., *Electrically Conductive LCP–carbon Composite with Low Carbon Content for Bipolar Plate Application in Polymer Electrolyte Membrane Fuel Cell.* **Journal of Power Sources**, 2006. **153**: p. 41–46.
121. Kunststofftechnik, M.D., *Injection Moulding Pocketbook*, ed. 1. 1997, Germany: Mannesman Demag Kunststofftechnik.
122. Ivanov, Y., Cheshkov, V., and Natova, M., *Polymer Composite Materials-Interface Phenomena & Process*. 2001, Netherlands: Kluwer Academic Publishers.
123. King, J.A., T.M. Tambling, Morrison, F. A., Keith, J. M., Cole, A. J., and Pagel, R. M., *Effects of Carbon Fillers on the Rheology of Highly Filled Liquid-Crystal Polymer Based Resins.* **Journal of Applied Polymer Science**, 2008. **108**: p. 1646–1656.
124. Yang, W., Liu, Z.Y., Shan,G.F., Li, Z.M., Xie, B.H., and Yang,M.B., *Study on The Melt Flow Behavior of Glass Bead Filled Polypropylene.* **Polymer Testing**, 2005. **24**: p. 490-497.
125. King, J.A., Keith, J. M., Smith,R. C., and Morrison, F. A., *Electrical Conductivity and Rheology of Carbon Fiber/Liquid Crystal Polymer Composites.* **Polymer Composites**, 2007: p. 168-174.
126. Gubbels, F., Jerome, R., Vanlathem, E., Deltour,R., Blacher, S., and Brouers,F., *Kinetic and Thermodynamic Control of The Selective Localization of Carbon Black at the Interface of Immiscible Polymer Blends.* **Chemical Materials**, 1998. **10**(5): p. 1227-1235.
127. GmbH, S.K., *Schunck Molded Bipolar Plate for Fuel Cell*. 2006, Germany.
128. Houshyar, S., Shanks, R.A., and Hodzic, A., *Tensile Creep Behaviour of Polypropylene Fibre Reinforced Polypropylene Composites.* **Polymer Testing**, 2005. **24**: p. 257-264.
129. Acha, B.A., Reboredo, M.M., and Marcovich, N.E., *Creep and Dynamic Mechanical Behavior of PP–jute Composites: Effect of The Interfacial Adhesion.* **Composites: Part A**, 2007. **38**: p. 1507–1516.
130. Murariu, M. and Dechief, A.L., *The Production and Properties of Polylactide Composites Filled with Expanded Graphite.* **Polymer Degradation and Stability**, 2010. **95**: p. 889-900.
131. King, J.A. and Keith, J.M., *Synergistic Effects of Carbon Fillers on Tensile and Flexural Properties in Liquid-Crystal Polymer Based Resins.* Journal of Applied Polymer Science, 2008. **108**: p. 1657–1666.
132. Fu, S.-Y., Lauke, B., Mäder, E., Yue, C. -Y. and Hu, X., *Tensile Properties of Short-glass-fiber- and Short-carbon-fiber-reinforced Polypropylene Composites.* **Composites: Part A**, 2000. **31**: p. 1117-1125.
133. Entegris, *Bipolar and Monopolar Plate Standard Properties* 2004: USA.

134. Heizel, A., Mahlendrof, F., Niemzig,O., and Kreuz, C., *Injection Moulded Low Cost Bipolar Plates for PEM Fuel Cells*. 2003, University Duisburg-Essen: Duisburg, Germany. p. 1-7.
135. Yuan, X., Wang, H., Sun, J. C., and Zhang, J, *AC Impedance Technique in PEM Fuel Cell Diagnosis—A review.* **International Journal of Hydrogen Energy**, 2007. **32**: p. 4365 – 4380.
136. Karim, M.R. and Lee, C.J., *Radiolytic Synthesis of Conducting polypyrrole/carbon Nanotube Composites.* **Materials Letters**, 2007. **61**(8-9): p. 1688-1692.
137. FourBier, J., Boiteuxa,G., Seytrea,G., and Marichyb, G., *Percolation Network of Polypyrrole in Conducting Polymer Composites.* **Synthetic Metals**, 1997. **84**: p. 839-840.
138. Omastova, M., Podhradska, S. Prokes, J. Janigova, I., and Stejskal, J., *Thermal Ageing of Conducting Polymeric Composites.* **Polymer Degradation and Stability**, 2003. **82**: p. 251–256.
139. Ketpang, K. and Park, J.S., *Electrospinning PVDF/PPy/MWCNTs Conductingcomposites.* **Sythetic Metals**, 2010. **in Press, Corrected Proof** p. 1-6.
140. Lee, W.J., Kim, Y.J., Jung, M.O., Kim, D.H., Cho, D.L., and Kaang, S., *Preparation and Properties of Conducting Polypyrrole Sulfonated Polycarbonated Composites.* **Synthetic Mctals**, 2001. **123**: p. 327-333.
141. Pan, Y., Li, L., Chan,S.H., and Zhao, J., *Correlation Between Dispersion State and Electrical Conductivity of MWCNTs/PP Composites Prepared by Melt Blending.* **Composites: Part A**, 2010. **Part A 41** p. 419–426.
142. Al-Saleh, M.H. and Sundararaj, U., *A Review of Vapor Grown Carbon Nanofiber/polymer Conductive Composites.* **Carbon**, 2009. **47**: p. 2-22.
143. Sui, G., Jana, S., Zhong,W.H., Fuqua,M.A., Ulven, C.A., *Dielectric Properties and Conductivity of Carbon Nanofiber/semi-crystalline Ppolymer Composites.* **Acta Materialia**, 2008. **56**: p. 2381–2388.
144. Thiébaud, F. and Gelin, J.C., *Characterization of Rheological Behaviors of Polypropylene/carbon Nanotubes Composites and Modeling Their Flow in a Twin-screw Mixer.* **Composites Science and Technology**, 2010. **70**: p. 647–656.
145. Teng, C.-C., M. Ma,C-C., Huang, Y-W., Yuen, S-M., Weng,C-C., Chen, C-H., and Su,S-F., *Effect of MWCNT Content on Rheological and Dynamic mechanical Properties of Multiwalled Carbon Nanotube/polypropylene Composites.* **Composites: Part A**, 2008. **39**: p. 1869–1875.
146. Kinumoto, T., Nagano, K., Tsumura, T., and Toyoda, M., *Thermal and Electrochemical Durability of Carbonaceous Composites used as a Bipolar plate of Proton Exchange Membrane Fuel Cell.* **Journal of Power Sources**, 2010. **195**: p. 6473–6477.
147. Thomason, J.L., *The Influence of Fibre Length, Diameter and Concentration on the Modulus of Glass Fibre Reinforced Polyamide 6,6.* **Composites: Part A**, 2008. **39**: p. 1732–1738.
148. Campus, M.T., *Data sheet of ElectroPhen: EP1105*. 2009, Bac2 Limited: United Kingdom.
149. Kakati, B.K. and Deka, D., *Differences in Physico-mechanical Behaviors of Resol(e) and Novolac Type Phenolic Resin Based Composite Bipolar Plate for Proton*

Exchange Membrane (PEM) Fuel Cell. **Electrochimica Acta**, 2007. **52**: p. 7330–7336.
150. Othman, N., Ismail, H., and Mariatti, M., *Effect of Compatibilisers on Mechanical and Thermal Properties of Bentonite Filled Polypropylene Composites.* **Polymer Degradation and Stability**, 2006. **91**: p. 1761-1774.
151. Yu, G., Zhang,M. Q., Zeng,H. M., Houy.Y. H., and Zhang,H. B., *Effect of Filler Treatment on Temperature Dependence of Resistivity of Carbon-black-filled Polymer Blends.* **Journal of Applied Polymer Science**, 1999. **73**: p. 489-494.
152. Wah, C.A., Choong, L.Y., and Neon, G.S., *Effects of Titanate Coupling Agent on Rheological Behaviour, Dispersion Characteristics and Mechanical Properties of Talc Filled Polypropylene.* **European Polymer Journal**, 2000. **36**: p. 789-801.
153. Chiang, Y.C., C.Y. Lee, and H.C. Lee, *Surface Chemistry of Polyacrylonitrile- and Rayon-based Activated Carbon Fibers After Post-heat Treatment.* **Materials Chemistry and Physics**, 2007. **101**: p. 199–210.
154. Xie, Y., Hill, C. A.S., Xiao, Z., Militz, H., Mai,C., *Silane Coupling Agents Used for Natural Fiber/polymer Composites: A review.* **Composites: Part A**, 2010. **41**: p. 806–819.
155. Lee, S.H., Kim, M. W., Kim, S. H., Youn,J. R., *Rheological and Electrical Properties of Polypropylene/MWCNT Composites Prepared with MWCNT Masterbatch Chips.* **European Polymer Journal**, 2008. **44**: p. 1620–1630.
156. Prashantha, K., Soulestin, J., Lacrampe, M. F., Claes,M., Dupin,G., and Krawczak,P., *Multi-walled Carbon Nanotube filled Polypropylene Nanocomposites Based on Masterbatch Route: Improvement of Dispersion and Mechanical Properties Through PP-g-MA Addition.* **eXPRESS Polymer Letters**, 2008. **2**(10): p. 735-745.
157. Wang, K., Liang,S., Zhao, P., Qu,C.,Tan, H., Du,R., Zhang,Q., and Fu,Q., *Correlation of Rheology–orientation–tensile Property in Isotactic Polypropylene/organoclay Nanocomposites.* **Acta Materialia**, 2007. **55**: p. 3143-3154.
158. Drubetski, M., Siegmann, A., and Narkis, M., *Electrical Properties of Hybrid Carbon Black/carbon Fiber Polypropylene Composites.* **Journal of Materials Science**, 2007. **42**: p. 1-8.
159. Lutz, W., Herrmann,J., Kockelmann, M., Hosseini, H.S., Jäckel, A., Schmauder,S., Predak,S., and Busse, G., *Damage Development in Short-fiber Reinforced Injection Molded Composites.* **Computational Materials Science**, 2009. **45**: p. 698–708.
160. Chandra, A., Kramschuster, A.J., Hu,X., Turng, L.S., *Effect of Injection Molding Parameters on The Electrical Conductivity of Polycarbonate/carbon nanotube Nanocomposites.* **ANTEC 2007**, 2007.
161. Zheng, G.Q., Yang,W., Huang,L., Yang,M.B., Li,W., Liu,C.T., and Shen,C.Y., *Flow-induced Fiber Orientation in Gas-assisted Injection Molded part.* **Materials Letters**, 2007. **61**(3436–3439).
162. Asghari, S., Mokmeli, A., and Samavati, M., *Study of PEM Fuel Cell Performance by Electrochemical Impedance Spectroscopy.* **International Journal of hydrogen energy**, 2010. **In Press Corrected Proof**: p. 1-8.
163. Fu, Y., Hou, M., Liang, D., Yan,X., Fu,Y., Shao, Z., Hou,Z., Ming,P., Yi,B., *The Electrical Resistance of Flexible Graphite as Flowfield Plate in Proton Exchange Membrane Fuel Cells.* **Carbon**, 2008. **46**: p. 19-23.

164. Freire, T. and Gonzalez, E., *Effect of Membrane Characteristics and Humidification Conditions on The Impedance Response of Polymerelectrolyte Fuel Cells.* **Journal of Electroanalytical Chemistry**, 2001. **503**: p. 57-68.
165. Avasarala, B. and Haldar, P., *Effect of Surface Roughness of Composite Bipolar Plates on the Contact Resistance of a Proton Exchange Membrane Fuel Cell.* **Journal of Power Sources**, 2009. **188**: p. 225-229.
166. Blunk, R., F. Zhong, and Owens J., *Automotive Composite Fuel Cell Bipolar Plates: Hydrogen Permeation Concerns.* **Journal of Power Sources**, 2006. **159**(1): p. 533-542.
167. Enomoto, K., Fujiwara,S., Yasuhara,T., Murakami, H., Teraki,J., Ohtake, N., *Effect of Filler Orientation on Thermal Conductivity of Polypropylene Matrix Carbon Nanofiber Composites.* **Japanese Journal of Applied Physics**, 2005. **44**(27): p. L 888–L 891.
168. Khizhnyak, P.E., Chechetkin, A.V., and Glybin, A.P., *Thermal Conductivity of Carbon Black,* **Journal of Engineering Physics and Thermophysics**, 1979. **37**(3): p. 1073-1075.
169. Hauser, R.A., Keith, J. M., King,J. A., and Holdren, J. L., *Thermal Conductivity Models for Single and Multiple Filler Carbon/Liquid Crystal Polymer Composites.* **Journal of AppliedPolymer Science**, 2008. **110**: p. 2914–2923
170. Hwang, I.U., Yu,H. N., Kim, S. S., Lee,D. G., Suh,J. D., Lee,S. H., Ahn, B. K., Kim, S. H., and Lim,T., *Bipolar Plate Made of Carbon Fiber Epoxy Composite for Polymer Electrolyte Membrane Fuel Cells.* **Journal of Power Sources**, 2008. **184**: p. 90-94.
171. Dhakate, S.R., Sharma, S., Chauhan,N., Seth,R.K., and Mathur,R.B., *CNTs Nanostructuring Effect on The Properties of Graphite Composite Bipolar Plate.* **International Journal of hydrogen energy**, 2010. **35**: p. 4195-4200.
172. Heiser, A.H. and King J.A, *Thermally Conductive Carbon Filled Nylon 6,6.* **Polymer Composites**, 2004. **25**: p. 186-193.

Appendix A

A-1 MATERIAL SPECIFICATIONS

Table A-1: The Properties of PP35FU01

Physical Properties Property	Nominal Value	Units	ASTM Test Method
Melt Flow Rate	**20**	**g/10 min**	**D 1238**
Tensile Strength @ Yield[1]	3,780 (26)	psi (MPa)	D 638
Elongation @ Yield[1]	4.0	%	D 638
Flexural Modulus[2]	190,000 (1,310)	psi (MPa)	D 790
Izod, Notched @ 23°C	2.0 (107)	ft-lb/in (J/m)	D 256
Unnotched Impact @ -18°C	20 (1,070)	ft-lb/in (J/m)	D 4812
Gardner Impact, 23°C	295 (33)	in-lb (J)	D 3029
Gardner Impact, -18°C	180 (20)	in-lb (J)	D 5420
Rockwell Hardness	92	R	D 785
Heat Deflection Temperature @ 66 psi[3]	219 (104)	°F (°C)	D 648
Heat Deflection Temperature @ 264 psi[3]	131 (55)	°F (°C)	D 648

[1] Crosshead Speed – 2 in/min, [2] Crosshead Speed – 0.05 in/min,

[3] Data are for control and development work and not intended for use in design or predicting endurance

Table A-2: The Properties of PP36KK01

Physical Properties Property	Nominal Value	Units	ASTM Test Method
Melt Flow Rate	7.0	g/10 min	D 1238
Tensile Strength @ Yield	3,200 (22.0)	psi (MPa)	D 638
Elongation @ Yield	6	%	D 638
Flexural Modulus	160,000 (1,100)	psi (MPa)	D 790

Table A-2: The Properties of PP36KK01 (continue)

Physical Properties Property	Nominal Value	Units	ASTM Test Method
Izod, Notched @ 23°C	9.5 (500)	ft-lb/in. (J/m)	D 256
Izod Impact, Notched @ -18°C	1.4 (75)	ft-lb/in. (J/m)	D 256
Unnotched Impact @ -18°C	31 (1,655)	ft-lb/in. (J/m)	D 4812
Gardner Impact, @ -18°C	320 (36)	in-lb. (J)	D 5420
Rockwell Hardness	78	R	D 785
Heat Deflection @ 66 psi	73 (163)	°C (°F)	D 648

Table A-3: The properties of Asbury synthetic graphite

Asbury Synthetic Graphite (4012)				
Type	**Carbon Content (%)**	**Typical Size (microns)**	**Surface Area (m^2/gram)**	**Typical Resistivity (Ohm-cm)**
4012	99	44 × 250	1.5	0.03

Asbury Carbon Fiber (AGM-99)							
Type	**Fiber Diameter (microns)**	**Density (g/cc)**	**Carbon (%)**	**Tensile Strength (MPa)**	**Young's Modulus (GPa)**	**Resistivity (ohm-cm)**	**Lengths (microns)**
PAN	7-9	1.79-1.85	>99	3600-3900	220-260	0.0014	Milled 150

Table A-4: The properties of fortafil carbon fiber and carbon nanafiber

Fortafil carbon fiber			
Typical continues fiber properties	English	SI	Metric
Tensile Strength	>500 ksi	>3,450 MPa	>350 kgf/ mm^2
Tensile Modules	>30 Msi	>207 GPa	>21,100 kgf/ mm^2
Ultimate Elongation	1.7 %	1.7 %	1.7 %
Density	0.065 Ib/ in^3	1.8 g/cm^3	1.8 g/cm^3
Cross-Sectional Area/Filament	4.7 or 6.5 x 10^{-8} in^2	3.3 or 4.2 x 10^{-5} mm^2	3.3 or 4.2 x 10^{-5} mm^2

Table A-4: The properties of Fortafil carbon fiber and Carbon nanofiber (continue)

Fortafil carbon fiber			
Typical continues fiber properties	**English**	**SI**	**Metric**
Filament Shape	Round	Round	Round
Filament Diameter	0.24 or 0.29 x 10^{-3} in	6 or 7 μm	6 or 7 μm
Electrical Resistivity		1,670 $\mu\Omega - cm$	
Chopped products			
Physical Form	Flakes		
Fiber Length	1/8, 1/4 in	3, 6 mm	3, 6 mm
Bulk Density	Dictated by the fiber length sizing level, and sizing type		
Moisture Content	<0.3 %		
Sizing Content	Dependent on the fiber length, fiber grade, and end use		
Ferromagnetic Metals Content	None >0.25 mm		

Conductive Carbon Nanofiber		
Property		
Outsider Diameter	50 – 200	nm
Insider Diameter	0.5 – 3	nm
Length	10 - 70	µm
BET Surface Area	25	m^2/g

Table A-5: The properties of Cabot vulcan XC-72 (VCB)

Property	**Value**	**Test Method**
Iodine number (mg/g)	253	ASTM D-1510
OAN (cc/100g)	174	ASTM D-2414
325 Mesh residue (ppm)	<25	ASTM D-1514
Moisture as packed (%)	<1.0	ASTM D-1509
Density (kg/m^3)	264	

Table A-6: The properties of Polypyrrole

Application	Conductive additive for thermoplasitics and thermosets.
Other Notes	Stable up to at least 290°C in air
Packaging	5, 25 g in glass bottle
Properties	contains proprietary organic sulfonic acid as dopant
solubility	H_2O: insoluble organic solvents: insoluble

Table A-7: The properties of Titanate coupling agent

Composition of blend :	Ken-React® LICA 38 = 65% (CAS # 103432-54-8) Silicon Dioxide = 35% (CAS # 112926-00-8)
Chemical description:	neopentyl(diallyl)oxy, tri(dioctyl)pyrophosphate titanate (Titanium IV 2,2 (bis 2-propenolatomethyl)butanolato, tris (dioctyl) pyrophosphato-O
Chemical structure:	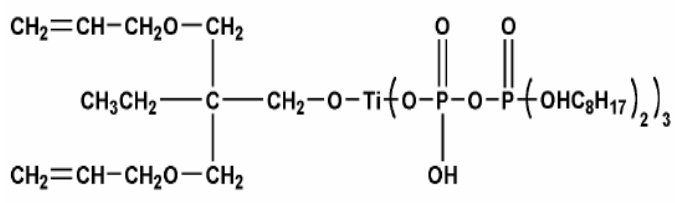
Titanate type:	Neoalkoxy

Color – Descriptive	Greenish Brown
Viscosity, cps @ 25ºC (77ºF)	1,200 – 9,000
Specific Gravity @ 16ºC (60ºF)	1.11 ± 0.02
Flash Point, ºF (TCC)	128
Initial Boiling Point, ºF, ASTM	160
pH (saturated solution)	3.0 ± 0.5
Solubility	>5% in mineral oil, aromatic plasticizer, DOP, DIDP, MEK , xylene and toluene. <5% in IPA. Insoluble in H2O. May be made water emulsifiable via emulsification using surfactants such as sodium dodecylbenzene-sulfonate (anionic), ethoxylated nonyl phenol (non-anionic) or cetyl trimethyl ammonium chloride (cationic).
Properties of silicon dioxide:	**Properties Of CAPOW L 38/H:**
Particle Size = 6.0 micrometer	Physical Form = Powder
pH (5.0%) = 7.0	Color = Off White
Oil Absorption = 190 (cc/100g)	% Ash = 54.0 ± 2.0
Surface Area = 140 (m^2/g)	Dispersion = Free flowing powder, no foreign matter.

A-2 MIXING PROCESSES

Figure A-1: Leistritz twin-screw extruder

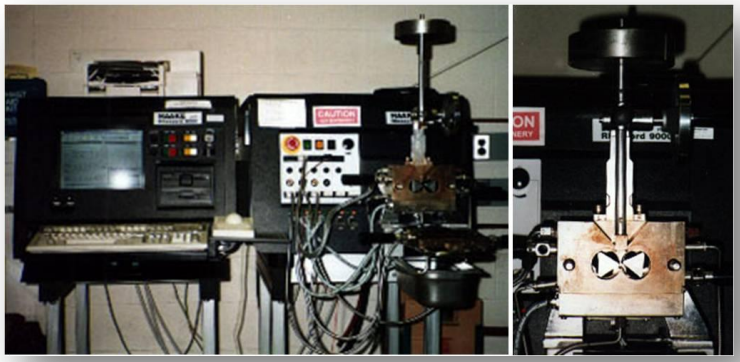

Figure A-2: Haake Fisons Rheocord 90

Figure A-3: Haake MiniLab Machine

Table A-8: Twin screw extruder elements

Configuration Name: ZSE 27 HP 40 L/D Screw Design McMaster University (Screw for use with side stuffer)

Enter Elements	**Length**
Spacer-10	10
GFA 2-40-90	90
GFA 2-30-90	90
GFA 2-20-60	60
KB 5-2-30-30 RE	30
KB 5-2-30-60 RE	30
KB 5-2-30-60 RE	30
KB 5-2-30-90	30
GFA 2-40-90	90
GFA 2-40-90	90
GFA 2-30-60	60
Comb	30
Comb	30
GFA 2-30-30	30
GFF 1-30-90	90
GFF 1-20-30	30
Comb R	30
KB 5-2-30-90	30
KS 1-2-10-E	10
GFA 2-40-90	90
GFA 2-30-30	30
Comb R	30
GFA 2-20-60	60
Total Length	**1100**

Inventory List

Element	**Length**	**Total Available**	**Remaining**
Spacer-5	5	8	**8**
Spacer-10	10	2	**0**
GFA 2-40-90	90	8	**0**
GFA 2-30-90	90	2	**0**
GFA 2-30-60	60	4	**2**
GFA 2-20-60	60	4	**0**
GFA 2-30-30	30	4	**0**
GFA 2-20-30	30	6	**6**
GFA 2-20-30 R	30	4	**4**
GFF 1-30-90	90	2	**0**
GFF 1-30-30	30	2	**2**
GFF 1-20-30	30	4	**2**
KS 1-2-10-M	10	10	**10**
KS 1-2-10-A	10	2	**2**
KS 1-2-10-E	10	2	**0**
KB 5-2-30-30 RE	30	6	**4**
KB 5-2-30-60 RE	30	10	**6**
KB 5-2-30-90	30	6	**2**
Comb	30	4	**0**
Comb R	30	4	**0**

Quick Check --> 0 (should equal 0)

(Should equal 1100)

Table A-9: The operating conditions of master batch productions using twin screw extruder

PP/Carbon black master batch											
TEMPERATURE (°C)											
zone:	**Feed Barrel**	**1**	**2**	**3**	**4**	**5**	**6**	**7**	**8**	**9**	**10**
set:	0	150	180	200	210	220	220	220	220	220	220
real:	38-42	150	180	200	210	220	220	220	220	220	224
SCREW SPEED (rpm)											
extruder speed:	100										
side stuffer speed:	82										
Output (kg/h)											
extruder output:	10										
extruder load:	6										
side stuffer load:	4										
MELT TEPERATURE (°C)					**MELT PRESSURE (bar)**						
238					304						
PP/Carbon black master batch (mixing PP with Titanate coupling agent)											
TEMPERATURE (°C)											
zone:	**Feed Barrel**	**1**	**2**	**3**	**4**	**5**	**6**	**7**	**8**	**9**	**10**
set:	0	150	180	200	210	220	220	220	220	220	220
real:	38	150	180	200	210	220	220	220	220	220	224
SCREW SPEED (rpm)											
extruder speed:	150										
side stuffer speed:	82										
Output (kg/h)											
extruder output:	10										
extruder load:	6										
side stuffer speed:	4										
MELT TEPERATURE (°C)					**MELT PRESSURE (bar)**						
238					340						
PP/synthetic graphite master batch											
TEMPERATURE (°C)											
zone:	**Feed Barrel**	**1**	**2**	**3**	**4**	**5**	**6**	**7**	**8**	**9**	**10**
set:	0	150	180	200	210	220	220	220	220	220	220
real:	36	150	180	200	210	220	220	220	220	220	224
SCREW SPEED (rpm)											
extruder speed:	152										
side stuffer speed:	87										
Output (kg/h)											
extruder output:	15										
extruder load:	6										
side stuffer load:	9										
MELT TEPERATURE (°C)					**MELT PRESSURE (bar)**						
240					316						

A-3 INJECTION AND COMPRESSION PROCESSES

Figure A-4: Engel 85 ton rotary injection-molding machine

Table A-10: The injection molding conditions of bipolar plate fabrication using Engle 85

Barrel Temperature (4 zones) (°C)	**Screw Speed (rpm)**	**Cooling Time (sec)**	**Cooling Temp (°C)**	**Injection Pressure (bar)**	**Hold Pressure (bar)**	**Injection Speed (mm/s)**	**Screw Recovery Time (sec)**	**Shot Size (mm)**	**Injection Time (sec)**
Z1, Z2, Z3: 190 to 200 Z4: 200 to 210	420	12 to 20	38 to 66	6 to 55	18.8	60 to 100	6.8	90 to 125	1.4 to 1.99

Figure A-5: Ray-Ran Injection Molding Machine

Figure A-6 Carver compression molding machine

A-4 CHARACTERIZATIONS

A-4.1 THE PROCEDURE OF LEAK TEST

The leak tests were performed to establish if there were any major defects in the cell assembly or membrane.

A-4.1.2 BLOCKING TEST

After single cell was assembled, a blocking test was demanded to certify gases can fully flow through gas-flow-channels on bipolar plates. The steps of the blocking test are shown as follows (Figure A-7).

1. Close the inlet and outlet of the cathode end plate
2. Plug nitrogen gas port to the anode inlet and pressurize cell to 30 psi using a knob on the nitrogen regulator
3. If the nitrogen flow from the anode outlet can be checked and the sound of the flow can be heard, the gas flow channels are not obstructed.
4. Repeat this procedure for the blocking test of the cathode side

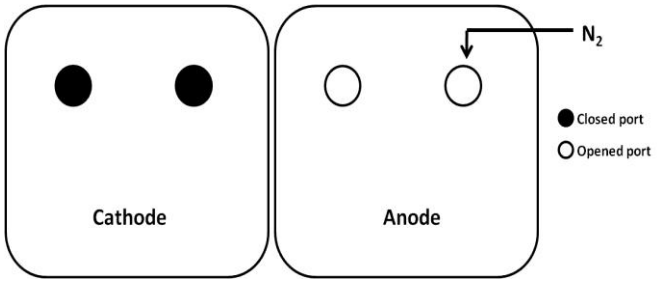

Figure A-7: The schematic of blocking test

A-4.1.3 SEALING TEST

The leak testing was required to ensure the fuel cell was tightened sufficiently to seal in both fuel and oxidant gases. The test consists of the procedure and schematic (Figure B-8) of test can be found as follows.

1. Hook up two a nitrogen port to inlet of cathode and anode together with a triple connection
2. Close cathode and anode outlets
3. Pressurize both the anode and cathode to an equal at 30 psi using the knob on the nitrogen regulator
4. Submerge the cell in water
5. If there was a sealing problem the gas would bubble out of the fuel cell, otherwise the fuel cell was sealed appropriately.

A-4.1.4 CROSS OVER TEST

The cross over test was conducted in order to ensure the fuel and oxidant gases cannot mix. This would be possible if there was a hole in the membrane or the membrane was not sealed between the gaskets. The test follows the method below (Figure A-9).

1. Plug nitrogen gas tube to the anode inlet port
2. Close the anode outlet and the cathode inlet
3. Connect the cathode outlet port to a specific pipette to measure the flow of gas
4. Pressurize the cell up to 5 psi
5. If there was no flow, then there was no cross over problems and the fuel cell was ready to be tested.

Note: It does not matter which side of cell is plugged in by nitrogen tube, as long as the measurement of the flow gas out is taken place on the other side.

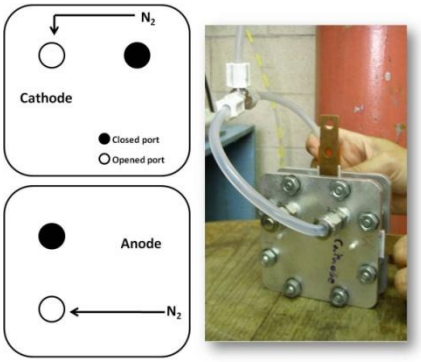

Figure A-8: The schematic of sealing test

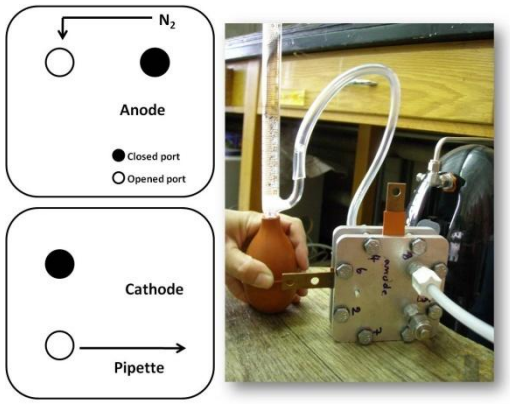

Figure A-9: The schematic of cross over test

A-4.2 ELECTRICAL CONDUCTIVITY PROCEDURE

Plates were tested using an Enlight Corp. Model EN 820212 power source. Voltage and current measurements were performed using an Agilent Model 34401A 6.5 Digit, Dual Input Multimeter. Both methods are arranged to measure voltage and current independently as shown in Figure 3-8. The procedure for determining in-plane electrical conductivity is:

1. Put the composite plates between the electrodes as shown in Figure 3-8.
2. The test apparatus is tightened at each corner by applying an evenly distributed torque of 0.5 Nm, which clamped the sample between the current electrodes
3. The multimeter outputs are checked ensuring a current and voltage of zero prior to start testing.
4. The power source is turned on, and the current and voltage are recorded at 10 s, 20 s, 30 s, 40 s, 1 min, 2 min, 3 min, 4 min, 5min, and 6 min intervals following power source commencement. Calculations are based on the average values.
5. Test at least 5 pieces for each sample.

Note: In case of the mini-tester, the apparatus is put between two plates of compression moulding machine to control the compressive force (500 lbs) instead of tightening by a torque wrench as depicted in the picture below.

The procedure of the through-plane electrical conductivity is as follows.

1. Place clean sample between gold plates, ensuring a complete contact.
2. Clamp the layered assembly to a pressure of 5,000 lbs and 1,500 psig.
3. The multimeter outputs are checked ensuring a current and voltage of zero prior to start testing.

4. The power source is turned on, and the current and voltage are recorded at 10 s, 20 s, 30 s, 40 s, 1 min, 2 min, 3 min, 4 min, 5min, and 6 min intervals following power source commencement. Calculations are based on the average values.
5. Test at least 5 pieces for each sample.

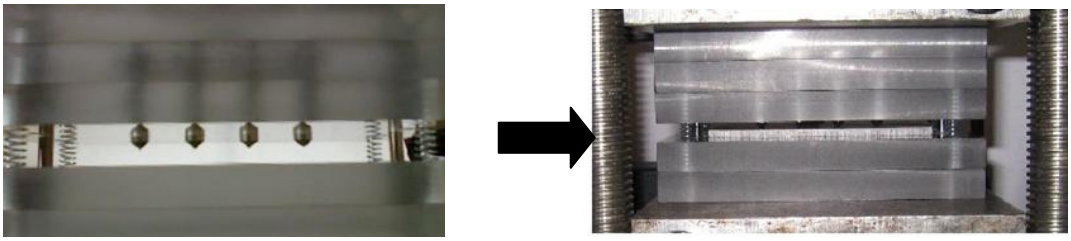

Figure A-10: The picture of mini-electrical conductivity tester that is under compression force

A-4.3 An Electrical Conductivity Apparatus Design

A-4.3.1 Four Point Probe Apparatus From ASTM D-991

The in-plane conductivity test procedure follows the outline in ASTM D-991 as portrayed in Figure A-11.The electrical conductivity test equipment was composed of half inch thick plastic pieces (Lexan). The insulators were made with two a quarter inch bolts, plastic swage pieces, Teflon disks, and electric tape. The electrodes were machined using 5/8 inch bolts. The supporting legs were assembled with metal tubes, nuts, and a quarter inch threaded rods. The Lexan pieces were cut and drilled using the band-saw and the drill-press. The electrodes were machined with a lathe. The band-saw was used to cut the threaded rods for the legs, while the tubes were shaped with the milling machine.

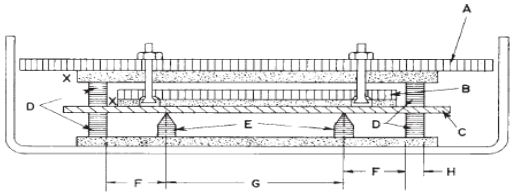

Figure A-11: Four probe testing apparatus from ASTM D-991

A-4.3.2 Mini Four Point Probe Apparatus

A mini conductivity tester was designed to accommodate small composite bars (6.2 × 1.6 cm.), and the design was concerned about applying compression force (500 lbs) during the measurement to diminish contact resistance between material layers. The new design was based on the design of ASTM four-probe tester, but the size of each part was modified to be appropriate for the specimen size. The tester was designed with four electrodes encased in Lexan plastic, and the electrodes were

fabricated from hex head brass bolts, machined to a precise length and sharpened. The three top and two bottom Lexan sheets were also machined with high precision dimensions, holes, channels and depressions. There are four screws to hold the top section together and four screws for the bottom section, and two dowels were used to keep the sections aligned. The tester has four springs to hold up the top section. All the specifications are displayed in Figure 3-9 and Figure A-12 exhibits a four probe compartment.

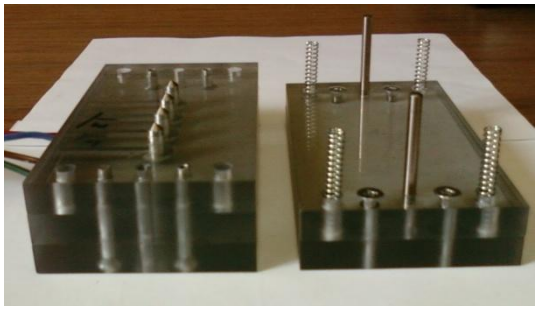

Figure A-12: The four probe compartment

To make the tester easy to use, the top section must float above the bottom section when no pressure is applied as seen in Figure B-10. There is naturally a 3 mm gap between the probes and sample to make insertion and removal of samples easy. At the same time, the springs have a negligible countering effect on the force of the hydraulic press during testing. To achieve this principle, a calculation of spring forces was required, using Equation A-1.

$$k = \frac{Gd^4}{8nD^3} \tag{A-1}$$

Variable	Description	Units
G	Modulus of rigidity	psi
D	Wire diameter	inches
N	Number of working coils	coils
D	Mean diameter of coils	inches

From the calculation, the top section weighs about 530 grams, or 1.2 pounds and the springs that were eventually selected have a k value of 9.1 pounds per inch. So the springs compress about 0.033 inches when there is no force applied to the tester. Under the pressure of the hydraulic press, which is about 500 pounds, the springs counteract with a force of about 4 pounds. The rest of the force goes into the test sample as a requirement, thus the effect of the springs on reducing the pressure is negligible.

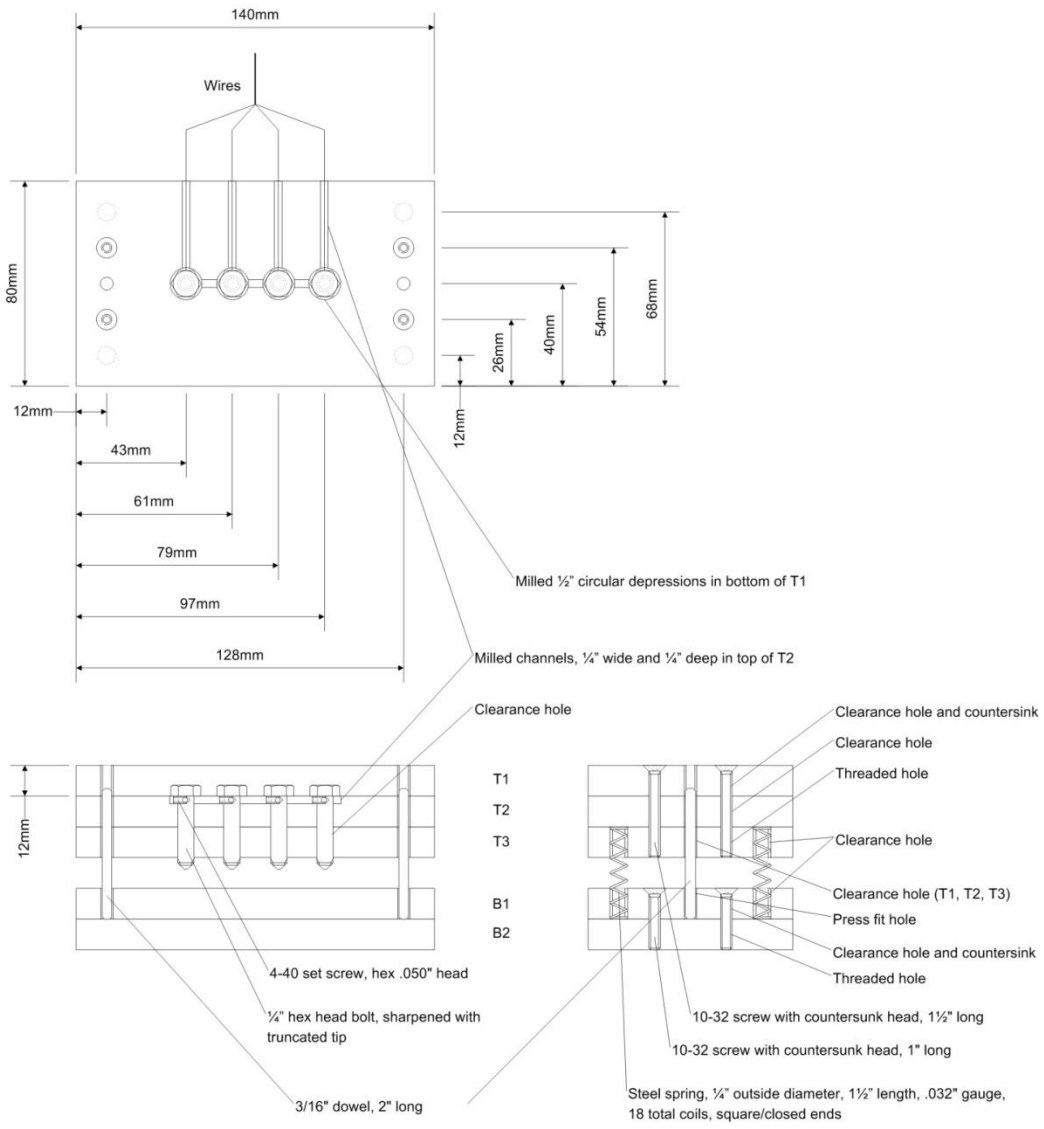

Figure A-13: The electrical conductivity tester design

A-4.4 THERMAL DIFFUSIVITY INSTRUMENT

Netzsch LFA 427 Instrument

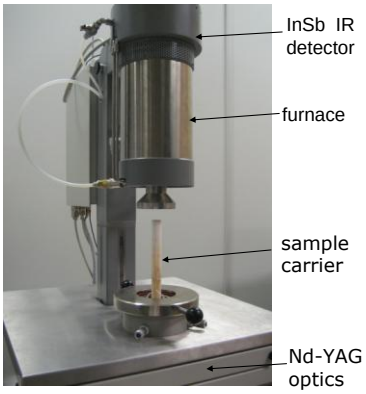

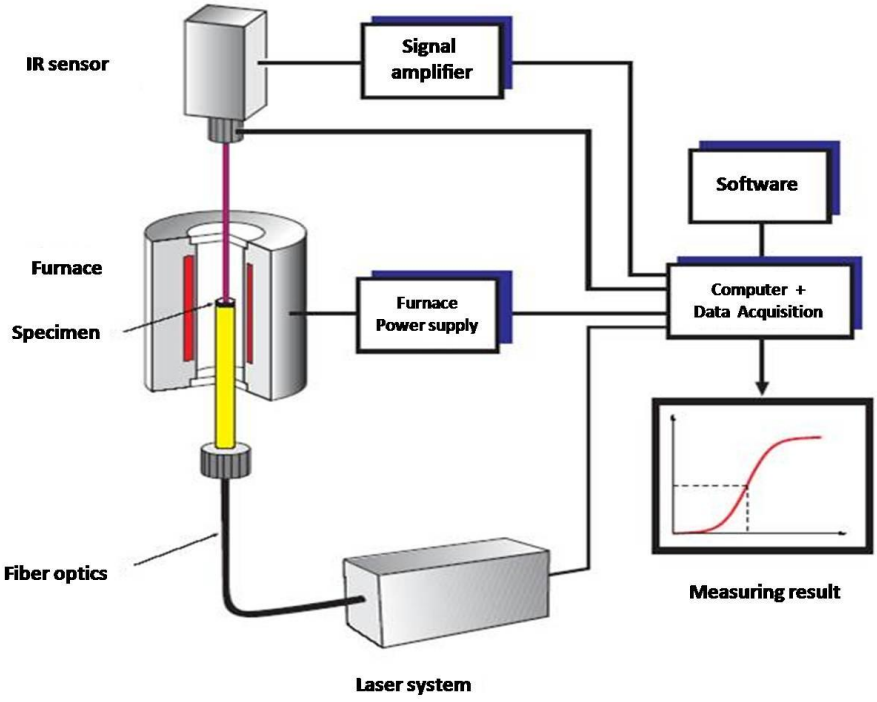

Figure A-14: Laser Flash Instrument and its layout

The instrument consists of four essential components: (1) measuring unit with furnace, sample carrier and IR detector, (2) controller for measuring unit, (3) laser system connected via fiber optics, and (4) data acquisition system computer. The laser system is connected with the measurement part by a sheeted glass fiber. The beam emerges from the outlet of the fiber optics. A recipient block is located above the laser optics, and a toggle quick seal permits a vacuum/gas-tight coupling between the recipient block and the furnace. A solid-state laser

produces a pulse with the energy, which is required for the flash method. The emission wave length of 1064 nm is in the infrared range. A thermocouple measures the absolute temperature of the sample. An IR detector measures the temperature increase on the rear face of the sample. Further features of these detectors are the germanium lens, which also acts as a filter for the laser light, and a motor-driven iris diaphragm.

Appendix B

B-1 Performance Test in "Synergistic Effect" Section

In this work, polarization curves from increasing and decreasing current were performed to investigate the different cell performance after normal polarization curve. After drawing current from OCV to 0.45 V, the current was drawn out to OCV. The Figure B-1 indicates that the second polarization was higher than the first polarization. The reason for its slight change may be that the water generated will be more with current density increasing; therefore, the membrane will be more hydrated, leading to the slight decrease of the ohmic resistance of stack.

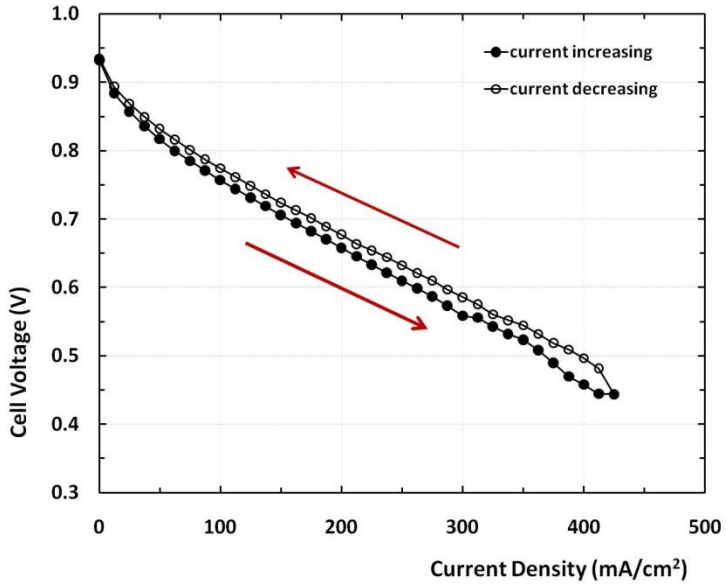

Figure B-1: Polarization curves of single cell assembled with FR8 bipolar plates

In this research the AC impedance measurement was conducted by using cathode as a working electrode. The impedance test using anode as the working electrode was also perform to ensure whether the selection of cathode or anode electrode as a working electrode does not affect to ohmic resistance of fuel cell. Figure B-2 represents ohmic resistance of the fuel cell using FR8 bipolar plates. The results illustrate the identical ohmic resistance which means a research can use any cathode or anode electrode to be the working electrode. However bigger arc size occurs when using anode as a working electrode. This is because the oxygen reduction is rate-determining step of electrochemical reaction in PEMFC. For that reason, charge transfer resistance will be higher than the one at anode side.

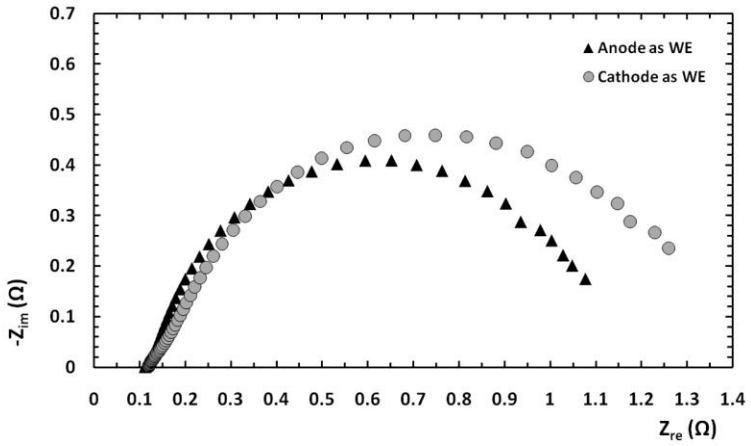

Figure B-2: Nyquist plots of single cell assembled with FR8 bipolar plates using different working electrodes

B-2 CHARACTERIZATION IN EFFECT OF PPY AND CARBON FIBERS

Table B-1: Mixing parameter of composites with different PPy loadings

PPy loading (wt%)	Temperature(^{o}C)	Screw speed (rpm)	Torque (Ncm)
0.5	175	180	127
1.0	175	180	130
1.5	175	180	132
2.0	175	180	149
2.5	175	180	150
3	175	180	165
4	175	180	170

Figure B-3 illustrates that combination of two different carbon fillers increased thermal stability of composites. Two steps of weight loss in filler decomposition region can be found when the composites contain two types of fillers.

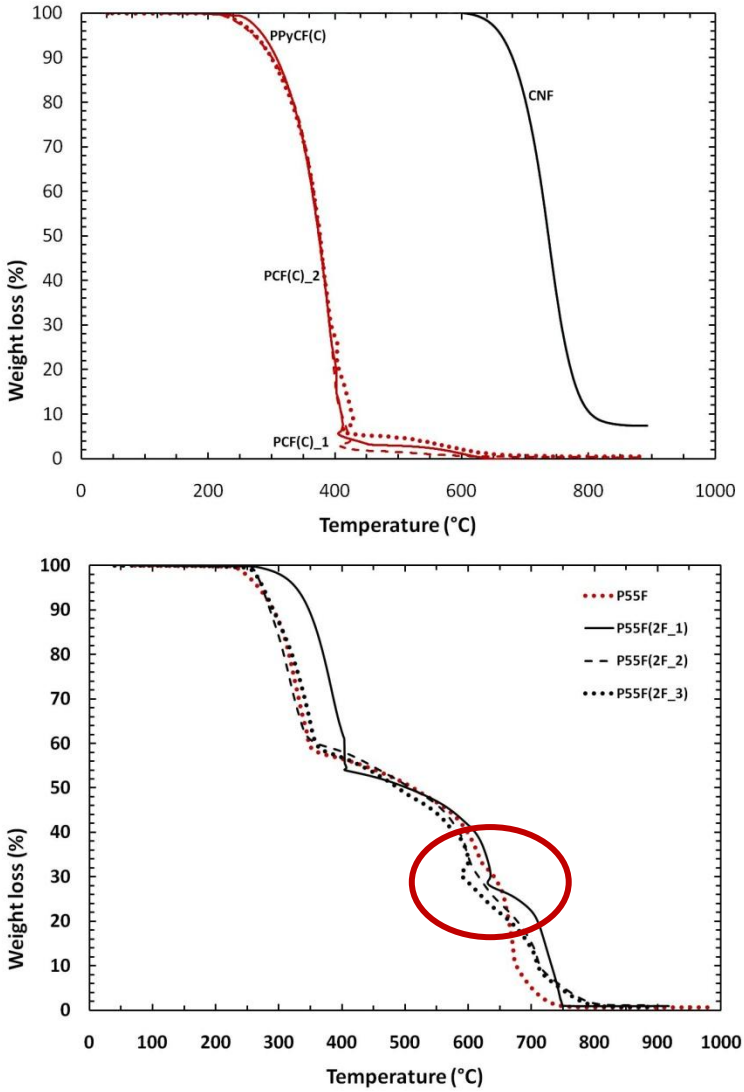

Figure B-3: TGA thermograms of composites in carbon fibers effects observation

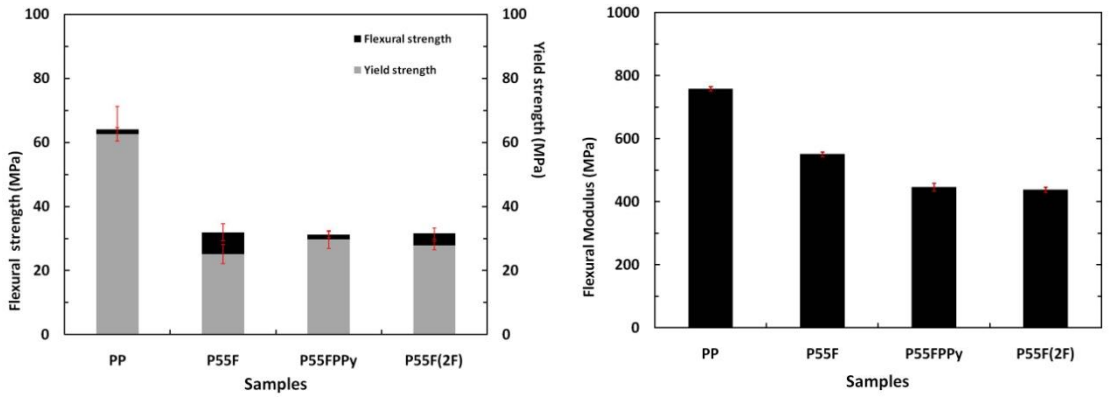

Figure B-4: Flexural properties of PP/carbon fiber composites

(specimens were cut in injection flow direction)

B-3 CHARACTERIZATION IN EFFECT OF TITANATE COUPLING AGENT

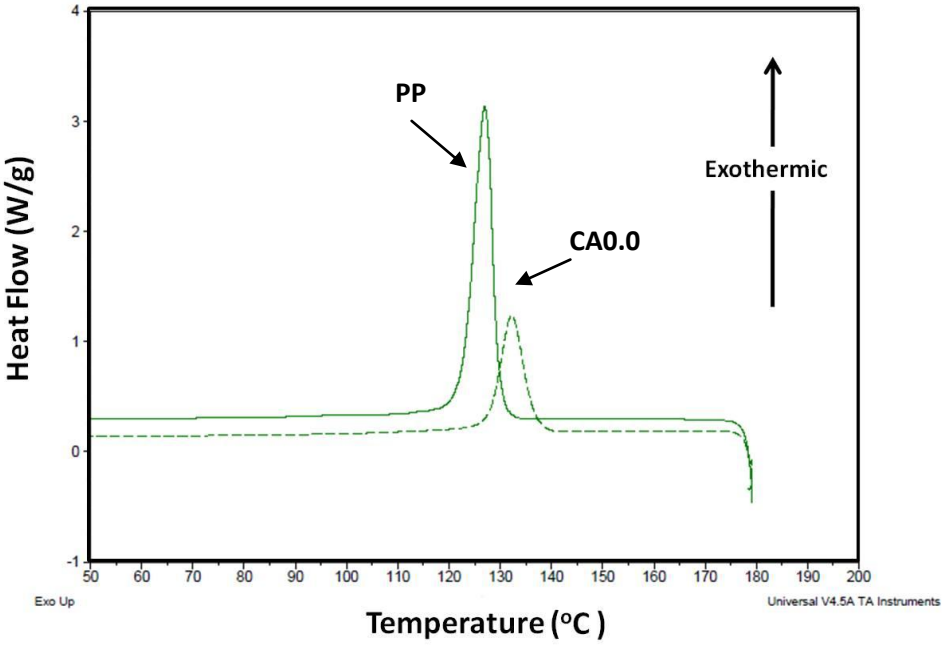

Figure B-5: Crystallization peaks of neat PP and PP/filler composite

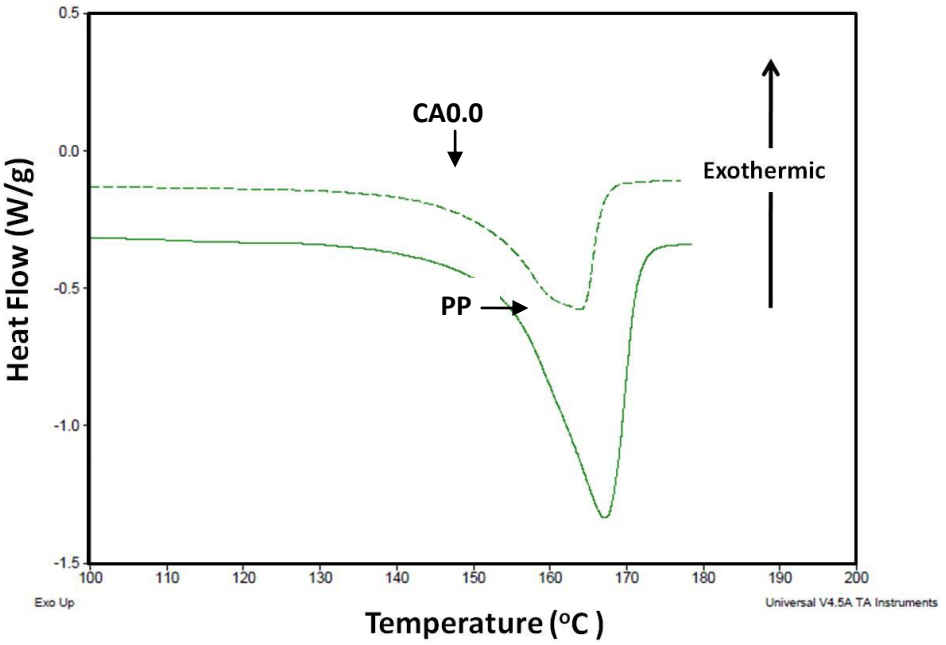

Figure B-6: Melting crystallization peaks of neat PP and PP/filler composite

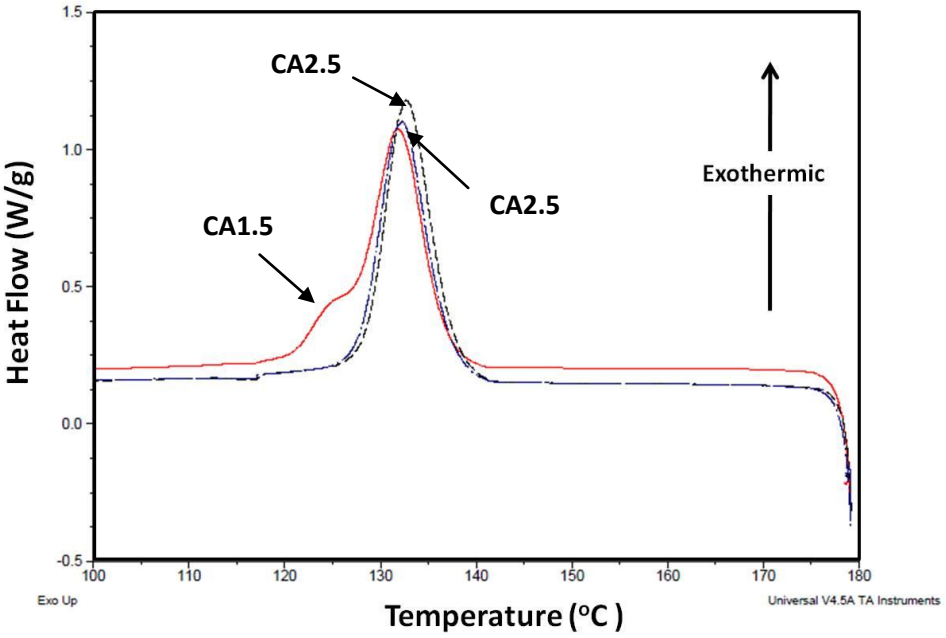

Figure B-7: Effect of Titanate coupling agent on crystallization peaks

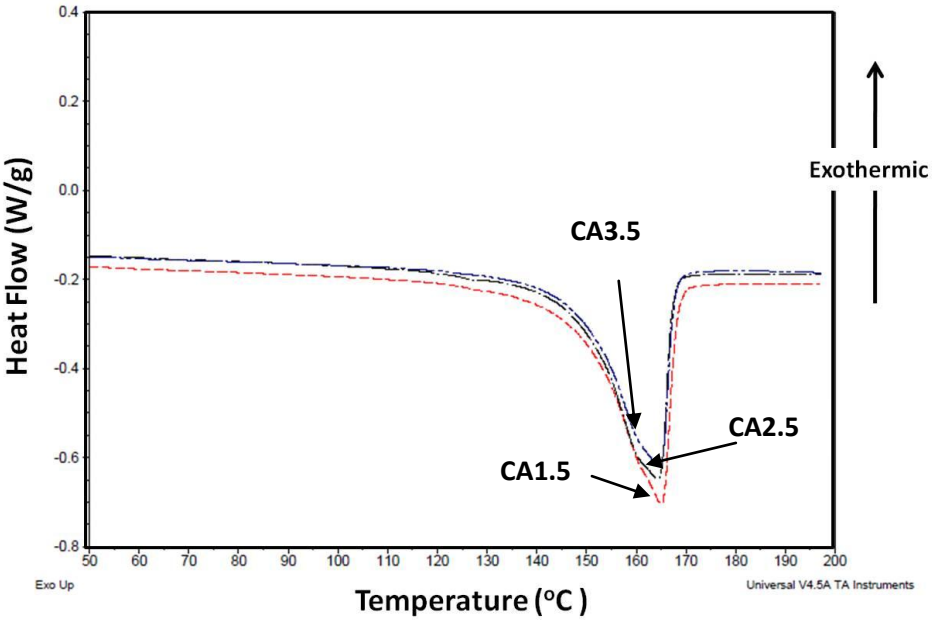

Figure B-8: Effect of Titanate coupling agent on melting crystallization peaks

B-4 Effect of Injection Flow on Conductive Network

The setting process condition for injection simulation:

Material	Polypropylene with 8g/10 min
Filler	Carbon fibre with 21 wt%
Stroke time	2.914 sec.
Actual Fill Time	2.914 sec.
Melt Temperature	200 ^{o}C
Mould temperature	45 ^{o}C
Maximum Injection Pressure	350 MPa
Mould thermal Boundary Condition Type	Heat Transfer Coefficient
Heat Transfer Coefficient	500 W/m^2.K

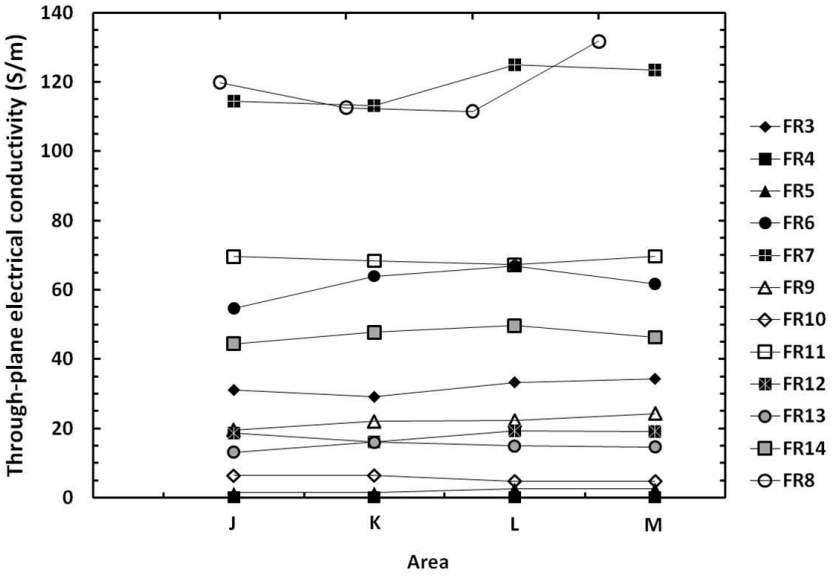

Figure B-9: Through-plane electrical conductivity of composite plates in different locations

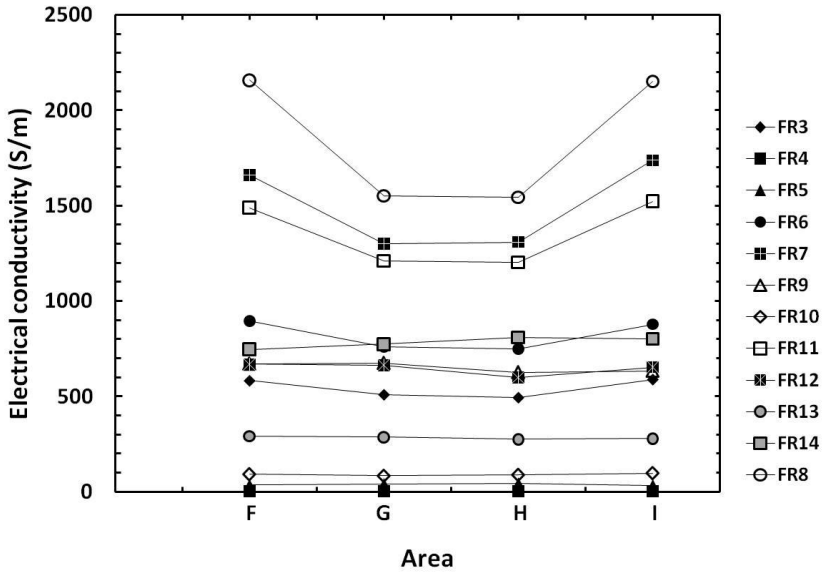

Figure B-10: In-plane electrical conductivity of composite plates in different locations (1)

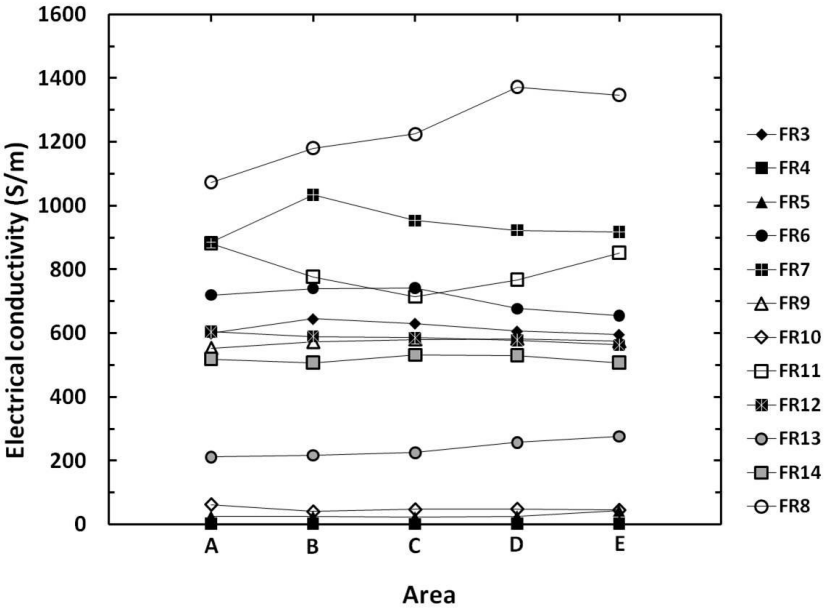

Figure B-11: In-plane electrical conductivity of composite plates in different locations (2)

B-5 CONTACT RESISTANCE

Figure B-12: An order of tightening supportive screws for fuel cell assembly

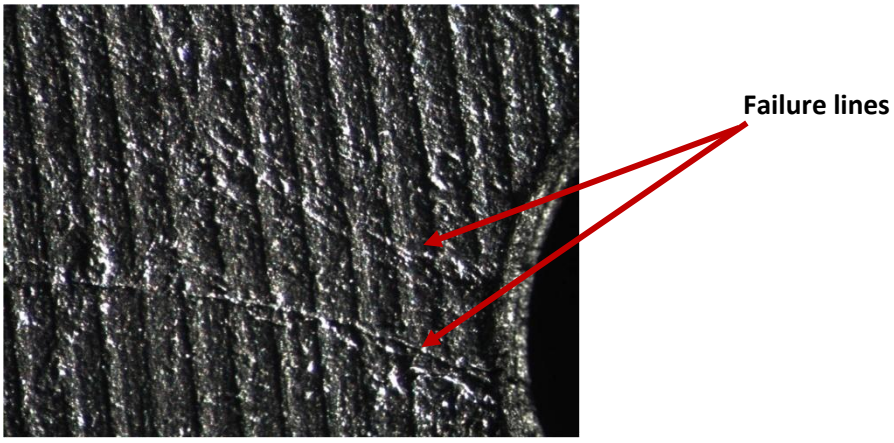

Figure B-13: A graphite bipolar plate was cracked under too much tightening torque

B-6 COPPER INSERT BIPOLAR PLATE

Copper sheet insert bipolar plates were prepared from injection molding process, since Wang recommended the compression molding is not suitable for producing the metal insert composite bipolar plate. First copper sheet with dimension of 100.0 × 24.0 × 0.5 mm were cut and its surface was cleaned with isopropanol. After that the copper sheet was transferred to the mould of injection molding machine. As expectation of this procedure, the copper sheet should be covered with molten composite, when the polypropylene composite is injected into the mould. In fact, injection pressure caused the copper insert to move from the original position; hence, one part of copper sheet was covered by the polymer composite. In order to solve this problem, an appropriate mould design must be provided for a metal insert plate. In this work, the researcher solved this problem by cutting another half of a composite plate, and compression molded the plate with the copper composite plate (from injection processed). The compression molding can sandwich copper sheet with composite polymer and also provide gas flow channel.

Appendix C

C-1 Example Electrical Conductivity

C-1: List of terms

Variable	Description	Units
ρ	Electrical resistivity	Ωm
σ	Electrical conductivity	S/m
V	Voltage	V
I	Current	A
W	Sample width	mm
T	Sample thickness	mm
L	Distance between 2 probes	mm
L_s	Sample Length	mm
k	Constant value (for unit conversion)	
S	Probe spacing	mm
F_1	Rectangular specimen of thickness	
F_2	Rectangular specimen of length	

In-plane Electrical Conductivity

Calculations for in-plane electrical conductivity following ASTM D-991 are shown below.

Calculations are based on Equation 2-30 in chapter 2:

$$\rho = \frac{(VWT)}{IL}$$

$$\sigma = \frac{IL}{(V \times W \times T \times k)}$$

Sample: P55FPPy

σ = (0.36A × 26.71mm)/ (0.144V×23.85mm×2.98mm×0.001)

σ = 956.2576 S/m

In case of mini in-plane tester, the calculation corresponds to Equation 2-28 and 2-29 (chapter 2)

$$\rho = \frac{\pi T}{\ln 2}\left(\frac{V}{I}\right)F_1F_2$$

F_1 = 1 can be assumed, when the ratio of a sample thickness/a probe spacing is lower than 0.4. The ratio of S/W of this tester very low; thus, F_2 is negligible. The electrical conductivity can be calculated from the equation below.

$$\rho = \frac{\pi T}{\ln\left(\frac{\sinh\left(\frac{T}{S}\right)}{\sinh\left(\frac{T}{2S}\right)}\right)}\left(\frac{V}{I}\right)$$

$$\ln\left(\frac{\sinh\left(\frac{T}{S}\right)}{\sinh\left(\frac{T}{2S}\right)}\right) = \ln\left(\frac{\sinh\left(\frac{3}{18}\right)}{\sinh\left(\frac{3}{2\times18}\right)}\right) = 0.6873$$

$$\sigma = \frac{0.6873}{\pi T}\left(\frac{I}{V}\right) = \frac{0.2190}{T}\left(\frac{I}{V}\right)$$

Sample: FR8 (2F_2)

$$\sigma = \frac{0.2190}{0.3\ cm}\left(\frac{0.5810\ A}{1.8191 \times 10^{-3}\ V}\right)$$

$$\sigma = 2.10\ \times 10^{1} S/cm = 2.10\ \times 10^{3} S/m$$

THROUGH-PLANE ELECTRICAL CONDUCTIVITY

Sample: P55FPPy with 4%wt of PPy

$$\sigma = \frac{I}{V} \times \frac{T}{W \times Ls} = Scm^{-1}$$

$$\sigma = \frac{0.552\ A}{2.3433\ \times\ 10^{-2} V} \times \frac{3.0\ (mm)}{12.55\ (mm) \times 63.40\ (mm)} = 8.84\ \times 10^{-1} Scm^{-1}$$

$$= 88.40\ Sm^{-1}$$

C-2 EXAMPLE THERMAL CONDUCTIVITY

The thermal diffusivity is relevant to thermal conductivity following the equation below.

$$\alpha = \frac{k}{\rho Cp}$$

C-2: List of terms

Variable	Description	Units
ρ	Density	kg/m^3
k	Thermal conductivity	W/ (m.K)
C_p	Heat capacity	J/(kg.K)
α	Thermal diffusivity	(m^2/s)

Sample: P55FPPy at 80°C

$$k = \alpha \rho Cp$$

$$k = (3.890 \times 10^{-7})(\frac{m^2}{s}) \times 1.23 \times 10^3 (\frac{kg}{m^3}) \times (879.6)(\frac{J}{kg.K})$$

$$k = 4.4413 \times 10^{-1} (\frac{W}{m.K}$$

Appendix D

D-1 SUMMARY PROPERTIES OF COMPOSITES

Table D-1: Summary of composite properties (1)

Composites	Electrical Conductivity (S/m)			Fuel cell Resistance (Ω)	Fuel cell Power (mW/cm^2)	Rheological characteristics		Mechanical properties
	In-plane (1)	In-plane (2)	Through-plane			n	k ($Pa.s^n$)	Compressive strength (MPa)
P55F	793	496	50	0.2104	52.152	0.3898	34914.030	58.76
P55FTi	812	503	52	0.1648	77.961	0.4117	26914.728	57.53
P55FTi(s)	613	437	34	0.3110	34.944	0.3648	26497.201	60.04
P55FZn	627	454	40	0.2745	36.056	0.5501	5601.440	59.62
P55FTiZn	636	468	46	0.2672	37.256	0.5130	7883.450	57.53
P55FPPy	971	532	53	0.1411	101.688	0.3278	56584.84	60.34
FR2 [1:0:0]	-	-	-	-	-	-	-	-
FR3 [1:1:0]	543	615	32	-	-	0.1769	10502.677	-
FR4 [0:0:1]	2	2	0.1	-	-	0.6122	414.572	-
FR5 [0:1:1]	38	29	2.1	-	-	0.5330	803.896	-
FR6 [1:0:1]	820	707	62	-	-	0.5937	7471.366	-
FR7 [1:1:0]	1502	943	119	-	-	0.1991	49945.918	-
FR8 [4:1:1]	1851	1239	120	0.0800	192.002	0.2121	161621.823	66.84
FR9 [1:4:1]	651	572	22	0.2286	47.226	0.2475	6410.6195	52.32
FR10 [1:1:4]	90	49	6	0.4799	21.679	0.2213	29369.733	48.75
FR11 [2:1:1]	1356	798	69	0.1134	99.142	0.2206	68611.988	67.91
FR12 [1:2:1]	646	584	18	0.2217	57.259	0.2531	9210.856	58.37
FR13 [1:1:2]	282	237	15	0.2168	56.476	0.2751	16512.012	51.54
FR14 [1:1:1]	782	519	47	0.2104	52.152	0.3086	16919.986	54.73
CA0.5	785	521	47	-	-	0.4254	18117.570	57.79
CA1.0	795	529	51	0.1744	77.961	0.4117	26914.728	54.73
CA1.5	838	545	56	-	-	0.3775	32976.154	56.31
CA2.0	890	628	48	0.1454	84.721	0.3804	32854.889	57.23
CA2.5	750	526	45	-	-	0.3546	38317.750	58.34
CA3.0	726	503	37	-	-	0.3366	43591.318	55.76
CA3.5	722	433	21	0.3281	29.166	0.3480	41361.854	-
CA4.0	704	431	22	-	-	0.3460	41257.224	55.99
VE1	90	49	6	-	-	0.2213	29369.733	-
VE2	782	519	47	-	-	0.3086	16919.986	-
VE3	113	64	8	-	-	0.4372	19306.342	-
VE4	1021	576	55	-	-	0.4113	34316.263	-

Table D-1: Summary of composite properties (1) (continued)

Composites	Electrical Conductivity (S/m)			Fuel cell Resistance (Ω)	Fuel cell Power (mW/cm^2)	Rheological characteristics		Mechanical properties
	In-plane (1)	In-plane (2)	Through-plane			n	k ($Pa.s^n$)	Compressive strength (MPa)
P55FPPy(0.0)	115	-	47	-	-	-	-	-
P55FPPy(0.5)	158	-	53	-	-	-	-	-
P55FPPy(1.0)	172	-	56	-	-	-	-	-
P55FPPy(1.5)	194	-	63	-	-	-	-	-
P55FPPy(2.0)	196	-	82	-	-	-	-	-
P55FPPy(2.5)	232	-	85	-	-	-	-	-
P55FPPy(3.0)	271	-	89	-	-	-	-	-
P55FPPy(4.0)	258	-	88	-	-	-	-	-
PPy(1.8)	-	-	1.266E-10	-	-	-	-	-
PPy(4.0)	-	-	3.611E-10	-	-	-	-	-
PCBPPy	-	-	-	-	-	-	-	-
PCFPPy	-	-	36	-	-	-	-	-
PSGPPy	-	-	1	-	-	-	-	-
P55F(2F_1)	115/ 1065	47/ 674	59	-	-	0.2292	171711.700	60.34
P55F(2F_2)	86	-	40				-	-
P55F(2F_3)	119	-	64	-	-	-	-	-
PCF(C)_1	-	-	4.835E-09	-	-	-	-	-
PCF(C)_2	-	-	4.493E-05	-	-	-	-	-
PPyCF(C)	-	-	7.167E-05	-	-	-	-	-
								-
FR8PPy_1	863	-	379	-	-	-	-	-
FR8PPy_2	1120	-	533	-	-	-	-	-
FR8(2F)_1	1896	-	503	-	-	-	-	-
FR8(2F)_2	2139	-	773	-	-	-	-	-
FR8(2F)_3	1034	-	386	-	-	-	-	-

Note: *(1) Parallel to injection flow direction, (2) Perpendicular to injection flow direction*

Table D-2: Summary of composite properties (2)

Composites	**Mechanical properties**				**Thermal conductivity ($W(mK)^{-1}$)**	**Thermal stability (°C)**	**H_2 Permeability ($cm^3cm^{-2}s^{-1}$)**	**Contact angle (degree)**
	Tensile strength (MPa)	**Flexural strength (MPa)**	**Creep behavior (%)**	**Hardness (shore D)**	**80°C**		**T = 1mm**	
P55F	40.33	33.38	-	79.0	3.8328E-01	327	4.95E-06	95
P55FTi	40.16	39.01	-	79.7	-	325	-	100
P55FTi(s)	43.70	31.77	-	-	-	343	-	103
P55FZn	38.30	28.15	-	-	-	326	-	93
P55FTiZn	31.23	29.30	-	-	-	326	-	99
P55FPPy	42.03	32.76	-	78.9	4.4413E-01	327	1.77E-06	110
FR2 [1:0:0]	-	-	-	-	-	372	-	-
FR3 [1:1:0]	-	-	~0.82	-	-	331	-	-
FR4 [0:0:1]	-	-	~0.55	-	-	334	-	-
FR5 [0:1:1]	-	-	~0.17	-	-	326	-	-
FR6 [1:0:1]	-	-	~0.86	-	-	347	-	-
FR7 [1:1:0]	-	-	~0.75	-	-	326	-	-
FR8 [4:1:1]	29.28	-	~0.17	80.0	3.1334E-01	320-321	9.44E-06	-
FR9 [1:4:1]	39.74	-	~0.12	-	-	320-321	-	-
FR10 [1:1:4]	30.59	-	~0.79	-	-	320-321	-	-
FR11 [2:1:1]	32.53	-	~0.19	-	-	320-321	-	-
FR12 [1:2:1]	37.83	-	~0.41	-	-	327	-	-
FR13 [1:1:2]	35.33	-	~0.089	-	-	320-321	-	-
FR14 [1:1:1]	40.33	-	~0.098	-	-	326	-	-
CA0.5	40.69	-	~0.090	-	-	327-329	-	98
CA1.0	43.33	-	~0.090	-	-	327-329	-	99
CA1.5	44.34	-	~0.25	-	-	327-329	-	100
CA2.0	44.82	-	~0.25	-	-	327-329	-	114
CA2.5	39.37	-	~0.23	-	-	327-329	-	95
CA3.0	33.71	-	~1.2	-	-	327-329	-	95
CA3.5	-	-	~1.6	-	-	327-329	-	89
CA4.0	33.17	-	~1.5	-	-	327-329	-	88
VE1	-	-	-	-	-	317	-	-
VE2	-	-	-	-	-	322	-	-
VE3	-	-	-	-	-	324	-	-
VE4	-	-	-	-	-	317	-	-

Table D-2: Summary of composite properties (2) (continued)

Composites	Mechanical properties				Thermal conductivity ($W(mK)^{-1}$)	Thermal stability (°C)	H_2 Permeability ($cm^3cm^{-2}s^{-1}$)	Contact angle (degree)
	Tensile strength (MPa)	Flexural strength (MPa)	Creep behavior (%)	Hardness (shore D)			T = 1mm	
P55FPPy(0.0)	-	-	-	-	-	305	-	-
P55FPPy(0.5)	-	-	-	-	-	306	-	-
P55FPPy(1.0)	-	-	-	-	-	312	-	-
P55FPPy(1.5)	-	-	-	-	-	304	-	-
P55FPPy(2.0)	-	-	-	-	-	315	-	-
P55FPPy(2.5)	-	-	-	-	-	322	-	-
P55FPPy(3.0)	-	-	-	-	-	320	-	-
P55FPPy(4.0)	-	-	-	-	-	320	-	-
PPy(1.8)	-	-	-	-	-	-	-	-
PPy(4.0)	-	-	-	-	-	-	-	-
PCBPPy	-	-	-	-	-	-	-	-
PCFPPy	-	-	-	-	-	-	-	-
PSGPPy	-	-	-	-	-	-	-	-
P55F(2F_1)	35.04	31.86	-	79.5	4.0443E-01	374	3.26E-05	-107
P55F(2F_2)	-	-	-	-	-	310	-	-
P55F(2F_3)	-	-	-	-	-	320	-	-

D-2 STANDARD DEVIATION OF ELECTRICAL CONDUCTIVITY VALUES

Table D-3: In-plane electrical conductivity of composites (parallel to injection flow): The effect of filler ratios

Composites	Component Loading (wt %)				Electrical conductivity (S/m)	SD	n
	CB (XC72)	CF (Fortafil)	SG (4012)	PP	In-plane (parallel to injection flow)		
FR2	55	0	0	45	-	-	-
FR3	0	55	0	45	543.00	21.50	16
FR4	0	0	55	45	2.00	0.54	16
FR5	0	27.5	27.5	45	38.00	8.52	16
FR6	27.5	0	27.5	45	820.00	38.86	16
FR7	27.5	27.5	0	45	1,502.00	55.91	16
FR8	36.66	9.17	9.17	45	1,851.00	123.08	16
FR9	9.17	36.66	9.17	45	651.00	11.74	16
FR10	9.17	9.17	3.66	45	90.00	8.19	16
FR11	27.5	13.75	13.75	45	1,356.00	67.66	16
FR12	13.75	27.5	13.75	45	646.00	15.21	16
FR13	13.75	13.75	27.5	45	282.00	27.95	16
FR14	18.33	18.33	18.33	45	782.00	11.96	16

Table D-4: In-plane electrical conductivity of composites (perpendicular to injection flow): The effect of filler ratios

Composites	Component Loading (wt %)				Electrical conductivity (S/m)	SD	n
	CB (XC72)	CF (Fortafil)	SG (4012)	PP	In-plane (perpendicular to injection flow)		
FR2	55	0	0	45	-	-	-
FR3	0	55	0	45	615.00	49.17	16
FR4	0	0	55	45	2.00	0.89	16
FR5	0	27.5	27.5	45	29.00	4.57	16
FR6	27.5	0	27.5	45	707.00	76.93	16
FR7	27.5	27.5	0	45	943.00	229.91	16
FR8	36.66	9.17	9.17	45	1,239.00	350.59	16
FR9	9.17	36.66	9.17	45	572.00	24.53	16
FR10	9.17	9.17	3.66	45	49.00	5.86	16
FR11	27.5	13.75	13.75	45	798.00	173.47	16
FR12	13.75	27.5	13.75	45	584.00	32.19	16
FR13	13.75	13.75	27.5	45	237.00	7.29	16
FR14	18.33	18.33	18.33	45	519.00	28.32	16

Table D-5: Through-plane electrical conductivity of composites: The effect of filler ratios

Composites	Component Loading (wt %)				Electrical conductivity (S/m)	SD	n
	CB (XC72)	CF (Fortafil)	SG (4012)	PP	Through-plane		
FR2	55	0	0	45	-	-	-
FR3	0	55	0	45	32.00	2.32	16
FR4	0	0	55	45	0.10	0.01	16
FR5	0	27.5	27.5	45	2.00	0.68	16
FR6	27.5	0	27.5	45	62.00	4.50	16
FR7	27.5	27.5	0	45	119.00	6.04	16
FR8	36.66	9.17	9.17	45	120.00	8.77	16
FR9	9.17	36.66	9.17	45	22.00	1.94	16
FR10	9.17	9.17	3.66	45	6.00	0.82	16
FR11	27.5	13.75	13.75	45	69.00	1.17	16
FR12	13.75	27.5	13.75	45	18.00	1.51	16
FR13	13.75	13.75	27.5	45	15.00	1.00	16
FR14	18.33	18.33	18.33	45	47.00	2.02	16

Table D-6: In-plane electrical conductivity of composites: The effect of PPy concentrations

Sample	PPy concentration (wt%)	In-plane electrical conductivity (S/m)	SD	n
P55FPPy(0.0)	0.0	115.09	8.85	16
P55FPPy(0.5)	0.5	157.98	3.90	16
P55FPPy(1.0)	1.0	172.48	3.15	16
P55FPPy(1.5)	1.5	193.65	5.26	16
P55FPPy(2.0)	2.0	196.00	4.47	16
P55FPPy(2.5)	2.5	232.20	5.72	16
P55FPPy(3.0)	3.0	270.90	7.20	16
P55FPPy(4.0)	4.0	258.23	5.13	16

Table D-7: Through-plane electrical conductivity of composites: The effect of PPy concentrations

Sample	PPy concentration (wt%)	Through-plane electrical conductivity (S/m)	SD	n
P55FPPy(0.0)	0.0	46.59	0.22	16
P55FPPy(0.5)	0.5	53.10	0.17	16
P55FPPy(1.0)	1.0	56.16	1.23	16
P55FPPy(1.5)	1.5	62.77	2.98	16
P55FPPy(2.0)	2.0	81.89	2.67	16
P55FPPy(2.5)	2.5	85.33	2.20	16
P55FPPy(3.0)	3.0	89.22	0.49	16
P55FPPy(4.0)	4.0	88.39	0.44	16

Table D-8: In-plane electrical conductivity of composites: The effect of additives

Sample	In-plane electrical conductivity (S/m) (parallel)	SD	In-plane electrical conductivity (S/m) (perpendicular)	SD
P55F	792.84	18.00 (n = 16)	495.61	18.00 (n = 16)
P55FTi	812.45	7.00 (n = 16)	503.78	25.00 (n = 16)
P55FTi(s)	613.34	7.00 (n = 16)	436.94	11.00 (n = 16)
P55FZn	627.14	12.00 (n = 16)	453.67	10.00 (n = 16)
P55FTiZn	636.27	8.00 (n = 16)	468.20	11.00 (n = 16)
P55FPPy(1.8)	971.07	12.00 (n = 16)	532.78	14.00 (n = 16)
P55F(2F_1)	1,064.73	18.00 (n = 16)	673.80	18.00 (n = 16)

Table D-9: Through-plane electrical conductivity of composites: The effect of additives

Sample	Through-plane electrical conductivity (S/m) (parallel)	SD	Through-plane electrical conductivity (S/m) (perpendicular)	SD
P55F	49.71	1.70 (n = 16)	47.19	18.00 (n = 16)
P55FTi	52.17	1.60 (n = 16)	53.72	25.00 (n = 16)
P55FTi(s)	34.20	2.70 (n = 16)	31.59	11.00 (n = 16)
P55FZn	40.34	2.60 (n = 16)	42.41	10.00 (n = 16)
P55FTiZn	46.91	1.60 (n = 16)	45.53	11.00 (n = 16)
P55FPPy(1.8)	53.30	1.70 (n = 16)	51.91	14.00 (n = 16)
P55F(2F_1)	56.66	1.92 (n = 16)	59.03	18.00 (n = 16)

Table D-10: Electrical conductivity of composites: The effect of fiber aspect ratios

Sample	In-plane electrical conductivity (S/m) (parallel)	SD	Through-plane electrical conductivity (S/m) (perpendicular)	SD
P55F(2F_1)	115.00	8.85 (n = 16)	46.59	0.22 (n = 16)
P55F(2F_2)	86.00	1.39 (n = 16)	40.00	0.19 (n = 16)
P55F(2F_3)	119.00	1.85 (n = 16)	64.00	0.34 (n = 16)

Table D-11: In-plane electrical conductivity of composites (parallel to injection flow): The effect of titanate coupling agent concentrations

Sample	Titanate coupling agent concentration (wt%)	In-plane electrical conductivity (S/m) (parallel)	SD	n
CA(0.0)	0.0	784.98	12.11	16
CA(0.5)	0.5	785.28	2.60	16
CA(1.0)	1.0	794.60	3.27	16
CA(1.5)	1.5	837.77	6.67	16
CA(2.0)	2.0	889.69	18.23	16
CA(2.5)	2.5	750.19	46.25	16
CA(3.0)	3.0	726.30	35.24	16
CA(3.5)	4.0	721.82	43.49	16
CA(4.0)	4.0	704.36	39.51	16

Table D-12: In-plane electrical conductivity of composites (perpendicular to injection flow): The effect of titanate coupling agent concentrations

Sample	Titanate coupling agent concentration (wt%)	In-plane electrical conductivity (S/m) (perpendicular)	SD	n
CA(0.0)	0.0	519.03	5.98	16
CA(0.5)	0.5	521.00	7.44	16
CA(1.0)	1.0	529.31	5.33	16
CA(1.5)	1.5	544.77	5.05	16
CA(2.0)	2.0	627.94	13.17	16
CA(2.5)	2.5	525.82	14.70	16
CA(3.0)	3.0	502.73	20.49	16
CA(3.5)	4.0	433.44	13.92	16
CA(4.0)	4.0	431.33	10.39	16

Table D-13: Through-plane electrical conductivity of composites: The effect of titanate coupling agent concentrations

Sample	Titanate coupling agent concentration (wt%)	Through-plane electrical conductivity (S/m)	SD	n
CA(0.0)	0.0	46.52	1.67	16
CA(0.5)	0.5	47.12	0.90	16
CA(1.0)	1.0	50.72	1.15	16
CA(1.5)	1.5	56.02	0.86	16
CA(2.0)	2.0	47.82	1.86	16
CA(2.5)	2.5	45.32	0.95	16
CA(3.0)	3.0	36.66	0.71	16
CA(3.5)	4.0	20.96	0.66	16
CA(4.0)	4.0	21.67	1.16	16

Table D-14: In-plane electrical conductivity of composites (parallel to injection flow): The effect of polypropylene viscosity

Sample	Filler ratio [CB:CF:SG]	In-plane electrical conductivity (S/m) (parallel)	SD	n
VE1	[1:1:4]	89.70	2.93	16
VE2	[1:1:1]	782.48	14.16	16
VE3	[1:1:4]	112.66	2.69	16
VE4	[1:1:1]	1,021.31	26.95	16

Table D-15: In-plane electrical conductivity of composites (perpendicular to injection flow): The effect of polypropylene viscosity

Sample	Filler ratio [CB:CF:SG]	In-plane electrical conductivity (S/m) (perpendicular)	SD	n
VE1	[1:1:4]	48.78	4.09	16
VE2	[1:1:1]	519.03	5.98	16
VE3	[1:1:4]	64.40	6.03	16
VE4	[1:1:1]	575.66	21.34	16

Table D-16: Through-plane electrical conductivity of composites: The effect of polypropylene viscosity

Sample	Filler ratio [CB:CF:SG]	Through-plane electrical conductivity (S/m)	SD	n
VE1	[1:1:4]	5.54	0.41	16
VE2	[1:1:1]	46.52	1.01	16
VE3	[1:1:4]	8.46	0.15	16
VE4	[1:1:1]	54.84	0.84	16

Table D-17: Electrical conductivity of composites: Additive combination

Sample	In-plane electrical conductivity (S/m)	SD	Through-plane electrical conductivity (S/m)	SD
P55F	115.09	4.42 (n = 16)	46.59	0.11 (n = 16)
FR8	514.33	11.39 (n = 16)	133.34	0.89 (n = 16)
P55F(2F_1)	368.02	38.43 (n = 16)	107.59	1.71 (n = 16)
FR8PPy_1	863.36	19.89 (n = 16)	379.31	6.68 (n = 16)
FR8PPy_2	1,120.15	15.78 (n = 16)	533.13	11.48 (n = 16)
FR8(2F)_1	1,895.90	53.66 (n = 16)	503.03	8.85 (n = 16)
FR8(2F)_2	2,139.18	89.76 (n = 16)	773.33	11.20 (n = 16)
FR8(2F)_3	1,034.33	39.78 (n = 16)	386.50	6.46 (n = 16)

Table D-18: Estimated Material costs

Materials	Cost (USD/lb)
Polypropylene	0.6
Polypyrrole	7,806
Carbon fiber (Fortafil)	10.0
Synthetic graphite (Asbery 4012)	1.5
Carbon black (Vulcan XC-72)	5.0
Carbon fiber (AGM99)	19.3
Titanate coupling agent - CA (LICA 38)	29.4

Note: These material prices are the prices in September 2010, and estimated based on commercially available materials that the lab has access to.

Table D-19: Percent contribution of material costs of a small bipolar plate

Bipolar plates	Percent weight in a bipolar plate (wt%)	Percent weight in a bipolar plate (grams)	Material cost in a bipolar plate (USD)	Material cost contribution to a bipolar plate
P55F	PP = 45 CB = 18.33 SG = 18.33 CF(Fortafil) = 18.33	PP = 5.4 CB = 2.2 SG = 2.2 CF(Fortafil) = 2.2	PP = 0.007 CB = 0.024 SG = 0.007 CF(Fortafil) = 0.048 ***Total cost/plate = 0.086***	PP = 8% CB = 28% SG = 8% CF(Fortafil) = 56%
P55FPPy(3.0)	PP = 45 CB = 18.33 SG = 18.33 CF(Fortafil) = 18.33 PPy = 3 wt% of total weight	PP = 5.4 CB = 2.2 SG = 2.2 CF(Fortafil) = 2.2 PPy = 0.36	PP = 0.007 CB = 0.024 SG = 0.007 CF(Fortafil) = 0.048 PPy = 6.189 ***Total cost/plate = 6.275***	PP = 0.1% CB = 0.4% SG = 0.1% CF(Fortafil) = 0.8% PPy = 99%
Blend with Titanate CA (2.0%)	PP = 45 CB = 18.33 SG = 18.33 CF(Fortafil) = 18.33 CA = 2 wt% of total weight	PP = 5.4 CB = 2.2 SG = 2.2 CF(Fortafil) = 2.2 CA = 0.24	PP = 0.007 CB = 0.020 SG = 0.007 CF(Fortafil) = 0.048 CA = 0.015 ***Total cost/plate = 0.097***	PP = 7% CB = 21% SG = 7% CF(Fortafil) = 49% CA = 15%
P55F(2F_1) (Two carbon fibers, no additives)	PP = 45 CB = 18.33 SG = 18.33 CF(Fortafil) = 9.17 CF(AGM99) = 9.17	PP = 5.4 CB = 2.2 SG = 2.2 CF(Fortafil) = 1.1 CF(AGM99) = 1.1	PP = 0.007 CB = 0.024 SG = 0.007 CF(Fortafil) = 0.003 CF(AGM99) = 0.046 ***Total cost/plate = 0.087***	PP = 8% CB = 28% SG = 8% CF(Fortafil) = 3% CF(AGM99) = 53%

Note: Assumed weight of a small bipolar plate is 12.0 grams